ON THE PERFORMANCE AND CAPACITY OF SPACE-TIME BLOCK CODED MULTICARRIER CDMA COMMUNICATION SYSTEMS

HU XIAOYU

NATIONAL UNIVERSITY OF SINGAPORE

2005

ON THE PERFORMANCE AND CAPACITY OF SPACE-TIME BLOCK CODED MULTICARRIER CDMA COMMUNICATION SYSTEMS

HU XIAOYU

(*B. Eng, M. Eng*)

A THESIS SUBMITTED

FOR THE DEGREE OF DOCTOR OF PHILOSOPHY

DEPARTMENT OF ELECTRICAL AND COMPUTER ENGINEERING

NATIONAL UNIVERSITY OF SINGAPORE

2005

Acknowledgements

The work of this dissertation could not have been accomplished without the contribution of friendship, support and guidance of many people.

First and foremost, I would like to express my deepest appreciation and most heartfelt gratitude to my supervisor, Dr. Chew Yong Huat, for his continual and thoughtful inspiration and guidance, enthusiastic encouragement, as well as tremendous technical support throughout my years at National University of Singapore and Institute for Infocomm Research, Singapore. Had it not been for his valuable advices, direction, patience, encouragement, and other unconditional support, this dissertation would certainly not be possible. Not only his conscious attitude towards research work but also his never giving up facing difficulties leaves indelible impact on me forever.

I dedicate this dissertation to my parents and my sister for their great caring, dedicated long-life supports and endless love to me throughout the years, and I will be forever indebted to them for all that they have done.

I would like to thank Dr. Mo Ronghong for her constant help and collaboration in the research work. My sincere thanks also go to my friends in the laboratory for their generous friendship, spiritual support, continual care and help, as well as many helpful discussions in my research work.

I am also greatly grateful to all my friends for their sincere care, warm concern and true friendship. Sharing with them the joy and frustration has made the life fruitful and complete.

Last but not least, my thanks go to the Department of Electrical and Computer Engineering in National University of Singapore and the Institute for Infocomm Research for giving me the opportunity to study here.

Contents

Abstract

Future wireless mobile systems are required to transport multimedia traffics at much higher bit rates and this motivates the author to work on the technologies suitable for the next generation of wireless mobile communication systems. Multicarrier (MC-) code division multiple access (CDMA) has emerged as a powerful candidate due to its capabilities of achieving high capacity over frequency selective fading channel. It inherits the substantial advantages from both the orthogonal frequency division multiplexing (OFDM) and code division multiple access (CDMA) systems. Space-time coding (STC) which integrates the techniques of spatial diversity and channel coding to combat the channel destructive multipaths is also a promising diversity technique to increase the system capacity of future wireless communication systems. This thesis focuses research on space-time block coded (STBC) multicarrier (MC-) CDMA system.

The thesis first investigates the bit error ratio (BER) performance and bandwidth efficiency of STBC MC-CDMA systems in the presence of carrier frequency offset (CFO) over frequency selective fading channels. The closed form expressions to compute BER theoretically when either equal gain combining (EGC) or maximum ratio combining (MRC) is used are derived. From these expressions, the effect of CFO on the performance and capacity can be easily investigated. It can be shown that if CFO is below certain threshold, it has insignificant effect on the BER and capacity of STBC MC-CDMA systems. This conclusion could be important in transceiver design.

Then various multirate access schemes for STBC MC-CDMA systems are proposed. The performance and capacity comparisons among the multicode, variable spreading gain (VSG) and multiple symbol rate (MSR) multirate access schemes over frequency selective fading channels are investigated. Power control is made to maintain the link quality and to improve the system capacity. From the numerical results, it can be concluded that the multicode access scheme when the orthogonal Gold sequence is used and the VSG access scheme have the similar performance and capacity. Both multicode and VSG access scheme are better than the three spectrum configurations of the MSR access scheme.

Next, the thesis looks into some of design and implementation issues of STBC MC-CDMA systems. First, the timing and frequency synchronization is studied. A subspace-based blind joint timing and frequency synchronization algorithm for STBC MC-CDMA systems over frequency selective fading channels is proposed. Through properly choosing the oversampling factor and the number of received samples, the timing and frequency synchronizations of all mobiles can be achieved. The use of subspace approach allows the multiuser estimations to be decoupled into multiple singe user estimations, and hence makes it computational efficient in multiuser environment.

After all the mobile users have adjusted and achieved synchronous transmission, the semi-blind channel estimation and linear multiuser detection are performed to recover the data from all the mobile users at the receivers of base station. Simulation results show the robustness and effectiveness of the estimation algorithm in the presence of near-far problems, multipath fading and large number of users**.** Finally the linear zero-forcing (ZF) and minimum-mean-square-error (MMSE) multiuser detection techniques are investigated in the thesis using the estimated channel gain.

Abbreviations

ACF	auto-correlation function
A/D	analog-to-digital
AWGN	additive white Gaussian noise
ARIB	association of radio industries and businesses
BER	bit-error-rate
BLAST	Bell-Labs layered space time
BPSK	binary phase shift keying
CCF	cross-correlation function
CDMA	code division multiple access
CFO	carrier frequency offset
CHF	characteristic function
CLT	central limit theorem
CP	cyclic prefix
CRB	Cramér-Rao bound
CSI	channel state information
D/A	digital-to-analog
DFT	discrete Fourier transform
DS-CDMA	direct sequence code division multiple access
DSP	digital signal processing
EGC	equal gain combining
ETSI	European telecommunications standards institute

FDMA	frequency division multiple access
FFT	fast Fourier transform
FIM	Fisher’s information matrix
FIR	finite impulse respons
FM	frequency modulation
FSK	frequency shift keying
FPLMTS	future public land mobile telecommunication system
GMSK	Gaussian minimum shift keying
GSM	global system for mobile communications
HPA	high power amplifier
ICI	inter-channel interference
IDFT	inverse discrete Fourier transform
IFFT	inverse fast Fourier transform
IMT-2000	international mobile telecommunication system in the year 2000
ISDN	integrated services digital network
ISI	inter-symbol interference
ITU-R	international telecommunications union’s radiocomm sector
MAI	multiple access interference
MCM	multicarrer modulation
MC-CDMA	multi-carrier code division multiple access
MC-DS-CDMA	multi-carrier direct sequence code division multiple access
MCR	multiple chip rate
MIMO	multiple-input and multiple-output
ML	maximum likelihood
MMSE	minimum mean squared error

MRC	maximum ratio combining
MSE	mean square error
MSR	multiple-symbol-rate
MT-CDMA	multitone code division multiple access
MUI	multiuser interference
NCFO	normalized carrier frequency offset
NFR	near-far ratio
NSV	normalized standard variance
OFDM	orthogonal frequency division multiplexing
PAPR	peak to average power ratio
PDF	probability density function
P/S	parallel to serial
PSD	power spectral density
QoS	quality of service
QPSK	quadratic phase shift keying
RTT	radio transmission technology
RV	random variable
SI	self-interference
SINR	signal-to-interference and noise-ratio
SIR	signal-to-interference ratio
SNR	signal-to-noise ratio
SISO	single input single output
S/P	serial-to-parallel
STBC	space-time block coding
STC	space-time coding

STTC	space-time trellis codes
SVD	Singular Value Decompositio*n*
TDMA	time division multiple access
TIA	telecommunications industry association
UTRA	UMTS terrestrial radio access
UWB	ultra wide band
VSG	variable spreading gain
WCDMA	wideband- code division multiple access
WLAN	wireless local area network
ZF	zero-forcing

List of Figures

List of Tables

List of Notations

$\underline{\mathbf{a}}$	symbol vector after STBC encoder (Chapter 3 and 4)
$\underline{\mathbf{a}}$	information vector defined in page 137 (Chapter 5)
$\overline{\underline{\mathbf{a}}}$	vector which is a function of time delay τ and vector $\mathbf{a}$ (Chapter 5)
$\tilde{\underline{\mathbf{a}}}$	vector which is a function of time delay τ and vector $\mathbf{a}$ (Chapter 5)
$\underline{\mathbf{b}}$	symbol vector before STBC encoder (Chapter 3 and 4)
b	symbol after STBC encoder (Chapter 5 and 6)
$\mathbf{c}$	spreading code
E_s	symbol energy
d	symbol before STBC encoder (Chapter 5 and 6)
f	carrier frequency
f_D	Doppler frequeny
$\mathbf{F}$	FFT processing
g	subscript to refer the multiple path
G	channel order
G_k	number of multiple paths for user k
$\underline{\mathbf{h}}$	channel frequency response vector
H	oversampling factor
i	subscript to refer the transmit antenna
I	total number of transmit antennas
j	subscript to refer the receive antenna

J	total number of receive antennas
k	subscript to refer the user
K	total number of users
l	subscript to refer the spreading chip
L	spreading gain
m	subscript to refer the class service
M	total number of class services
N_0	noise energy
n	subscript to refer the sampling time
p	subscript to refer the substream
P	number of parallel substreams
S	transmit power
V	total number of samples in one MC-CDMA symbol period
α	coefficient
β	channel fading gain
$\underline{\boldsymbol{\beta}}$	actual channel vector in without noise (Chapter 6)
$\underline{\tilde{\boldsymbol{\beta}}}$	actual channel vector in the presence of noise (Chapter 6)
$\underline{\boldsymbol{\beta}\!\!\!\!-}$	the channel vector solution of (6.17)
$\underline{\tilde{\boldsymbol{\beta}}\!\!\!\!-}$	the channel vector solution of (6.20)
$\underline{\hat{\boldsymbol{\beta}}}$	the estimated channel vector (Chapter 6)
η	AWGN noise
τ	time delay
ε	normalized carrier frequency offset
ω	normalized angular carrier frequency offset

Chapter 1

Introduction

The next generation wireless communication systems (sometimes also referred as 4G systems or beyond 3G) are required to support multimedia services such as speech, audio, video, image and data at much higher transmission rate. In future wireless networks, the various services such as circuit switched traffic, IP data packets and broadband streaming services are needed to be provided seamlessly. To ensure this, the development of wireless communication systems with generic protocols and multiple-physical layers or software defined radio interfaces are expected to allow users to seamlessly switch access among existing and future standards.

The idea behind of 4G wireless communication systems will be not only the application of new technologies to cover the need for high data rate services and new services, but also the integration of a multitude of existing and new wireless access technologies over a common platform in a manner that, at any given time, a user (or rather his/her terminal) may select the best suited of all access technologies that are available at her current location. These could include short-range technologies such as Bluetooth and wireless local area network (WLAN) as well as various types of cellular access technologies and even access through satellite. Hence, the selection of generic air-interface for future wireless communication system is of great importance. First, the new air-interface in the 4G system should be generic, so that it can integrate the existing access technologies; secondly, it should be spectrum efficient so that the high data rate can be supported in the system; thirdly, it should have high adaptability and reconfigurability so that the different standards and technologies can be supported; fourthly, it should have high scalability so that the system can provide different cell configurations hence better coverage; finally, it should be low cost so that a rapid market can be introduced.

1.1 Evolution of Cellular Mobile Communication Systems

1.1.1 Analogue First Generation Cellular Systems

In the late of 1970s and early 1980s, various first generation (1G) cellular mobile communication systems were introduced, characterized by analogue (frequency modulation) voice transmission and limited flexibility. The first such system, the *Advanced Mobile Phone System* (AMPS), was introduced in the US in the late 1970s [1][2]. Other 1G systems include the *Nordic Mobile Telephone System* (NMTS), and the *Total Access Communications System* (TACS). The former was introduced in 1981 in Sweden, then soon afterwards in other Scandinavian countries followed by the Netherlands Switzerland, and a large number of central and eastern

European countries, the latter was deployed from 1985 in Ireland, Italy, Spain and UK [1][2].

These systems used analog frequency modulation (FM) for speech transmission and frequency shift keying (FSK) for signaling. Individual calls use different frequencies. This way of sharing the spectrum is called frequency division multiple access (FDMA). While these systems offer reasonably good voice quality, they provide limited spectral efficiency. They also suffer from the fact that network control messages — for handover or power control, for example — are carried over the voice channel in such a way that they interrupt speech transmission and produced audible clicks, which limits the network control capacity [3]. This is one reason why the cell size cannot be reduced indefinitely to increase capacity.

1.1.2 Digital Second Generation Cellular Systems

Capacity increase was one of the main motivations for introducing second generation (2G) systems in the early 1990s. Compared to the 1G system, 2G offers:

1) increased capacity due to application of low-bit-rate speech codec and lower frequency reuse factors;
2) security (encryption to provide privacy, and authentication to prevent unauthorized access and use of the system);
3) integration of voice and data owing to the digital technology; and
4) dedicated channels for the exchange of network control information between mobile terminals and the network infrastructure during a call, in order to overcome the limitations in network control of 1G systems.

Digitization allows the use of time division multiple access (TDMA) and code division multiple access (CDMA) as alternatives to FDMA. With TDMA, the usage of each radio channel is partitioned into multiple timeslots and each user is assigned a specific frequency/timeslot combination. With CDMA (which uses direct sequence spreading), a frequency channel is used simultaneously by multiple mobiles in a given cell and the signals are distinguished by spreading them with different codes [8]. The use of TDMA and CDMA offers advantages such as the capability of supporting much higher number of mobile subscribers within a given frequency allocation, better voice quality, lower complexity and flexible support of new services. The digital cellular has become a real success. The vast majority of the subscribers are based on the Global System for Mobile Communications (GSM) Standard proposed by Europe, which today is deployed in more than 100 countries. The GSM standard uses Gaussian minimum shift keying (GMSK) modulation scheme and it adopts TDMA as the access technology. A very important contribution of GSM is that it brought forward strict criteria on its interfaces such that every system following such criteria can be compatible with each other. Another feature of GSM is that it has an interface compatible with Integrated Services Digital Network (ISDN). Other systems that are based on TDMA are Digital AMPS (DAMPS) in North America and Personal Digital Cellular (PDC) in Japan. DAMPS system, based on the IS-54 standard, operates in the same spectrum with the existing AMPS systems, thus making the standard IS-54 a "dual mode" standard that provides for both analog (AMPS) and digital operations. Another standard by North America is IS-95, which is based on narrow-band CDMA and can operate in AMPS mode as well. This standard has very attractive features such as increased capacity, eliminating the need for planning frequency assignments to cells and flexibility for accommodating different transmission rates. Cellular systems such as GSM and DAMPS are optimized for wide-area coverage; giving bit rates around

100 kbps. Further development will be capable of providing user data rates of up to 384kbps.

1.1.3 Third Generation Cellular Systems

Already before the launch of 2G systems, research on the third-generation (3G) wireless communication system started in the late 1980s. The international telecommunications union’s radio communication sector (ITU-R) task group 8/1 defined the requirements for the 3G mobile radio systems. This initiative was then known as future public land mobile telecommunication system (FPLMTS) [4][5]. The tongue-twisting acronym of FPLMTS was also aptly changed to IMT-2000, which refers to the international mobile telecommunication system in the year 2000. Besides possessing the ability to support services from rates of a few kbps to as high as 2Mbps in a spectrally efficient way, IMT-2000 aimed to provide seamless global radio coverage for global roaming. This implied the ambitious goal of aiming to connect virtually any two mobile terminals worldwide. The IMT-2000 system was designed to be sufficiently flexible in order to operate in any propagation environment, such as indoor, outdoor to indoor and vehicular scenarios. It’s also aiming to be sufficiently flexible to handle circuit as well as packet mode services and to handle services of variable data rates. In addition, these requirements must be fulfilled with a quality of service (QoS) comparable to that of the current wired network at an affordable cost.

Several regional standard organizations — led by the European telecommunications standards institute (ETSI) in Europe, the association of radio industries and businesses (ARIB) in Japan, and the telecommunications industry association (TIA) in the United States — have been dedicating their efforts to specifying the standards for IMT-2000. Most standardizations bodies have based their terrestrial oriented solutions on wideband-CDMA (W-CDMA), due to its advantageous properties, which satisfy most of the requirements specified for 3G mobile radio systems. W-CDMA is aiming to provide improved coverage in most propagation environments in addition to an increased user capacity. Furthermore, it has the ability to combat, or to benefit from, multipath fading through RAKE multipath diversity combining [6][7][29]. W-CDMA also simplifies frequency planning due to its unity frequency reuse.

Several of the regional standard organizations have agreed to cooperate and jointly prepare the technical specifications for the 3G mobile systems in order to assist as well as accelerate the ITU process for standardization of IMT-2000. This led to the formation of two partnership projects, which known as 3GPP [9] and 3GPP2 [10]. 3GPP was officially launched in December 1998 with the aim of establishing the ethnical specifications for IMT-2000 based on the evolved GSM core networks and the UMTS terrestrial radio access (UTRA) radio transmission technology (RTT) proposal. In contrast to 3GPP, the objective of 3GPP2 is to produce the ethnical specifications for IMT-2000 based on the evolved ANSI-41 core networks, the CDMA2000 RTT.

The objectives of the 3G standards by 3GPP or 3GPP2 went far beyond the 2G systems, especially with respect to:

1) the high quality of service requirements (better speech/image quality, lower bit error, higher number of active users.);
2) operation in mixed cell scenarios (macro, micro, oicp);
3) operation in different environments (indoor/outdoor, business/domestic, cellular/cordless)
4) finally flexibility in frequency (variable bandwidth), data rate (variable) and radio resource management (variable power/channel allocation).

1.2 Future or Fourth Generation Cellular Mobile Communication Systems

Wireless service providers are slowly beginning to deploy 3G cellular services. Voice, video, multimedia, and broadband data services are becoming integrated into the same network. However, the hope once envisioned for 3G as a true broadband service has dwindled away. Maintaining the possible 2Mbps data rate in the standard, 3G systems that were built so far can only realistically achieve 384kbps rates. To achieve the goals of a true broadband cellular service, the systems have to make the leap to a fourth generation (4G) network. 4G is intended to provide high speed, high capacity, low cost per bit and IP based services. The goal is to achieve data rates of up to 20Mbps, even when used in scenarios such as a vehicle traveling at 200km per hour. New modulation and signal processing techniques, however, are needed to make this happen. 4G does not have any solid specification defined yet, but it is clear that some standardization effort is in process.

Future mobile terminals will have to coexist in a world of multiple standards – both 2G and those members of the IMT-2000 (3G) family. Also, standards themselves are expected to evolve. In order to provide universal coverage, seamlessly roaming and non-standardized services, some of the elements of the radio interface (i.e., channel coder, modulator, transcoder, etc.) will no longer have fixed parameters; rather they will take the form of a toolbox whereby key parameters can be selected or negotiated to match the requirements of the local radio channel. In addition to the ability to adapt to different standards, downloadable terminals will enable network operators to distribute the new communications software over the air in order to improve the terminal’s performance in the network or to fix minor problems.

Besides offering new services and applications, the success of the 4G of cellular mobile communication systems will strongly depend on the choice of the concept and technology innovations in architecture, spectrum allocation, spectrum utilization and exploitation. Therefore, new high performance physical layer and multiple access technologies are needed to provide high speed data rates with flexible bandwidth allocation. A low-cost generic radio interface, being operational in mixed cell and in different environments with scalable bandwidth and data rates, is expected to have better acceptance.

1.2.1 Multicarrier Modulation

The technique of CDMA may allow the above requirements to be at least partially fulfilled because of its apparent advantages: high immunity against multipath distortion through the use of Rake receiver, able to overcome narrowband jamming due to the spectrum spreading of signal, and high flexibility to make variable rate transmission through changing the spreading gain [29]. However, the CDMA technology relies on spreading the data stream using an assigned spreading code for each user in time domain. In the presence of severe multipath propagation in mobile communications, the capability of distinguishing one component from others in the composite received signal is offered by the autocorrelation properties of the spreading codes. The RAKE receiver should contain multiple correlators, each matched to a different resolvable path in the received composite signal. Hence the system performance and capacity will strongly depend on the number of fingers employed in the RAKE. It is difficult for the CDMA receivers to make full use of the received energy scattered in time domain and usually the number of fingers is limited due to the hardware complexity.

Multicarrer modulation (MCM) has recently been attracting wide interest, especially for high data rate broadcast applications. The history of orthogonal multicarrier transmission dates back to the mid of 1960s, when Chang published his paper on the synthesis of band-limited signals for multichannel transmission [11][12]. He introduced the basic principle of transmitting data simultaneously through a band-limited channel without interference between subcarriers (without inter-channel interference, ICI) and without interference between consecutive transmitted symbols (without inter-symbol interference, ISI) in time domain. Later, Saltzberg performed futher analyses [13]. However, the major contribution to multicarrier transmission was presented in 1971 by Weinstein and Ebert [14] who used Fourier transform for baseband processing instead of a bank of subcarrier oscillators. To combat ICI and ISI, they introduced the guard time between the OFDM symbols.

The main advantages of multicarrier transmission are its robustness in frequency selective fading channels, and in particular, the reduced signal processing complexity by performing equalization in the frequency domain. The basic principle of multicarrier modulation relies on the transmission of data by dividing a high rate data stream into several parallel low rate substreams. These substreams are modulated on different subcarriers [15][16]. By using a sufficient number of subcarriers, a high immunity against multipath dispersion can be provided since the useful symbol duration on each subcarrier will be much larger than the channel time dispersion. Hence, the effect of ISI will be minimized. Since the large number of filters and oscillators necessary have to be used for a number of subcarriers, an efficient digital implementation of a special form of multicarrier modulation, known as orthogonal frequency division multiplexing (OFDM), with rectangular pulse shaping and guard time was proposed in [15]. OFDM can be easily realized by using the discrete Fourier transform (DFT). It divides the full bandwidth into a number of narrowband subcarriers each having bandwidth less than the channel coherent bandwidth, the transmission over each subcarrier will experience frequency nonselective fading. With the insertion of cyclic prefix (CP), ISI free system can be obtained as long as the number of CP is greater than the channel order.

The complementary advantages for CDMA and MCM have led to the thought to combine both CDMA and MCM to realize the so-called multi-carrier (MC-) CDMA. This combination of the techniques was proposed in 1993 by several authors independently [17]-[22]. It allows one to benefit from several advantages of both multicarrier modulation and spread spectrum system by offering, for instance, high flexibility, high spectral efficiency, simple and robust detection techniques and narrow band interference rejection ability. It is today emerged as the powerful candidate for the future generation (4G) high-speed wireless communication systems.

1.2.2 Diversity Techniques

Wireless channel suffers from attenuation due to destructive addition of multipaths in the propagation media and due to interference from other users. Severe attenuation makes it impossible for the receiver to determine the transmitted signal unless some less-attenuated replica of the transmitted signal is provided to the receiver. This resource is called diversity and it is the single most important contributor to achieve reliable wireless communications. Examples of diversity techniques are [43]:

- Temporal Diversity: Channel coding in conjunction with time interleaving is used. Thus replicas of the transmitted signal are provided to the receiver in the form of redundancy in temporal domain.

- Frequency Diversity: The fact that waves transmitted on different frequencies induce different multipath structure in the propagation media is exploited. Thus replicas of the transmitted signal are provided to the receiver in the form of redundancy in the frequency domain.
- Spatial Diversity: Spatially separated or differently polarized antennas are used. The replicas of transmitted signal are provided to the receiver in the form of redundancy in spatial domain. This can be provided with no penalty in bandwidth efficiency.

Encompassing all forms of diversity is required in the future wireless communication system (4G) to ensure high performance of capacity and spectral efficiency. Furthermore, the future generation of broadband mobile/fixed wireless system will aim to support a wide range of services and bit rates. The transmission rate may vary from voice to very high rate multimedia services requiring data rates up to 100Mbps. Communication channel may change in terms of their level of mobility, cellular infrastructure, required symmetrical or asymmetrical transmission capacity, and whether they are indoor or outdoor. Hence, air interfaces with highest flexibility are demanded in order to maximize the spectral efficiency in a variety of communication environments.

Temporal and frequency diversity techniques has been exploited in the conventional 2G or 3G wireless communication systems to achieve the spectral and power efficiency. For instance, cellular systems typically use channel coding in combination with time interleaving to obtain some form of temporal diversity [43][52]. In TDMA systems, frequency diversity is obtained using a nonlinear equalizer [43][53] when multipath delays are a significant fraction of symbol interval, In DS-CDMA, RAKE receivers are used to obtain frequency diversity [43].

However, spatial diversity so far only for cell sectorization will play much more important role in future wireless communication systems. In the past most of the work has concentrated on the design of intelligent antennas, known as space-time processing. In the meantime, more general techniques have been introduced where arbitrary antenna configurations at the transmit and receive sides are considered. For a general space-time processing systems where multiple antennas are employed at both the transmitter and receiver, such a signal model is so-called as multiple-input and multiple-output (MIMO) model.

Two approaches exist to exploit the capacity in MIMO channels. The information theory shows that with I transmit antennas and $J = I$ receive antennas, I independent data streams can be simultaneously transmitted, hence, increasing the system capacity. The BLAST (Bell-Labs Layered Space Time) architecture can be referred to [49][50]. The basic concept of BLAST architecture is to exploit channel capacity by increasing the data rate through simultaneous transmission of independent data stream over I transmit antennas. In this architecture, the number of receive antennas should be at least equal to the number of transmit antennas $J \geq I$. For m-ary modulation, the receiver has to choose the most likely out of m^I possible signals in each symbol time interval. Therefore, the receiver complexity grows exponentially with the number of modulation constellation points and the number of transmit antennas. Furthermore, the BLAST architecture for mobile communications is the needs of high number of receive antennas, which is not practical in a small mobile terminal.

An alternative approach is known as space-time coding (STC) [43][44][48] to obtain transmit diversity with I transmit antennas, where the number of receive antennas is not necessarily equal to the number of transmit antennas. Even with one receive antenna the system should work. This approach is more suitable for mobile communications. The basic philosophy with STC is different from the BLAST architecture. In stead of transmitting independent data streams, the same data stream is transmitted in an appropriate manner over all antennas. All transmit signals occupy the same bandwidth, but they are constructed such that the receiver can exploit antenna diversity.

1.3 Multicarrier CDMA and Space Time Coding

1.3.1 Multicarrier CDMA

Since 1993, various combinations of multicarrier modulation with the spread spectrum technique have been introduced. It has been shown that multicarrier CDMA offers high spectral efficiency, robustness and flexibility. Three different systems exist, namely MC-CDMA, MC-DS-CDMA and multitone (MT-) CDMA.

MC-CDMA is based on a serial concatenation of direct sequence (DS) spreading with multicarrier modulation. The high-rate DS spread data stream of process gain P_G is multicarrier modulated in the way that the chips of a spread data symbol are transmitted in parallel and the same assigned data symbol is simultaneously transmitted on each subcarrier. As for DS-CDMA, a user may occupy the total bandwidth for the transmission of a single data symbol. Separation of the user's signal is performed in the code domain. Each data symbol is copied on the substreams before multiplying it with a chip of the spreading code assigned to the specific user. This reflects that an MC-CDMA system performs the spreading in the frequency domain, and thus, has an additional degree of freedom compared to a DS-CDMA system.

Mapping of the chips in the frequency domain allows for simple methods of signal detection. This concept was proposed with OFDM for optimum use of available bandwidth. The realization of this concept implies a guard time between adjacent OFDM symbols to prevent ISI or to assume that the symbol duration is significantly larger than the time dispersion of the channel. The number of subcarriers has to be chosen sufficiently large to guarantee frequency nonselective fading on each subcarrier. Since the fading on the narrowband subcarriers can be considered as flat, simple equalization using one complex-valued multiplication per subcarrier can be realized.

MC-DS-CDMA modulates substreams on subcarriers with a subcarrier spacing proportional to the inverse of the chip duration. This wills guarantee orthogonality between the spectra of the substreams. If the spreading code length is smaller or equal to the number of subcarrier, a single data symbol is not spread in the frequency domain; instead it is spread in the time domain. Spread spectrum is obtained by modulating the time spread data symbols on parallel subcarriers. By using high numbers of subcarriers, this concept benefits from time diversity. However, due to the frequency nonselective fading per subcarrier, frequency diversity can only be exploited if channel coding with interleaving or subcarrier hopping is employed or if the same information is transmitted on several subcarriers in parallel. Furthermore, high frequency diversity could be achieved if the subcarrier spacing is chosen larger than the chip rate. The MC-DS-CDMA scheme can be subdivided into the scheme with broadband subcarriers and the scheme with narrowband subcarriers. System with broadband subcarriers typically applies only a small number of subcarriers, where each subcarrier can be considered as a classical DS-CDMA system with reduces data rate and ISI. The system with narrowband subcarrier typically uses high numbers of subcarriers and can be efficiently realized by using the OFDM operation.

MT-CDMA is a combined technique employing time domain spreading and a similar multicarrier transmission scheme to that of the MC-DS-CDMA scheme. However, the spectrum of each subcarrier prior to the spreading operation satisfies the orthogonal condition which subsequently loses the orthogonal quality after spreading. In this way, the system has a multiple access capability. The main intention of this operation is to increase the spreading gain within a given bandwidth. However, the system will experience ICI and ISI since the subcarriers do not maintain the orthogonality.

It has been shown that MC-CMDA outperforms than MC-DS-CDMA and MT-CDMA in the synchronous downlink and uplink channel [24]. However, in the asynchronous uplink channel, direct multicarrier transmission using OFDM operation without any pre-processing will lead to high peak to average power ratio (PAPR). Thus multicarrier modulated system using OFDM operation are more sensitive to high power amplifier (HPA) non-linearity than single carrier modulated system [26], and leading to severe clipping effects. One of possible approach is to use MC-DS-CDMA with low number of subcarriers in asynchronous mode. The low number of subcarriers results in the possibility to use the broadband transmission instead of OFDM operation and this leads to lower PAPR. However, for this implementation of MC-DS-CDMA, the each subcarrier experience frequency selective fading instead of flat fading, then much more complex RAKE receivers and multiuser detectors have to be needed. Hence, the BER performance and system capacity decreases. Another possible approach is to use pre-distortion technique or to properly select the spreading codes to reduce the influence of HPA non-linearity [27][28]. It can be shown in [27] (Table 4-

8) that the total degradation for MC-CDMA with the pre-distortion is less than the DS-CDMA and MC-DS-CDMA implemented without OFDM transmission in the uplink channels. And with the appropriate selection of spreading codes, the degradation of MC-CDMA decreases greatly. Hence, the MC-CDMA system is also a choice for uplink channel with pre-distortion or appropriate selection of spreading codes.

1.3.2 Space-Time Coding

Information theoretic studies have shown that antenna diversity provided by multiple transmit and receive antennas allows for a dramatic increase in the capacity and is an effective technique for combating fading in wireless communication systems [40][41]. Only recently has transmit diversity been studied extensively as a method of combating detrimental effects in wireless fading channels because of its relative simplicity of implementation and feasibility to support transmission in multiple antennas at the base station. The first bandwidth efficient transmit diversity scheme was proposed by Wittneben [45], and it includes the delay diversity scheme of Seshadri and Winters [46] as a special case. Later Foschini introduced multilayered space–time architecture [49].

More recently, a considerable amount of research in multiple antennas has addressed the design and implementation of space-time coded systems. These systems integrate the techniques of antenna diversity and channel coding, can combat the channel attenuation due to the destructive multipath and interference from other users, and can provide significant capacity gains [43][44][48]. The spatial nature of space-time codes can guarantee that the diversity burden is put at the base station while maintaining optional receive diversity. The temporal nature, on the other hand guarantees that the diversity advantage is achieved, without any sacrifices in the transmission rate. The design of space-time codes guarantees the highest possible transmission rate at a given diversity gain. In fact, it has shown that the space-time coding approach provides the best theoretical trade-off between diversity gain, transmission rate, constellation size, and trellis complexity [43]. For this reason, transmit diversity schemes become very attractive after the space-time coding techniques are proposed. Theoretically, we can add more antennas and receivers to all the remote units to implement such system. Although it is definitely not so economical at this state of art, however, its potential to achieve higher capacity has attracted the attention of many researchers.

A number of space-time coding schemes have been proposed so far, including space time trellis codes (STTC) and space time block codes (STBC). Space–time trellis coding has been proposed [43] which combines signal processing at the receiver with coding techniques appropriate to multiple transmit antennas and provides significant gain. Space–time trellis codes are designed for two or four transmit antennas perform extremely well in slow fading environments (typical in indoor transmission) by Telatar [51] and independently by Foschini and Gans [41]. The bandwidth efficiency is about three to four times that of current systems without any expansion in the bandwidth used. The space–time trellis codes presented in [43] provide the best possible tradeoff between constellation size, data rate, diversity advantage, and trellis complexity. When the number of transmit antennas is fixed, the decoding complexity of space–time trellis coding (measured by the number of trellis states in the decoder) increases exponentially as a function of both the diversity level and the transmission rate.

In addressing the issue of decoding complexity in space-time trellis codes, Alamouti discovered a remarkable scheme for transmission using two transmit antennas [44]. Space–time block coding, introduced in [48], generalizes the transmission scheme discovered by Alamouti to an arbitrary number of transmit antennas and is able to achieve the full diversity promised by the transmit and receive antennas. These codes retain the property of having a very simple maximum likelihood decoding algorithm based only on linear processing at the receiver [48]. For real signal constellations (such as PAM), they provide the maximum possible transmission rate allowed by the theory of space–time coding [43]. For complex constellations, space–time block codes can be constructed for any number of transmit antennas, and again these codes have remarkably simple decoding algorithms based only on linear processing at the receiver. They provide full spatial diversity and half of the maximum possible transmission rate allowed by the theory of space–time coding. For complex constellations and for the specific cases of three and four transmit antennas, these diversity schemes were improved to provide 3/4 of the maximum possible transmission rate [48].

1.4 Motivations

As we discussed above, MC-CDMA and space-time block coding (STBC) are emerged as powerful technologies for the future wireless communication system. This motivates the author to concentrate his studies in their combination - STBC MC-CDMA as the candidate of radio techniques for the next generation wireless communication system.

In the thesis, we concentrate the research on the uplink transmission of STBC MC-CDMA systems. In the first part, the thesis focuses on the theoretical analysis of BER performance and system capacity for STBC MC-CDMA systems. The analysis on the system performance in the presence of carrier frequency offset is first made, and the performance comparison among different multirate access schemes is also studied. In the second part, the thesis focuses on the receiver design and implementation for STBC MC-CDMA systems. First, the timing and frequency synchronizations are investigated. A joint timing and frequency synchronization is performed at the base station where the timing delays and carrier frequency offset of all users are estimated. Then the estimated timing delay and carrier frequency offset will be feed back to mobile users at the control channel. The mobile users then adjust its transmitted signal so that it is in alignment with other users' signals, and adapt to the base station's oscillator frequency by adjusting their own oscillators' frequency, according to the time and frequency offset information obtained from the control channel. After timing and frequency synchronization processing, the signals from all the mobile users arrive at the base station synchronously. Then the channel estimation is made at the base station where the channel state information of all users are obtained. Finally, with the estimated channel state information, multiuesr detection and STBC decoder is performed, so that the source information from all mobile users are resolved.

1.4.1 Performance and Capacity in the Presence of Carrier Frequency Offset

The performance and capacity of STBC MC-CDMA systems in the presence of carrier frequency offset is studied. There are many literatures on the BER performance of MC-CDMA [1][61] and STBC MC-CDMA systems [57]-[60] using synchronous and asynchronous transmissions, however, perfect carrier frequency synchronization is assumed. A major drawback of multicarrier modulation is that it is sensitive to the carrier frequency offset between the transmitter and receiver oscillator. Carrier frequency offset causes a loss of orthogonality between subcarriers and thus inevitably results in inter-subcarrier interference (ICI), which will cause severe performance degradation in MC-CDMA systems. In [62], the effect of frequency offset on the downlink performance of MC-CDMA systems was investigated. They used a computer simulation approach to study the multiuser case, while the analytical approach was only for a single user situation. In [63], the effect of carrier frequency offset on the performance of downlink MC-CDMA system in the frequency selective fading channels was studied, but not for uplink transmission. There were only a few reports considered the effect of carrier frequency offset on asynchronous MC-CDMA systems. In [64], the impact of frequency offset in the uplink of MC-CDMA systems was investigated, but only additive white Gaussian noise (AWGN) channels was considered. In [65], although frequency selective fading channels were studied in the uplink of MC-CDMA systems, only synchronous transmission was assumed. In [66], the effect of frequency offset on asynchronous MC-CDMA systems in correlated Rayleigh fading channel was studied, however, the approach needed complicated multi-dimensional integration when computing the BER performance.

To the author’s best knowledge, there are no closed form expressions available to compute the BER performance of asynchronous STBC MC-CDMA systems in the presence of carrier frequency offset over frequency selective fading channels. Many of methods to obtain the BER performance over such channels in the literature always need complicated multi-dimensional integrations.

1.4.2 Multirate Access Schemes

The future wireless communication systems are required to support various multimedia application services. And the multimedia services entail variable data rates and may have different Quality of Service (QoS) requirements. Future system should thus support flexible QoS for these multirate services. There were many works in the literature investigating the performance and capacity of multirate direct sequence code division multiple access (DS-CDMA) systems [68]-[70]. To be accommodated with the multirate information sources, different access schemes were employed under DS-CDMA scenario: (i) multicode (mc) [68], (ii) variable spreading gain (VSG)[68], and (iii) multiple chip rate (MCR) access schemes [69][70]. However, only a few publications were related to the system performance and capacity of multirate MC-CDMA systems [72]. The performance of multicode and VSG schemes for asynchronous MC-DS/CDMA system was studied in [71]. The performance of multicode schemes for quasi-synchronous generalized MC-CDMA system was studied in [72]. Although multirate STBC MC-CDMA systems was considered in [67], only VSG access scheme was studied. To the author’s best knowledge, MCR multiple access scheme (in MC-CDMA, named as MSR) has not been considered for multicarrier systems, and there are also no attempt to study the comparisons of performance and capacity of all possible multirate access schemes (multicode, VSG and MSR access schemes) for STBC MC-CDMA systems.

1.4.3 Timing and Frequency Synchronization

In this part of research, some important issues related to the receiver design and implementations which have not been fully researched on will be investigated. Firstly, the joint timing and frequency synchronization scheme for STBC MC-CDMA systems is studied.

Since MC-CDMA is basically multicarrier transmission, it is very vulnerable to the synchronization errors, i.e. timing error at the receiver and carrier frequency offset [73][74]. Symbol timing synchronization is to find the correct starting position of fast

Fourier transform (FFT) window while frequency synchronization is to compensate the frequency offset due to the mismatch in frequencies between the local oscillators in the transmitter and receiver. Timing error results in the rotation of the subcarrier constellation, whilst frequency offset causes the loss of subcarrier orthogonality and results in ICI – both will severely degrade the system performance [73][74].

The timing and frequency synchronization in OFDM systems has been studied in the literature [78][79], however, these methods cannot be directly applied to MC-CDMA systems due to the presence of multiuser interference (MUI). There are also some approaches proposed to perform code synchronization in CDMA systems [80][81]. These approaches cannot be directly used in MC-CDMA systems since the use of multicarrier modulation is vulnerability to frequency offset. In the literature, some schemes have been proposed to recover the timing and frequency offset for MC-CDMA systems [82]-[88]. However, in [82][83], only timing synchronization was studied and zero frequency offset was assumed. Conversely, in some of the studies [84][85], only frequency offset was estimated and perfect timing synchronization was assumed. Joint timing and frequency synchronization were studied in [86]-[88]. But only downlink synchronous transmission was considered in [86] and only single user uplink asynchronous transmission was investigated in [87][88].

To the author’s best knowledge, there is still no attempt to investigate the joint timing and frequency synchronization for asynchronous MC-CDMA or STBC MC-CDMA in multiuser scenario.

1.4.4 Channel Estimation and Multiuser Detection

After all mobile users have adapted to the base station’s receiver clock and oscillator by adjusting their own oscillators’ frequency and scheduling their transmission time according to the time and frequency offset information obtained through control channel, the signals of all the users arrive at the base station aligned in time and frequency. The channel estimation and multiuser detection will be performed to recover the data from all the mobile users.

To facilitate coherent detection, channel state information (CSI) is required – this is difficult especially for the frequency dispersive fading channels in the multiuser environment and multiple-input and multiple-output (MIMO) system. In practice, CSI is obtained through channel estimation. The conventional methods used are training and blind estimation. When training method is used, the number of training symbols required increases proportionally with the number of transmit/ receive antennas and the number of users. This can cause a substantial decrease in the system throughput. On the other hand, blind detection methods [91]-[94] (such as subspace-based algorithm) do not require training data but suffer from other limitations such as scalar ambiguity, hence restrict its usefulness in some applications. This is due to that when using the second order statistics, the channel impulse response can be only estimated up to a complex constant, which represents the phase ambiguity in coherent detection system.

Semi-blind channel estimation is then adopted to overcome this limitation [95][96][97][98]. This method allows a significant reduction in the number of training symbols and reduces the bit error rate (BER) in severe reception conditions. In this thesis, the subspace-based semi-blind channel estimation is studied in uplink STBC MC-CDMA systems over frequency selective channels. The work here is the extension of our previous research in [95]. We investigate the channel identifiablity of semi-blind channel estimation, present more accurate perturbation analysis of channel estimation error and also calculate the Cramér-Rao bound (CRB) of channel estimation.

There were no attempts in the literature to study the semi-blind techniques in MC-CDMA system as well as STBC MC-CDMA for the multiuser scenario. And there were no analysis about the theoretical error of channel estimation and the effect of channel estimation error on system performance of STBC MC-CDMA systems for the semi-blind techniques as well.

1.5 Contributions

In Chapter 3, the effect of carrier frequency offset (CFO) on the system capacity and performance for the STBC MC-CDMA systems in frequency selective Rayleigh fading channels is first studied. A method for applying equal gain combining (EGC) technique and an approximate approach for applying maximum ratio combining (MRC) technique at the receiver were presented. In both cases, the BER expressions obtained were verified through computer simulations. Using these BER expressions, system capacities for both EGC and MRC receiver in the presence of CFO were studied. Although independent channel characteristics between neighboring subcarriers were assumed in the analysis, the theoretical analysis could be a good approximation to the practical correlated channels whose correlation coefficients among subcarriers are small, i.e. the correlation coefficient between neighboring subcarriers was less than 0.5, and could be a good lower bound when the neighboring subcarriers had large correlation coefficients [100]. Through theoretical analysis and computer simulation, the thesis gives a clear range of allowed CFO in which it would have only a slight effect on system capacity and performance. It is very important to keep the CFO within this range when doing receiver design.

In Chapter 4, the thesis studied the three possible multirate access schemes for STBC MC-CDMA systems. One of them is the multicode access scheme, where each high rate user is divided into multiple low rate parallel substreams and each is assigned different codes for spreading. The second is variable spreading gain (VSG) access scheme, where each user is assigned one periodic code sequence with its code length determined by its data rate. In these two access schemes, symbol rates at each subcarrier for different service classes remain the same. The third is multiple-symbol-rate (MSR) scheme, which is similar as multiple-chip-rate (MCR) scheme in DS-CDMA, where each user is assigned with one code sequence with symbol rate determined by its data rate. In MSR scheme, symbol rates at each subcarrier for different service classes are different, and there are three possible spectrum configurations for MSR access scheme. In these multirate access schemes for STBC MC-CDMA systems, an adaptive power control was proposed to maintain the link quality and improve the system capacity. The multiple access interferences and hence the system performance and capacity of these three multirate access schemes for asynchronous multirate STBC MC-CDMA systems are obtained. And the thesis presents the clear comparisons among these three schemes.

In Chapter 5, a joint blind multiuser timing and frequency synchronization scheme for asynchronous STBC MC-CDMA systems over frequency selective fading channels is proposed. Through properly choosing the oversampling factor and the number of received samples, the joint timing and frequency synchronization are resolved using the subspace approach. The proposed subspace based algorithm is derived by taking all users and all transmitters into consideration, and then the algorithm transforms the joint multiuser and multiple input multiple output (MIMO) synchronization problem into a set of single user and single input single output (SISO) timing and frequency synchronization problems. Each single user and single input problem is then reduced and generalized as a one-dimensional unconstrained optimization, and solved using the numerical iterative algorithm, such as Newton approach. Simulation results show the robustness and effectiveness of the proposed synchronization algorithm in the presence of noises, near far problem, multipath fading and Doppler Effect. Performance of the proposed algorithm is studied using the small perturbation analysis and is verified by computer simulations. The efficiency of the proposed algorithm is demonstrated by comparing its performance with the Cramér-Rao bound (CRB) being derived in the paper.

Finally, in Chapter 6, the subspace-based semi-blind channel estimation is studied in uplink STBC MC-CDMA systems over frequency selective channels. We assume perfect timing and frequency synchronization at the receiver of base station, and the signals from different users are synchronized at the receiver. In the uplink context, we have to simultaneously estimate the multipath channels corresponding to the different links between the different mobile users and base station. It is a $K \times I \times J$ -dimension estimation problem if there are K active users, each having I transmit antennas and J receiver antennas. Again, subspace-based technique decouples this multiuser channel estimation to a series of single user and single-input single output (SISO) estimation problems. To resolve the inherent scalar ambiguity existing in all the second-order statistic blind estimation, a training symbol is introduced to obtain this scalar. To access the performance of the proposed subspace-based semi-blind channel estimation technique, we quantify its resilience to the additive noise. Using the subspace perturbation result in [101], we develop a first-order analysis of the channel estimation covariance matrix in a closed form. As a benchmark to measure the relative accuracy of the proposed channel estimation algorithm, a closed-form expression for the Cramér-Rao bound (CRB) is derived in the thesis by assuming the unknown transmitted symbols as the deterministic or nuisance parameters and independent additive Gaussian white noise (AWGN). We prove that the estimation approach is statistically efficient at the practical SNR values. Finally linear zero-forcing (ZF) and minimum mean squared error (MMSE) detectors are constructed to recover the data of the different users using the estimated channel parameters.

1.6 Outline

The work of the thesis provides the efficient theoretical analysis model and implementation solutions in the practical system design for the STBC MC-CDMA systems which has emerged as a good candidate for the next generation of wireless communication systems.

Chapter 2 presents the literature reviews for the STBC MC-CDMA systems. Chapter 3 provides the theoretical BER performance and bandwidth efficiency system capacity analysis for STBC MC-CDMA systems in the presence of the carrier frequency offset. In Chapter 4, the system capacity comparisons among three multirate access schemes (multicode, VSG, MSR) for STBC MC-CDMA systems are present. Chapter 5 proposes a subspace-based blind joint timing and frequency synchronization for STBC MC-CDMA systems. In Chapter 6, subspace-based semi-blind channel estimation and multiuser detection are proposed. The motivation and detail summary of the work can be found in respective subsection in Chapter 1.4 and 1.5.

Some of the commonly used notations in this thesis are as follows. Matrices are shown in upper case bold while column vectors are shown in lower case bold with an underscore. $(\cdot)^T$, $(\cdot)^{\mathcal{H}}$, $(\cdot)^*$ and $(\cdot)^\dagger$ are used to denote the transpose, Hermitian, conjugate and pseudo-inverse of the matrix, respectively. $\mathcal{D}(\cdot)$ is the diagonalization operation converting a vector to diagonal matrix. $vec(\cdot)$ is the vectorization operator that turns a matrix into a vector by stacking the column of the matrix one below another and $\otimes$ denotes the Kronecker product. $\|\cdot\|^2$ denotes the vector norm. For a given matrix, $\mathbf{M}[a,b]$ denotes the (a,b)th element of the matrix. The notation $\mathbf{M}(\cdot)$, $f(\cdot)$ is to indicate that it is a function of the random variables (or vectors) given in the bracket. The subscripts k, i, j and g are used to refer the user, transmitter, receiver and multipath of the channels under consideration, respectively. The notation I and J is to represent the number of transmit antennas and receiver antennas, respectively.

Chapter 2

Fundamentals of Multicarrier CDMA and Space-Time Coding

Future wireless radio systems are required to transport multimedia traffic at much higher bit rates and this motivates the communications research community to work on the possible technologies and system configurations for next generation of cellular mobile communication system. As mentioned in Chapter 1, multicarrier CDMA and space-time coding are the powerful potential candidates to fulfill the requirement of next generation high-speed wireless multimedia communication systems.

Since the mutlicarrier CDMA techniques rely on the combination of CDMA and OFDM, these two techniques will be reviewed briefly in this chapter. The concept of multicarrier CDMA will be presented next, followed by the fundamentals on space-time coding.

2.1 Combining DS-CDMA and OFDM

2.1.1 DS-CDMA

Direct-sequence (DS-) CDMA is a spread spectrum communication technique. DS-CDMA systems [29] are capable of supporting multiple users transmission in the same bandwidth by assigning different orthogonal codes to different users, in order to distinguish their signals from each other at the receiver. Spread spectrum techniques were developed originally for military applications [30].

In spread spectrum system, the original information signal is spread over a wide frequency band, much wider than the minimum bandwidth required to transmit the information. In general, the idea behind spread spectrum system is the information signal having a bandwidth B_s is spread into a signal having bandwidth B, where $B >> B_s$. The spreading gain is defined as

$$L = \frac{B}{B_s} \tag{2.1}$$

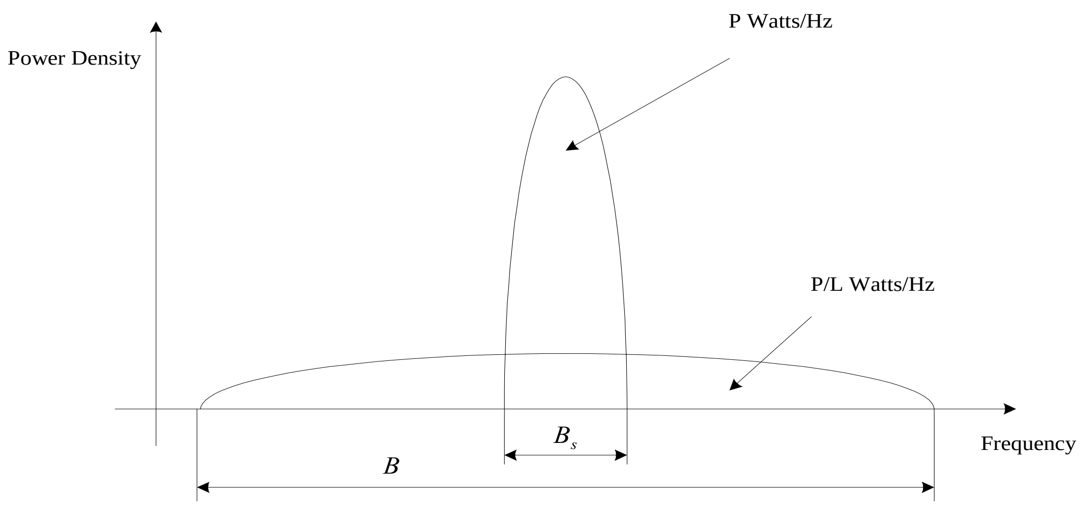

Fig. 2.1 Power spectral density of signal before and after spreading

The frequency domain spreading concept is illustrated in Fig. 2.1. The power of the transmitted spread spectrum signal is spread over L times of the original bandwidth, while its spectral density is correspondingly reduced by the same amount. The higher the spreading gain, the lower the power spectral density (PSD) of the transmitted signal. If the spreading gain is very large, the transmitted signal exhibits the PSD of a noise.

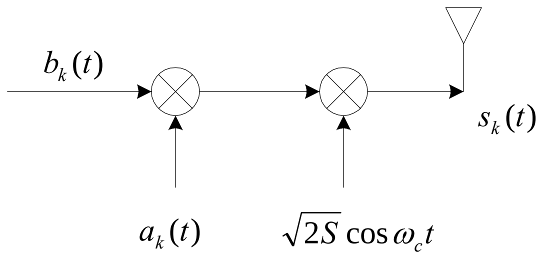

Fig. 2.2 BPSK modulated DS spread spectrum transmitter

The block diagram of a typical binary phase shift keying (BPSK) modulated DS-SS transmitter is shown in Fig. 2.2. We will now express the associated signals mathematically. The binary data signal of kth user may be written as:

$$b_k(t) = \sum_{j=-\infty}^{j=\infty} b_{k,j}\, p_{T_b}(t - jT_b) \tag{2.2}$$

where T_b is the bit duration, $b_{k,j} \in \{+1,-1\}$ denotes the jth data bit, $k = 0,1,\cdots,K-1$, K is the total number of active users, and $p_{T_b}(t)$ is the pulse shape of the data bit. In practical applications, $p_{T_b}(t)$ is a bandlimited waveform, such as a raised cosine Nyquist pulse. However, for analysis and simulation simplicity, we will assume that $p_{T_b}(t)$ is a rectangular pulse throughout this chapter, which is defined as:

$$p_\tau(t) = \begin{cases} 1, & 0 \le t < \tau \\ 0, & otherwise \end{cases}. \tag{2.3}$$

Similarly, the spreading sequence with the length L for kth user may be written as

$$a_k(t) = \sum_{l=0}^{l=L-1} a_{k,l} p_{T_c}(t - lT_c) \tag{2.4}$$

where $a_{k,l} \in \{+1,-1\}$ denotes the lth chip and $p_{T_c}(t)$ is the chip-pulse with a chip duration of T_c. The proper choice of spreading sequence is a crucial problem in DS-CDMA, since the multiple access interference (MAI) strongly depends on the cross-correlation function (CCF) of the used spreading sequences. To minimize the MAI, the CCF values should be as small as possible. In order to guarantee equal interference among all transmitting users, the cross-correlation properties between different pairs of spreading sequences should be similar. Moreover, the auto-correlation function (ACF) of the spreading sequence should have low out-of phase peak magnitudes in order to achieve a reliable synchronization.

As shown in Fig. 2.2, the data signal and spreading sequence are multiplied, and the resultant baseband spread signal $s_k(t)$ for kth user is given by

$$s_k(t) = b_k(t)a_k(t)\,. \tag{2.5}$$

At the intended receiver, the signal is multiplied by the conjugate of the transmitter's spreading sequence, which is known as dispreading sequence, in order to retrieve the information. Ideally, in a single-user, nonfading, noiseless environment, the original information can be decoded without errors.

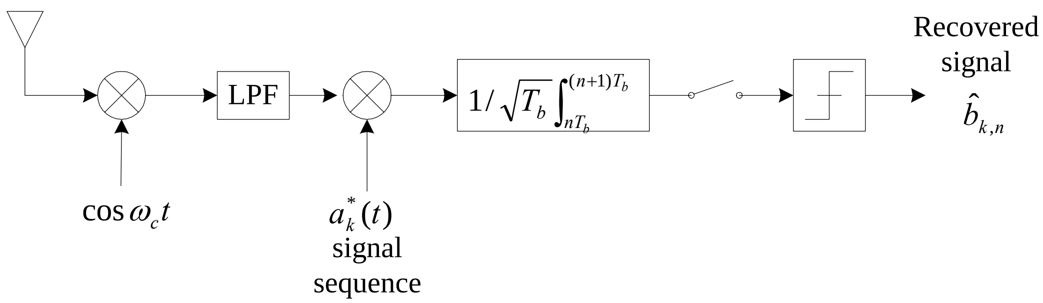

Fig. 2.3 BPSK DS spread spectrum receiver for AWGN channel

In reality, however, the channel conditions are never so perfect. The received signal will be corrupted by noise, interfered by both multipath fading and the existence of other users. Of course it's possible to reduce the interference due to multipath fading and MUI, and it will not be discussed in this chapter.

Fig. 2.3 shows the diagram of the receiver for a noise-corrupted channel using a correlator for detecting the transmitted signal, yielding

$$\begin{aligned}\hat{b}_{k,n} &= \operatorname{sgn}\left\{\frac{1}{\sqrt{T_b}}\int_{nT_b}^{(n+1)T_b} a_k^*(t)\left(\sum_{m=0}^{K-1} a_m(t)b_m(t)+\eta(t)\right)\right\} \\ &= \operatorname{sgn}\left\{b_{k,n}+\frac{1}{\sqrt{T_b}}\int_{nT_b}^{(n+1)T_b} a_k^*(t)\sum_{m=0,m\neq k}^{K-1} a_m(t)b_m(t)+\frac{1}{\sqrt{T_b}}\int_{nT_b}^{(n+1)T_b} a_k^*(t)\eta(t)\right\}, \qquad (2.6)\end{aligned}$$

if the downlink transmission is considered. The first term is the desired signal, the second term is known as MUI, and the third term is known as noise interference.

DS-CDMA has numerous inherent advantages that are derived from the spectral spreading. These advantages, to name a few, include: improved capacity, narrow-band interference rejection, ISI rejection and higher privacy, etc. While in the hostile mobile communications channel, frequency selective multipath fading causes severe degradation in a CDMA system. As mentioned in [61], multipath propagation causes ISI in the DS- CDMA system and severe ISI in high data rate systems if the channel delay spread exceeds the symbol duration. Due to the severe ISI and the difficulty in synchronization, conventional CDMA has been designed only for low- or medium-bit-rate transmission. OFDM is the technique prompted to solve this problem.

2.1.2 OFDM

The principle of multicarrier transmission is to convert a serial high-rate data stream onto multiple parallel low-rate substreams. Each substream is modulated on one subcarrier. Since the symbol rate on each subcarrier is much less than the initial serial data symbol rate, the effect of ISI significantly decreases, and hence reduces the complexity of the equalizer. Orthogonal frequency division multiplexing (OFDM) is a specific form of multicarrier modulation technique [16] [34]-[36],[54][55].

An important design goal for multicarrier transmission scheme is that the channel can be considered as time-invariant during one OFDM symbol and that fading of each subcarrier can be considered as flat. Thus, the OFDM symbol duration should be smaller than the coherent time of the channel and the subcarrier spacing should be smaller than the coherent bandwidth of the channel. By fulfilling these conditions, the realization of low-complex receivers is possible.

The OFDM communication system transmits N complex-valued source symbols b_n, $n = 0,1,\cdots,N-1$, in parallel on N subcarriers. The source symbols, for instance, be obtained after source and channel coding, interleaving and symbol mapping. The source symbol duration T_b of the serial data symbols results after serial-to-parallel (S/P) conversion in the OFDM symbol duration $T_s = NT_b$. The principle of OFDM is to modulate the N substreams on subcarriers with a spacing $1/T_s$. The complex baseband equivalent OFDM signals with rectangular pulse shaping can be represented as

$$s(t) = \sum_{n=0}^{N-1} b_n e^{j2\pi \frac{n}{T_s} t} . \tag{2.7}$$

At the receiver, the received signal is multiplied by $e^{-j2\pi \frac{n}{T_s} t}$ and integrated over a symbol duration in order to recover b_n. The resultant signal becomes, assuming perfect carrier frequency and symbol time synchronization over the idea channel:

$$\frac{1}{T_s}\int_0^{T_s} s(t)e^{-j2\pi\frac{n}{T_s}t}dt = \frac{1}{T_s}\sum_{k=0}^{N-1} b_k \int_0^{T_s} e^{-j2\pi\frac{k}{T_s}t} e^{-j2\pi\frac{n}{T_s}t} dt = b_n . \tag{2.8}$$

In order to implement directly the transmitter and the receiver of an OFDM system, N oscillators are required.

Weinstein and Ebert [14] presented a method involving the discrete Fourier Transform (DFT) to perform baseband modulation and demodulation, which spurred the development of OFDM systems with the advent of efficient real-time digital signal processing (DSP) technology. By sampling the modulated signal N times during a OFDM symbol at instants of $t = \frac{m}{N}T_s$, (2.7) becomes:

$$s(\frac{m}{N}T_s) = \sum_{n=0}^{N-1} b_n e^{j2\pi\frac{nm}{N}} , \quad m = 0,1,\cdots,N-1 \tag{2.9}$$

Since $s(\frac{m}{N}T_s)$ depends only on m, it can be represented as s_m in discrete form, and (2.9) can also be written as:

$$s_m = N \cdot \mathrm{IDFT}(\{b_n\}),\ m = 0,1,\cdots,N-1 , \tag{2.10}$$

where IDFT represents the inverse discrete Fourier transform operator. The efficient implementation of IDFT is the inverse fast Fourier transform (IFFT). The overall block diagram of OFDM transmission system is shown in Fig. 2.4.

The N message sequence b_0, b_1, $\cdots$, b_{N-1}, form a frame, which is converted into a parallel form, where b_n is modulated at nth subcarrier. The IFFT module takes the parallel data and calculates N sampled time domain signals, s_0, s_1, $\cdots$, s_{N-1}. The IFFT eliminates the use of N oscillators and renders the OFDM transmitter implementationally attractive.

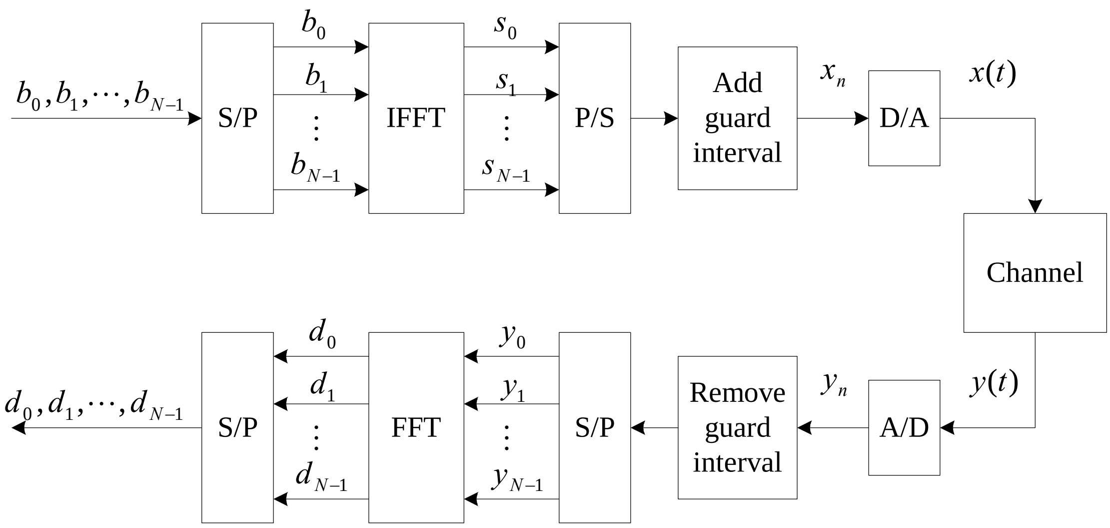

Fig. 2.4 OFDM transmission system

When the number of subcarriers increases, the OFDM symbol duration T_s becomes large compared to the duration of the impulse response time delay spread τ_m of the channel, and the amount of ISI reduces. However, to completely avoid the effects of ISI and, thus, to maintain the orthogonality between the signals on the subcarriers, i.e., to also avoid the inter-channel interference (ICI), a guard interval of $T_g \geq \tau_m$ has to be inserted between the adjacent OFDM symbols. The guard interval is the cyclic extension of each OFDM symbol which is obtained by extending the duration of an OFDM symbol to $T_s' = T_s + T_g$. The discrete length of guard interval has to be

$$L_g \geq \left\lceil \frac{\tau_m N}{T_s} \right\rceil \tag{2.11}$$

samples in order to prevent ISI. The sampled sequence with cyclic extended guard interval results in

$$x_m = \sum_{n=0}^{N-1} b_n e^{j2\pi \frac{nm}{N}}, \quad m = -L_g, \cdots, 0, 1, \cdots, N-1 \tag{2.12}$$

This sequence is passed through a digital-to-analog (D/A) converter whose output ideally would be the signal waveform $x(t)$ with increased duration T_s'. The signal is up-converted and the RF signal is transmitted to the channel. The output of the channel, after RF down conversion, is received signal waveform $y(t)$ obtained from the convolution of $x(t)$ and the channel impulse response $h(\tau,t)$ and additive noise $\eta(t)$, i.e.,

$$y(t)=\int_{-\infty}^{\infty}x(t-\tau)h(\tau,t)d\tau+\eta(t). \tag{2.13}$$

The received signal $y(t)$ is passed through an analog-to-digital (A/D) converter, whose output sequence y_n, $n=-L_g,\cdots,0,1,\cdots,N-1$, is the samples of $y(t)$ sampled at rate $1/T_b$. Since ISI is only presented in the first L_g samples of the received sequence, these L_g samples are removed before multicarrier demodulation. Then the ISI-free part $n=0,1,\cdots,N-1$ of y_n is multicarrier demodulated by FFT. The output of the FFT is the multicarrier demodulated sequence d_n, $n=0,1,\cdots,N-1$, consisting of N complex-valued samples

$$d_n=\sum_{m=0}^{N-1}y_m e^{-j2\pi\frac{nm}{N}}, \quad n=0,1,\cdots,N-1 \quad . \tag{2.14}$$

Since ICI can be avoided due to the guard interval, each subcarrier can be considered separately. Furthermore, when assuming that the fading on each subcarrier is flat and ISI is removed, a received sample d_n is obtained from the frequency domain representation according to

$$d_n=H_n b_n+N_n,\ n=0,1,\cdots,N-1 \tag{2.15}$$

where H_n is the frequency response of nth subcarrier and N_n represents the noise in the nth subcarrier.

In summary, OFDM systems are attractive with advantages as: (1) High spectral efficiency due to nearly rectangular frequency spectrum; (2) Simple digital realization by using the FFT operation; (3) Low complex receivers due to the avoidance of ISI and ICI with a sufficiently long guard interval; (4) Different modulation schemes can be used on individual subcarriers which are adapted to the transmission conditions on each subcarriers.

2.2 Multicarrier CDMA Systems

In 1993, the first MC-CDMA system was proposed by N. Yee, J-P. Linnartz and G. Fettweis [22]. Shortly after that, the MC-DS-CDMA was proposed by V. DaSilva and E. S. Sousa [18] and the MT-CDMA by Vandendorpe [37]. Although there are other versions of the MC-CDMA system, these three systems are the foundation for which other MC-CDMA systems are built. A systematic overview of MC-CDMA systems was presented by S. Hara and R. Prasad in [24].

2.2.1 MC-CDMA

In MC-CDMA, instead of applying spreading sequences in the time domain, it applies them in the frequency domain, mapping a different chip of a spreading sequence to an OFDM subcarrier. Hence, each OFDM subcarrier has a data rate identical to the original input data rate and the multicarrier system absorbs the increased rate due to the spreading in a wider frequency band. The basic MC-CDMA signal is generated by a serial concatenation of classical DS-CDMA and OFDM. With MC-CDMA, the chips of a spread data symbol are transmitted in parallel on different subcarriers, in contrast to a serial transmission with DS-CDMA. The transmitted signal of the *k*th user $s_k(t)$ is written as [25]:

$$s_k(t) = \sum_{n=0}^{N-1} b_k c_{k,n} e^{j2\pi(f_0 + nf_d)t} \tag{2.16}$$

where *N* is the number of subcarriers, b_k is the source symbol of the *k*th user with the data duration T_b, $c_{k,n}$, $n = 0, \cdots, N-1$, represents the spreading sequence for *k*th user, f_0 is the lowest subcarrier frequency, f_d is subcarrier separation.

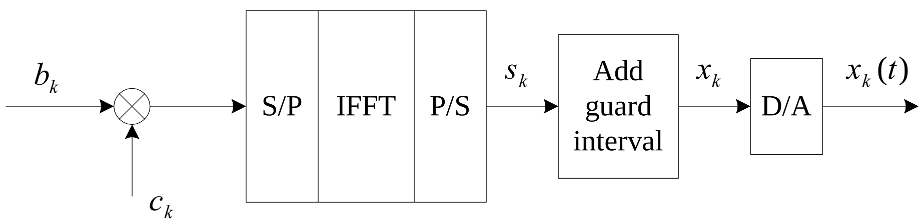

Fig. 2.5 Transmitter of MC-CDMA

If $1/T_b$ is used for f_d, the transmitted signal can be generated using the IFFT, as in the case of an OFDM system. The overall transmitter structure is implemented by concatenating a DS-CDMA spreader and an OFDM transmitter, as shown in Fig. 2.5. The rate of the serial data symbols is $1/T_b$. In the transmitter, the complex-valued data symbol b_k is spread in the time domain by the user specific spreading sequence $\underline{\mathbf{c}}_k = [c_{k,0}, \quad c_{k,1}, \quad \cdots \quad c_{k,L-1}]^T$ with the spreading gain equal to the number of subcarriers, i.e., $L = N$. The chip rate of the serial spreading sequence $\mathbf{c}_k$ before S/P conversion is $\frac{1}{T_c} = \frac{N}{T_b}$, and it is *N* times higher than the data symbol rate $1/T_b$. In this implementation, high speed operations are required at the output of the spreader in order to carry out the chip-related operations. The spread chips are fed into the S/P block and IFFT is applied to these N parallel chips. With multicarrier spread spectrum, each data symbol is spread over N subcarriers. The OFDM symbol duration with multicarrier spread spectrum including a guard interval results in

$$T_s' = T_g + NT_c \,. \tag{2.17}$$

In this case one data symbol per user is transmitted in one OFDM symbol. This OFDM symbol is passed through a digital-to-analog (D/A) converter whose output ideally would be the signal waveform $x(t)$ with increased duration T_s'. The signal is up-converted and the RF signal is transmitted to the channel.

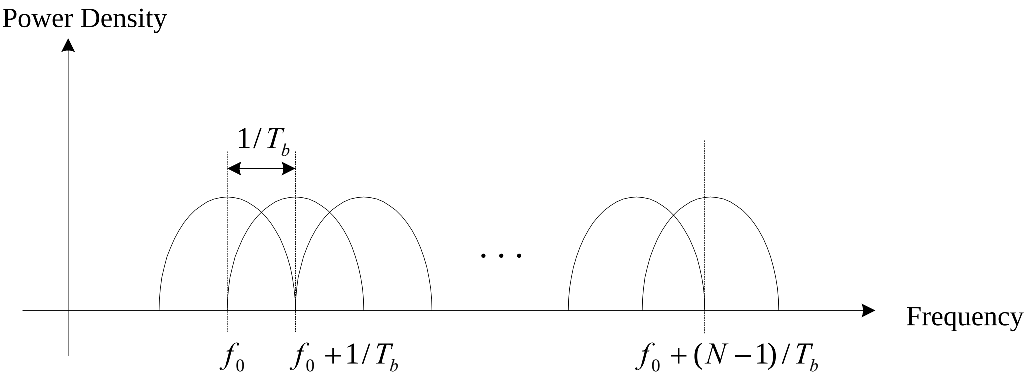

Fig. 2.6 Power spectrum of MC-CDMA

The power spectrum of the MC-CDMA signal is shown in Fig. 2.6. Assume the rectangular pulse shape, the required bandwidth for this MC-CDMA scheme is $(N+1)/T_b$.

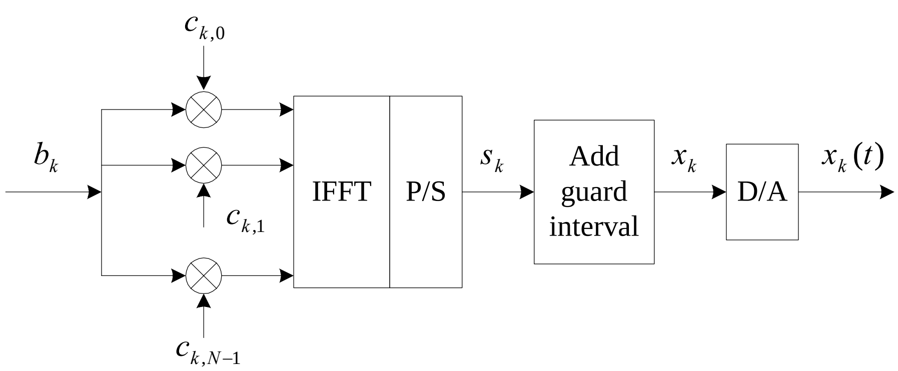

Fig. 2.7 Alternative transmitter of MC-CDMA

Fig. 2.7 shows an alternative implementation of MC-CDMA, which removes the time domain spreader. In this implementation, the spreading sequence is applied directly to the identical parallel bits. Hence, the high speed spreading operation is not required. And the spreading of the symbol is done in the frequency domain before modulating to the carrier frequencies.

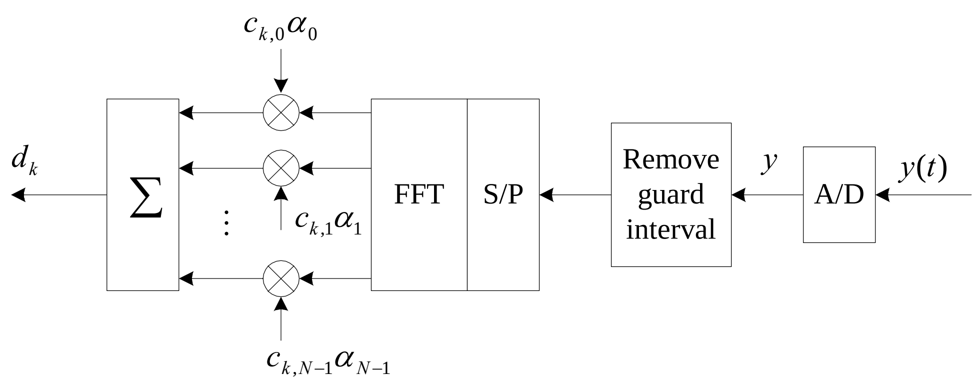

Fig. 2.8 Receiver of MC-CDMA

At the MC-CDMA receiver shown in Fig. 2.8 each subcarrier's symbol, i.e. the corresponding chip $c_{k,n}$ of user k at nth subcarrier, is recovered using FFT after sampling at a rate of $1/T_c$ and the recovered chip sequence is correlated with the desired user's spreading code in order to recover the original information b_k. Let us define the received sample at the nth subcarrier as

$$y_n = \sum_{m=0}^{K-1} H_n b_m c_{m,n} + \eta_n \tag{2.18}$$

where K is the number of active users, H_n is the frequency channel response at nth subcarrier and η_n is the corresponding noise samples. The MC-CDMA receiver of the kth user multiplies y_n in (2.18) by its spreading sequence $c_{k,n}$, as well as by the gain, α_n, which is given by the reciprocal of the estimated channel transfer factor of subcarrier n, for each received subcarrier symbol $n = 0,1,\cdots,N-1$, and sum all these products, in order to arrive at the decision variable d_k, which is given by

$$d_k = \sum_{n=0}^{N-1} c_{k,n} \alpha_n y_n \tag{2.19}$$

2.2.2 MC-DS-CDMA

This scheme is the combination of time domain spreading and multicarrier modulation, originally proposed in [18]. MC-DS-CDMA signal is generated by S/P converting data symbols into N substreams followed by DS-CDMA spreading on each individual substream. Thus with MC-DS-CDMA, each data symbol is spread within its subcarrier bandwidth ($N > 1$), but in contrast to MC-CDMA or DS-CDMA not over the whole transmission bandwidth. A MC-DS-CDMA system with one subcarrier is identical to a single-carrier DS-CDMA system. MC-DS-CDMA systems can be distinguished in systems where the subcarriers are narrowband and the fading over each subcarrier appears flat and in systems with broadband subcarrier where the fading is frequency selective over each subcarrier. The fading over the whole transmission bandwidth can be frequency selective in both cases. The complexity of the receiver with flat fading per subcarrier is comparable to that of MC-CDMA receiver, when OFDM is assumed for multicarrier modulation. As long as the fading in each subcarrier is frequency selective, ISI occurs and more complex detectors have to be applied.

Fig. 2.9 shows the block diagram of the transmitter for MC-DS-CDMA. The data symbol rate is $1/T_b$. A sequence of N complex-valued data symbols $b_{k,n}$, $n = 0,\cdots,N-1$, of kth user is S/P converted into N substreams. The data symbol rate on each substream becomes $1/NT_b$. Within each single substream, a data symbol is spread in the time domain with the user specific spreading code

$$c_k(t) = \sum_{l=0}^{L-1} c_{k,l} p_{T_c}(t - lT_s) \tag{2.20}$$

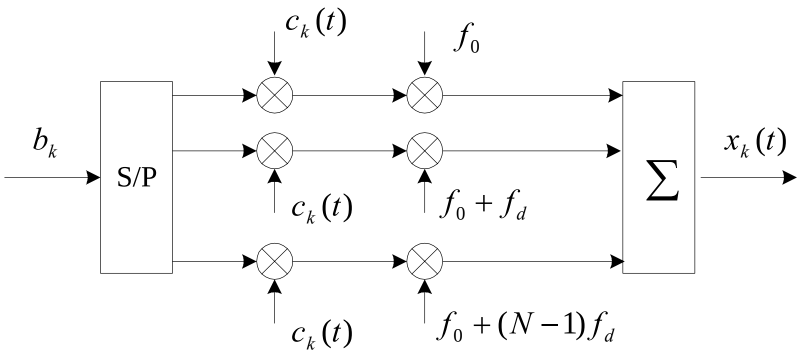

Fig. 2.9 Transmitter of MC-DS-CDMA

with spreading gain L. The pulse form of the chips is given by $p_{T_c}(t)$. The duration of a chip with a substream is

$$T_c = T_s = \frac{NT_b}{L}. \tag{2.21}$$

The complex-valued sequence obtained after spreading is given by

$$x_k(t) = \sum_{n=0}^{N-1} b_{k,n} c_k(t) e^{j2\pi(f_0 + (N-1)f_d)}, \quad 0 \le t < LT_s \tag{2.22}$$

where f_0 is the lowest subcarrier frequency, f_d is the subcarrier spacing. If $f_d = 1/T_s$, the transmitted signal can be generated using the IFFT, as in the case of OFDM system. However, OFDM might not necessarily be the choice in the asynchronous uplink transmission since the MC-DS-CDMA with broadband subcarrier has the lower PAPR than the MC-DS-CDMA system with narrowband subcarrier when using OFDM. However, the spectral efficiency of the system decreases.

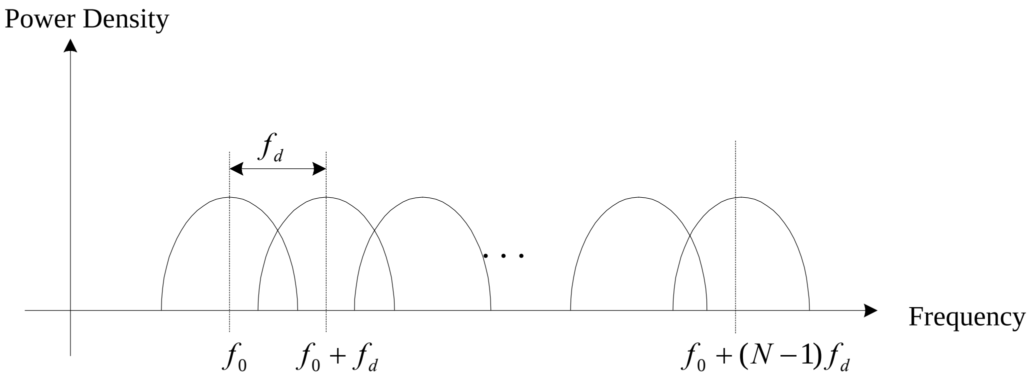

Fig. 2.10 Power spectrum of MC-DS-CDMA

Fig. 2.10 shows the typical power spectrum of the MC-DS-CDMA signal using the schematic shown in Fig. 2.9. If $f_d = 1/T_s$ and $L = N$, the MC-DS-CDMA spectrum has the same shape of a MC-CDMA system.

It is important to note that each symbol in the MC-DS-CDMA is spread in time by the same spreading sequence per subcarrier while in the MC-CDMA, each symbol is spread by a spreading sequence in frequency but one chip per subcarrier.

2.2.3 Multi-tone (MT-) CDMA

MT-CDMA is similar to the MC-DS-CDMA with the incoming bit stream divided into N different bit streams, after which the spreading of each stream is done in time domain with a long spreading sequence aimed at maintaining a constant bandwidth for each of the subcarriers. The ratio of the length of spreading codes, r, to the number of sub-carriers is kept at a constant. The relationship is $r/N = L$, where L has been denoted previously as the spreading gain of the MC-CDMA and MC-DS-CDMA system.

The MT-CDMA transmitter has the same structure as that of MC-DS-CDMA. The only difference from MC-DS-CDMA is that the spectrum of each subcarrier prior to the spreading operation satisfies the orthogonal condition, while subsequently loses the orthogonal quality after spreading. This is achieved by separating the subcarrier frequency with $1/NT_b$ and keeping the chip duration as $NT_b/r = T_b/L$, where r is the spreading gain of the MT-CDMA system. Note that in MC-DS-CDMA system, the chip duration is T_bN/L and the separation of the subcarrier is L/T_bN. Loss of orthogonality after spreading results in ICI. In the frequency domain, the bandwidth of each subcarrier after spreading is larger than the coherence bandwidth of the channel, therefore, with a high spreading gain, each subcarrier will experience frequency selective fading. The frequency domain power spectrum is shown in Fig. 2.11.

The transmitter design is performed using the same data mapping and spreading (in time) as in the MC-DS-CDMA except that longer codes are used to spread each subcarrier signal such that it experiences frequency selective fading. Therefore, a Rake receiver or other multiuser detector must be used at the receiver. It is important to note that because the adjacent carriers are separated by $1/NT_b$ the N modulators/demodulators in the transmitter/receiver can be implemented by the IFFT/FFT.

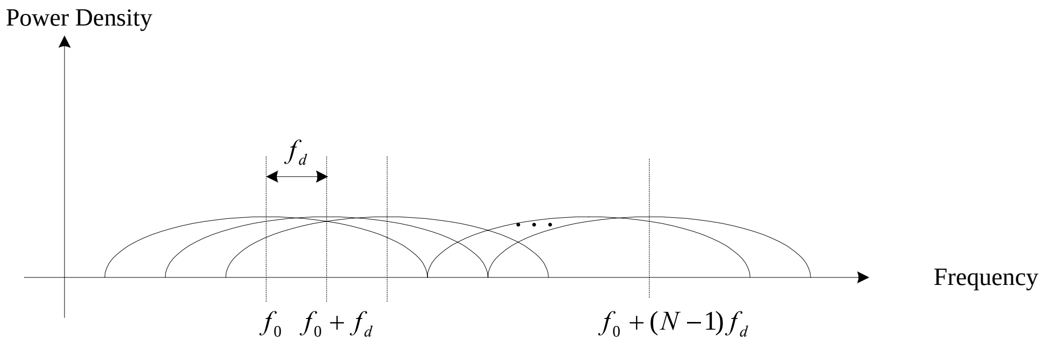

Fig. 2.11 Power spectrum of MT-CDMA

2.2.4 Systems Comparison

Table 2.2 briefly compares the advantages and disadvantages of three multicarrier CDMA systems.

The simulation in [24] compared the BER performance of MC-CDMA, MC-DS-CDMA, MT-CDMA, from which it is evident that the MC-CDMA scheme outperforms the other two multicarrier schemes in synchronous transmission.

Table 2.1 Comparison of advantages and disadvantages of three multicarrier CDMA systems

Scheme	Advantages	Disadvantages
MC-CDMA	▪ Performance is the best in the synchronous transmission ▪ Transmits multiple carrier per symbol, therefore diversity combining can be applied. ▪ Spreads the signal in frequency domain, the frequency diversity can be obtained.	▪ Sensitive to timing errors and frequency offsets
MC-DS-CDMA	▪ It needs fewer carriers and thus allows the spreading gain to be increased ▪ Robust to timing errors and frequency offsets.	▪ Performance is not as good as MC-CDMA
MT-CDMA	▪ Longer spreading codes result in a reduction in self-interference and multiple access interference as compared to those experienced in conventional CDMA system. ▪ Detection can be done non-coherently.	▪ The modulated signal experience ISI and ICI.

In asynchronous uplink channel, direct multicarrier transmission using OFDM operation without any pre-processing will lead to high PAPR. Thus multicarrier modulated system with OFDM operation are more sensitive to high power amplifier (HPA) non-linearity than single carrier modulated system [26], and lead to severe clipping effects. One of possible approach is to use MC-DS-CDMA with small number of subcarriers in asynchronous mode. The small number of subcarriers results in the possibility to use the broadband transmission instead of OFDM and this leads to lower PAPR. However, for this implementation of MC-DS-CDMA, each subcarrier experiences frequency selective fading instead of flat fading when a large number of sucarriers used, therefore much more complex RAKE receivers and multiuser detectors are needed. This results in the loss of the BER performance and system capacity. Another possible approach is to use pre-distortion technique or to properly select the spreading codes to reduce the influence of HPA non-linearity [27][28]. It can be shown in [27] that the total degradation for MC-CDMA with the pre-distortion is less than the DS-CDMA and MC-DS-CDMA without OFDM operation in the uplink channels. And with the appropriate selection of spreading codes, the degradation of MC-CDMA decreases greatly. Hence, the MC-CDMA system is also a choice for uplink channel with pre-distortion or appropriate selection of spreading codes.

Therefore, with the above advantages of MC-CDMA, the focus of our work is mainly on MC-CDMA system.

2.3 Space-Time Coding

Information theoretic studies have shown that spatial diversity provided by multiple transmit and receive antennas allows for a dramatic increase in the capacity and is an effective technique for combating fading in wireless communication systems [40][41]. Space-time coding (STC) systems, which integrate the techniques of antenna array spatial diversity and channel coding to combat the channel destructive multipaths and interference from other users, have been one of the key research focus over the last few years [42]-[48].

STC is a transmit diversity techniques with multiple transmit antennas, where the number of receiver antennas is not necessarily equal to the number of transmit antennas. The basic idea of STC is different from the BLAST [49][50]. Instead of transmitting independent data streams, the same data stream is transmitted in an appropriate manner over all antennas. This could be, for instance, a downlink mobile communication, where in the base station I transmit antennas are used while in the terminal mobile station either one or a few antennas can be applied.

The principle of STC is illustrated in Fig. 2.12. The basic idea is to provide through coding constructive superposition of the signals transmitted from different antennas. Constructive combining can be achieved for instance by modulation diversity, where orthogonal signals are used in different transmit antennas. The receiver uses the respective matched filters, where the contributions of all transmit antennas can be separated and combined with the diversity combining techniques, such as maximum ratio combining (MRC).

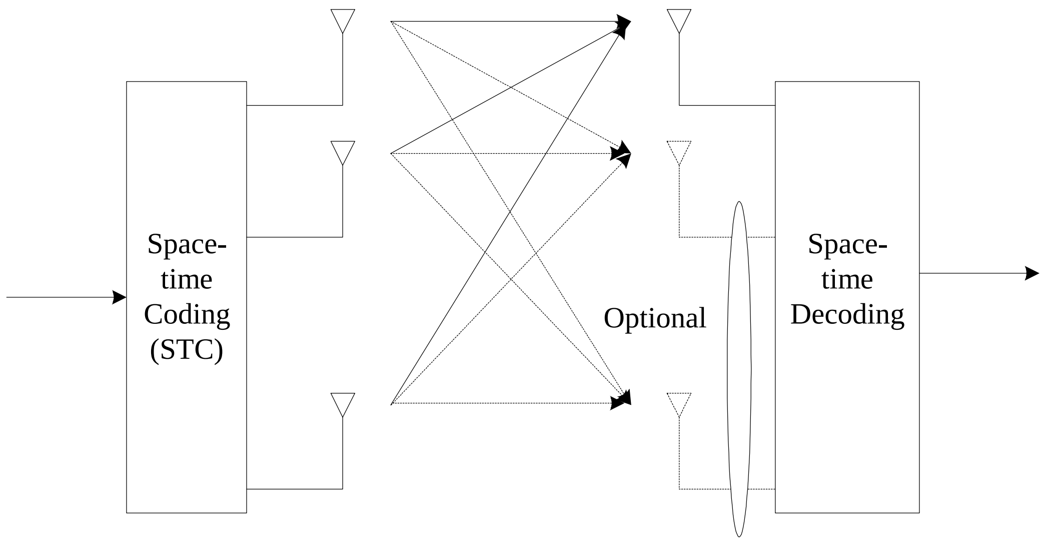

Fig. 2.12 General Principle of space-time coding (STC)

The first attempt to develop STC was presented in [38] and was inspired by the delay diversity scheme of Wittneben [39]. However, the key development of the STC concept was originally revealed in [43] in the form of trellis codes, which required a multi-dimensional Viterbi algorithm at the receiver for decoding. These codes were shown to provide a diversity benefit equal to product of the number of transmit antennas and receiver antennas, in addition to a coding gain that depends on the complexity of the code (i.e., number of states in the trellis) without any loss in bandwidth efficiency. Then, the popularity of STC really took off with the discovery of the so-called space-time block codes (STBC). This is due to the way of their coding construction. STBC can be decoded using simple linear processing at the receiver in contrast to the vector Viterbi decoding algorithms required for ST trellis codes (STTC). Although STBC codes give the same diversity gain as STTC for the same number of transmit and receiver antennas, they provide zero or minimal coding gain. Below, we will briefly summarize the basic concepts of STTC and STBC.

2.3.1 Space-Time Trellis Codes

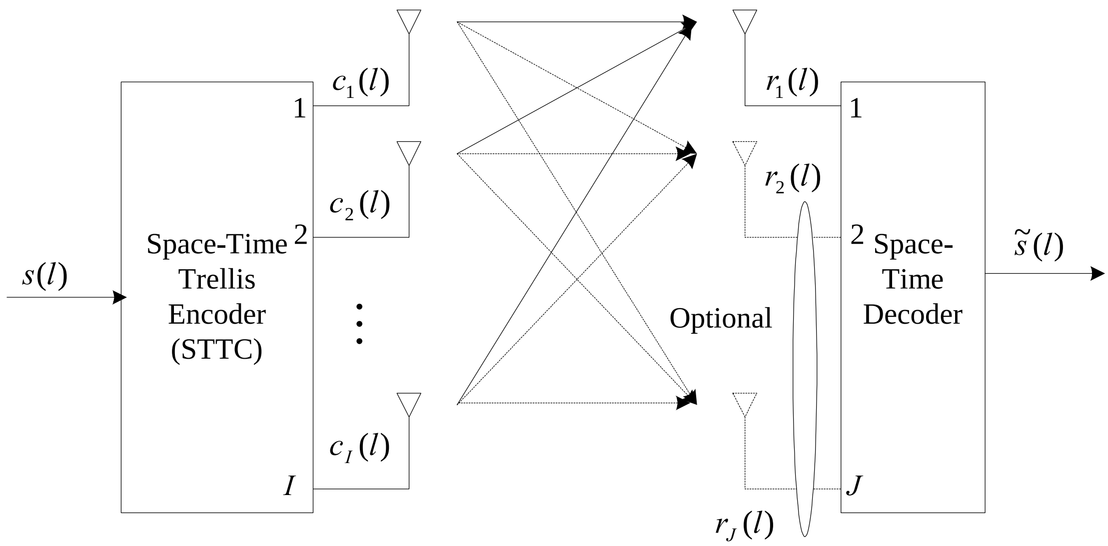

Fig. 2.13 Transceiver of space-time trellis code

Fig. 2.13 shows the diagram of the transceiver for STTCs. For every input symbol s_l, a space-time trellis encoder generates *I* code symbols $c_{l1}, c_{l2}, \cdots, c_{lI}$. These *I* code symbols are transmitted simultaneously from the *I* transmit antennas. We define the code vector $\underline{\mathbf{c}}_l = [c_{l1}, c_{l2}, \cdots, c_{lI}]^T$. Suppose that the *code vector* sequence

$$\mathbf{C} = \{\underline{\mathbf{c}}_1, \quad \underline{\mathbf{c}}_2, \quad \cdots, \quad \underline{\mathbf{c}}_L\}$$

is transmitted. We consider the probability that the decoder decides erroneously in favor of the legitimate code vector sequence

$$\tilde{\mathbf{C}} = \{\underline{\tilde{\mathbf{c}}}_1, \quad \underline{\tilde{\mathbf{c}}}_2, \quad \cdots, \quad \underline{\tilde{\mathbf{c}}}_L\}$$

Consider a frame or block of data of length *L* and define the $I \times I$ error matrix $\mathbf{A}$ as

$$\mathbf{A}(\mathbf{C}, \tilde{\mathbf{C}}) = \sum_{l=1}^{L} (\underline{\mathbf{c}}_l - \underline{\tilde{\mathbf{c}}}_l)(\underline{\mathbf{c}}_l - \underline{\tilde{\mathbf{c}}}_l)^{\mathcal{H}} . \tag{2.23}$$

If ideal channel state information (CSI) is available at the receiver, then it is possible to show the probability of transmitting $\mathbf{C}$ and defining in favor of $\tilde{\mathbf{C}}$ is upper bounded for a Rayleigh fading channel by [104]

$$P(\mathbf{C} \to \tilde{\mathbf{C}}) \leq \left(\prod_{i=1}^{r} \lambda_i \right)^{-J} \cdot (E_s / 4N_0)^{-rJ} \tag{2.24}$$

where E_s is the symbol energy and N_0 is the noise spectral density, *r* is the rank of the error matrix $\mathbf{A}$ and λ_i, $i = 1, 2, \cdots, r$ are the nonzero eigenvalues of the error matrix $\mathbf{A}$. We can easily see that the probability of error bound in (2.24) is similar to the probability of error bound for trellis coded modulation for fading channel, The term $g_r = \prod_{i=1}^{r} \lambda_i$ represents the coding gain achieved by the STC and the term $(E_s / 4N_0)^{-rJ}$ represents a diversity gain of *rJ*. Since $r < I$, the overall diversity order is always less than or equal to *IJ*. It is clear that in designing a STTC, the rank of error matrix *r* should be maximized (thereby maximizing the diversity gain) and at the same time g_r should be also be maximized, thereby maximizing the coding gain.

However, there is no general rule how to obtain good space-time trellis codes for arbitrary number of transmit antennas and modulation methods. Powerful STTCs are given in [48] and obtained from an exhaustive search. And the problem of STTCs is that the detection complexity measured in the number of states grows exponentially with m^I, where *m* is the modulation level, and *I* is the number of transmit antennas.

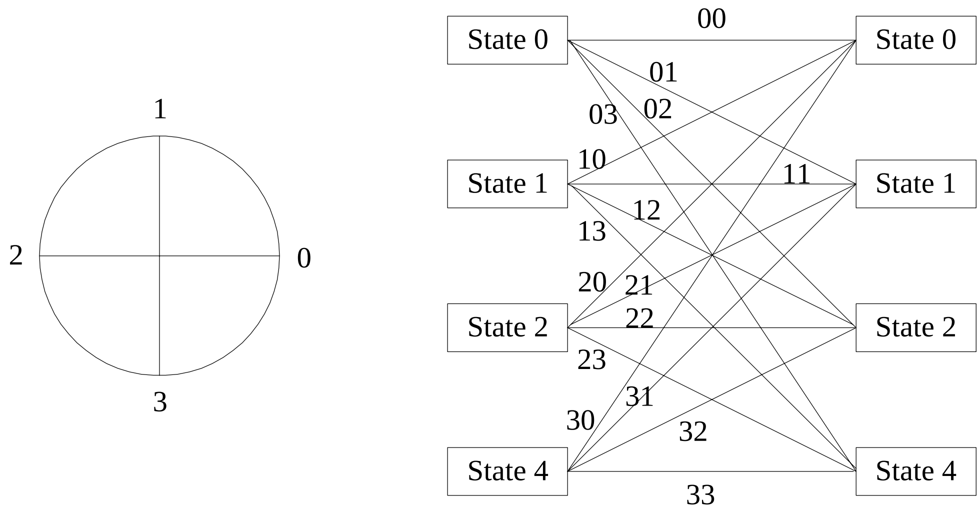

Fig. 2.14 Space-time trellis code with four states

In Fig. 2.14, an example of a STTC for two transmit antennas $I = 2$ in case of quadratic phase shift keying (QPSK) $m = 2$ is given. This code has four states. Assuming ideal channel, the decoding of this code at the receive antenna *j* can be performed by minimizing the following metric:

$$D = \sum_{j=1}^{J} \left| r_j - \sum_{i=1}^{I} \beta_{i,j} x_i \right|^2 \tag{2.25}$$

where r_j is the received signal at *j*th receive antenna and x_i is the branch metric in the transition of the encoder trellis, *I* and *J* is the number of transmit and receive antennas, respectively, and $\beta_{i,j}$ is the channel response between the *i*th transmit antenna and *j*th receive antenna. Here, the Viterbi algorithm can be used to choose the best path with the lowest accumulated metric.

2.3.2 Space-Time Block Codes

In addressing the issue of decoding complexity, Alamouti [44] introduces a remarkable scheme for transmissions using two transmit antennas in 1998. This scheme is much less complex than space-time trellis coding for two transmit antennas but there is a loss in performance compared to space-time trellis codes. Despite this performance penalty, Alamouti's scheme is still appealing in terms of simplicity and performance. In 1999, Tarokh [48] generalized the Alamouti's scheme to an arbitrary number of transmit antennas, namely as space-time block codes (STBC), and is able to achieve the full diversity promised by the transmit and receive antennas. These codes remain the property of having a very simple maximum likelihood decoding algorithm based only on linear processing at the receiver. For real signal constellations, they provide the maximum possible transmission rate allowed by the theory of space-time coding [43]. However, the orthogonal block codes design exists if and only if the code size equal to two, four and eight [48]. For complex constellations, STBCs can be constructed for any number of transmit antennas, and again these codes also have remarkably simple decoding algorithms based only on linear processing at the receiver. They provide full spatial diversity and half of the maximum possible transmission rate allowed by the theory of space-time coding. For complex constellations and for the specific cases of three and four transmit antennas, these diversity schemes were improved to provide ¾ of the maximum possible transmission rate [48].

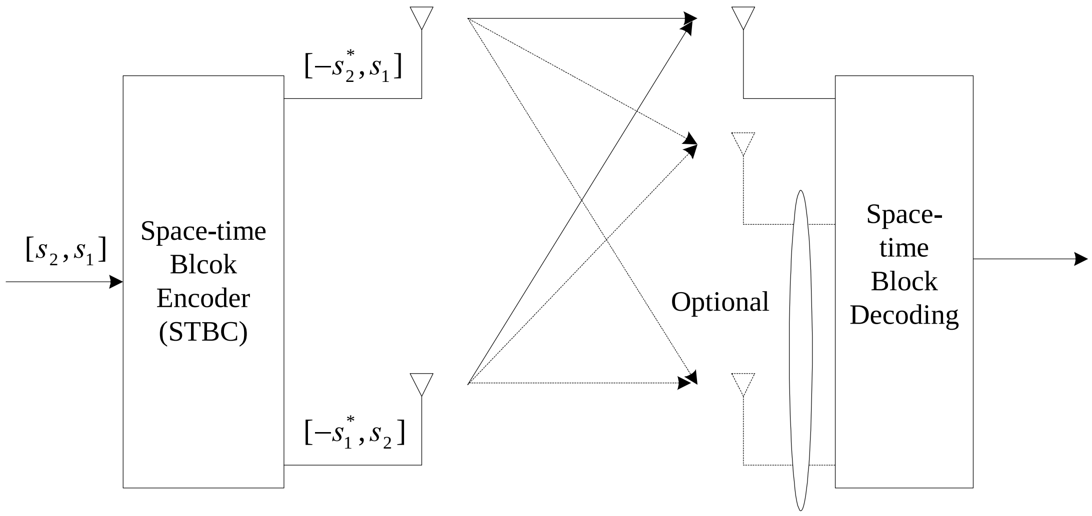

Fig. 2.15 Transceiver of space-time block codes with two transmit antennas

Basically, STBCs are designed as pure diversity schemes and provide no additional coding gain as with STTCs. The transceiver of space-time block coding can be referred to Fig. 2.12. For the case of two transmit antennas, $I = 2$, (see Fig. 2.15), the successive transmitted symbols $[s_2, s_1]$ are mapped to the transmit antenna with the STBCs shown as follows [44][48]:

$$\begin{pmatrix} s_2^* & s_1 \\ -s_1^* & s_2 \end{pmatrix} \begin{array}{l} \leftarrow \quad \text{time} \\ \downarrow \quad \text{space} \end{array} \tag{2.26}$$

where the row corresponds to the time index and the column corresponds to the transmit antenna index. In the first symbol time interval s_1 is transmitted at 1st antenna and s_2 is transmitted at 2nd antenna simultaneously, while in the second symbol time interval s_2^* is transmitted at 1st antenna and $-s_1^*$ is transmitted at 2nd antenna simultaneously. More general STBCs for other number of transmit antennas can be found in [48]

Due to the orthogonality of STBCs, the symbols can be recovered at the receiver by a simple linear processing [43]. The maximum likelihood detection amounts to minimizing the decision metric

$$\sum_{j=1}^{J}\left(\left|r_{j,1}-\beta_{1,j}s_1-\beta_{2,j}s_2\right|^2+\left|r_{j,2}+\beta_{1,j}s_2^*-\beta_{2,j}s_1^*\right|^2\right) \tag{2.27}$$

over all possible values of s_1 and s_2, where $r_{j,t}$ is the received signal at time t and at receive antenna j, $\beta_{i,j}$ is the channel response between the ith transmit antenna and jth receive antenna, and I and J is the number of transmit and receive antennas, respectively. Note that due to the quasi-static nature of the channel, the path gains are constant over two transmissions. The minimizing values are the receiver estimates of s_1 and s_2, respectively. We expand the above metric and delete the terms are independent of the codewords and minimizing metrics are given by

$$\left|\left(\sum_{j=1}^{J}r_{j,1}\beta_{1,j}^*+r_{j,2}^*\beta_{2,j}\right)-s_1\right|^2+\left(-1+\sum_{j=1}^{J}\sum_{i=1}^{2}\left|\beta_{i,j}\right|^2\right)\left|s_1\right|^2 \tag{2.28}$$

for detecting s_1 and

$$\left|\left(\sum_{j=1}^{J}r_{j,1}\beta_{2,j}^*-r_{j,2}^*\beta_{1,j}\right)-s_2\right|^2+\left(-1+\sum_{j=1}^{J}\sum_{i=1}^{2}\left|\beta_{i,j}\right|^2\right)\left|s_2\right|^2 \tag{2.29}$$

for detecting s_2.

STBCs techniques are prompted as the most promising antenna diversity techniques for the future wireless mobile communication system because of its low coding and decoding complexity and the full diversity gain obtained by transmit and receive antenna. It has been demonstrated in [43][47] that the significant diversity gain and performance improvement can be achieved by increasing the number of transmit and receive antennas with very little decoding complexity.

2.4 Related Mathematics

In this section, we present some fundamentals and definitions of the mathematics used in this thesis.

2.4.1 Subspace Approach

Basis: Let $\{\underline{\mathbf{x}}_1, \quad \cdots, \quad \underline{\mathbf{x}}_n\}$ be a set of $m \times 1$ vectors in a vector space *S*. This set is called a basis of *S* if it spans the vector space *S* and the vectors $\underline{\mathbf{x}}_1, \quad \cdots, \quad \underline{\mathbf{x}}_n$ are linearly independent.

Subspace of C^n [56]: Let $X \subseteq C^n$, X is subspace if (a) $\mathbf{0} \in X$; (b) for each $\underline{\mathbf{u}}$, $\underline{\mathbf{v}} \in X$, $\underline{\mathbf{u}} + \underline{\mathbf{v}} \in X$ (closure under addition); (c) for each $\underline{\mathbf{u}} \in X$, $c \in C$, $c\underline{\mathbf{u}} \in X$ (closure under scalar multiplication), where C^n is *n*-dimensional complex space.

Range of $\mathbf{A}$ [56]: the range (or column space) of $\mathbf{A}^{m\times n}$ is a set of all linear combinations of the columns of $\mathbf{A}$. In other words, if $\mathbf{A} = [\underline{\mathbf{a}}_1 \quad \cdots \quad \underline{\mathbf{a}}_n]$, $\underline{\mathbf{a}}_1 \quad \cdots \quad \underline{\mathbf{a}}_n \in C^m$, then

$$R(\mathbf{A}) = Span\{\underline{\mathbf{a}}_1 \quad \cdots \quad \underline{\mathbf{a}}_n\}. \tag{2.30}$$

This is the subspace of C^m.

Right Null Space of $\mathbf{A}$ [56]: the null space of $\mathbf{A}^{m\times n}$ is a set of all solutions of $\mathbf{A}\underline{\mathbf{x}} = \underline{\mathbf{0}}$, i.e.,

$$N_R(\mathbf{A}) = \{\underline{\mathbf{x}} : \mathbf{A}\underline{\mathbf{x}} = \underline{\mathbf{0}}, \underline{\mathbf{x}} \in C^n\}. \tag{2.31}$$

This is a subspace of C^n.

Left Null Space of $\mathbf{A}$: the null space of $\mathbf{A}^{m\times n}$ is a set of all solutions of $\underline{\mathbf{x}}^{\mathcal{H}}\mathbf{A} = \underline{\mathbf{0}}$, i.e.,

$$N_L(\mathbf{A}) = \{\underline{\mathbf{x}} : \underline{\mathbf{x}}^{\mathcal{H}} \mathbf{A} = \underline{\mathbf{0}}, \underline{\mathbf{x}} \in C^m\}. \tag{2.32}$$

This is a subspace of C^m.

Singular Value Decomposition (SVD): Let $\mathbf{A}$ be an arbitrary $m \times n$ matrix. There exist two orthonormal matrices, $\mathbf{U}$ and $\mathbf{V}$, such that

$$\mathbf{A} = \mathbf{U}\ \mathbf{\Sigma}\ \mathbf{V}^{\mathcal{H}} \tag{2.33}$$

where $\mathbf{\Sigma} = \begin{pmatrix} \mathbf{\Sigma}_s & \mathbf{0} \\ \mathbf{0} & \mathbf{0} \end{pmatrix}$, $\mathbf{\Sigma}_s$ is the diagonal matrix, $\mathbf{\Sigma}_s = diag(\lambda_1, \ \lambda_2, \ \cdots, \ \lambda_r)$, $\mathbf{U} = [\underline{\mathbf{u}}_1 \ \ \underline{\mathbf{u}}_2 \ \ \cdots \ \ \underline{\mathbf{u}}_n]$ and $\mathbf{V} = [\underline{\mathbf{v}}_1 \ \ \underline{\mathbf{v}}_2 \ \ \cdots \ \ \underline{\mathbf{v}}_n]$ are unitary matrix. The r values $\lambda_1, \ \lambda_2, \ \cdots, \ \lambda_r$ are arranged such that $\lambda_1 \geq \lambda_2 \geq \cdots \geq \lambda_r$, together with the values of $\lambda_{r+1} = \lambda_{r+2} = \cdots = \lambda_n = 0$. We rewrite (2.33) as

$$\mathbf{AV} = \mathbf{U\Sigma}. \tag{2.34}$$

By partitioning multiplication on the left and backward multiplying on the right, we have

$$\mathbf{A}\underline{\mathbf{v}}_i = \lambda_i \underline{\mathbf{u}}_i \tag{2.35}$$

for $i = 1,2,\cdots,r$ and otherwise

$$\mathbf{A}\underline{\mathbf{v}}_i = \underline{\mathbf{0}}. \tag{2.36}$$

Recall from [56], if $\underline{\mathbf{v}}_1 \ \ \underline{\mathbf{v}}_2 \ \ \cdots \ \ \underline{\mathbf{v}}_n$ is a basis for C^n, then $\mathbf{A}\underline{\mathbf{v}}_1 \ \ \mathbf{A}\underline{\mathbf{v}}_2 \ \ \cdots \ \ \underline{\mathbf{A}\mathbf{v}}_n$ form a spanning set for the range of $\mathbf{A}$. Thus, the vectors $\lambda_1\underline{\mathbf{u}}_1 \ \ \lambda_2\underline{\mathbf{u}}_2 \ \ \cdots \ \ \lambda_r\underline{\mathbf{u}}_r$ and thus $\underline{\mathbf{u}}_1 \ \ \underline{\mathbf{u}}_2 \ \ \cdots \ \ \underline{\mathbf{u}}_r$ span the range of $\mathbf{A}$, i.e.,

$$R(\mathbf{A}) = Span\{\underline{\mathbf{u}}_1 \ \ \underline{\mathbf{u}}_2 \ \ \cdots \ \ \underline{\mathbf{u}}_r\} \tag{2.37}$$

Let $\underline{\mathbf{x}} = \alpha_1\underline{\mathbf{v}}_1 + \alpha_2\underline{\mathbf{v}}_2 + \cdots + \alpha_n\underline{\mathbf{v}}_n$ and suppose $\mathbf{A}\underline{\mathbf{x}} = \underline{\mathbf{0}}$, and noting (2.36), we see that

$$\mathbf{A}\underline{\mathbf{x}} = \alpha_1\lambda_1\underline{\mathbf{u}}_1 + \alpha_1\lambda_2\underline{\mathbf{u}}_2 + \cdots + \alpha_r\lambda_r\underline{\mathbf{u}}_r = \underline{\mathbf{0}}. \tag{2.38}$$

Since $\underline{\mathbf{u}}_1 \quad \underline{\mathbf{u}}_2 \quad \cdots \quad \underline{\mathbf{u}}_r$ are linearly independent, $\alpha_1\lambda_1 = 0$, …, $\alpha_r\lambda_r = 0$ or $\alpha_1 = 0$, …, $\alpha_r = 0$. Thus $\underline{\mathbf{x}} = \alpha_{r+1}\underline{\mathbf{v}}_{r+1} + \alpha_{r+2}\underline{\mathbf{v}}_{r+2} + \cdots + \alpha_n\underline{\mathbf{v}}_n$. And any vector in this form is in *Right Null Space* $N_R(\mathbf{A})$, so

$$N_R(\mathbf{A}) = Span\{\underline{\mathbf{v}}_{r+1} \quad \underline{\mathbf{v}}_{r+2} \quad \cdots \quad \underline{\mathbf{v}}_n\}. \tag{2.39}$$

If we rewrite (2.33) as

$$\mathbf{U}^{\mathcal{H}}\mathbf{A} = \mathbf{\Sigma}\mathbf{V}^{\mathcal{H}} \tag{2.40}$$

and we have

$$\underline{\mathbf{u}}_i^{\mathcal{H}}\mathbf{A} = \lambda_i\underline{\mathbf{v}}_i^{\mathcal{H}} \tag{2.41}$$

for $i = 1,2,\cdots,r$ and otherwise

$$\underline{\mathbf{u}}_i^{\mathcal{H}}\mathbf{A} = \underline{\mathbf{0}}. \tag{2.42}$$

Similarly, the vectors $\lambda_1\underline{\mathbf{v}}_1 \quad \lambda_2\underline{\mathbf{v}}_2 \quad \cdots \quad \lambda_r\underline{\mathbf{v}}_r$ and thus $\underline{\mathbf{v}}_1 \quad \underline{\mathbf{v}}_2 \quad \cdots \quad \underline{\mathbf{v}}_r$ span the range of $\mathbf{A}$, i.e.,

$$R(\mathbf{A}) = Span\{\underline{\mathbf{v}}_1 \quad \underline{\mathbf{v}}_2 \quad \cdots \quad \underline{\mathbf{v}}_r\}. \tag{2.43}$$

Let $\underline{\mathbf{x}} = \alpha_1\underline{\mathbf{u}}_1 + \alpha_2\underline{\mathbf{u}}_2 + \cdots + \alpha_n\underline{\mathbf{u}}_n$ and suppose $\underline{\mathbf{x}}^{\mathcal{H}}\mathbf{A} = \underline{\mathbf{0}}$, similarly, we can obtain $\alpha_1 = 0$, …, $\alpha_r = 0$. Thus $\underline{\mathbf{x}} = \alpha_{r+1}\underline{\mathbf{u}}_{r+1} + \alpha_{r+2}\underline{\mathbf{u}}_{r+2} + \cdots + \alpha_n\underline{\mathbf{u}}_n$. And any vector in this form is in *Left Null Space* $N_L(\mathbf{A})$, so

$$N_L(\mathbf{A}) = Span\{\underline{\mathbf{u}}_{r+1} \quad \underline{\mathbf{u}}_{r+2} \quad \cdots \quad \underline{\mathbf{u}}_n\}. \tag{2.44}$$

We partition the SVD into blocks corresponding to the location of the zero and nonzero singular values, we can exploit the following properties of the matrices $\mathbf{U}$ and $\mathbf{V}$:

$$\mathbf{A} = \mathbf{U}\ \mathbf{\Sigma}\ \mathbf{V}^{\mathcal{H}} = [\mathbf{U}_s \quad \mathbf{U}_o]\begin{bmatrix}\mathbf{\Sigma}_s & \mathbf{0}\\ \mathbf{0} & \mathbf{0}\end{bmatrix}\begin{bmatrix}\mathbf{V}_s^{\mathcal{H}}\\ \mathbf{V}_o^{\mathcal{H}}\end{bmatrix}. \tag{2.45}$$

By the above discussion, it can be shown that the columns of matrix $\mathbf{U}_s$ or $\mathbf{V}_s$ span the range space (or signal space in signal communication) of $\mathbf{A}$, and the columns of $\mathbf{U}_o$ spans the left null space of $\mathbf{A}$, the columns of $\mathbf{V}_o$ spans the right null space of $\mathbf{A}$. Thus, we have

$$\mathbf{U}_o^{\mathcal{H}}\mathbf{A} = \mathbf{0} \tag{2.46a}$$

or

$$\mathbf{AV} = \mathbf{0}. \tag{2.46b}$$

Hence, the orthogonality shown in (2.46) is the basic principle of subspace approach in the signal estimation theory.

2.4.2 Cramér-Rao Bound

Estimation accuracy is often measured in the terms of the mean-square errors of the estimates. The Cramér-Rao bound (CRB) provides a lower bound for the variance of an unbiased estimator. If an estimator can be found to achieve the bound, then it must be the minimum variance unbiased estimator.

We denote the measurement vector (the received signal) by $\underline{\mathbf{x}}$, an unknown parameter by θ, the probability density function of $\underline{\mathbf{x}}$ by $p(\underline{\mathbf{x}} \mid \theta)$ and unbiased estimate θ by $\hat{\theta}$, then the variance of any unbiased estimator $\hat{\theta}$ must satisfy [105]

$$\mathrm{var}(\hat{\theta}) \geq \frac{1}{E\left\{\left(\dfrac{\partial^2 \ln p(\underline{\mathbf{x}} \mid \theta)}{\partial \theta^2}\right)\right\}} \tag{2.47}$$

where the expectation is taken with respect to $p(\underline{\mathbf{x}} \mid \theta)$, which is given by

$$E\left\{\left(\frac{\partial^2 \ln p(\underline{\mathbf{x}} \mid \theta)}{\partial \theta^2}\right)\right\} = \int_{-\infty}^{\infty} \frac{\partial^2 \ln p(\underline{\mathbf{x}} \mid \theta)}{\partial \theta^2} p(\underline{\mathbf{x}} \mid \theta) d\underline{\mathbf{x}}. \tag{2.48}$$

Since the second derivative is a random variable dependent on $\underline{\mathbf{x}}$, the bound will depend on θ.

For the vector parameter $\underline{\boldsymbol{\theta}}$, we let $\underline{\boldsymbol{\theta}} = \begin{bmatrix}\theta_1 & \theta_2 & \cdots & \theta_N\end{bmatrix}^T$ a set of N unknown parameters. The estimator for the ith parameter is denoted by $\underline{\boldsymbol{\theta}}_i(\underline{\mathbf{x}})$. Then

$$\mathrm{var}(\theta_i) \geq J_{ii}^{-1}(\underline{\boldsymbol{\theta}}) \tag{2.49}$$

where

$$\begin{aligned} J_{ij}^{-1}(\underline{\boldsymbol{\theta}}) &= -E\left\{\left(\frac{\partial \ln p(\underline{\mathbf{x}} \mid \underline{\boldsymbol{\theta}})}{\partial \theta_i}\right)\left(\frac{\partial \ln p(\underline{\mathbf{x}} \mid \underline{\boldsymbol{\theta}})}{\partial \theta_j}\right)\right\} \\ &= -E\left\{\left(\frac{\partial^2 \ln p(\underline{\mathbf{x}} \mid \underline{\boldsymbol{\theta}})}{\partial \theta_i \partial \theta_j}\right)\right\} \end{aligned} \tag{2.50}$$

where $i = 1,2,\cdots,N$, $j = 1,2,\cdots,N$ and J_{ij} is the (*i, j*)th element of the $N \times N$ square matrix $\mathbf{J}$, and $\mathbf{J}$ is known as the Fisher's information matrix (FIM) [105].

2.5 Conclusion

With the above introductory knowledge of MC-CDMA, space-time block coding (STBC) and their potential advantages to dramatically increase the capacity and to effectively combat the destructive fading channel in wireless communication system, the author is motivated to focus his research on the combined technology, namely STBC MC-CDMA. In the next chapters, the thesis studies and investigates the performance and capacity analysis of STBC MC-CDMA systems. Some implementation issues for STBC MC-CDMA systems, such as timing and frequency synchronization, channel estimation and multiuser detections are investigated.

Chapter 3

Performance and Capacity in the presence of Carrier Frequency Offset

In the following two chapters of the thesis, we focus on the theoretical study of bit-error-rate (BER) performance and system capacity of STBC MC-CDMA systems. We begin the studies with the BER performance and capacity analysis in the presence of carrier frequency offset (CFO) between the transmitter and receiver oscillators. The exact BER expression when using equal gain combining (EGC) and the approximate BER expression when using maximum ratio combining (MRC) are derived. These BER expressions are verified through simulations. Using these derived expressions, the achievable system capacity satisfying a minimum BER requirement can be studied for the two cases when EGC and MRC are used, and hence possible to compare the achievable capacity of STBC MC-CDMA systems with that of MC-CDMA systems. It is concluded that small CFO has insignificant effect on the BER and capacity of STBC

MC-CDMA systems, and this range of CFO is important in transceiver design. Besides, STBC MC-CDMA systems with multiple receive antennas can achieve higher capacity than that of the MC-CDMA systems, and this amount can be obtained analytically using the theoretical BER expressions derived.

Although independent channel characteristics between neighboring subcarriers are assumed, the theoretical performance analysis can be a good approximation to the practical channels when the correlation coefficients between neighboring subcarriers are small, for example, less than 0.5, and can be a good lower bound when the neighboring subcarriers have large correlation coefficients [100]. The expressions obtained provides a simple way to study the effect of CFO on the BER performance and capacity of asynchronous STBC MC-CDMA systems.

3.1 System Model

The equivalent block diagram of the transmitter and receiver of a STBC MC-CDMA systems used in our analysis is shown in Fig. 3.1. The stream of binary phase-shift keying (BPSK) symbols of the k^{th} user first goes through the ST block encoder. Without incurring any power or bandwidth penalty, the Alamouti's orthogonal ST block coding scheme for 2 transmit antennas is employed [44][48], and more general ST codes for other number of transmit antennas can be found in [48]. Two successive block symbols $\underline{\mathbf{b}}_k(2n)$ and $\underline{\mathbf{b}}_k(2n+1)$ for the k^{th} user are mapped to the following matrix

$$\begin{pmatrix} \underline{\mathbf{a}}_{k,1}(2n+1) & \underline{\mathbf{a}}_{k,1}(2n) \\ \underline{\mathbf{a}}_{k,2}(2n+1) & \underline{\mathbf{a}}_{k,2}(2n) \end{pmatrix} = \frac{1}{\sqrt{2}} \begin{pmatrix} -\underline{\mathbf{b}}_k(2n+1) & \underline{\mathbf{b}}_k(2n) \\ \underline{\mathbf{b}}_k(2n) & \underline{\mathbf{b}}_k(2n+1) \end{pmatrix}$$

where $\underline{\mathbf{b}}_k(n) = \begin{bmatrix} b_{k,1}(n) & \cdots & b_{k,P}(n) \end{bmatrix}^T$ denotes the n^{th} block symbols for k^{th} user with length P, and $\underline{\mathbf{a}}_{k,i}(n) = \begin{bmatrix} a_{k,i,1}(n) & \cdots & a_{k,i,P}(n) \end{bmatrix}^T$ denotes the n^{th} block symbols at i^{th} transmit antenna for k^{th} user with length P. The columns are transmitted in successive block time with the symbols in the upper and lower blocks simultaneously sent through the two transmit antennas, respectively. The factor $1/\sqrt{2}$ is to normalize the transmitted symbol energy.

Next every block symbol $\underline{\mathbf{a}}_{k,i}(n)$ ($i = 1,2$) at the i^{th} transmit antenna is serial-to-parallel converted to P parallel data streams. Each data stream is spread and transmitted on L different subcarriers, where L is the spreading gain. Random spreading sequence is used in this paper. The symbol duration T_s on each subcarrier is P times of the input symbol duration T_b, i.e., $T_s = PT_b$, therefore, frequency selective fading over each subcarrier can be avoided by increasing P if T_b is less than the channel delay spread. The MC-CDMA modulator transmits a total of PL chips resulting from the P BPSK symbols over a total of PL subcarriers. The frequency separation between the neighboring subcarriers is $1/T_s$ Hz and passband null-to-null bandwidth of each subcarrier is $2/T_s$. The ideal central baseband frequency of each subcarrier is given by

$$f_x = x/T_s \qquad x = 1,2,\cdots,PL. \tag{3.1}$$

In order to achieve frequency diversity, the assignment of PL subcarriers to the PL chips is made such that the frequency separation among subcarriers conveying the chips of the same data symbol is kept at maximum, as shown in Fig. 3.1. It means that data in the p^{th} $(p = 1, 2, \cdots, P)$ data stream is transmitted on the l^{th} subcarrier with the frequency $\{f_{p+(l-1)P}, l = 1, 2, \cdots, L\}$ and the adjacent frequency separation between these subcarriers is P/T_s. Let B as the null-to-null passband bandwidth of the STBC MC-CDMA systems with PL subcarriers, then $B = (PL+1)/T_s$.

Symbol duration T_s in each subcarrier is assumed to be longer than channel delay spread so that each subcarrier signal undergone flat fading, and fading process of a given user on different subcarriers is assumed to be independent throughout this paper. In the literature, when using this model, no cyclic prefixes (CP) need to be considered since all subcarriers undergo flat fading [61]-[66]. In practical implementation where inverse fast Fourier transform (IFFT) is used, the intersymbol interferences (ISI) for MC-CDMA symbol have to be considered since the channel fading is modeled at chip period interval over the full bandwidth instead of at symbol period interval over each subcarrier bandwidth. Normally, the use of CP requires the use of additional bandwidth, which does not account for in this analysis since our system model is equivalent to the IFFT/FFT implemented system with CP has been removed at the receiver. This bandwidth expansion factor needs to be compensated when applying the results obtained in this paper to IFFT/FFT implemented system.

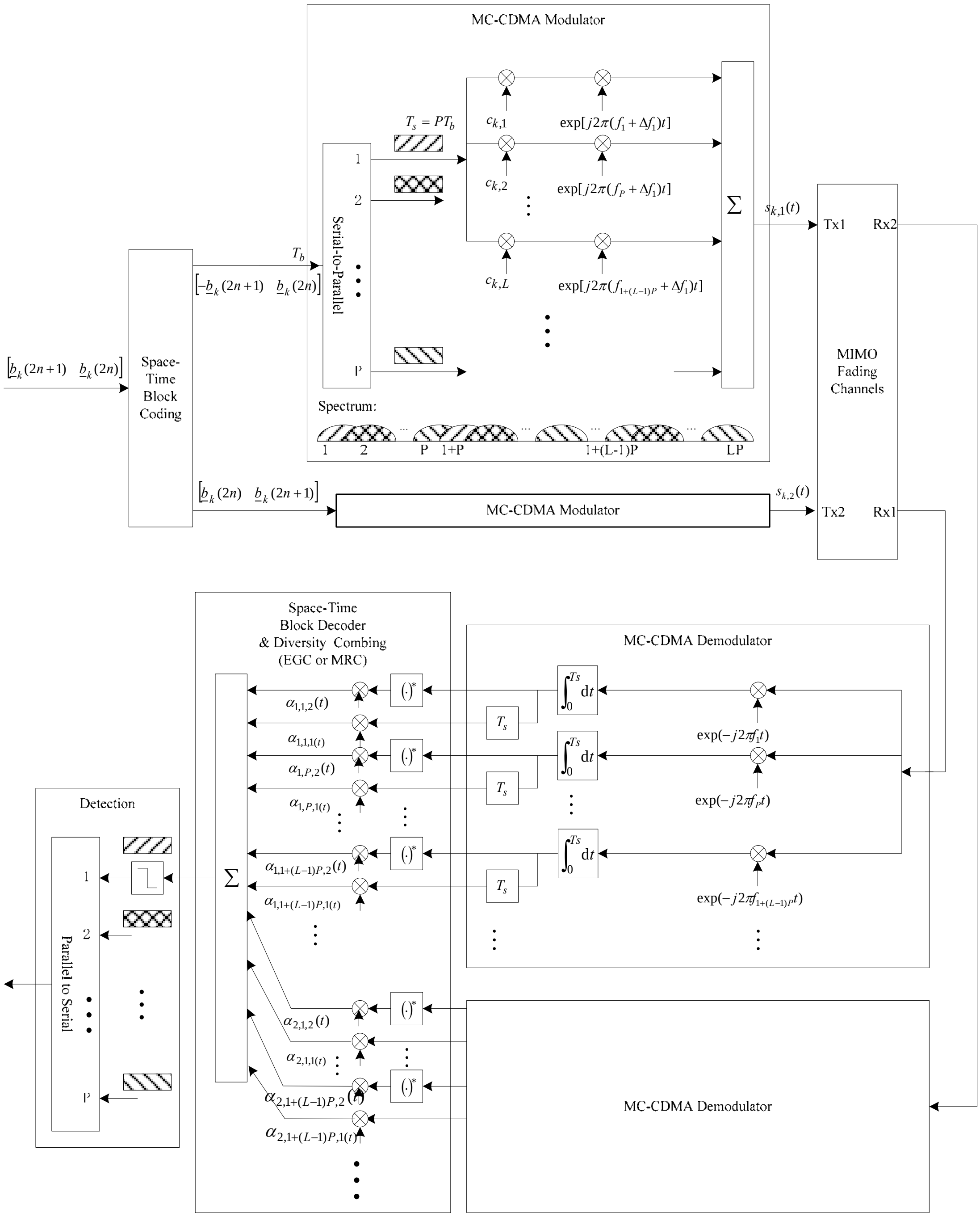

Fig. 3.1 STBC MC-CDMA system model with 2Tx2Rx

Assume that there is K asynchronous users, each employing BPSK with the same transmitting power S and at the same data bit rate $1/T_b$. The transmitted signal at the i^{th} antenna of user k can be expressed as

$$s_{k,i}(t) = \sum_{n=-\infty}^{n=+\infty} \sqrt{2S} \sum_{p=1}^{P} \sum_{l=1}^{L} a_{k,i,p}(n) c_{k,l}(n) u(t - nT_s) \cdot \exp[j2\pi(f_x + \Delta f_k)t],\ i = 1,2 \quad (3.2)$$

where $a_{k,i,p}(n)$ denotes the n^{th} data bit of the p^{th} data stream at the i^{th} antenna of user k, $c_{k,l}(n)$ $(l=1,\cdots,L)$ is the l^{th} spreading chip for the n^{th} data bit of the k^{th} user, $u(t)$ is the rectangular pulse define over $[0,T_s]$. The subscript

$$x = p + (l-1)P \tag{3.3}$$

and f_x is the ideal central baseband frequency at x^{th} subcarrier given by (1), Δf_k is the CFO between the k^{th} user's transmitter and the oscillator at the receiver of base station.

Consider uplink transmission, the received signal at the j^{th} receive antenna ($j=1,\cdots,J$) is given by

$$r_j(t) = \sum_{n=-\infty}^{n=+\infty} \sqrt{2S} \sum_{k=1}^{K} \sum_{i=1}^{2} \sum_{p=1}^{P} \sum_{l=1}^{L} a_{k,i,p}(n) c_{k,l}(n) u(t - nT_s - \tau_{k,i,j}) \cdot$$

$$\beta_{k,i,j,x} \exp[j(2\pi(f_x + \Delta f_k)t + \phi_{k,i,j,x}(t))] + \eta_j(t) \tag{3.4}$$

where $\tau_{k,i,j}$ is the transmission delay from i^{th} transmit antenna of user k to the j^{th} receive antenna, which is independently and uniformly distributed over $[0,T_s)$ for different k, i and j. $\phi_{k,i,j,x}(t) = \varphi_{k,i,j,x}(t) - 2\pi(f_x + \Delta f_k)\tau_{k,i,j}$, $\beta_{k,i,j,x}(t)$ and $\varphi_{k,i,j,x}(t)$ are respectively the amplitude and phase of the channel fading gain of user k when signal is transmitted from the i^{th} transmit antenna to the j^{th} receive antenna through the x^{th} subcarrier, $\beta_{k,i,j,x}(t)$ is Rayleigh distributed with $E\{\beta^2_{k,i,j,x}\} = \sigma^2$, $\varphi_{k,i,j,x}(t)$ is uniformly distributed over $[0, 2\pi]$. $\eta_j(t)$ denotes AWGN at the j^{th} receive antenna with zero mean and double-sided power spectral density (PSD) $N_0/2$.

Assume user 1 is of interest and coherent receiver is used. Without loss of generality, let $\tau_{1,i,j} = 0$. At the l^{th} subcarrier of the p^{th} parallel data stream, the coherent receiver output for the n^{th} symbol of the j^{th} antenna is given by

$$Y_{j,p,l}(n) = \frac{1}{T_s} \int_{nT_s}^{(n+1)T_s} r_j(t) \exp(-j2\pi f_x t) dt = D_{j,p,l}(n) + I_{j,p,l}(n) \tag{3.5}$$

where $D_{j,p,l}(n)$ is the desired signal term before decision is made, and

$$I_{j,p,l}(n) = I_{SO,j,p,l}(n) + I_{MS,j,p,l}(n) + I_{MO,j,p,l}(n) + \eta_{j,p,l}(n) \tag{3.6}$$

where $I_{SO,j,p,l}(n)$ denotes the self-interference from the remaining subcarriers, $I_{MS,j,p,l}$ and $I_{MO,j,p,l}(n)$ denote the multiuser interference (MUI) from the same subcarriers and other subcarriers, respectively, and $\eta_{j,p,l}(n)$ is the AWGN.

3.2 Interference Analysis

Channel fading is assumed to be quasi-stationary over the two successive symbol intervals $2T_s$, i.e., the channel gain remains constant over the time interval $\left[2nT_s \quad (2n+2)T_s\right]$,

$$\beta_{k,i,j,x}(2n) \approx \beta_{k,i,j,x}(2n+1) = \beta_{k,i,j,x}\,,$$

$$\varphi_{k,i,j,x}(2n) \approx \varphi_{k,i,j,x}(2n+1) = \varphi_{k,i,j,x}\,. \tag{3.7}$$

Let $\varepsilon_k = \Delta f_k T_s$ be the CFO normalized by the subcarrier spacing for user *k*. We assume that $\varepsilon_1 \in [0,1)$ and ε_k $(k = 2,\cdots,K)$ is uniformly distributed over $[0,\varepsilon_1)$. This corresponds to the case where user 1 will have the worst performance among the group of users since its offset frequency observed by the base station receiver is the largest. The signal and respective interference terms can be derived using (3.4), (3.5) and (3.6). The desired $(2n)^{\text{th}}$ and $(2n+1)^{\text{th}}$ block symbols at the l^{th} subcarrier of the p^{th} data stream of the j^{th} antenna can be shown to be given by

$$\begin{aligned} D_{j,p,l}(2n) = \sqrt{\Xi}[&\beta_{1,1,j,x}\exp(j\Phi_{1,1,j,x})\cdot c_{1,l}(2n)b_{1,p}(2n) \\ &+\beta_{1,2,j,x}\exp(j\Phi_{1,2,j,x})\cdot c_{1,l}(2n)b_{1,p}(2n+1)], \end{aligned} \tag{3.8}$$

$$D_{j,p,l}(2n+1) = \sqrt{\Xi}[\beta_{1,1,j,x}\exp(j\Phi_{1,1,j,x})\cdot c_{1,l}(2n+1)(-b_{1,p}(2n+1))$$

$$+\beta_{1,2,j,x}\exp(j\Phi_{1,2,j,x})\cdot c_{1,l}(2n+1)b_{1,p}(2n)] \quad (3.9)$$

where $\Xi = S\cdot \mathrm{sinc}^2(\varepsilon_1)$, $\mathrm{sinc}(x)=\sin(\pi x)/(\pi x)$ and $\Phi_{1,i,j,x}=\pi\varepsilon_1+\phi_{1,i,j,x}$ ($i=1,2$). In the following, we derive the respective interference terms defined in (3.6) for a referenced subcarrier $x=p+(l-1)P$ at the receive antenna *j* of user 1.

3.2.1 Self-Interference from the other subcarriers

Here we consider only those terms corresponding to $k=1$. There are altogether $PL-1$ subcarriers that will interfere the referenced subcarrier *x*.

$$I_{SO,j,p,l}(2n)=\sum_{q=1}^{P}\sum_{h=1,y\neq x}^{L}\sqrt{S}\,\mathrm{sinc}(x-y-\varepsilon_1)\cdot\big\lfloor\beta_{1,1,j,y}\exp(-j\Phi'_{1,1,j})\cdot c_{1,h}(2n)b_{1,q}(2n)$$

$$+\beta_{1,2,j,y}\exp(-j\Phi'_{1,2,j})\cdot c_{1,h}(2n)b_{1,q}(2n+1)\big\rfloor, \quad (3.10)$$

$$I_{SO,j,p,l}(2n+1)=\sum_{q=1}^{P}\sum_{h=1,y\neq x}^{L}\sqrt{S}\,\mathrm{sinc}(x-y-\varepsilon_1)\cdot$$

$$\big\lfloor\beta_{1,1,j,y}\exp(-j\Phi'_{1,1,j})\cdot c_{1,h}(2n+1)(-b_{1,q}(2n+1))$$

$$+\beta_{1,2,j,y}\exp(-j\Phi'_{1,2,j})\cdot c_{1,h}(2n+1)b_{1,q}(2n)\big\rfloor \quad (3.11)$$

where $y=q+(h-1)P$, $\Phi'_{1,i,j}=\pi[x-y+\varepsilon_1]-\phi_{1,i,j,y}$, and is uniformly distributed over $[0,2\pi]$.

3.2.2 Multiuser Interference from the same subcarrier

Here we consider only terms in (3.5) resulting from other users ($k\neq 1$) who transmit using subcarrier *x*.

$$I_{MS,j,p,l}(2n)=\sum_{k=2}^{K}\sqrt{S}\,/\,\pi\varepsilon_k\cdot$$

$$\{\big\lfloor\sin(\pi\varepsilon_k\tau_{k,1,j}/T_s)\cdot\beta_{k,1,j,x}\exp(j\Phi''_{k,1,1,j})\cdot c_{k,l}(2n-1)(-b_{k,p}(2n-1))$$

$$+\sin(\pi\varepsilon_k\tau_{k,2,j}/T_s)\cdot\beta_{k,2,j,x}\exp(j\Phi''_{k,1,2,j})\cdot c_{k,l}(2n-1)b_{k,p}(2n-2)\big]$$

$$+\big[\sin[\pi\varepsilon_k(T_s-\tau_{k,1,j})/T_s]\cdot\beta_{k,1,j,x}\exp(j\Phi''_{k,2,1,j})\cdot c_{k,l}(2n)b_{k,p}(2n)$$

$$+\sin[\pi\varepsilon_k(T_s-\tau_{k,2,j})/T_s]\cdot$$

$$\beta_{k,2,j,x}\exp(j\Phi''_{k,2,2,j})\cdot c_{k,l}(2n)b_{k,p}(2n+1)\big]\big\}, \tag{3.12}$$

$$I_{MS,j,p,l}(2n+1)=\sum_{k=2}^{K}\sqrt{S}/\pi\varepsilon_k\cdot$$

$$\big\{\big[\sin(\pi\varepsilon\tau_{k,1,j}/T_s)\cdot\beta_{k,1,j,x}\exp(j\Phi''_{k,1,1,j})\cdot c_{k,l}(2n)b_{k,p}(2n)$$

$$+\sin(\pi\varepsilon_k\tau_{k,2,j}/T_s)\cdot\beta_{k,2,j,x}\exp(j\Phi''_{k,1,2,j})\cdot c_{k,l}(2n)b_{k,p}(2n+1)\big]$$

$$+\big[\sin[\pi\varepsilon_k(T_s-\tau_{k,1,j})/T_s]\cdot$$

$$\beta_{k,1,j,x}\exp(j\Phi''_{k,2,1,j})\cdot c_{k,l}(2n+1)(-b_{k,p}(2n+1))$$

$$+\sin[\pi\varepsilon_k(T_s-\tau_{k,2,j})/T_s]\cdot$$

$$\beta_{k,2,j,x}\exp(j\Phi''_{k,2,2,j})\cdot c_{k,l}(2n+1)b_{k,p}(2n)\big]\big\} \tag{3.13}$$

where $\Phi''_{k,1,i,j}=\pi\varepsilon_k\tau_{k,i,j}/T_s+\phi_{k,i,j,x}$ and $\Phi''_{k,2,i,j}=\pi\varepsilon_k(T_s+\tau_{k,i,j})/T_s+\phi_{k,i,j,x}$, $i=1,2$, are all uniformly distributed over $[0,2\pi]$.

3.2.3 Multiuser Interference from the other subcarriers

Here we consider those terms in (3.5) resulting from other users ($k\neq 1$) who transmit using different subcarrier.

$$I_{MO,j,p,l}(2n)=\sum_{k=2}^{K}\sum_{q=1}^{P}\sum_{h=1,y\neq x}^{L}\sqrt{S}/\pi(x-y-\varepsilon_k)\cdot$$

$$\big\{\big[\sin[\pi(x-y-\varepsilon_k)\tau_{k,1,j}/T_s]\cdot$$

$$\beta_{k,1,j,y}\exp(-j\Phi'''_{k,1,1,j})\cdot c_{k,h}(2n-1)(-b_{k,q}(2n-1))$$

$$+\sin[\pi(x-y-\varepsilon_k)\tau_{k,2,j}/T_s]\cdot$$

$$\beta_{k,2,j,y}\exp(-j\Phi'''_{k,1,2,j})\cdot c_{k,h}(2n-1)b_{k,q}(2n-2)\Big]$$

$$+\Big[\sin[\pi(x-y-\varepsilon_k)(T_s-\tau_{k,1,j})/T_s]\cdot$$

$$\beta_{k,1,j,y}\exp(-j\Phi'''_{k,2,1,j})\cdot c_{k,h}(2n)b_{k,q}(2n)$$

$$+\sin[\pi(x-y-\varepsilon_k)(T_s-\tau_{k,2,j})/T_s]\cdot$$

$$\beta_{k,2,j,y}\exp(-j\Phi'''_{k,2,2,j})\cdot c_{k,h}(2n)b_{k,q}(2n+1)\Big]\Big\}, \qquad (3.14)$$

$$I_{MO,j,p,l}(2n+1)=\sum_{k=2}^{K}\sum_{q=1}^{P}\sum_{h=1,y\neq x}^{L}\sqrt{S}\Big/\pi(x-y-\varepsilon_k)\cdot$$

$$\Big\{\Big[\sin[\pi(x-y-\varepsilon_k)\tau_{k,1,j}/T_s]\cdot$$

$$\beta_{k,1,j,y}\exp(-j\Phi'''_{k,1,1,j})\cdot c_{k,h}(2n)b_{k,q}(2n)$$

$$+\sin[\pi(x-y-\varepsilon_k)\tau_{k,2,j}/T_s]\cdot$$

$$\beta_{k,2,j,y}\exp(-j\Phi'''_{k,1,2,j})\cdot c_{k,h}(2n)b_{k,q}(2n+1)\Big]$$

$$+\Big[\sin[\pi(x-y-\varepsilon_k)(T_s-\tau_{k,1,j})/T_s]\cdot$$

$$\beta_{k,1,j,y}\exp(-j\Phi'''_{k,2,1,j})\cdot c_{k,h}(2n+1)(-b_{k,q}(2n+1))$$

$$+\sin[\pi(x-y-\varepsilon_k)(T_s-\tau_{k,2,j})/T_s]\cdot$$

$$\beta_{k,2,j,y}\exp(-j\Phi'''_{k,2,2,j})\cdot c_{k,h}(2n+1)b_{k,q}(2n)\Big]\Big\} \qquad (3.15)$$

where $\Phi'''_{k,1,i,j}=\pi(x-y-\varepsilon_k)\tau_{k,i,j}/T_s-\phi_{k,i,j,y}$, $\Phi'''_{k,2,i,j}=\pi(x-y-\varepsilon_k)(T_s+\tau_{k,i,j})/T_s$ $-\phi_{k,i,j,y}$, $i=1,2$, all are uniformly distributed over $[0,2\pi]$.

3.2.4 Noise

The AWGN noise term $\eta_{j,p,l}$ has zero mean and variance

$$\sigma^2_{\eta_{j,p,l}}=N_0\big/2T_s\ . \qquad (3.16)$$

3.3 BER Performance and Capacity Analysis

At the x^{th} subcarrier of the j^{th} receive antenna, we denote the factors used to weight the received signals $Y_{j,p,l}(2n)$ and $Y_{j,p,l}(2n+1)$ from the two successive intervals to be $\alpha_{j,x,1}(2n)$, $\alpha_{j,x,2}(2n)$ and $\alpha_{j,x,1}(2n+1)$, $\alpha_{j,x,2}(2n+1)$, respectively. The values are to be chosen depending on the combining scheme used. For BPSK only the real part of the signal is used for making decision. The decision variables for $b_{1p}(2n)$ and $b_{1p}(2n+1)$ are respectively given by

$$U_p(2n) = \sum_{j=1}^{J}\sum_{l=1}^{L}\mathrm{Re}\{Y_{j,p,l}(2n)\alpha_{j,x,1}(2n) + Y^*_{j,p,l}(2n+1)\alpha_{j,x,2}(2n)\}, \tag{3.17}$$

$$U_p(2n+1) = \sum_{j=1}^{J}\sum_{l=1}^{L}\mathrm{Re}\{Y_{j,p,l}(2n)\alpha_{j,x,1}(2n+1) + Y^*_{j,p,l}(2n+1)\alpha_{j,x,2}(2n+1)\} \tag{3.18}$$

where $(\cdot)^*$ denotes the complex conjugate. In the following BER analysis, $U_p(2n)$ will be used as an example and we shall simply use U_p to denote $U_p(2n)$. Eq.(3.17) can be expressed as

$$U_p = D_p + I_p \ , \tag{3.19}$$

where $I_p = I_{SO,p}(2n) + I_{MS,p}(2n) + I_{MO,p}(2n) + \eta_p(2n)$. The desired signal is given by

$$D_p = D_p(2n) = \sum_{j=1}^{J}\sum_{l=1}^{L}\mathrm{Re}\left\{D_{j,p,l}(2n)\alpha_{j,x,1}(2n) + D^*_{j,p,l}(2n+1)\alpha_{j,x,2}(2n)\right\}. \tag{3.20}$$

The self-interference (SI) from other subcarriers is given by

$$I_{SO,p}(2n) = \sum_{j=1}^{J}\sum_{l=1}^{L}\mathrm{Re}\left\{I_{SO,j,p,l}(2n)\alpha_{j,x,1}(2n) + I^*_{SO,j,p,l}(2n+1)\alpha_{j,x,2}(2n)\right\}. \tag{3.21}$$

The MUI from same subcarriers is given by

$$I_{MS,p}(2n) = \sum_{j=1}^{J}\sum_{l=1}^{L}\mathrm{Re}\left\{I_{MS,j,p,l}(2n)\alpha_{j,x,1}(2n) + I^*_{MS,j,p,l}(2n+1)\alpha_{j,x,2}(2n)\right\}. \tag{3.22}$$

And the MUI from other subcarriers is given by

$$I_{MO,p}(2n)=\sum_{j=1}^{J}\sum_{l=1}^{L}\mathrm{Re}\left\{I_{MO,j,p,l}(2n)\alpha_{j,x,1}(2n)+I^{*}_{MO,j,p,l}(2n+1)\alpha_{j,x,2}(2n)\right\}. \quad (3.23)$$

For large value of JL, $I_{SO,p}(2n)$, $I_{MS,p}(2n)$ and $I_{MO,p}(2n)$ can be approximately assumed to be Gaussian distributed with zero mean. The variance for $I_{SO,p}$ defined in (3.21) is given by

$$\sigma^2_{I_{SO,p}}=\sum_{j=1}^{J}\sum_{l=1}^{L}A_{SO,l,p}\left(\left|\alpha_{j,x,1}(2n)\right|^2+\left|\alpha_{j,x,2}(2n)\right|^2\right) \quad (3.24)$$

where $A_{SO,l.p}=\sum_{q=1}^{P}\sum_{h=1,y\neq x}^{L}\sigma^2 S\,\mathrm{sinc}^2(x-y+\varepsilon_1)$. Here we assume that all the terms corresponding to different subscripts are all independent from each other. Similarly for (3.22),

$$\sigma^2_{I_{MS,p}}=\sum_{j=1}^{J}\sum_{l=1}^{L}A_{MS,l,p}\left(\left|\alpha_{j,x,1}(2n)\right|^2+\left|\alpha_{j,x,2}(2n)\right|^2\right) \quad (3.25)$$

where $A_{MS,l,p}=(K-1)\sigma^2 S\left[-1+{}_1F_2(\{-\tfrac{1}{2}\};\{\tfrac{1}{2},\tfrac{3}{2}\};-\pi^2\varepsilon_1^2)\right]/\pi^2\varepsilon_1^2$. ${}_pF_q(\underline{\mathbf{a}};\underline{\mathbf{b}};z)$ is the generalized hypergeometric function and its definition can be found in [107]. And for (3.23),

$$\sigma^2_{I_{MO,p}}=\sum_{j=1}^{J}\sum_{l=1}^{L}A_{MO,l,p}\left(\left|\alpha_{j,x,1}(2n)\right|^2+\left|\alpha_{j,x,2}(2n)\right|^2\right) \quad (3.26)$$

where $A_{MO,l,p}=(K-1)\sigma^2 S/\varepsilon_1\pi^2\sum_{q=1}^{P}\sum_{h=1,y\neq x}^{L}g(x-y,\varepsilon_1)-g(x-y,0)$,

$$g(a,b)=\{2-\cos[2\pi(a-b)]-\mathrm{sinc}[2(a-b)]-2\pi(a-b)\cdot\mathrm{Si}[2\pi(a-b)]\}/2(a-b),$$

and $\mathrm{Si}[z]=\int_0^z \sin(t)/t\,dt$.

The noise term can be written as

$$\eta_p(2n)=\sum_{j=1}^{J}\sum_{l=1}^{L}\mathrm{Re}\{\eta_{j,p,l}(2n)\alpha_{j,x,1}(2n)+\eta^{*}_{j,p,l}(2n+1)\alpha_{j,x,2}(2n)\}. \quad (3.27)$$

It is a Gaussian RV with zero mean and variance

$$\sigma_{\eta_p}^2 = \sum_{j=1}^{J}\sum_{l=1}^{L}\frac{N_0}{2T_s}\left(\left|\alpha_{j,x,1}(2n)\right|^2 + \left|\alpha_{j,x,2}(2n)\right|^2\right). \tag{3.28}$$

Since interference items $I_{SO,p}(2n)$, $I_{MS,p}(2n)$, $I_{MO,p}(2n)$ and $\eta_p(2n)$ are mutually uncorrelated, the total interference I_p is also a Gaussian RV with zero mean and variance

$$\sigma_{I_p}^2 = \sigma_{I_{SO,p}}^2 + \sigma_{I_{MS,p}}^2 + \sigma_{I_{MO,p}}^2 + \sigma_{\eta_p}^2 . \tag{3.29}$$

3.3.1 Equal Gain Combining

For EGC scheme, the factors used to weight the received signal at the x^{th} subcarrier of the j^{th} antenna are given by

$$\alpha_{j,x,1}(2n) = \beta_{1,1,j,x}\exp(-j\hat{\Phi}_{1,1,j,x})\cdot c_{1,l}(2n)\big/\beta_{1,j,x} ,$$

$$\alpha_{j,x,2}(2n) = \beta_{1,2,j,x}\exp(j\hat{\Phi}_{1,2,j,x})\cdot c_{1,l}(2n+1)\big/\beta_{1,j,x} \tag{3.30}$$

and

$$\alpha_{j,x,1}(2n+1) = \beta_{1,2,j,x}\exp(-j\hat{\Phi}_{1,2,j,x})\cdot c_{1,l}(2n)\big/\beta_{1,j,x}$$

$$\alpha_{j,x,2}(2n+1) = \beta_{1,1,j,x}\exp(j\hat{\Phi}_{1,1,j,x})\cdot c_{1,l}(2n+1)\big/\beta_{1,j,x} \tag{3.31}$$

where $\beta_{1,j,x} = \sqrt{\beta_{1,1,j,x}^2 + \beta_{1,2,j,x}^2}$, and $\hat{\Phi}_{1,i,j,x}$ can be obtained by using a carrier synchronizer to estimate the phase $\Phi_{1,i,j,x} = \pi\varepsilon_1 + \phi_{1,i,j,x}$. We assume perfect synchronization, i.e. $\hat{\Phi}_{1,i,j,x} \cong \Phi_{1,i,j,x}$ throughout this paper. Substitute (3.8), (3.9) and (3.30) in (3.20), the desired signal is given by

$$D_p = \sum_{j=1}^{J}\sum_{l=1}^{L}\sqrt{\Xi}\cdot\sqrt{\beta_{1,1,j,x}^2 + \beta_{1,2,j,x}^2}\cdot b_{1p}(2n) . \tag{3.32}$$

Assuming that a “+1” is transmitted, (3.19) can be rewritten as

$$U_p = \sum_{j=1}^{J}\sum_{l=1}^{L}\sqrt{\Xi}\cdot\beta_{1,j,x} + I_p\,. \tag{3.33}$$

Since BPSK is used, then the BER for p^{th} data stream can be obtained by using [103]

$$\mathrm{P}_{e,p} = \frac{1}{2} - \frac{1}{\pi}\int_0^\infty \omega^{-1}\,\mathrm{Im}[\Psi_{U_p}(\omega)]d\omega \tag{3.34}$$

where $\Psi_{U_p}(\omega)$ is the characteristic function (CHF) of the decision variable U_p. Im(z) is the imaginary part of complex number z. And it can be easily shown that

$$\Psi_{U_p}(\omega) = \prod_{j=1}^{J}\prod_{l=1}^{L}\Psi_{\beta_{1,j,x}}(\sqrt{\Xi}\omega)\cdot\Psi_{I_p}(\omega)\,. \tag{3.35}$$

Since $\beta_{1,1,j,x}$ and $\beta_{1,2,j,x}$ are independent Rayleigh RVs, then RV $\beta_{1,j,x}$ is Nakagami-m ($m = 2$) [105] distributed with parameter $2\sigma^2$. Its CHF is given by [106]

$$\Psi_{\beta_{1,j,x}}(\omega) = \left\lfloor {}_1F_1(-\tfrac{3}{2};\tfrac{1}{2};\sigma^{2}\omega^2/4) + j\cdot 3\,\omega\sigma\sqrt{\pi}\big/4\cdot\ {}_1F_1(-1;\tfrac{3}{2};\sigma^{2}\omega^2/4)\right\rfloor\cdot\exp(-\sigma^{2}\omega^2/4)\,, \tag{3.36}$$

where ${}_1F_1(a;b;\omega)$ denotes the confluent hypergeometric function [107]. The CHF of Gaussian RV I_p is given by [104]

$$\Psi_{I_p}(\omega) = \exp(-\sigma_p^2\omega^2/2)\,. \tag{3.37}$$

Substitute (3.36) and (3.37) into (3.35), then the CHF of U_p is given by

$$\Psi_{U_p}(\omega) = \Big\lfloor {}_1F_1(-\tfrac{3}{2};\tfrac{1}{2};\Xi\sigma^2\omega^2/4) + j\cdot 3\,\omega\sigma\sqrt{\pi\Xi}\big/4\cdot$$

$${}_1F_1(-1;\tfrac{3}{2};\Xi\sigma^2\omega^2/4)\Big\rfloor^{JL}\cdot\exp[-(2\sigma_{I_p}^2 + JL\Xi\sigma^{2})\omega^2/4]\,. \tag{3.38}$$

Let $\omega = 2z\Big/\sqrt{2\sigma_{I_p}^2 + JL\Xi\sigma^2}$, the exact BER for the p^{th} data stream is given by [107]

$$\mathrm{P}_{e,p}^{EGC} = \frac{1}{2} - \frac{1}{\pi}\int_0^\infty G(z)\exp(-z^2)dz = \frac{1}{2} - \frac{1}{\pi}\sum_{m=1}^{N_p} H_{x_m}G(x_m) \tag{3.39}$$

where

$$G(z) = \mathrm{Im}\Big\{\Big[{}_1F_1(-\tfrac{3}{2};\tfrac{1}{2};\Xi\sigma^2 z^2\big/(2\sigma_{I_p}^2 + JL\Xi\sigma^2)) + j\cdot 3\,z\sigma\sqrt{\pi\Xi\big/(2\sigma_{I_p}^2 + JL\Xi\sigma^2)}\Big/2\cdot$$

$${}_1F_1(-1;\tfrac{3}{2};\Xi\sigma^2 z^2\big/(2\sigma_{I_p}^2 + JL\Xi\sigma^2))\Big]^{JL} z^{-1}\Big\}, \tag{3.40}$$

and N_p is the order of the Hermite polynomial, and we found that $N_p = 20$ is sufficient for good accuracy. x_m is the m^{th} zero of the $N_p{}^{\text{th}}$ order Hermite polynomial, and H_{x_m} are the weight factors given by

$$H_{x_m} = \frac{2^{N_p-1} N_p!\sqrt{\pi}}{N_p^2 H_{N_p-1}(x_m)}. \tag{3.41}$$

It is assumed that any bit can be sent via any of the P data streams with equal probability. Therefore, the system average BER if EGC scheme used is given by

$$\mathrm{P}_e^{EGC} = \frac{1}{P}\sum_{p=1}^{P}\mathrm{P}_{e,p}^{EGC}. \tag{3.42}$$

Under a guaranteed quality-of-service (QoS) requirement, the BER performance with EGC receiver has to be better than a given BER threshold $\mathrm{Ber}_{\mathrm{THR}}$. It means that the system BER performance needs to satisfy

$$\mathrm{P}_e^{EGC} \le \mathrm{Ber}_{\mathrm{THR}}. \tag{3.43}$$

We define $K_{\max}^{EGC}$ as the largest number of users that the system can accommodate while satisfying the QoS requirement (3.43), i.e.,

$$K_{\max}^{EGC} = \max\left\{K \mid \mathrm{P}_e^{EGC} \le \mathrm{Ber}_{\mathrm{THR}}\right\}. \tag{3.44}$$

The system capacity (bandwidth efficiency) if EGC is used is given by

$$\rho_{EGC} = K_{\max}^{EGC} R_b\big/B, \tag{45}$$

where $R_b = 1/T_b$ is the data rate of the system and B is the total bandwidth of the system.

3.3.2 Maximum Ratio Combining

For MRC scheme, the factors used to weight the received signal at x^{th} subcarrier of j^{th} antenna are given by

$$\alpha_{j,x,1}(2n) = \beta_{1,1,j,x} \exp(j\hat{\Phi}_{1,1,j,x}) \cdot c_{1,l}(2n),$$

$$\alpha_{j,x,2}(2n) = \beta_{1,2,j,x} \exp(-j\hat{\Phi}_{1,2,j,x}) \cdot c_{1,l}(2n+1), \tag{3.46}$$

and

$$\alpha_{j,x,1}(2n+1) = \beta_{1,2,j,x} \exp(j\hat{\Phi}_{1,2,j,x}) \cdot c_{1,l}(2n),$$

$$\alpha_{j,x,2}(2n+1) = \beta_{1,1,j,x} \exp(-j\hat{\Phi}_{1,1,j,x}) \cdot c_{1,l}(2n+1). \tag{3.47}$$

Assume a "+1" is transmitted, (3.33) becomes

$$U_p = \sum_{j=1}^{J} \sum_{l=1}^{L} \sqrt{\Xi} \cdot \beta_{1,j,x}^2 + I_p, \tag{3.48}$$

where $\beta_{1,j,x}^2 = \beta_{1,1,j,x}^2 + \beta_{1,2,j,x}^2$, and similarly, $\hat{\Phi}_{1,i,j,x}$ can be obtained by using a carrier synchronizer. The variance of the total interference I_p can be written as

$$\sigma_{I_p}^2 = \sum_{j=1}^{J} \sum_{l=1}^{L} A_{l,p} \beta_{1,j,x}^2 \tag{3.49}$$

where $A_{l,p}$ is the interference coefficient at the l^{th} subcarrier of p^{th} data stream, which is given by

$$A_{l,p} = A_{SO,l,p} + A_{MS,l,p} + A_{MO,l,p} + N_0/2T_s \ . \tag{3.50}$$

The variances of the respective terms in (3.50) have been given in (3.24), (3.25) and (3.26). The conditional signal-to-interference and noise ratio (SINR) is therefore defined as

$$\gamma_p = \frac{\Xi \cdot \left(\sum_{j=1}^{J} \sum_{l=1}^{L} (\beta_{1,1,j,x}^2 + \beta_{1,2,j,x}^2) \right)^2}{2 \sum_{j=1}^{J} \sum_{l=1}^{L} A_{l,p} (\beta_{1,1,j,x}^2 + \beta_{1,2,j,x}^2)}. \tag{3.51}$$

The BER for the p^{th} data stream conditioned on $\{\beta_{1,i,j,x}$, $i=1,2$, $j=1,\cdots,J$, $x=p+(l-1)P$, $l=1,\cdots,L\}$ is given by

$$\mathrm{P}_{e,p|\{\beta_{1,i,j,x}\}} = Q(\sqrt{2\gamma_p}) . \tag{3.52}$$

The BER for p^{th} data stream is obtained via averaging over $\{\beta_{1,i,j,x}$, $i=1,2$, $j=1,\cdots,J$, $x=p+(l-1)P$, $l=1,\cdots,L\}$,

$$\mathrm{P}_{e,p}^{MRC} = \int_0^\infty \int_0^\infty \cdots \int_0^\infty \ \mathrm{P}_{e,p|\{\beta_{1,i,j,x}\}} f(\beta_{1,1,1,1}) \cdots f(\beta_{1,2,J,p+(L-1)P}) \,\mathrm{d}\,\beta_{1,1,1,1} \cdots \mathrm{d}\,\beta_{1,2,J,p+(L-1)P} \tag{3.53}$$

where $f(\beta_{1,i,j,x})$ is the probability density function (PDF) for RV $\beta_{1,i,j,x}$. It can be seen that (3.53) involves computing the complicated $2JL$-dimensional integrations. To avoid such complexity in computing the BER, an approximate approach is proposed in this section.

In the following, we first introduce a lemma, and then use it to simplify the expression given in (3.51). The conditions for such approximation to be valid are also stated. The theoretical justification on these conditions is presented in the Appendix.

Lemma 1*:* Given v_l $(l=1,2,\cdots,L)$ are positive independent and identical distributed (i.i.d.) random variables (RVs) with mean μ_v and variance σ_v^2, and w_l $(l=1,2,\cdots,L)$ are positive i.i.d. RVs with mean $\mu_w=\lambda\Omega$ and variance $\sigma_w^2=\lambda\Omega^2$, where $\lambda >> 1/L$, $\Omega > 0$. Then it can be shown that

$$\sum_{l=1}^{L} v_l w_l \approx \mu_v \sum_{l=1}^{L} w_l \ . \tag{3.54}$$

The conditions for the approximation in (3.54) to be held is given by

$$\text{(i)} \qquad L \ge \max\left\{ \left[Q^{-1}(1-\kappa)\right]^2 \cdot \left[\frac{\sigma_v^2}{\mu_v^2} + \frac{1}{\lambda}(1+\frac{\sigma_v^2}{\mu_v^2})\right] + \frac{2}{\lambda}, \quad 23 \right\}, \tag{3.54a}$$

(ii) $$\frac{\sigma_v}{\mu_v} \le \zeta(2\pi L)^{1/4} \cdot \left(\frac{\lambda^2}{\lambda^2+\lambda}\right)^{1/2} \tag{3.54b}$$

where κ is the level of inaccuracy to be defined in Appendix 3.B, ζ is the desired bound of the normalized standard deviation for z to be defined in (3.B.20) of Appendix 3.B. The correctness of this lemma is also verified through simulations by arbitrarily choosing some probability density functions with appropriate values of mean and variance.

Since $\beta_{1,1,j,x}$ and $\beta_{1,2,j,x}$ are independent Rayleigh RVs with $E\{\beta_{1,i,j,x}^2\} = \sigma^2$, $i = 1, 2$, $\beta_{1,j,x}^2 = \beta_{1,1,j,x}^2 + \beta_{1,2,j,x}^2$ can be shown to be Gamma distributed [105]. The mean and variance are given by

$$\mu_\beta = 2\sigma^2 \ , \quad \sigma_\beta^2 = 2\sigma^4 . \tag{3.55}$$

Denote $\mu_{A,p} = \sum_{l=1}^{L} A_{l,p} / L$ and $\sigma_{A,p}^2 = \sum_{l=1}^{L} (A_{l,p} - \mu_{A,p})^2 / L$ as the mean and the variance of the interference coefficients $A_{l,p}$ $(\forall l \in \{1, \cdots L\})$, we show in Appendix 3.C that for all values of $\varepsilon_1 \le 1$,

$$\sigma_{A,p} \big/ \mu_{A,p} \le 0.125 , \quad p = 1,2,\cdots,P \tag{3.56}$$

when $L \ge 32$. We show in Appendix 3.B that by applying $v_l = A_{l,p}$, $w_l = \beta_{1,j,x}^2$ $(l = 1,2,\cdots,L)$, $\lambda = 2$, $\Omega = \sigma^2$ to *Lemma* 1, the two conditions given by (3.54a) and (3.54b) are both satisfied. Under this circumstance, the variance of I_p in (3.49) can be approximated by

$$\sigma_{I_p}^2 \approx \mu_{A,p} \sum_{j=1}^{J} \sum_{l=1}^{L} \beta_{1,j,x}^2 . \tag{3.57}$$

Then the conditional SINR for p^{th} data stream can be simplified as

$$\gamma_p \approx \frac{\Xi}{2\mu_{A,p}} \sum_{j=1}^{J} \sum_{l=1}^{L} (\beta_{1,1,j,x}^2 + \beta_{1,2,j,x}^2) \tag{3.58}$$

To simplify the notation, (3.58) can be written as

$$\gamma_p \approx \frac{\Xi}{2\mu_{A,p}} \sum_{m=1}^{2JL} \beta_m^2 \tag{3.59}$$

where { β_m , $m = 1, 2, \cdots, 2JL$ } denotes { $\beta_{1,i,j,x}$, $i = 1, 2$, $j = 1,2,\cdots,J$, $x = l + (p-1)P$, $l = 1,2,\cdots,L$ }, hereafter. Then the approximate BER for p^{th} data stream is given by

$$\mathrm{P}_{e,p}^{MRC} \approx \int_0^{\infty} Q(\sqrt{2\gamma_p}) f_{\gamma_p}(\gamma_p) d\gamma_p \tag{3.60}$$

where $f_{\gamma_p}(\gamma_p)$ is PDF for RV γ_p, which can be given by [104]

$$f_{\gamma_p}(\gamma_p) = \frac{1}{(2JL-1)!\,\bar{\gamma}_{c,p}^{2JL}} \gamma_p^{2JL-1} \exp(-\gamma_p / \bar{\gamma}_{c,p}) \tag{3.61}$$

where $\bar{\gamma}_{c,p} = \Xi\sigma^2 / 2\mu_{A,p}$. Therefore, the closed form expression of BER for the p^{th} data stream is given by [104]

$$\mathrm{P}_{e,p}^{MRC} \approx \left[(1-u_p)/2\right]^{2JL} \sum_{m=0}^{2JL-1} \binom{2JL-1+m}{m} \left[(1+u_p)/2\right]^m \tag{3.62}$$

where $u_p = \sqrt{\bar{\gamma}_{c,p} / (1+\bar{\gamma}_{c,p})}$. It is assumed that any bit can be sent via any of the P data streams with equal probability. Therefore, the system average BER if MRC scheme is used is given by

$$\mathrm{P}_e^{MRC} = \frac{1}{P} \sum_{p=1}^{P} \mathrm{P}_{e,p}^{MRC} \ . \tag{3.63}$$

It can be seen that it will be much easier to use the closed form expression (3.62) rather than (3.53) to obtain the BER performance for MRC receiver.

Similarly, the BER performance with MRC receiver has to be better than the given BER threshold $\mathrm{Ber}_{\mathrm{THR}}$ to satisfy the QOS requirement. It means that the system performance is required to satisfy

$$\mathrm{P}_e^{MRC} \le \mathrm{Ber}_{\mathrm{THR}}\,. \tag{3.64}$$

Similarly, we define $K_{\max}^{MRC}$ as the largest number of users fulfils the QoS requirement if MRC is used.

$$K_{\max}^{MRC} = \max\left\{K \mid \mathrm{P}_e^{MRC} \le \mathrm{Ber}_{\mathrm{THR}}\right\}. \tag{3.65}$$

Therefore, the system capacity (bandwidth efficiency) if MRC is used can be obtained by

$$\rho_{MRC} = K_{\max}^{MRC} R_b \big/ B\,. \tag{3.66}$$

3.4 Numerical Results

The effect of CFO on BER performance and system capacity for asynchronous STBC MC-CDMA systems can be easily obtained by using (3.42), (3.45) and (3.63), (3.66). The results obtained are also compared with the conventional MC-CDMA systems [102]. For comparison, BPSK is used and the total system bandwidth and fading channel statistics for all subcarriers are chosen to be the same. The BER threshold $\mathrm{Ber}_{\mathrm{THR}}$ is set to 10^{-3} to satisfy the QoS requirement. The symbol energy is defined as $E_s = LST_s$. The normalized CFO is set to ε_1 for desired user 1 and ε_k for k^{th} user which is assumed to be uniformly distributed over $[0, \varepsilon_1)$. The simulation results are obtained by taking average over 500 sets of uniformly distributed random ε_k $(k = 2, \cdots K)$ for each given value of ε_1. In the following numerical results, the BER performance and system capacity of (i) MC-CDMA systems with 1 transmitter and 1 receiver, (ii) STBC MC-CDMA systems with 2 transmitters and 1 receiver, and (iii) STBC MC-CDMA systems with 2 transmitters and 2 receivers are investigated.

Fig. 3.2 and Fig. 3.3 show the BER performance and system capacity as a function of the normalized CFO ε_1 when E_s / N_0 =20dB, and with the number of data streams P is set to 1. The ratio L/K is kept at a constant for fair comparison when L increases. It can be found that the BER performance and system capacity remains almost the same when ε_1 is less than 0.01 for the three systems. When ε_1 is between 0.01 and 0.1, the system performance degrades very slightly since MUI is the main impairment source and results in the error floor. Hence, maintaining CFO within this range is already sufficient in transceiver design. When ε_1 is larger than 0.1, BER performance and system capacity deteriorate severely. The performance of MC-CDMA systems obtained by using our expressions are in good agreement with [66] where the fading correlation coefficients between neighboring subcarriers is equal to 0.26. In general, the performance and system capacity of STBC MC-CDMA systems with 2 transmitters and 1 receiver are only slightly better than that of MC-CDMA systems despite of the diversity combining schemes applied. On the other hand, the BER performance and system capacity of STBC MC-CDMA systems with 2 transmitters and 2 receivers are much better than that of previous two systems despite of the diversity combining schemes used. The system capacity is about 1.5~2 times higher than that of MC-CDMA systems. Besides, the computed BER results using our proposed analysis well agree with the results obtained from our simulations. This verifies the correctness and effectiveness of our analysis for both the asynchronous STBC MC-CDMA and MC-CDMA systems with either EGC or MRC receivers. It can be also found that MRC receivers outperform EGC receivers in the presence of CFO for these three asynchronous systems.

Fig. 3.4 shows BER versus the number of parallel data streams P given $L = 32$, $K = 8$ and E_s / N_0 =20dB. In the case if $P > 1$, the results we obtained are almost the same as that of $P = 1$ due to the assumption that fading processes of a given user on different subcarriers are independent each other, and the slight change is due to the slight different in the interference. However, the introduction of P is necessary in practice because through properly choosing the value of P, it can be guaranteed that all subcarriers used by a given user undergo flat fading, since the symbol duration over subcarriers used by a particular user will be increased by P times.

Fig. 3.5 shows the BER performance versus E_s / N_0 given $L = 32$, $K = 8$ and $P = 1$. And Fig. 3.6 shows the system capacity versus E_s / N_0 given $L = 32$ and $P = 1$. It can be observed that the BER performance and system capacity improved gradually as E_s / N_0 increases when ε_1 is small. And BER performance and system capacity remain almost the same when E_s / N_0 is greater than 20dB. For large ε_1, the BER performance and system capacity degraded dramatically.

Fig. 3.7 shows the BER performance versus the number of users when E_s / N_0=20dB, L=32 and $P = 1$. It can be seen that BER degrades gradually as K increases when ε_1 is small. For large ε_1, BER has already been large even for small number of users.

3.5 Conclusion

The BER performance and system capacity of asynchronous STBC MC-CDMA systems in the presence of CFO are theoretically analyzed in this chapter. A closed form BER expression is obtained for EGC receiver, and an expression to estimate the BER for MRC receiver is also derived. These expressions are verified through simulations. The BER performance and system capacity degrade significantly as the normalized CFO is larger than 0.1 but remain nearly the same when the normalized CFO is less than 0.1. Our results show that the performance and system capacity of STBC MC-CDMA systems are better than that of MC-CDMA systems without ST coding, regardless of the diversity combining schemes used. STBC MC-CDMA systems with two receive antennas will obtain 1.5~2 times higher in system capacity.

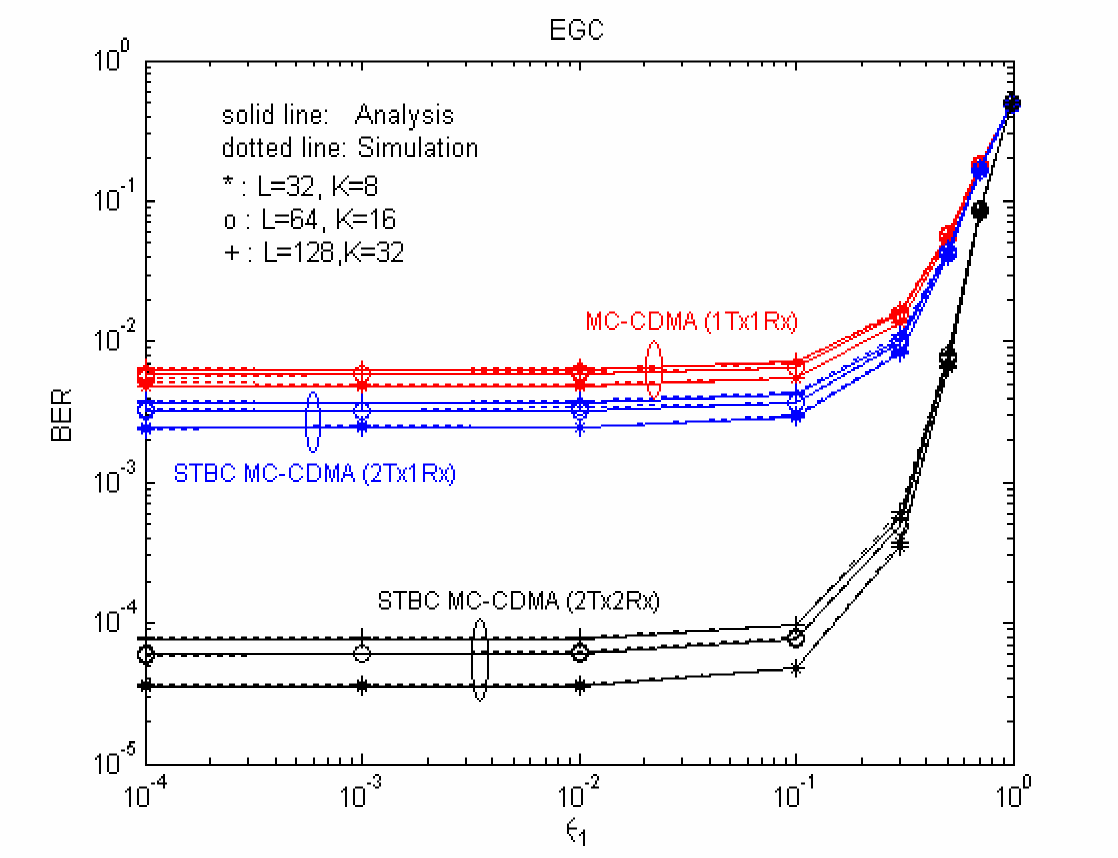

(a)

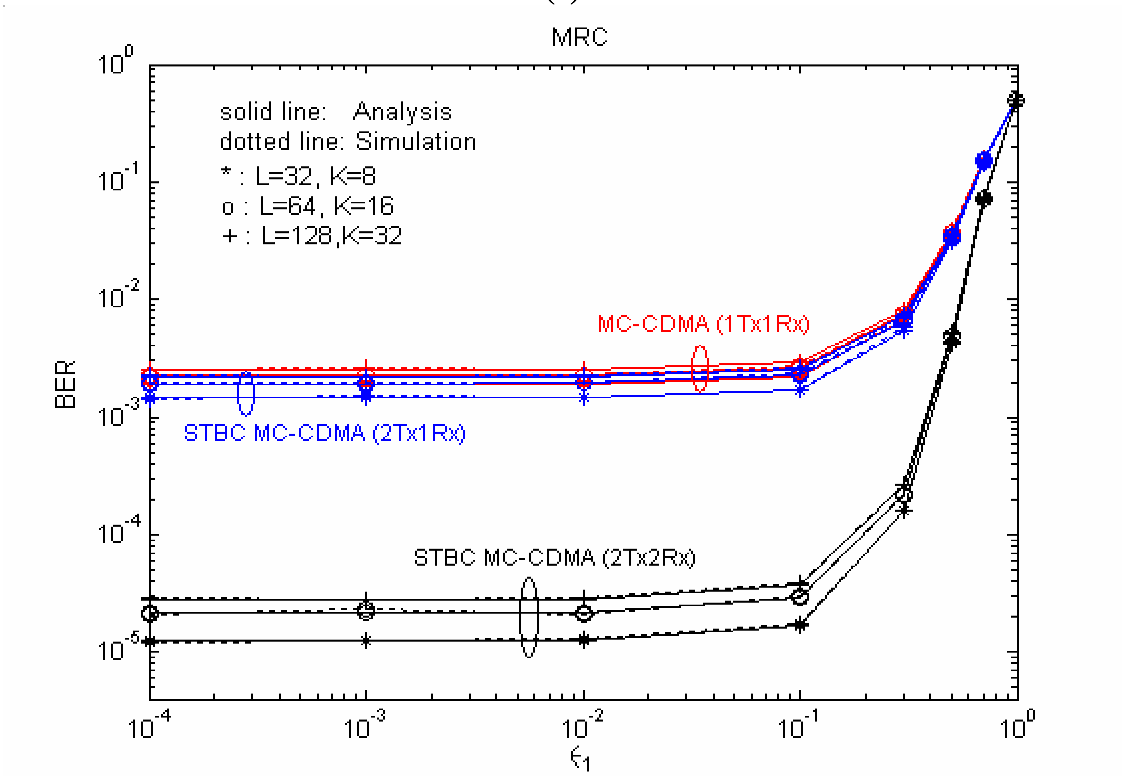

(b)

Fig. 3.2 BER versus normalized carrier frequency offset ε_1 (a) EGC and (b) MRC

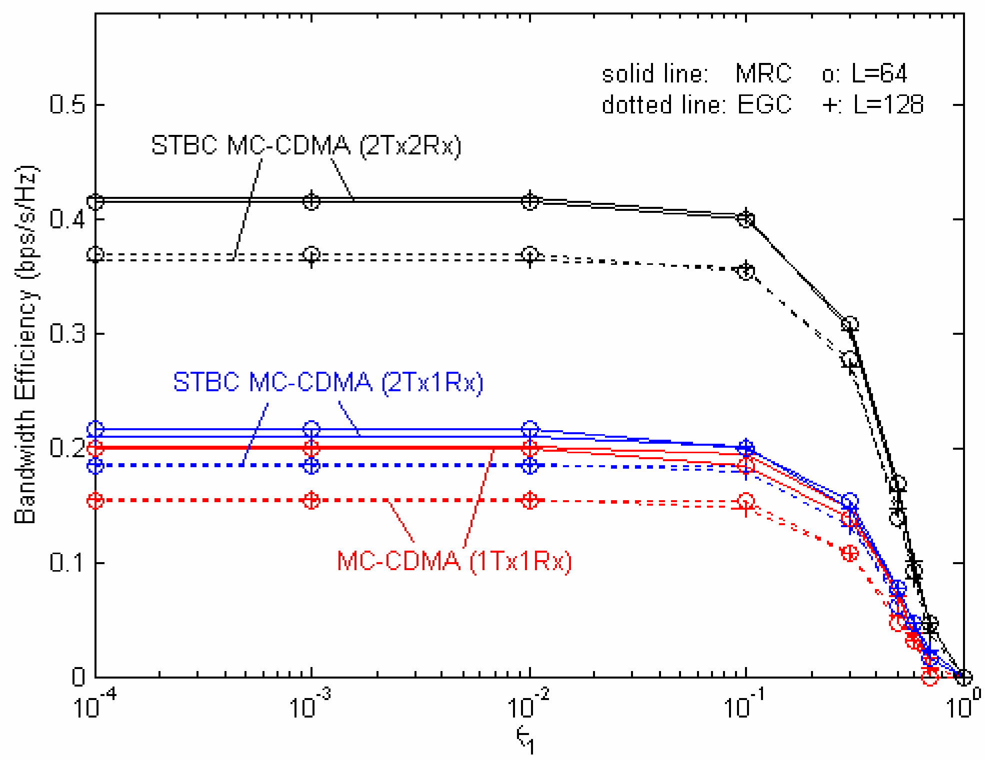

Fig. 3.3 System capacity versus normalized carrier frequency ε_1

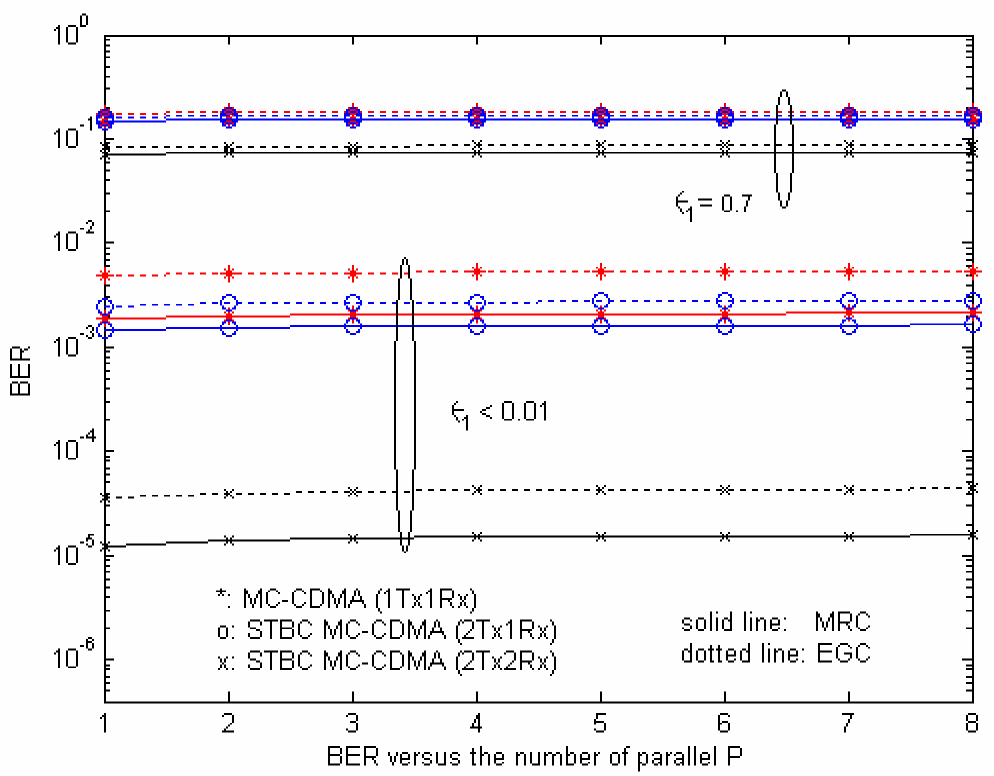

Fig. 3.4 BER versus the number of parallel data streams P

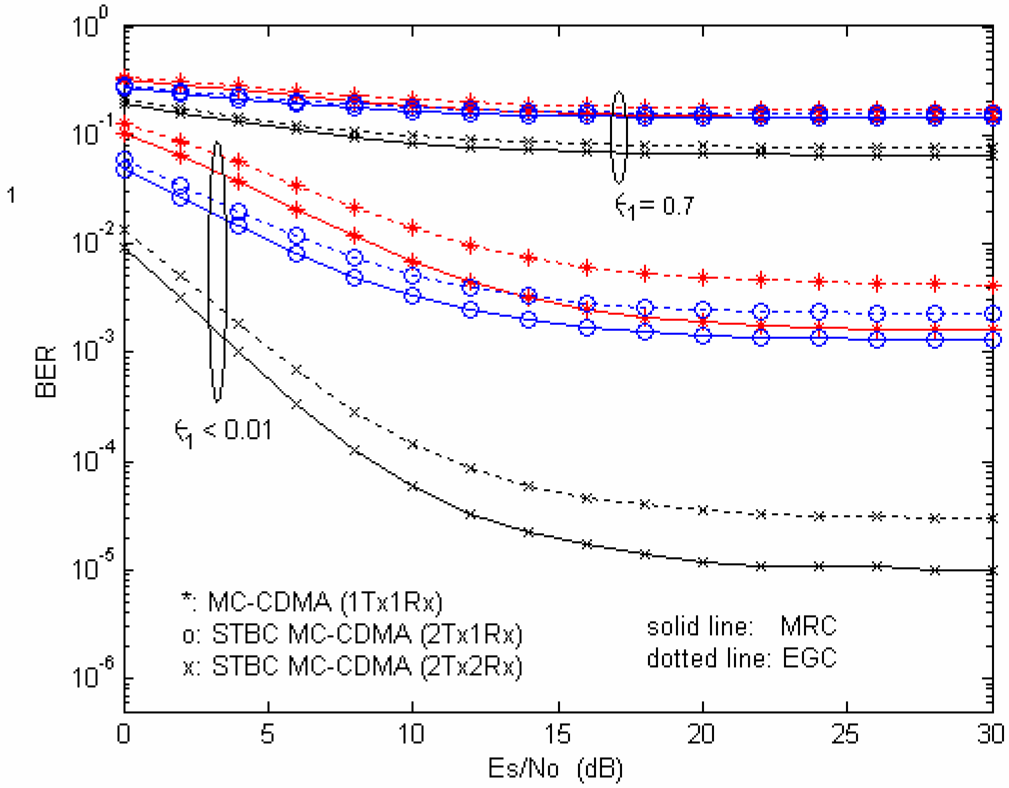

Fig. 3.5 BER versus *Es/No* dB

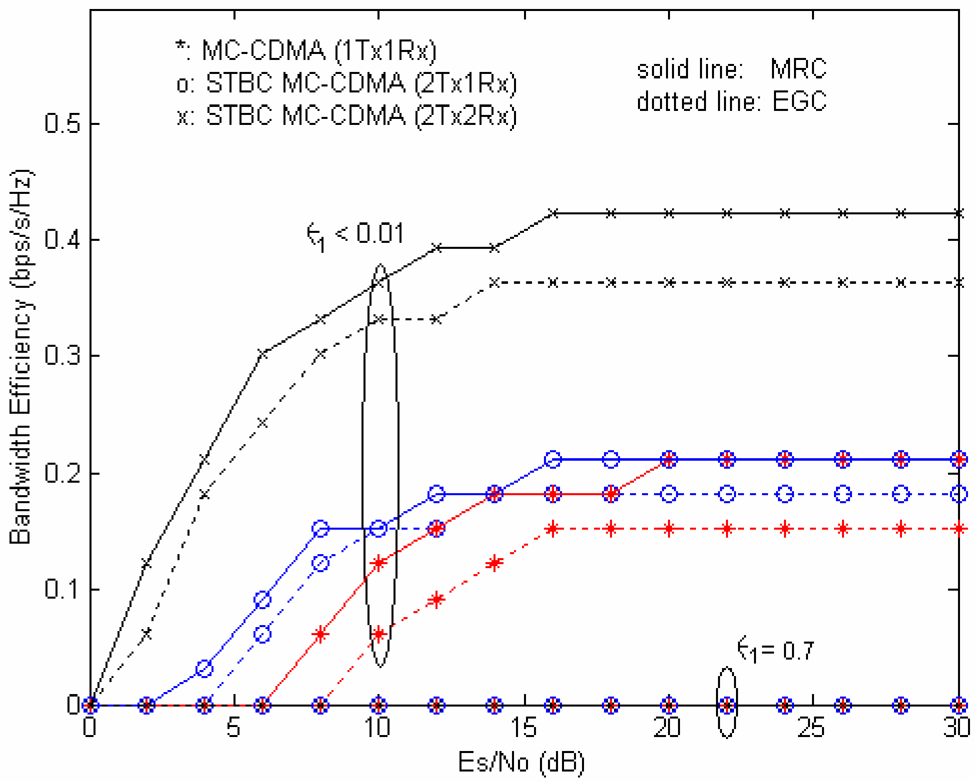

Fig. 3.6 System capacity versus *Es/No* dB

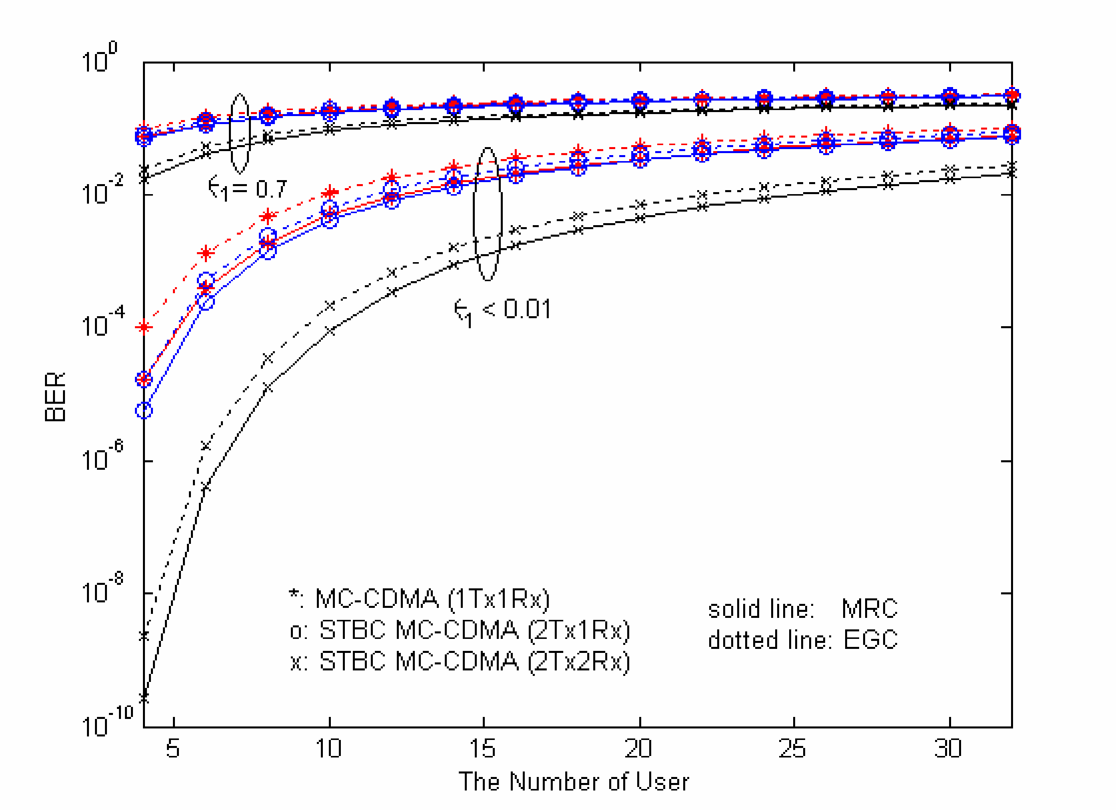

Fig. 3.7 BER versus the number of users

Appendix 3.A

Proposition 1: X_i $(i = 1,2,\cdots,L)$ are positive i.i.d. RVs with mean μ_x and variance σ_x^2. Let $Y = \sum_{i=1}^{L} X_i$, then by central limit theorem (CLT), for large *L*, *Y* can be approximated by a Gaussian RV with mean $L\mu_x$ and variance $L\sigma_x^2$. The PDF of RV *Y* is given by

$$f_Y(y) = \frac{1}{\sqrt{2\pi L}\sigma_x} \exp\left[-\frac{(y - L\mu_x)^2}{2L\sigma_x^2}\right] \quad -\infty < y < \infty . \tag{3.A.1}$$

However, since *Y* is a positive RV, inaccuracy occurs by assuming that *Y* follows a Gaussian distributed RV because $\int_{-\infty}^{0} f_Y(y) \neq 0$. Denote

$$\Theta(L, \kappa) = \mathrm{P}(Y \le 0) = 1 - Q\left(-\sqrt{L}\,\frac{\mu_x}{\sigma_x}\right) \le \kappa , \tag{3.A.2}$$

we define κ as *the level of inaccuracy* when applying CLT. This means that a small amount of inaccuracy exists to positive RVs when applying CLT. κ is a small value, and ideally $\kappa \to 0$ as $L \to \infty$. $Q(x) = \int_x^{\infty} \frac{1}{\sqrt{2\pi}} \exp(-x^2/2)dx$ represents the Gaussian cumulative function. Conversely, to guarantee a given level of accuracy κ, it is required that

$$L > \left[Q^{-1}(1-\kappa)\right]^2 \sigma_x^2 \big/ \mu_x^2 , \tag{3.A.3}$$

Lemma 2: X_i $(i = 1,2,\cdots,L)$ are positive i.i.d. RVs with mean μ_x and variance σ_x^2. Let $Y = \sum_{i=1}^{L} X_i$, for arbitrary δ, where $\delta << L$, it can be shown that Y/μ_x will always greater than δ with a level of inaccuracy κ if

$$L > \left[Q^{-1}(1-\kappa)\right]^2 \sigma_x^2 \big/ \mu_x^2 \; + \; 2\delta . \tag{3.A.4}$$

Proof: Since Y/μ_x can be approximated as a Gaussian RV with mean L and variance $L\sigma_x^2 / \mu_x^2$, then

$$P\left(\frac{Y}{\mu_x} \le \delta\right) = 1 - Q\left(\frac{\delta - L}{\sqrt{L}\sigma_x/\mu_x}\right) < 1 - Q\left(-\mu_x\sqrt{L-2\delta} / \sigma_x\right) = \Theta(L-2\delta,\kappa) \le \kappa\,,$$

(3.A.5)

where $\Theta(\cdot)$ is the level of inaccuracy when applying CLT defined in (3.A.2). By *Proposition* 1, κ is negligibly small when L is large. Conversely, given κ, we can lead to (3.A.4).

Appendix 3.B

In this appendix, we shall prove *Lamma* 1 stated in the main text. Define a RV as

$$z = \frac{X_1}{X_2} = \left(\sum_{l=1}^{L} v_l w_l - \mu_v \sum_{l=1}^{L} w_l\right) \Bigg/ \sum_{l=1}^{L} v_l w_l \ , \tag{3.B.1}$$

where $X_1 = \sum_{l=1}^{L} v_l w_l - \mu_v \sum_{l=1}^{L} w_l$, $X_2 = \sum_{l=1}^{L} v_l w_l$. In the following, the objective is to verify that $z \approx 0$ if both the mean and variance of z can be shown to be or approximately equal to zero under the two specific conditions given in (3.54a) and (3.54b).

By CLT, for large L, X_1 and X_2 can be approximated as Gaussian RVs with mean μ_1, μ_2 and variance σ_1^2, σ_2^2, respectively. Since v_l, w_l $(l = 1,2,\cdots,L)$ are i.i.d. RVs, the mean and variance of X_1 can be computed to be

$$\mu_1 = E\{X_1\} = L(\mu_v\mu_w) - u_v(L\mu_w) = 0\,, \tag{3.B.2}$$

$$\sigma_1^2 = E\{X_1^2\} = L\sigma_v^2(\mu_w^2 + \sigma_w^2)^2\,. \tag{3.B.3}$$

Similarly the mean and variance of X_2 can be easily found as

$$\mu_2 = E\{X_2\} = L\mu_v\mu_w, \tag{3.B.4}$$

$$\sigma_2^2 = E\{X_2^2\} - \mu_2^2 = L\sigma_v^2(\mu_w^2 + \sigma_w^2) + L\mu_v^2\sigma_w^2. \tag{3.B.5}$$

The covariance of X_1 and X_2 is given by

$$\mu_{12} = E\{X_1X_2) - \mu_1\mu_2 = L\sigma_v^2(\mu_w^2 + \sigma_w^2). \tag{3.B.6}$$

To obtain the mean and variance of RV z, we first obtain its PDF. Since X_1 and X_2 are Gaussian RVs, the joint PDF is given by

$$f_{X_1X_2}(x_1,x_2) = \exp\left[-[\underline{x}-\underline{\mu}]^T \underline{\underline{\xi}}^{-1}[\underline{x}-\underline{\mu}]/2\right] \Big/ \left[2\pi\sqrt{\left|\underline{\underline{\xi}}\right|}\right] \tag{3.B.7}$$

where $\underline{x} = [x_1 \quad x_2]^T$, $\underline{\mu} = [\mu_1 \quad \mu_2]^T$ and $\underline{\underline{\xi}} = \begin{bmatrix} \sigma_1^2 & \mu_{12} \\ \mu_{12} & \sigma_2^2 \end{bmatrix}$ with $\left|\underline{\underline{\xi}}\right|$ represents its determinant. As $\mu_1 = 0$,

$$f_{X_1X_2}(x_1,x_2) = \exp\left[-\left(\sigma_2^2x_1^2 + \sigma_1^2(x_2-\mu_2)^2\right)\Big/2\left|\underline{\underline{\xi}}\right|\right] \Big/ \left[2\pi\sqrt{\left|\underline{\underline{\xi}}\right|}\right]. \tag{3.B.8}$$

Since $z = X_1/X_2$, then the PDF of z is given by

$$f_z(z) = \int_{-\infty}^{\infty} x_2 f_{X_1X_2}(x_2z, x_2)dx_2 \ . \tag{3.B.9}$$

The mean of RV z is given by

$$\mu_z = E\{z\} = \int_{-\infty}^{\infty} zf_z(z)dz = \int_{-\infty}^{\infty} z\int_{-\infty}^{\infty} x_2 f_{X_1X_2}(x_2z,x_2)dx_2dz$$

$$= \int_0^{\infty} x_2 \exp\left[-\sigma_1^2(x_2-\mu_2)^2\Big/2\left|\underline{\underline{\xi}}\right|\right]\cdot T(x_2)dx_2 \Big/ \left[2\pi\sqrt{\left|\underline{\underline{\xi}}\right|}\right]$$

$$= 0 \tag{3.B.10}$$

since $T(x_2) = \int_{-\infty}^{\infty} z\exp\left[-\sigma_2^2x_2^2z^2\Big/2\left|\underline{\underline{\xi}}\right|\right]dz = 0$. The variance of z is given by

$$\sigma_z^2 = E\{z^2\} = \int_{-\infty}^{\infty} z^2 f_z(z)dz = \int_{-\infty}^{\infty} z^2\int_{-\infty}^{\infty} x_2 f_{X_1X_2}(x_2z,x_2)dx_2dz$$

$$= \int_{-\infty}^{\infty} x_2 \exp\left[-\sigma_1^2 (x_2 - \mu_2)^2 \Big/ 2\left|\underline{\underline{\xi}}\right|\right] \cdot J(x_2) dx_2 \Bigg/ \left[2\pi \sqrt{\left|\underline{\underline{\xi}}\right|}\right]$$

(3.B.11)

and can be shown that [108]

$$J(x_2) = \int_{-\infty}^{\infty} z^2 \exp\left[-\sigma_2^2 x_2^2 z^2 \Big/ 2\left|\underline{\underline{\xi}}\right|\right] dz = \frac{\sqrt{2\pi\left|\underline{\underline{\xi}}\right|^3}}{\sigma_2^3} \cdot \frac{1}{x_2^3} \quad . \tag{3.B.12}$$

Substitute (3.B.12) in (3.B.11), we have

$$\sigma_z^2 = \left|\underline{\underline{\xi}}\right| R \Big/ \left[\sqrt{2\pi}\sigma_2^3\right], \tag{3.B.13}$$

where

$$R = \int_{-\infty}^{\infty} \frac{1}{x_2^2} \exp\left[-\sigma_1^2 (x_2 - \mu_2)^2 \Big/ 2\left|\underline{\underline{\xi}}\right|\right] dx_2 \,. \tag{3.B.14}$$

Substitute (3.B.2)-(3.B.6) into (3.B.14), (3.B.14) can be rewritten as

$$R = \frac{1}{\mu_v \Omega} \int_{-\infty}^{\infty} \frac{\mu_v^2 \Omega^2}{x_2^2} \exp\left[-(\frac{x_2}{\mu_v \Omega} - L\lambda)^2 \Big/ 2L\lambda\right] d\,\frac{x_2}{\mu_v \Omega} . \tag{3.B.15}$$

We shall now estimate an upper bound for (3.B.15). Again X_2 in (3.B.1) is approximately Gaussian distributed and our objective is to have X_2 greater than some positive number. Applying *Lemma* 2 with $\delta = 1/\lambda$ and $\delta << L$ (conversely $\lambda >> 1/L$), $X_2 / \mu_v \lambda \Omega$ will always be greater than $1/\lambda$ for a given *level of inaccuracy* κ under the condition

$$L > \left[Q^{-1}(1-\kappa)\right]^2 \cdot \left[\frac{\sigma_v^2}{\mu_v^2} + \frac{1}{\lambda}(1 + \frac{\sigma_v^2}{\mu_v^2})\right] + \frac{2}{\lambda} \quad . \tag{3.B.16}$$

Then (3.B.15) can be evaluated by letting $Y = X_2 / \mu_v \Omega$ and expressed as

$$R = \frac{1}{\mu_v \Omega} \int_1^{\infty} \frac{1}{y^2} \exp\left[-(y - L\lambda)^2 / 2L\lambda\right] dy \,. \tag{3.B.17}$$

It can be verified that

$$R < \frac{1}{\mu_v \Omega L \lambda^{3/2}} \quad \text{when} \quad L \geq 23 \ . \tag{3.B. 18}$$

Combine (3.B.16) and (3.B.18) will give condition (3.54a). Substitute (3.B.18) in (3.B.13), we obtain

$$\sigma_z^2 \leq \frac{\left|\underline{\underline{\xi}}\right|}{\sqrt{2\pi}\sigma_2^3} \cdot \frac{1}{\mu_v \Omega L \lambda^{3/2}} = \frac{\sigma_1^2\sigma_2^2 - \mu_{12}^2}{\sqrt{2\pi} L \mu_v \Omega \lambda^{3/2} \sigma_2^3} \ . \tag{3.B.19}$$

Substitute (3.B.2) to (3.B.6) in (3.B.19)

$$\sigma_z^2 \leq \frac{1}{\sqrt{2\pi L}} \cdot \frac{\mu_v \sigma_v^2 \sigma_w^2 (\mu_w^2 + \sigma_w^2)}{\Omega \lambda^{3/2} \left[\mu_v^2 \sigma_w^2 + \sigma_v^2 (\mu_w^2 + \sigma_w^2)\right]^{3/2}}$$

$$< \frac{1}{\sqrt{2\pi L}} \cdot \frac{\sigma_v^2}{\mu_v^2} \cdot \frac{\lambda^2 + \lambda}{\lambda^2} \leq \zeta^2 , \tag{3.B.20}$$

where ζ is the desired bound of the standard deviation of z that we want to define. For a given ζ, it is required that

$$\frac{\sigma_v}{\mu_v} \leq \zeta (2\pi L)^{1/4} \cdot \left(\frac{\lambda^2}{\lambda^2 + \lambda} \right)^{1/2} , \tag{3.B.21}$$

which gives the condition (3.54b).

When L is large, $\zeta \to 0$ and $\sigma_z^2 \to 0$. Hence, for large L, the RV z has zero mean and zero variance or $z \approx 0$. It means that (3.54) holds under the conditions (3.54a) and (3.54b) for a predefined κ and ζ.

In particular, when $\lambda = 2$, with the upper bound of the normalized standard deviation $\zeta = 4.1\%$, and the level of inaccuracy of applying CLT is defined at $\kappa = 10^{-14}$, then the conditions given in (3.54a) and (3.54b) can be computed as

(i) $L \geq 32$; (3.B.22a)

(ii) $\sigma_v / \mu_v \leq 0.126$ (3.B.22b)

Appendix 3.C

Denote the mean and variance for $A_{l,p}$ which is defined in (3.50) by $\mu_{A,p} = \sum_{l=1}^{L} A_{l,p} / L$ and $\sigma^2_{A,p} = \sum_{l=1}^{L} (A_{l,p} - \mu_{A,p})^2 / L$, respectively, with L denoted the spreading gain. We define the normalized standard variance for the p^{th} data stream as $NSV_p = \sigma_{A,p} / \mu_{A,p}$ and $NSV = \max\{NSV_1, NSV_2 \cdots, NSV_P\}$. Fig. 3.8 shows the plot on NSV versus L as (a) the number of users $K = L$, (b) $K = 2$, when $P = 1$ and E_s / N_0=20dB, for various values of ε_1. It shows that NSV decreases as L increases. We purposely choose $K = L$ and $K = 2$ to over-estimate the normalized standard variance of a practical system; in general, $2 \le K \le L$. We then investigate the relationships (i) between NSV and P for a given K and E_s / N_0. For $P > 1$, the results we obtained are almost the same as that of $P = 1$ and the plot is not presented here. (ii) between NSV and K for a given L, P and E_s / N_0. Fig. 3.9 shows that there is a strictly monotonely increase as ε_1 is small or decrease as ε_1 is large in NSV. (iii) between NSV and E_s / N_0 for a given L, K, and P. Fig. 3.10 shows that when $E_s / N_0 \ge 20\text{dB}$, NSV attains a constant value and below 20dB, NSV decreases as $E_s / N_0 \ge 20\text{dB}$ decreases.

From all these observations, it can be concluded that the values of NSV shown in Fig. 3.8 give the worst case bound, Fig. 3.8 (a) gives the bound as ε_1 is small and Fig. 3.8 (b) gives the bound as ε_1 is large, for a practical range of E_s / N_0 and when $K < L$. We can use Fig. 3.8 to find whether the conditions (3.B.22a) and (3.B.22b) will be satisfied so as to apply *Lemma* 1 in the main text. For example, for all values of $\varepsilon_1 \le 1$, we need $L \ge 32$ to fulfill

$$\sigma_{A,p} / \mu_{A,p} \le 0.125 \qquad p = 1,2,\cdots,P. \tag{3.C.1}$$

Hence if we let $v_l = A_{l,p}$, the two conditions in (3.B.22a) and (3.B.22b) are satisfied from the above discussion. Similarly, if we are interested in the range where $\varepsilon_1 \leq 0.1$, then for any value of L will satisfy

$$\sigma_{A,p} / \mu_{A,p} \leq 0.06 \qquad p = 1,2,\cdots,P\,. \tag{3.C.2}$$

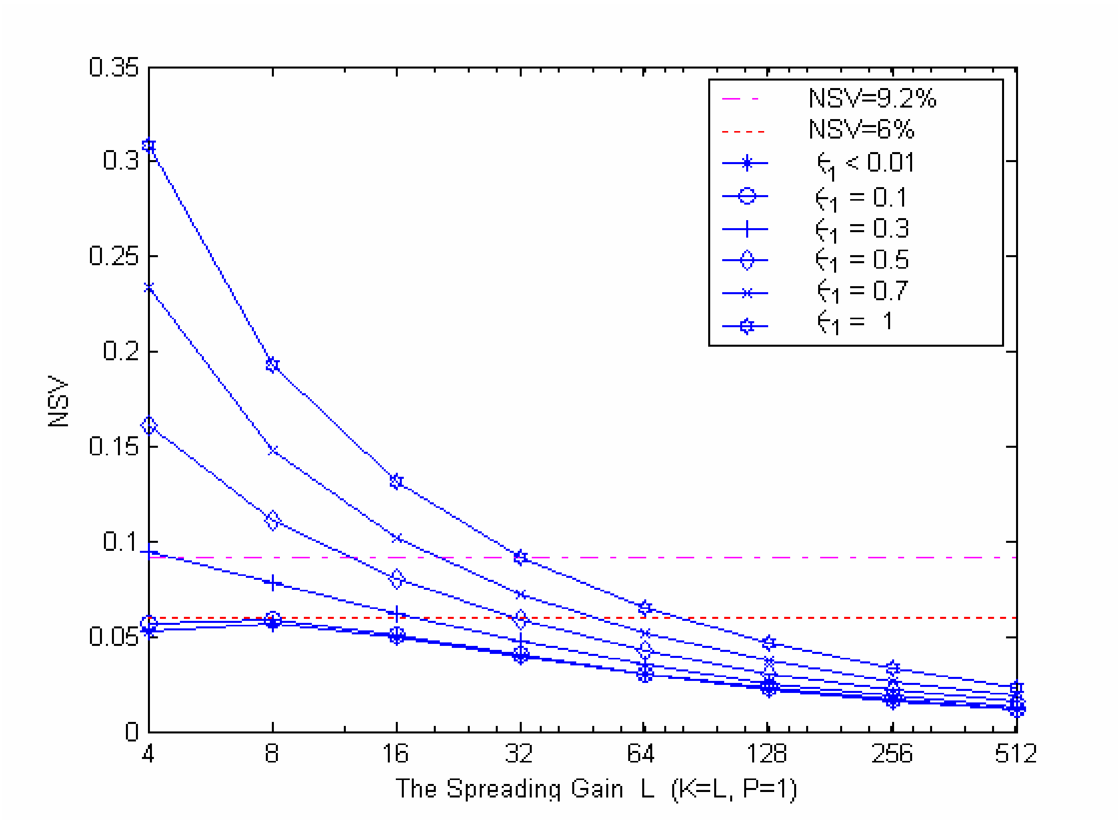

(a) $K = L$

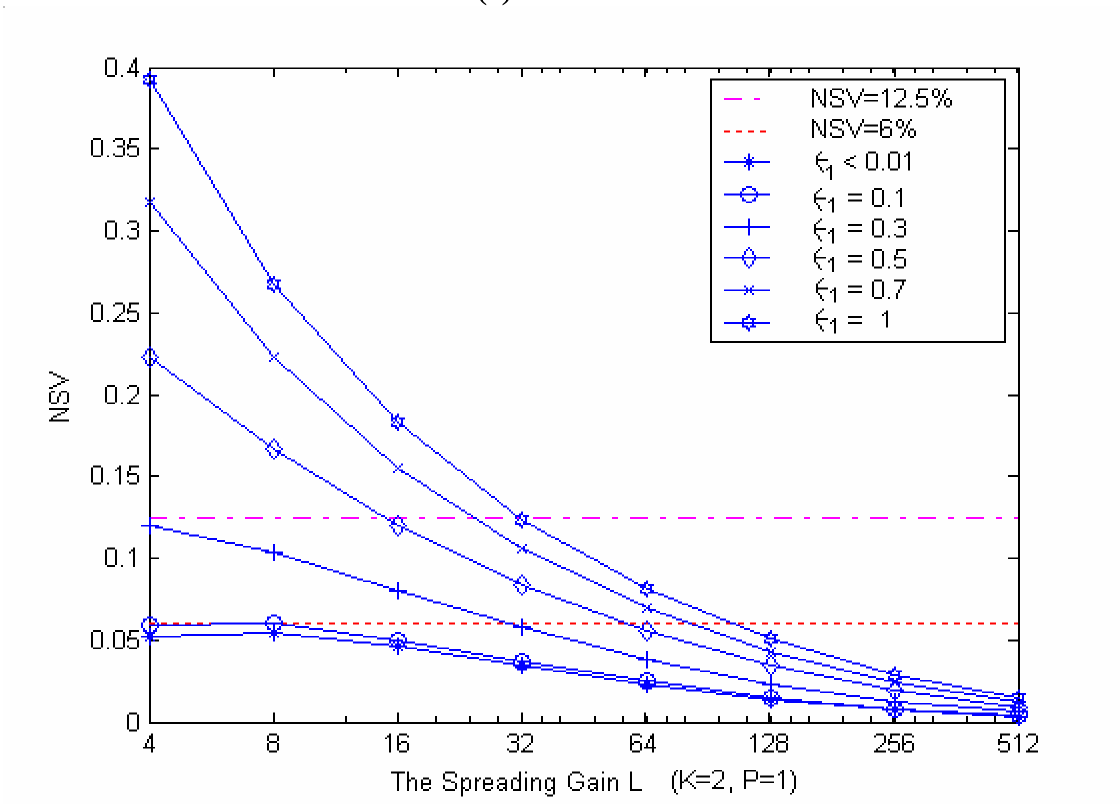

(b) $K = 2$

Fig. 3.8 NSV versus the spreading gain L

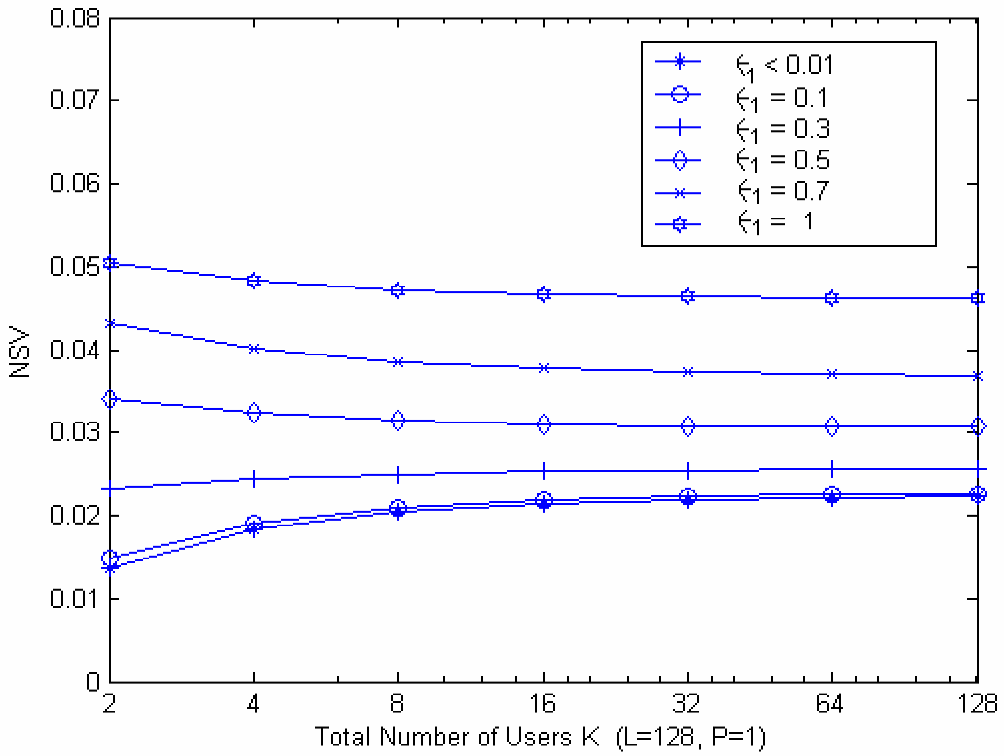

Fig. 3.9 NSV versus number of users *K*

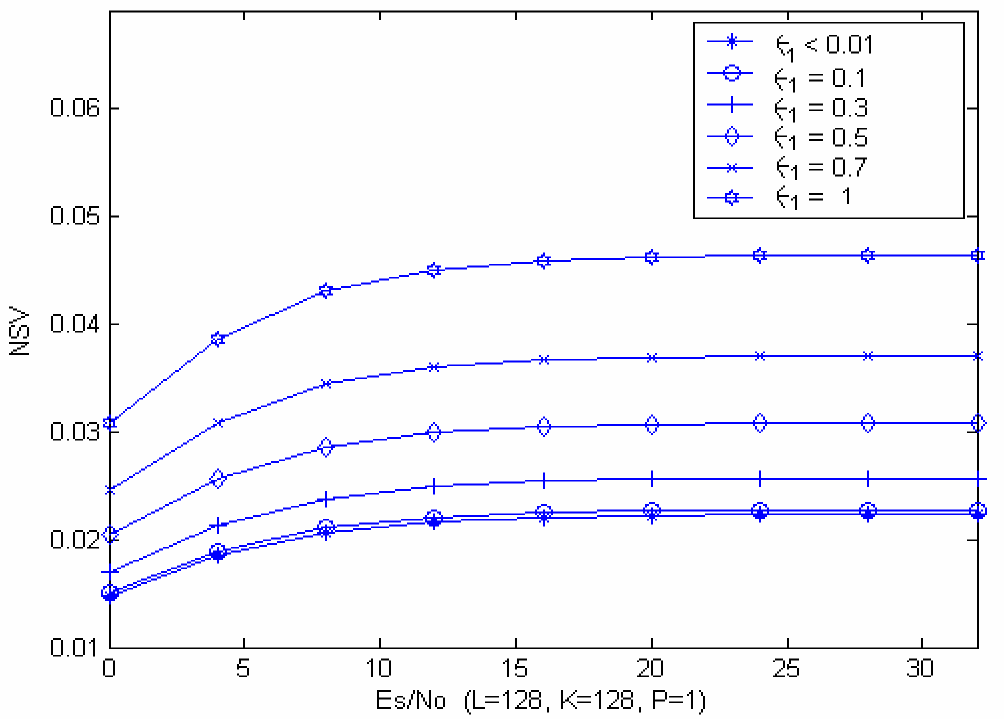

Fig. 3.10 NSV versus *Es/No*

Chapter 4

Multirate Access Schemes

In this chapter, the multicode, variable spreading gain (VSG) and spectral overlaid multiple-symbol-rate (MSR) multirate access schemes for asynchronous space-time block coded (STBC) multicarrer code division multiple access (MC-CDMA) systems are considered. The system performance and system capacity of these three multirate access schemes are investigated. Transmit power control is adjusted according to the service rates and the number of active users in each service class to maintain the link quality and to improve the system capacity. The multiple access interferences and hence the BER performance and system capacities of the three multirate access schemes for STBC MC-CDMA systems are studied. From the numerical results obtained, it can be concluded that the systems with mc access scheme when orthogonal Gold spreading sequence is applied and the VSG access scheme have similar system performance and capacity, and both perform better than the system with MSR access scheme for any spectrum configurations. In case when non-orthogonal Gold sequences are used, mc access scheme shows a degrading in the system capacity as compared to VSG, due to the presence of larger self-interference (SI) among the sequences used by each user.

The remaining of the chapter is organized as follows. The system models of mc, VSG and MSR multirate access scheme are presented in Section 4.1. The interference terms in these three multirate access schemes for STBC MC-CDMA systems are given in Section 4.2. Then Section 4.3 presents the BER performance analysis. The transmit power control and system capacity for the multirate STBC MC-CDMA systems are given in section 4.4. Numerical results are presented and discussed in Section 4.5. The conclusion is finally given in Section 4.6.

4.1 System Model

An asynchronous multirate STBC MC-CDMA system with K users over frequency selective Rayleigh fading channels is considered. Fig. 4.1 shows the transmitter diagram of multirate STBC MC-CDMA systems. Assume that the system supports M different data rates and there are K_m users in the mth class, each transmits at a data rate of R_m, where $K = \sum_{m=1}^{M} K_m$. Users in the 1st service class have the lowest data rate R_1, and users in Mth service class have the highest date rate R_M. The data rate for the mth class, denoted by R_m, is an integral multiple of R_1, i.e., $R_m = N_m R_1$, where N_m is an integer and $1 = N_1 < N_2 < \cdots < N_M$. And the total null-to-null wide bandwidth of the systems is fixed at B for all access schemes in our analysis for the ease of comparison.

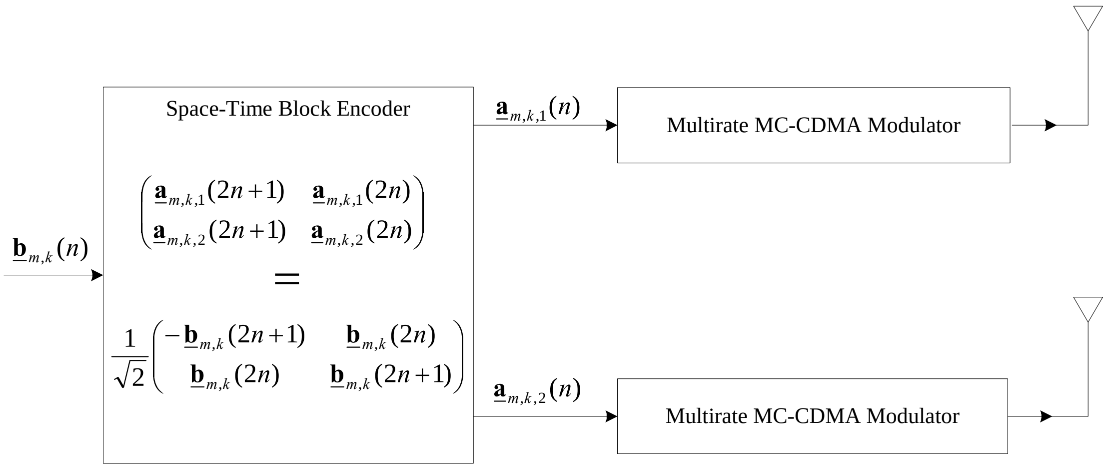

Fig. 4.1 Transmitter of multirate STBC MC-CDMA system

The stream of binary phase-shift keying (BPSK) symbols of the *k*th user from *m*th class is first passed through the ST block encoder. Without incurring any power or bandwidth penalty, the Alamouti's orthogonal ST block coding scheme is employed [44][48]. Two successive block symbols $\underline{\mathbf{b}}_{m,k}(2n)$ and $\underline{\mathbf{b}}_{m,k}(2n+1)$ for the *k*th user are mapped to the following matrix

$$\begin{pmatrix} \underline{\mathbf{a}}_{m,k,1}(2n+1) & \underline{\mathbf{a}}_{m,k,1}(2n) \\ \underline{\mathbf{a}}_{m,k,2}(2n+1) & \underline{\mathbf{a}}_{m,k,2}(2n) \end{pmatrix} = \frac{1}{\sqrt{2}}\begin{pmatrix} -\underline{\mathbf{b}}_{m,k}(2n+1) & \underline{\mathbf{b}}_{m,k}(2n) \\ \underline{\mathbf{b}}_{m,k}(2n) & \underline{\mathbf{b}}_{m,k}(2n+1) \end{pmatrix} \begin{matrix} \leftarrow \ \text{time} \\ \downarrow \ \text{space} \end{matrix}$$

where $\underline{\mathbf{b}}_{m,k}(n) = \left[b_{m,k,1}(n) \quad \cdots \quad b_{m,k,P_m}(n)\right]^T$ denotes the *n*th block symbols for *k*th user from *m*th service class with length P_m and $(\cdot)^T$ denotes the transpose, and $\underline{\mathbf{a}}_{m,k,i}(n) = \left[a_{m,k,i,1}(n) \quad \cdots \quad a_{m,k,i,P_m}(n)\right]^T$ denotes the *n*th STBC coded block symbols at *i*th transmit antenna for the *k*th user from the *m*th service class with length P_m. For mc and VSG access scheme, $P_m = N_m$; for MSR access scheme, $P_m = 1$. The columns are transmitted in successive block time with the block symbol in the upper and lower blocks simultaneously sent through the two transmit antennas, respectively. The factor $1/\sqrt{2}$ is to normalize the transmitted symbol energy.

Next every symbol $\underline{\mathbf{a}}_{m,k,i}(n)$ $(i = 1,2)$ at the *i*th transmitter antenna will go through the multirate MC-CDMA modulator before transmitted. In this chapter, three multirate access schemes will be studied.

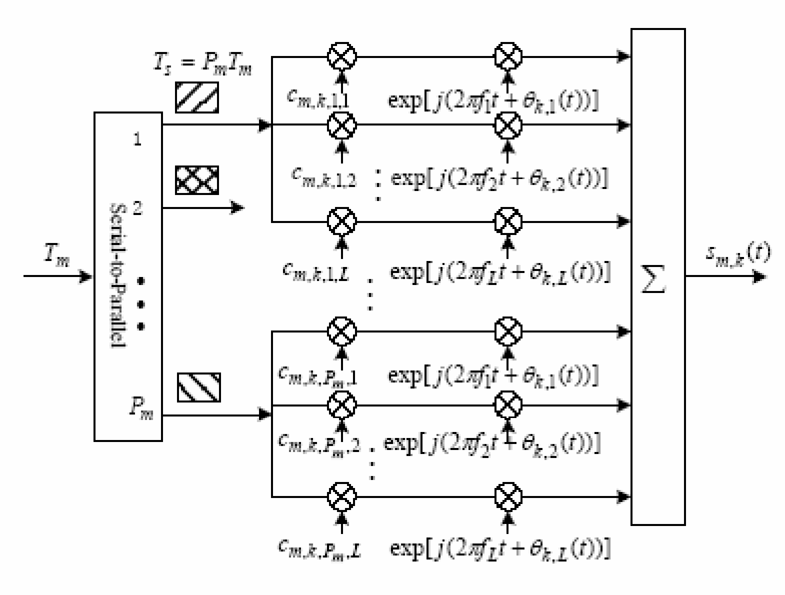

Fig. 4.2 Multirate MC-CDMA modulator with multicode access scheme

(a) mc access scheme. Fig. 4.2 shows multirate MC-CDMA modulator with multicode access scheme. The spreading gain (equal to the number of subcarriers as well) is the same for different classes, i.e. $L_1 = L_2 = \cdots = L_M = L$. The block symbols $\underline{\mathbf{a}}_{m,k,i}(n)$ $(i = 1,2)$ from the users in *m*th class is first serial-to-parallel converted to P_m parallel data streams (known as virtual users). Thus, the symbol rate on each data stream is the same and equal to the lowest data rate R_1, i.e., $T_s = P_m T_m = T_1$, where T_m is the input bit duration of *m*th class, T_s is the symbol duration at each data stream and also each subcarrier. Essentially, the higher rate user in the *m*th $(m > 1)$ class will be converted into P_m virtual users each with lowest data rate R_1. Each virtual user will then be spread via a different signature sequence with spreading gain L over the L subcarriers. The frequency separation between the neighboring subcarriers is $1/T_s$ Hz

and passband null-to-null bandwidth of each subcarrier is $2/T_s$. We therefore have $B=(L+1)/T_s$. The center frequency of each subcarrier is given by

$$f_{mc} = l/T_s \qquad l = 1,2,\cdots,L. \tag{4.1}$$

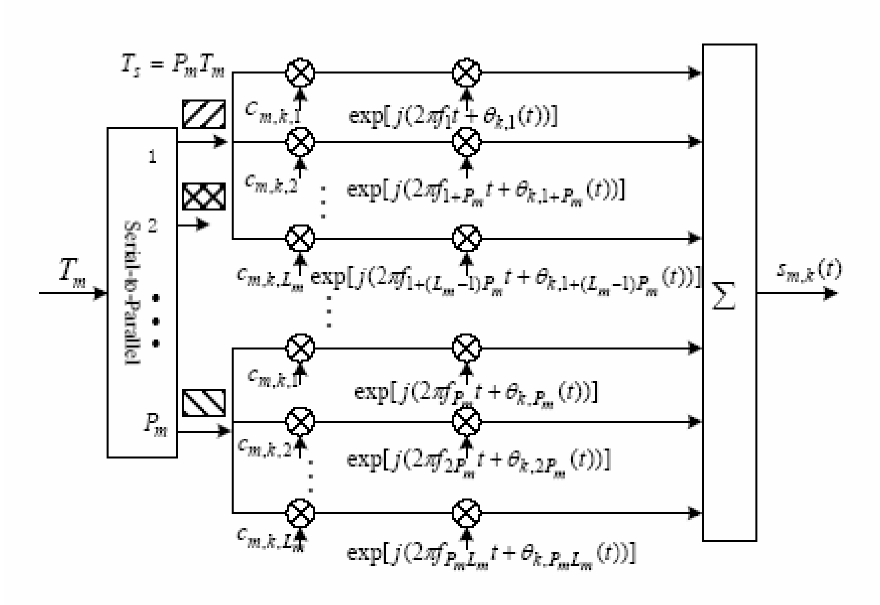

Fig. 4.3 Multirate MC-CDMA modulator with VSG access scheme

(b) VSG access scheme. Fig. 4.3 shows Multirate MC-CDMA modulator with VSG access scheme. Different classes are accommodated with the signature sequences having different spreading gains. The spreading gain for *m*th class is given by $L_m = L/P_m$. Hence, the highest transmission rate users will have the least spreading gain, i.e. $L = L_1 > L_2 > \cdots > L_M$. The block symbol $\underline{\mathbf{a}}_{m,k,i}(n)$ $(i=1,2)$ from the users in *m*th class is first serial-to parallel converted to P_m parallel data streams. Similarly, the symbol period on each data stream remains the same at $T_s = P_m T_m = T_1$. The data on each data stream is spread via the same spreading sequence with the spreading gain L_m in the frequency domain. A total of $P_m L_m = L$ chips resulting from the P_m BPSK symbols are transmitted over a total of $P_m L_m$ subcarriers. The frequency separation between the neighboring subcarriers is $1/T_s$ Hz and passband null-to-null bandwidth

of each subcarrier is $2/T_s$, hence $B=(P_m L_m+1)/T_s$. The center frequency of each subcarrier is given by

$$f_{VSG} = x_{VSG}/T_s \qquad x_{VSG} = 1,2,\cdots,P_m L_m, \tag{4.2}$$

where $x_{VSG} = p+(l-1)P_m$.

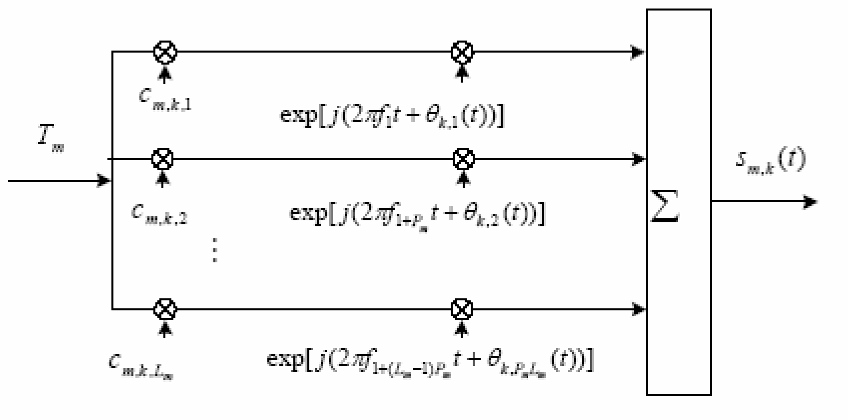

Fig. 4.4 Multirate MC-CDMA modulator with MSR access scheme

(c) MSR access scheme. Fig. 4.4 shows multirate MC-CDMA modulator with MSR access scheme. The symbol rates over each subcarrier for different service classes are different. This is the main difference compared to the former two access schemes. It means that the symbol duration over each subcarrier for *m*th service class is given by $T_s = T_m$. In this access scheme, no serial-to-parallel converter is needed since $P_m = 1$. The block symbol $\underline{\mathbf{a}}_{m,k,i}(n)$ ($i=1,2$) will directly go through MSR multirate modulator. Three possible spectrum configurations for the MSR access scheme are investigated.

(i) *MSR Configuration 1 and Configuration 2*. In these two spectrum configurations, the spreading gains for different service classes are the same, i.e. $L_1=\cdots=L_M=L$. The total bandwidth B is divided to L subcarriers. The maximum bandwidth of each subcarrier is given by $B_n = 2B/(L+1) = 2/T_M$. If we assume rectangular waveform is used, users transmitted at highest data rate will normally occupy the subcarrier bandwidth for transmission, as shown in Fig. 4.5 (a). The spectrum of the subsystems supporting lower data rate services is overlaid on the spectrum of the subsystems accommodating higher data rate users. Since lower rate users will only use part of the subcarrier bandwidth, there are two ways to place the subcarrier frequencies for MSR STBC MC-CDMA systems, as demonstrated by the layer structure shown in Fig. 4.5 (b) and (c). Configuration 1 shown in Fig. 4.5 (b) indicates that all the subcarrier frequencies of lower data rate users (class *m*) is offset from the corresponding subcarrier frequencies of highest data rate users (class *M*) by Δf_m, and there is only one subsystem to accommodate all the lower rate class *m* users. In MSR configuration 1, the central frequency of the *l*th subcarrier for *k*th user from *m*th class is given by

$$f_{MSR\_1} = f_{M,l} + \Delta f_{m,k}, \tag{4.3a}$$

where MSR_1 denotes the MSR configuration 1, $f_{M,l} = l / T_M$ is the central frequency of *l*th subcarrier for the highest data rate class and $\left|\Delta f_{m,k}\right| \leq 1/T_M - 1/T_m$. Configuration 2 shown in Fig. 4.5 (c) has $\overline{N}_m = 2\lfloor T_m / T_M \rfloor - 1$ subsystems similar to configuration 1, each with different subcarrier frequency offsets from the *M*th class users who occupied the whole bandwidth for transmission. All the lower rate class *m* users are evenly distributed among these $\overline{N}_m$ subsystems. In MSR configuration 2, the central frequency of *n*th subsystem at *l*th subcarrier for *k*th user from *m*th class is given by

$$f_{MSR\_2} = f_{M,l} - 1/T_M + n/T_m, \; n = 1,2,\cdots,\overline{N}_1, \tag{4.3b}$$

where MSR_2 denotes the MSR configuration 2.

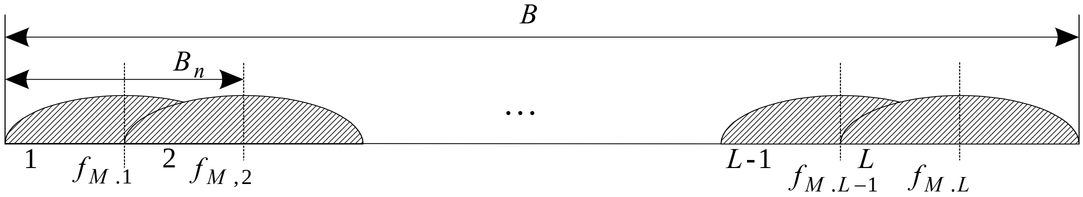

(a) Spectrum allocation for highest data rate user (class *M*)

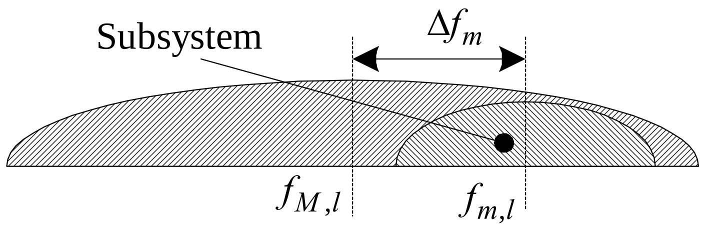

(b) Lower rate user configuration 1 (one subsystem per subcarrier)

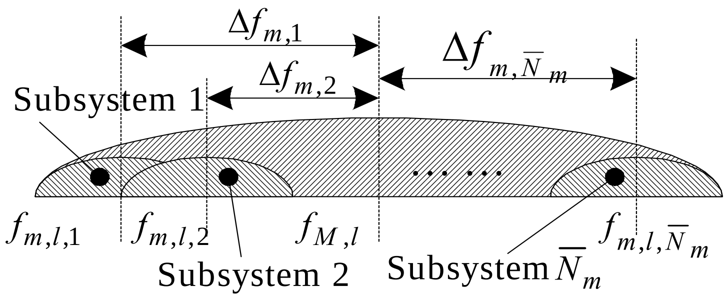

(c) Lower rate user configuration 2 ($\overline{N}_m$ subsystems per subcarrier)

Fig. 4.5 Spectrum Configuration 1 & 2 of MSR STBC MC-CDMA

(ii) *MSR Configuration 3*. In this configuration, the spreading gains for different service classes are different. i.e. $L_1 > L_2 > \cdots > L_M = L$. The spectrum of configuration 3 for MSR STBC MC-CDMA system is shown in Fig. 4.6. For *m*th class, the total bandwidth is divided into L_m subcarriers, i.e. $B = (L_m + 1)/T_m$ (conversely, $L_m = BT_m - 1$) and rectangular waveform is used. T_m is the symbol duration on subcarrier for *m*th class. In MSR configuration 3, the central frequency of the *l*th subcarrier for *k*th user from *m*th class is given by

$$f_{MSR\_3} = l / T_m . \tag{4.3c}$$

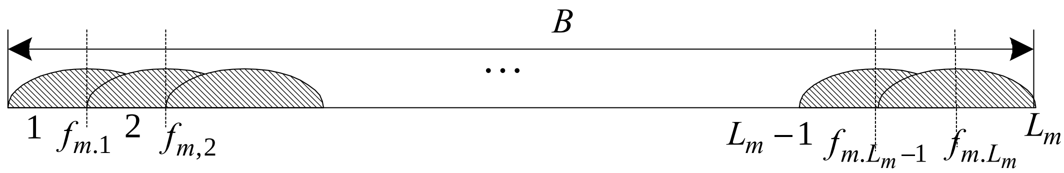

Fig. 4.6 Spectrum Configuration 3 of MSR STBC MC-CDMA system

Consider uplink transmission and each user is assumed to employ binary phase-shift keying (BPSK) symbols, the received signal at *jth* antenna can be expressed as

$$r_j(t) = \sum_{n=-\infty}^{n=+\infty}\sum_{m=1}^{M}\sqrt{2S_m / P_m L_m}\sum_{k=1}^{K_m}\sum_{i=1}^{2}\sum_{l=1}^{L_m}\sum_{p=1}^{P_m} a_{m,k,i,p}(n) c_{m,k,p,l}(n) \cdot$$

$$u(t - nT_s - \tau_{m,k,i,j}) \cdot \beta_{m,k,i,j,x_{sch}}(t)$$

$$\exp[j(2\pi f_{sch} t + \phi_{m,k,i,j,x_{sch}}(t))] + \eta_j(t), \tag{4.4}$$

where *sch* denotes either one of the mc, VSG or MSR (including MSR_1, MSR_2, MSR_3) access schemes. S_m denotes the transmit power for the *m*th class users with the value to be determined by the proposed power control algorithm presented in the next section, $a_{m,k,i,p}(n)$ is the *n*th data bit of the *p*th data stream at *i*th antenna for the *k*th user from *m*th service class. Note that $P_m = 1$ for MSR access scheme. $c_{m,k,p,l}(n)$ ($l = 1, \cdots, L_m$) is the spreading sequence used to spread the *n*th data bit of the *p*th data stream in the frequency domain. For mc access scheme $c_{m,k,1,l}(n) \neq \cdots \neq c_{m,k,P_m,l}(n)$, whereas, for VSG and MSR access scheme, $c_{m,k,1,l}(n) = \cdots = c_{m,k,P_m,l}(n) = c_{m,k,l}(n)$. $u(t)$ is the rectangular pulse defined in $[0, T_s]$, $\tau_{m,k,i,j}$ denotes the transmission delay and it is uniformly distributed over the time interval $[0, T_s]$. $\beta_{m,k,i,j,x_{sch}}(t)$ and $\varphi_{m,k,i,j,x_{sch}}(t)$ are respectively the amplitude and phase of the channel fading gain of user *k* from *m*th class when signal is transmitted from the *i*th transmit antenna to the *j*th receive antenna through the x_{sch} th subcarrier, where $x_{mc} = l$, $x_{VSG} = p + (l-1)P_m$ and $x_{MSR} = l$. $\beta_{m,k,i,j,x_{sch}}(t)$ is Rayleigh distributed with $E\{\beta^2_{m,k,i,j,x_{sch}}\} = \sigma^2$, $\varphi_{m,k,i,j,x_{sch}}(t)$ is uniformly distributed over $[0,2\pi]$. $\phi_{m,k,i,j,x_{sch}}(t) = \theta_{m,k,i,x_{sch}} + \varphi_{m,k,i,j,x_{sch}}(t)$ $-2\pi f_{x_{sch}}\tau_{m,k,i,j}$, where $\theta_{m,k,i,x_{sch}}$ is the random carrier phase uniformly distributed over $[0,2\pi]$. $\eta_j(t)$ denotes the additive white Gaussian noise (AWGN) at jth receive antenna with zero mean and double-sided PSD $N_0/2$.

Symbol duration in each subcarrier is assumed to be longer than channel delay spread so that each subcarrier signal undergone flat fading. Also with sufficient frequency separation between adjacent subcarriers relative to the channel's coherent bandwidth, fading process of a given user on different subcarriers can also be assumed to be independent; otherwise the results could be used as the upper limit. We assume that perfect timing and frequency sychnronization are achieved at the receiver throughout this chapter.

Assume that the 1st user from uth class is of interest, and coherent receiver is used. Without loss of generality, let $\tau_{u,1} = 0$. The correlator output for the nth data bit at the lth subcarrier of the pth data stream at the jth antenna for mc scheme is given by

$$Y^{sch}_{u,j,p,l}(n) = \frac{1}{T_s}\int_{nT_s}^{(n+1)T_s} r_j(t)\exp(-j2\pi f_{sch}t)dt$$

$$= D^{sch}_{u,j,p,l}(n) + I^{sch}_{u,j,p,l}(n) + \xi^{sch}_{u,j,p,l}(n), \tag{4.5}$$

where $D^{sch}_{u,j,p,l}(n)$, $I^{sch}_{u,j,p,l}(n)$ and $\xi^{sch}_{u,j,p,l}(n)$ are the desired signal, interference and AWGN noise, respectively. The noise term $\xi^{sch}_{u,j,p,l}(n)$ is Guassian distributed with zero mean and variance $\sigma^2_{\xi^{sch}_{u,j,p,l}} = N_0/2T_s$. The interference term $I^{sch}_{u,j,p,l}(n) = I^{sch}_{SI,u,j,p,l}(n) + I^{sch}_{MI,u,j,p,l}(n)$, where $I^{sch}_{SI,u,j,p,l}(n)$ denotes the self-interference

(SI), and $I_{MI,u,j,p,l}^{sch}(n)$ represent the multiuser interference (MUI). Note that for MSR access scheme, the signal will be filtered by a bandpass filter with its bandwidth adapted to the symbol rate of the desired class before decision making.

4.2 Interference Analysis

Channel fading is assumed to be quasi-stationary over the two successive symbol intervals $2T_s$, i.e., the channel gain remains constant over the time interval $\left[2nT_s \quad (2n+2)T_s\right]$, i.e.

$$\beta_{m,k,i,j,x_{sch}}(2n) \approx \beta_{m,k,i,j,x_{sch}}(2n+1) = \beta_{m,k,i,j,x_{sch}},$$

$$\varphi_{m,k,i,j,x_{sch}}(2n) \approx \varphi_{m,k,i,j,x_{sch}}(2n+1) = \varphi_{m,k,i,j,x_{sch}}. \tag{4.6}$$

The signal and respective interference terms can be derived using (4.4) and (4.5). The desired (2n)th and (2n-1)th block symbols at the lth subcarrier of the pth data stream of the jth antenna are given by

$$\begin{aligned} D_{u,j,p,l}(2n) = \sqrt{S_u / P_u L_u}\,[\beta_{u,1,1,j,x_{sch}} \exp(-j\phi_{u,1,1,j,x_{sch}}) \\ \cdot c_{u,1,p,l}(2n) \cdot b_{u,1,p}(2n) + \beta_{u,1,2,j,x_{sch}} \\ \cdot \exp(-j\phi_{u,1,2,j,x_{sch}}) \cdot c_{u,1,p,l}(2n) b_{u,1,p}(2n+1)], \end{aligned} \tag{4.7}$$

$$\begin{aligned} D_{u,j,p,l}(2n+1) = \sqrt{S_u / P_u L_u}\,[\beta_{u,1,1,j,x_{sch}} \exp(-j\phi_{u,1,1,j,x_{sch}}) \\ \cdot c_{u,1,p,l}(2n+1)(-b_{u,1,p}(2n+1)) + \beta_{u,1,2,j,x_{sch}} \cdot \\ \exp(-j\phi_{u,1,2,j,x_{sch}}) \cdot c_{u,1,p,l}(2n+1) b_{u,1,p}(2n)]. \end{aligned} \tag{4.8}$$

Assume that the equal gain combining (EGC) technique is used. The decision variables for $b_{u,1,p}(2n)$ and $b_{u,1,p}(2n+1)$ are respectively given by

$$U_{u,p}(2n) = \sum_{j=1}^{J}\sum_{l=1}^{L_u} \mathrm{Re}\{Y_{u,j,p,l}(2n)\alpha_1 c_{u,1,p,l}(2n)$$

$$+ Y^*_{u,j,p,l}(2n+1)\alpha_2^* c_{u,1,p,l}(2n+1)\}/\beta_{x_{sch}}, \tag{4.9a}$$

$$U_{u,p}(2n+1) = \sum_{j=1}^{J}\sum_{l=1}^{L_u} \mathrm{Re}\{Y_{u,j,p,l}(2n)\alpha_2 c_{u,1,p,l}(2n)$$

$$+ Y^*_{u,j,p,l}(2n+1)\alpha_1^* c_{u,1,p,l}(2n+1)\}/\beta_{x_{sch}}, \tag{4.9b}$$

where $\alpha_i = \beta_{u,1,i,j,x_{sch}} \exp(j\phi_{u,1,i,j,x_{sch}})$ ($i = 1,2$) and $\beta_{x_{sch}} = \sqrt{\beta^2_{u,1,1,j,x_{sch}} + \beta^2_{u,1,2,j,x_{sch}}}$. In the following analysis, $U_{u,p}(2n)$ will be used as an example and we shall simply use $U^{sch}_{u,p}$ to denote $U_{u,p}(2n)$. Eq.(4.9a) can be expressed as

$$U^{sch}_{u,p} = D^{sch}_{u,p} + I^{sch}_{u,p} + \xi^{sch}_{u,p}, \tag{4.10}$$

where $D^{sch}_{u,p} = \sum_{j=1}^{J}\sum_{l=1}^{L_u}\sqrt{S_u / P_u L_u}\cdot\beta_{x_{sch}}\cdot b_{u,1,p}(2n)$, and $I^{sch}_{u,p} = I^{sch}_{u,p}(2n)$. The noise is given by

$$\xi^{sch}_{u,p} = \xi^{sch}_{u,p}(2n) = \sum_{j=1}^{J}\sum_{l=1}^{L_u} \mathrm{Re}\{\xi^{sch}_{u,j,p,l}(2n)\alpha_1 c_{u,1,p,l}(2n)$$

$$+ {\xi^{sch}_{u,j,p,l}}^*(2n+1)\alpha_2^* c_{u,1,p,l}(2n+1)\}/\beta_{x_{sch}}. \tag{4.11}$$

Thus the variance of $\xi^{sch}_{u,p}$ is given by

$$\sigma^2_{\xi^{sch}_{u,p}} = N_0 J L_u / 2T_s. \tag{4.12}$$

In the following, we derive the respective interference terms defined in (4.10) for mc, VSG and MSR access schemes, either Gold sequence or orthogonal Gold sequences will be used. Gold sequence is one of pseudo-random sequences that exhibit noise-like randomness properties. And the orthogonal Gold sequences has the similar autocorrelation and cross-correlation as compared to Gold sequence except that orthogonal Gold sequence offer zero crosscorrelation value at zero time shift

[109][110]. In the following interference analysis, we use the statistical properties of pseudo-random sequences to simplify the analysis when we compute the variances of the various interference terms.

4.2.1 Multicode Access Scheme

The interference for mc access scheme is given by

$$I_{u,p}^{mc} = I_{SI,u,p}^{mc} + I_{MI,u,p}^{mc}, \tag{4.13}$$

where $I_{SI,u,p}^{mc}(n)$ denotes the self-interference (SI), and $I_{MI,u,p}^{mc}(n)$ represents the multiuser interference (MUI), respectively. Then, the SI from other parallel data streams (virtual users) for mc access scheme is given by

$$I_{SI,u,p}^{mc} = \sum_{j=1}^{J}\sum_{l=1}^{L} \mathrm{Re}\Big\{ I_{u,j,p,l}^{mc}(2n)\alpha_1 c_{u,1,p,l}(2n)$$

$$+ I_{u,j,p,l}^{mc\;*}(2n+1)\alpha_2^* c_{u,1,p,l}(2n+1) \Big\} / \beta_l, \tag{4.14}$$

where $I_{SI,u,j,p,l}^{mc}(n) = \sqrt{S_u / P_u L} \sum_{i=1}^{2} \sum_{q=1,q\neq p}^{P_u} c_{u,1,p,l} c_{u,1,q,l} \cdot \beta_{u,1,i,j,l} \exp(j\phi_{u,1,i,j,l}) \cdot b_{u,1,i,q}(n)$,

thus the SI can be simplified as

$$I_{SI,u,p}^{mc} = \sum_{j=1}^{J}\sum_{l=1}^{L} \sqrt{S_u / P_u L} \sum_{q=1.q\neq p}^{P_u} c_{u,1,p,l} c_{u,1,q,l} \cdot \beta_l \cdot b_{u,1,q}(2n). \tag{4.15}$$

If orthogonal Gold sequences are used, then we have $\sum_{l=1.q\neq p}^{L} c_{u,1,p,l} c_{u,1,q,l} = 0$, and let $\tilde{c} = c_{u,1,p,l} c_{u,1,q,l}$. This implies that a half of $\tilde{c}$ take the value "+1", the other half take the value "-1". Denote the index of $\tilde{c} =$"+1" as $a_{1,d}$, and the index of $\tilde{c} =$"−1"as $a_{2,d}$. Then (4.15) can be rewritten as

$$I_{SI,u,p}^{mc} = \sum_{j=1}^{J} \sum_{q=1.q\neq p}^{P_u} \sqrt{S_u / P_u L} \cdot b_{u,1,q}(2n) \cdot \sum_{d=1}^{L/2} (\beta_{a_{1,d}} - \beta_{a_{2,d}}). \tag{4.16}$$

By the central limit theorem (CLT), the RV $\sum_{d=1}^{L/2}(\beta_{a_{1,d}} - \beta_{a_{2,d}})$ can be approximated to be a Gaussian RV with zero mean and variance $(2-9\pi/16)L\sigma^2$ for large L. Therefore, the variance of $I_{SI,u,p}^{mc}$ is given by

$$Var(I_{SI,u,p}^{mc}) = (P_u - 1)/P_u \cdot J(2-9\pi/16)\sigma^2 \cdot S_u . \tag{4.17a}$$

If Gold sequences (nonorthogonal) are used, the value of $I_{SI,u,p}^{mc}$ can be obtained by

$$Var(I_{SI,u,p}^{mc}) = 2(P_u - 1)/P_u \cdot J\sigma^2 \cdot S_u . \tag{4.17b}$$

The MUI for mc access scheme is given by

$$\begin{aligned} I_{MI,u,p}^{mc} = \sum_{j=1}^{J}\sum_{l=1}^{L} \mathrm{Re}\Big\{ & I_{MI,u,j,p,l}^{mc}(2n)\alpha_1 c_{u,1,p,l}(2n) \\ & + I_{MI,u,j,p,l}^{mc}{}^{*}(2n+1)\alpha_2^{*} c_{u,1,p,l}(2n+1)\Big\}/\beta_l , \end{aligned} \tag{4.18}$$

where
$$\begin{aligned} I_{MI,u,j,p,l}^{mc}(n) = & \sum_{m=1}^{M}\sum_{k=1,(m,k)\neq(u,1)}^{K_m}\sqrt{S_m/P_m L}\sum_{i=1}^{2}\Bigg\{\sum_{q=1}^{P_m}\sum_{h=1,h=l}^{L}\beta_{m,k,i,j,l}\exp(-j\phi_{m,k,i,j,l})\cdot \\ & \big\lfloor b_{m,k,i,q}(n-1)c_{m,k,q,l}\cdot\tau_{m,k} + b_{m,k,i,q}(n)c_{m,k,q,l}(T_s - \tau_{m,k})\big\rfloor / T_s \cdot c_{u,1,p,l} \\ & + \sum_{q=1}^{P_m}\sum_{h=1,h\neq l}^{L} 1/\pi(h-l)\cdot c_{u,1,p,l}\cdot\beta_{m,k,i,j,l}\cdot\big\lfloor b_{m,k,i,q}(n-1)c_{m,k,q,h} \\ & \cdot\sin[\pi(h-l)\tau_{m,k}/T_s]\cdot\exp[-j(\pi(h-l)\tau_{m,k}/T_s + \phi_{m,k,i,j,l})] \\ & + b_{m,k,q}(0)c_{m,k,q,h}\cdot\sin[\pi(h-l)(T_s - \tau_{m,k})/T_s] \\ & \cdot\exp[-j(\pi(h-l)(T_s + \tau_{m,k})/T_s + \phi_{m,k,i,j,l})]\big\rfloor\Bigg\} . \end{aligned} \tag{4.18a}$$

Therefore, the variance of $I_{MI,u,p}^{mc}$ is given by

$$Var(I_{MI,u,p}^{mc}) = \sum_{m=1}^{M}\sum_{k=1,(m,k)\neq(u,1)}^{K_m}(2/3\cdot J\sigma^2 + \sum_{l=1}^{L}\sum_{h=1,h\neq l}^{L} J\sigma^2/L\pi^2(h-l)^2)\cdot S_m . \tag{4.19}$$

By central limit theory (CLT), and since $I^{mc}_{SI,u,p}$, $I^{mc}_{MI,u,p}$ are independent each other, the total interference $I^{mc}_{u,p}$ is also a Gaussian RV with zero mean and variance

$$\sigma^2_{I^{mc}_{u,p}} = Var(I^{mc}_{SI,u,p}) + Var(I^{mc}_{MI,u,p}) = \sum_{m=1}^{M} G_{u,m} S_m \ , \tag{4.20}$$

where $G_{u,m}$ can be obtained from (4.17) and(4.19).

4.2.2 VSG access scheme

The interference for VSG access scheme is given by

$$I^{VSG}_{u,p} = I^{VSG}_{SI,u,p} + I^{VSG}_{MI,u,p} \ , \tag{4.21}$$

where $I^{VSG}_{SI,u,p}(n)$ denotes the self-interference (SI), and $I^{VSG}_{MI,u,p}(n)$ represents the multiuser interference (MUI), respectively. In VSG access scheme, different parallel data streams will occupy different subcarriers, hence will not interfere each other, i.e. $I^{VSG}_{SI,u,p} = 0$.

The MUI for VSG access scheme is given by

$$I^{VSG}_{MI,u,p} = \sum_{j=1}^{J} \sum_{l=1}^{L} \mathrm{Re}\Big\{ I^{VSG}_{MI,u,j,p,l}(2n)\alpha_1 c_{u,1,p,l}(2n)$$

$$+ I^{VSG}_{MI,u,j,p,l}{}^{*}(2n+1)\alpha_2^{*} c_{u,1,p,l}(2n+1) \Big\} / \beta_{x_{VSG}} \ , \tag{4.22}$$

where $I^{VSG}_{MS,u,j,p,l}(n) = \sum_{m=1}^{M} \sum_{k=1,(m,k)\neq(u,1)}^{K_m} \sqrt{S_m / P_m L_m} \sum_{i=1}^{2} \{$

$$\sum_{q=1}^{P_m} \sum_{h=1, x_{VSG}=y_{VSG}}^{L_u} \beta_{m,k,i,j,y_{VSG}} \exp(-j\Phi_{m,k,i,j,x_{VSG}})$$

$$\cdot \big[b_{m,k,i,q}(n-1) c_{m,k,h}(n-1)\tau_{m,k} + b_{m,k,i,q}(n) c_{m,k,h}(n)(T_s - \tau_{m,k}) \big] / T_s \cdot c_{u,1,l}(n)$$

$$+ \sum_{q=1}^{P_m} \sum_{h=1, y_{VSG}\neq x_{VSG}}^{L_u} 1/\pi(y_{VSG} - x_{VSG}) \cdot c_{u,1,l}(n) \cdot \beta_{m,k,i,j,y_{VSG}}$$

$$\cdot \Big[b_{m,k,i,q}(n-1)c_{m,k,h}(n-1)\cdot$$

$$\sin[\pi(y-x)\tau_{m,k}/T_s]\exp[-j(\pi(y_{VSG}-x_{VSG})\tau_{m,k}/T_s+\Phi_{m,k,i,j,y_{VSG}})]$$

$$+b_{m,k,i,q}(n)c_{m,k,h}(n)\cdot\sin[\pi(y_{VSG}-x_{VSG})(T_s-\tau_{m,k})/T_s]\cdot$$

$$\exp[-j(\pi(y_{VSG}-x_{VSG})(T_s+\tau_{m,k})/T_s+\Phi_{m,k,i,j,y_{VSG}})]\Big]\Big\}. \tag{4.22a}$$

and $y_{VSG}=q+(h-1)P_m$. Therefore, the variance of $I_{MI,u,p}^{VSG}$ is given by

$$Var(I_{MI,u,p}^{VSG})=\sum_{m=1}^{M}\sum_{k=1,(m,k)\neq(u,1)}^{K_m}(2L_u/3P_mL_m\cdot J\sigma^2$$

$$+\sum_{l=1}^{L}\sum_{q=1}^{P_m}\sum_{h=1,y_{VSG}\neq x_{VSG}}^{L}J\sigma^2/\pi^2(y_{VSG}-x_{VSG})^2/P_mL_m)\cdot S_m\,. \tag{4.23}$$

Similarly, by central limit theorem (CLT), the total interference $I_{u,p}^{VSG}$ is also a Gaussian RV with zero mean and variance

$$\sigma^2_{I_{u,p}^{VSG}}=Var(I_{MI,u,p}^{VSG})=\sum_{m=1}^{M}G_{u,m}S_m\,, \tag{4.24}$$

where $G_{u,m}$ can be obtained from (4.23).

4.2.3 MSR access scheme

The MUI for MSR access scheme is given by

$$I_{u,p}^{MSR}=\sum_{m=1}^{M}\sum_{k=1,(m,k)\neq(u,1)}^{K_m}I_{m,k}^{MSR}\,, \tag{4.25}$$

where $I_{m,k}^{MSR}=\sum_{j=1}^{J}\sum_{l=1}^{L_u}\mathrm{Re}\Big\{I_{m,k,j,l}^{MSR}(2n)\alpha_1c_{u,1,l}(2n)+I_{m,k,j,l}^{MSR}{}^{*}(2n+1)\alpha_2^{*}c_{u,1,l}(2n+1)\Big\}/\beta_l\,.$

(4.25a)

The evaluation of $I_{m,k,j,l}^{MSR}$ is presented below. Since for MSR access scheme the symbol rate in each subcarrier is not the same for different service classes, extra care has to be taken when computing the average interference imposed by users in one of the service classes on the other. The correct number of consecutive symbols that will interfere the desired user has to be taken into consideration. The derivation details are omitted here, and [70] can be used as a reference source to fill up this gap.

A. $T_m \geq T_u$ (Lower rate and the same rate class)

This is corresponding to the case where desired user has higher or equal data rate than interference user. The MUI imposed from users in the lower and same data rate class can be separately considered.

(a) $\tau_{m,k,i,j} \leq T_u$

$$I_{m,k,j,l}^{MSR}(n) = \sum_{i=1}^{2} \sqrt{S_m / L_m} \cdot \beta_{m,k,i,j,l} \cdot c_{u,1,l}(n) \cdot \{ \sum_{h=1, f_{m,k,h}=f_{u,1,l}}^{L_m} \big[b_{m,k,i}(n-1) \cdot$$

$$c_{m,k,h}(n-1)\tau_{m,k,i,j} + b_{m,k}(n)c_{m,k,h}(n)(T_u - \tau_{m,k,i,j})\big] \cdot \exp(-j\Phi)/T_u$$

$$+ \sum\nolimits_{h=1, f_{m,k,h} \neq f_{u,1,l}}^{L_m} T_{conf} / (\overline{\Delta\omega}_{conf} T_u) \big[b_{m,k}(n-1)c_{m,k,h}(n-1)\sin(\overline{\Delta\omega}_{conf}\tau_{m,k} / T_{conf})$$

$$\exp[-j(\overline{\Delta\omega}_{conf}\tau_{m,k,i,j} / T_{conf} + \Phi)]$$

$$+ b_{m,k,i}(n)c_{m,k,h}(n)\sin[\overline{\Delta\omega}_{conf}(T_u - \tau_{m,k,i,j}) / T_{conf}]$$

$$\exp[-j(\overline{\Delta\omega}_{conf}(T_u + \tau_{m,k,i,j}) / T_{conf} + \Phi)] \big] \big\}, \tag{4.26}$$

where $\overline{\Delta\omega}_{conf} = \pi[h - l + (\Delta f_{m,k} - \Delta f_{u,1})T_M]$ $T_{conf} = T_M$ for MSR configuration 1 or 2, and, $\overline{\Delta\omega}_{conf} = \pi(hT_u / T_m - l)$, $T_{conf} = T_u$ for MSR configuration 3, $\Phi = \phi_{m,k,l} - \phi_{u,1,l}$.

(b) $T_u < \tau_{m,k,i,j} < T_m$

$$I_{m,k,j,l}^{MSR}(n) = \sum_{i=1}^{2} \sqrt{S_m / L_m} \cdot \beta_{m,k,i,j,l} c_{u,1,l}(n) \cdot \{$$

$$\sum_{h=1, f_{m,k,h}=f_{u,1,l}}^{L_m} \big[b_{m,k,i}(n-1) c_{m,k,h}(n-1) \cdot \exp(-j\Phi) +$$

$$\sum_{h=1, f_{m,k,h} \neq f_{u,1,l}}^{L_m} T_{conf} \, / (\overline{\Delta\omega}_{conf} T_u) \cdot \left[b_{m,k,i}(n-1) \cdot \right.$$

$$\left. c_{m,k,h}(n-1) \sin(\overline{\Delta\omega}_{conf} T_u / T_{conf}) \exp[-j(\overline{\Delta\omega}_{conf} T_u / T_{conf} + \Phi)] \right] \Big\}, \quad (4.27)$$

When $T_m \geq T_u$, the variance of $I_{m,k}^{MSR}$ is given by

$$Var(I_{m,k}^{MSR} \mid T_m \geq T_u) = P(\tau_{m,k} \leq T_u) Var(I_{m,k}^{MSR} \mid T_m \geq T_u, \tau_{m,k} \leq T_u)$$

$$+ P(T_u < \tau_{m,k} < T_m) Var(I_{m,k}^{MSR} \mid T_m \geq T_u, T_u < \tau_{m,k} < T_m)$$

$$= J\sigma^2 \sum_{l=1}^{L_u} S_m / L_m \cdot \{ \sum_{h=1, f_{m,k,h} = f_{u,1,l}}^{L_m} T_m / 3T_u + \sum_{h=1, f_{m,k,h} \neq f_{u,1,l}}^{L_m} T_{conf}^2 \, / (\overline{\Delta\omega}_{conf}^{\,2} T_u^2) \cdot T_u / T_m$$

$$\left[1 - T_{conf} \, / (\overline{\Delta\omega}_{conf} T_m) \cdot \sin(\overline{\Delta\omega}_{conf} T_m / T_{conf}) \cdot \cos[\overline{\Delta\omega}_{conf} T_u / T_{conf}] \right.$$

$$\left. \cdot \cos[\overline{\Delta\omega}_{conf} (T_m - T_u) / T_{conf}] \right] + (T_m - T_u) / 2T_m \sin^2(\overline{\Delta\omega}_{conf} T_u / T_{conf}) \, . \quad (4.28)$$

B. $T_m < T_u$ (Higher rate class)

This is corresponding to the case when desired user has a lower transmission rate than the interference user. The MUI from the users in the higher rate class is given by

$$I_{m,k,j,l}^{MSR}(n) = \sum_{i=1}^{2} \sqrt{S_m / L_m} \cdot \beta_{m,k,i,j,l} c_{u,1,l}(n) \cdot \{$$

$$\sum_{h=1, f_{m,k,h} = f_{u,1,l}}^{L_m} \left[b_{m,k,i}(n-1) \cdot c_{m,k,h}(n-1) \tau_{m,k,i,j} + \sum_{d=0}^{a-1} b_{m,k,i}(n+d) c_{m,k,h}(n+d) T_m \right.$$

$$\left. + b_{m,k,i}(n+a) c_{m,k,h}(n+a)(T_u - \tau_{m,k,i,j} - aT_m) \right] \cdot \exp(-j\Phi) / T_u$$

$$+ \sum_{h=1, f_{m,k,h} \neq f_{u,1,l}}^{L_m} T_{conf} \, / (\overline{\Delta\omega}_{conf} T_u) \cdot \left[b_{m,k,i}(n-1) c_{m,k,h}(n-1) \right.$$

$$\cdot \sin(\overline{\Delta\omega}_{conf} \tau_{m,k,i,j} / T_{conf}) \exp[-j(\overline{\Delta\omega}_{conf} \tau_{m,k,i,j} / T_{conf} + \Phi)]$$

$$+ \sum_{d=0}^{a-1} b_{m,k,i}(n+d) \cdot c_{m,k,h}(n+d) \cdot \sin(\overline{\Delta\omega}_{conf} T_m / T_{conf})$$

$$\exp[-j(\overline{\Delta\omega}_{conf}((2n+1)T_m+2\tau_{m,k,i,j})/T_{conf}+\Phi)]$$

$$+b_{m,k,i}(n+a)c_{m,k,h}(n+a)\sin[\overline{\Delta\omega}_{conf}(T_u-\tau_{m,k,i,j}-aT_m)/T_{conf}]$$

$$\exp[-j(\overline{\Delta\omega}_{conf}(T_u+\tau_{m,k}+aT_m)/T_{conf}+\Phi)]\big]\big\}, \tag{4.29}$$

where $a=\lfloor T_u/T_m \rfloor-1$. There are altogether ($a$+2) bits from higher rate user that will affect the decision symbol of the lower rate user. When $T_m<T_u$, by taking the PSD of interference signal into consideration, after the bandpass filter, the variance of $I_{u,p}^{MSR}$ is given by

$$Var(I_{m,k}^{MSR}\,|\,T_m<T_u)=J\sigma^2\sum_{m=1}^{M}\sum_{k=1,(m,k)\neq(u,1)}^{K_m}\chi_{u,m}S_m/L_m\cdot$$

$$\sum_{l=1}^{L_u}\{\sum_{h=1,f_{m,k,h}=f_{u,1,l}}^{L_m}\left[T_u^2-T_uT_m(2a+1)+T_m^2(a^2+2a+2/3)\right]/2T_u^2$$

$$+\sum_{h=1,f_{m,k,h}\neq f_{u,1,l}}^{L_m}T_{conf}^2/(\overline{\Delta\omega}_{conf}T_u)^2\cdot\ \big[1-T_{conf}/(\overline{\Delta\omega}_{conf}T_u)\cdot\sin(\overline{\Delta\omega}_{conf}T_m/T_{conf})\cdot$$

$$\cos[\overline{\Delta\omega}_{conf}(T_u-T_m)/T_{conf}]\cos[\overline{\Delta\omega}_{conf}(T_u-(a+1)T_m)/T_{conf}]$$

$$+a\sin^2[\overline{\Delta\omega}_{conf}T_m/T_{conf}]/2\big]\big\}, \tag{4.30}$$

where $\chi_{u,m}$ is to account for the effect of the receiver filter on the signal of the desired user and the PSD of the signal of the interference user. The significance of $\chi_{u,m}$ is defined by [70]

$$\chi_{u,m}=\int_{-1/T_u}^{1/T_u}\mathrm{sinc}^2[fT_m]df\Big/\int_{-1/T_m}^{1/T_m}\mathrm{sinc}^2[fT_m]df\ . \tag{4.31}$$

Similarly, by CLT, the interference $I_{u,p}^{MSR}$ can be assumed as Gaussian distributed with zero mean and variance

$$\sigma_{I_{u,p}^{MSR}}^2=\sum_{m=1}^{M}\sum_{k=1,(m,k)\neq(u,1)}^{K_m}Var(I_{m,k}^{MSR})=\sum_{m=1}^{M}G_{u,m}S_m\ , \tag{4.32}$$

where $G_{u,m}$ can be obtained from (4.28) and (4.30). To better understand the effect of MUI for different MSR spectrum configurations, we present a two-class service system in Appendix 4.A.

4.3 BER Performance Analysis

Assume that a "+1" is transmitted, (4.10) can be rewritten as

$$U_{u,p}^{sch} = \sum_{j=1}^{J} \sum_{l=1}^{L_u} \sqrt{S_u / P_u L_u} \cdot \beta_{x_{sch}} + I_{u,p}^{sch} + \xi_{u,p}^{sch} \tag{4.33}$$

and since BPSK is used, then the BER of *p*th data stream for mc or VSG or MSR access scheme can be obtained by using [103]

$$\mathrm{P}_{e,p}^{sch} = \frac{1}{2} - \frac{1}{\pi} \int_0^\infty \omega^{-1} \,\mathrm{Im}[\Psi_{U_{u,p}^{sch}}(\omega)] d\omega \,, \tag{4.34}$$

where $\Psi_{U_{u,p}^{sch}}(\omega)$ is the characteristic function (CHF) of the decision variable $U_{u,p}^{sch}$. Im(z) is the imaginary part of complex number z. And it can be easily shown that

$$\Psi_{U_{u,p}^{sch}}(\omega) = \prod_{j=1}^{J} \prod_{l=1}^{L_u} \Psi_{\beta_{x_{sch}}}(\sqrt{S_u / P_u L_u}\,\omega) \cdot \Psi_{I_{u,p}^{sch}}(\omega) \Psi_{\xi_{u,p}^{sch}}(\omega) \,. \tag{4.35}$$

Since $\beta_{u,1,1,j,x_{sch}}$ and $\beta_{u,1,2,j,x_{sch}}$ are independent Rayleigh RVs, then RV $\beta_{x_{sch}}$ is Nakagami-*m* ($m = 2$) distributed with parameter $2\sigma^2$. Its CHF is given by [106]

$$\Psi_{\beta_{x_{sch}}}(\omega) = \Big[{}_1F_1(-3/2; 1/2; \sigma^2 \omega^2 / 4) + j \cdot 3\omega\sigma\sqrt{\pi}/4 \cdot$$

$$ {}_1F_1(-1; 3/2; \sigma^2 \omega^2 / 4) \Big] \cdot \exp(-\sigma^2 \omega^2 / 4) \,, \tag{4.36}$$

where ${}_1F_1(a;b;\omega)$ denotes the confluent hypergeometric function. The CHF of Gaussian RV $I_{u,p}^{sch}$ and $\xi_{u,p}^{sch}$ is given by [105]

$$\Psi_{I_{u,p}^{sch}}(\omega) = \exp(-\sigma_{I_{u,p}^{sch}}^2 \omega^2 / 2) \,, \tag{4.37}$$

$$\Psi_{\xi_{u,p}^{sch}}(\omega) = \exp(-\sigma^2_{\xi_{u,p}^{sch}}\omega^2 / 2), \tag{4.38}$$

respectively. Substitute (4.36)-(4.38) into (4.35), the CHF of $U_{u,p}^{sch}$ is given by

$$\Psi_{U_{u,p}^{sch}}(\omega) = \Big[{}_1F_1(-3/2;1/2;S_u\sigma^2\omega^2/4P_uL_u)$$

$$+ j\cdot 3\,\omega\sigma\sqrt{\pi S_u / P_uL_u}\Big/4\cdot {}_1F_1(-1;3/2;S_u\sigma^2\omega^2/4P_uL_u)\Big]^{JL_u}$$

$$\cdot\exp[-(2\sigma^2_{I_{u,p}^{sch}} + 2\sigma^2_{\xi_{u,p}^{sch}} + JS_u\sigma^{2\cdot}/P_u)\omega^2/4]. \tag{4.39}$$

Let $\omega = 2z\Big/\sqrt{2\sigma^2_{I_{u,p}^{sch}} + 2\sigma^2_{\xi_{u,p}^{sch}} + JS_u\sigma^2/P_u}$, the exact BER for the pth data stream is given by [104]

$$\mathrm{P}_{e,u,p} = \frac{1}{2} - \frac{1}{\pi}\int_0^\infty W(z)\exp(-z^2)dz = \frac{1}{2} - \frac{1}{\pi}\sum_{m=1}^{N_p} H_{x_m} W(x_m), \tag{4.40}$$

where $W(z) = \mathrm{Im}\{[{}_1F_1(-3/2;1/2;S_u\sigma^2z^2/(2P_uL_u(\sigma^2_{I_{u,p}^{sch}} + \sigma^2_{\xi_{u,p}^{sch}}) + JL_uS_u\sigma^2))$

$$+ j\cdot 3z\sigma\sqrt{\pi S_u/(2P_uL_u(\sigma^2_{I_{u,p}^{sch}} + \sigma^2_{\xi_{u,p}^{sch}}) + JL_uS_u\sigma^2)}/2\cdot$$

$${}_1F_1(-1;3/2;S_u\sigma^2z^2/(2P_uL_u(\sigma^2_{I_{u,p}^{sch}} + \sigma^2_{\xi_{u,p}^{sch}}) + JL_uS_u\sigma^2))]^{JL_u}z^{-1}\}, \tag{4.40a}$$

and N_p is the order of the Hermite polynomial and we found that $N_p = 40$ is sufficient for good accuracy. The parameter x_m in (40) is the mth zero of the N_pth order Hermite polynomial, and H_{x_m} are the weight factors given by

$$H_{x_m} = 2^{N_p-1}N_p!\sqrt{\pi}\Big/N_p^2H_{N_p-1}(x_m). \tag{4.40b}$$

It is assumed that any bit can be sent via any of the P_u data streams with equal probability. Therefore, the system average BER for either mc , VSG or MSR access scheme is given by

$$\mathrm{P}_{e,u}^{sch} = \sum_{p=1}^{P_u}\mathrm{P}_{e,u,p}^{sch}/P_u \qquad (u = 1,2,\cdots,M). \tag{4.41}$$

4.4 Transmit Power Control and Capacity Analysis

We define the signal-to-interference ratio (SIR) for pth data stream as

$$\gamma_{u,p}^{sch} = E\{D_{u,p}^{sch\,2}\} / \sigma_{I_{u,p}^{sch}}^2 = S_u \tilde{L}_u / P_u \sigma_{I_{u,p}^{sch}}^2 , \tag{4.42}$$

where $\tilde{L}_u = J[2 + 9\pi(JL_u - 1)/16]\sigma^2$. It is assumed that any bit can be transmitted via any of data streams with equal probability, and define γ_u^{sch} as the average SIR given by

$$\gamma_u^{sch} = \frac{1}{P_u} \sum_{p=1}^{P_u} \gamma_{u,p}^{sch} \cong \gamma_{u,1}^{sch} \quad . \tag{43}$$

In the multirate STBC MC-CDMA systems, different service classes may have different QoS requirements, i.e. bit error rate (BER) requirements. We assume that the average BER for mth class service is demanded to be less than its threshold $Ber_{Trh,m}$. Equivalently, the SIR threshold can be defined as

$$\Gamma_m = \left[Q^{-1}(Ber_{Trh,m})\right]^2 \quad (m = 1, \cdots, M), \tag{4.44}$$

where $Q(x) = \int_x^\infty \exp(-x^2/2)/\sqrt{2\pi}dx$ represents the Gaussian cumulative function. The proposed power control algorithm is to maintain the ratio among the average SIR defined in (4.43) of different classes equal to the ratio among the corresponding SIR thresholds between different classes, i.e.,

$$\gamma_1^{sch} : \gamma_2^{sch} : \cdots : \gamma_M^{sch} = \Gamma_1 : \Gamma_2 : \cdots : \Gamma_M . \tag{4.45}$$

Then the transmit power of every user from each class has to be adapted according to the relation defined in (4.45). Let the average power $\bar{S}$ in the system is kept at a constant, given by

$$\bar{S} = \sum_{m=1}^{M} K_m S_m \Big/ \sum_{m=1}^{M} K_m , \tag{46}$$

by solving the M variables M independent linear equations (4.45) and (4.46), we can obtain the transmit power S_m ($m=1,\cdots,M$) for different classes. Particularly, if $M=2$, the transmit powers for each service class are given by

$$S_1 = \frac{\vartheta_{sch}(K_1+K_2)}{\vartheta_{sch}K_1+K_2}\bar{S}\ , \qquad S_2 = \frac{K_1+K_2}{\vartheta_{sch}K_1+K_2}\bar{S}\ , \tag{4.47}$$

respectively, where

$$\vartheta_{sch} = \Big[G_{1,1}^{sch}\tilde{L}_2P_1\Gamma_1/\Gamma_2 - G_{2,2}^{sch}\tilde{L}_1P_2 + \Big((G_{1,1}^{sch}\tilde{L}_2P_1\Gamma_1/\Gamma_2 - G_{2,2}^{sch}\tilde{L}_1P_2)^2 + 4G_{1,2}^{sch}G_{2,1}^{sch}\tilde{L}_1\tilde{L}_2P_1P_2\Gamma_1/\Gamma_2\Big)^{1/2}\Big]/2G_{2,1}^{sch}\tilde{L}_1P_2\ . \tag{4.47a}$$

Under a guaranteed QoS requirement, the average BER performance of mth class service has to be better than a given BER threshold $Ber_{Trh,m}$. It means that the system average BER performance of mth class service needs to satisfy

$$\mathrm{P}_{e,m}^{sch} \le Ber_{Trh,m}\ . \tag{4.48}$$

Define $K_{m,Max}^{sch}$ as the maximum number of users from mth class that the system with either mc, VSG or MSR scheme can accommodate under the QoS requirement (4.48), i.e.

$$K_{m,Max}^{sch} = \max\{K_m^{sch} \mid \mathrm{P}_{e,m}^{sch} \le Ber_{Trh,m}, m=1,\cdots,M\}\ . \tag{4.49}$$

Then the system capacity (bandwidth efficiency) of the system with mc or VSG or MSR access scheme is given by

$$\rho_{sch} = \sum_{m=1}^{M} K_{m,Max}^{sch} R_m / B\ . \tag{4.50}$$

4.5 Numerical Results

In this section, we investigate the performance and system capacity of mc, VSG and MSR access schemes for STBC MC-CDMA systems. The results obtained are also compared with the conventional MC-CDMA systems. Three systems i) MC-CDMA system (1 transmitter and 1 receiver), ii) STBC MC-CDMA system (2 transmitters and 1 receiver) and iii) STBC MC-CDMA system (2 transmitters and 2 receivers) are considered. For simplicity, a two-class service system ($M = 2$) is used. The transmission rate for a low and a high rate user are given to be R_1 and R_2, respectively, with $R_2 = N_2 R_1$. There are altogether K_1 low rate and K_2 high rate users in the systems. The total bandwidth B for the systems is fixed at 5MHz. The transmission rate R_1 of low rate class is fixed at 20kbps. The BER thresholds are the same for all classes, and we set $Ber_{Trh,m} = 10^{-3}$. The symbol energy is defined as $E_s = ST_s / P_m$.

Fig. 4.7 shows the BER performance of high rate users versus E_s / N_0 for different multirate access schemes when $K_1 = 32$, $K_2 = 8$ and $R_2 = 4R_1$ (The BER performance of low rate users is not presented here since the results are nearly the same as those of high rate users), with (a) shows the BER performance for multirate MC-CDMA systems, and (b) shows the BER performance of multirate STBC MC-CDMA systems. It can be observed that BER performance of multicode access scheme when orthogonal Gold sequences are used and VSG access scheme give the highest capacity. The performance of multicode access scheme when Gold sequences (non-orthogonal) are used will be a slightly worse. On the other hand, the BER performances of the three configurations of MSR access scheme are worse than that of multicode and VSG access schemes, although the performances of configuration 2 and

3 of MSR access scheme is approaching the that of multicode and VSG access schemes. The performance of configuration 1 of MSR access scheme is the worst among all the schemes because it does not fully make use of the whole bandwidth. It also can be seen that for any of the multirate access scheme, the performance of multirate STBC MC-CDMA systems is better than that of conventional multirate MC-CDMA system. Besides, the computed BER results using our proposed analysis method well agree with the results obtained from computer simulations. This verifies the correctness and effectiveness of our analysis for all the multirate access schemes (multicode, VSG and MSR access scheme) of both the asynchronous STBC MC-CDMA systems and MC-CDMA systems.

The system capacity for mc access scheme of STBC MC-CDMA systems is shown in Fig. 4.8 (a) and (b), where orthogonal and non-orthogonal Gold sequences are used, respectively. It can be observed that the system capacity of STBC MC-CDMA with 2 transmitters and 2 receivers will be much better, although the system capacity of STBC with 2 transmitters and 1 receiver will be only slightly better than that of conventional MC-CDMA. It also shows from Fig. 4.8 (b) that the system capacity is relatively worse when there a larger number of high rate users (i.e. smaller number of low rate users) in the system. This is due to the presence of self-interference (SI) resulting from all virtual users of a high rate user. On the other hand, if orthogonal sequences are used, interference between users exist (because of asynchronous transmission) but not between virtual users. Hence system capacity exhibits different behavior when the number of low rate users increases, as shown in Fig. 4.8 (a). As R_2 / R_1 increases, a larger "fluctuation" in the system capacity is observed. This is expected because we need to remove more low rate users in order to allow a high rate user to enter the system. The results presented in these curves also shown that there exist a maximum number of users that the system can support and beyond that, BER cannot be satisfied.

By comparing Fig. 4.8 (a) and (b), it can be observed that the system capacity for mc access scheme when the Gold sequence is used is worse than that when the orthogonal Gold sequence is used. The system capacity gets worse when the value of R_2 / R_1 increases. This is because SI from virtual users when non-orthogonal Gold sequence is used is much larger than that when orthogonal Gold sequence is used, since transmission among virtual users is synchronized.

Fig. 4.9 shows the system capacity for VSG multirate access scheme of STBC MC-CDMA system. As mentioned before, the system capacity when either orthogonal Gold sequence or Gold sequences is used will be the same. By comparing Fig. 4.9 with Fig. 4.8, it can be observed that the system capacity of the VSG access scheme is nearly the same as that of mc access scheme when orthogonal Gold sequence is used. In fact, very slight degradation is observed for VSG by comparing using the actual computed values. This observation is in contrast to MC-CDMA systems, where orthogonal Gold sequence mc scheme exhibits a higher capacity than VSG scheme, as can be seen by comparing the curves for MC-CDMA shown in Fig. 4.8 (a) and Fig. 4.9.

Fig. 4.10 shows the system capacity of three configurations of MSR access scheme for STBC MC-CDMA system, where (a) is for MSR system with spectrum configuration 1 ($\Delta f_1 = 0$, here the case when $\Delta f_1 \neq 0$ is not presented since the results we have evaluated have not much differences.), (b) is for the MSR system with spectrum configuration 2 and (c) is for the MSR system with spectrum configuration 3. It can be observed from (a) that as R_2 / R_1 increases, the system capacity and the maximum number of low rate users K_1 that the system can accommodate decreases dramatically for MSR system with CSG configuration 1. From (b) and (c), it can be seen that as the R_2 / R_1 increases, the system capacity and maximum number of low rate users that the system can accommodate changes only slightly for the MSR system with spectrum configuration 2 or the MSR system with spectrum configuration 3. By comparing (b) with (c), as K_1 is small, the system capacity of spectrum configuration 2 will be better than that of the system with spectrum configuration 3 when R_2 / R_1 is small, the result is reverse when R_2 / R_1 is large. As K_1 is moderate, the system capacity of configuration 2 will be better than that of the system with spectrum configuration 3. Besides, the larger the high transmission rate R_2 is, the larger fluctuation in the system capacity is observed. This is expected because more lower rate users are needed to replace a high rate user to enter the systems.

By comparing (a) with (b) and (c), the system capacity for MSR system with spectrum configuration 2 and the system with spectrum configuration 3 is getting much steadily than that for the system with spectrum configuration 1 as R_2 / R_1 is large. And the system capacity of MSR system with spectrum configuration 2 is the best when K_1 is moderate. And as expected, when the two service rates approach the same value, All the MSR system with different spectrum configuration will approach the nearly same system capacity.

By comparing Fig. 4.8, Fig. 4.9. and Fig. 4.10, it can be concluded that the systems with mc access scheme when orthogonal Gold spreading sequence applied and VSG access scheme have similar system performance and capacity, and both perform better and much steadily than the system with any spectrum configurations of MSR access scheme.

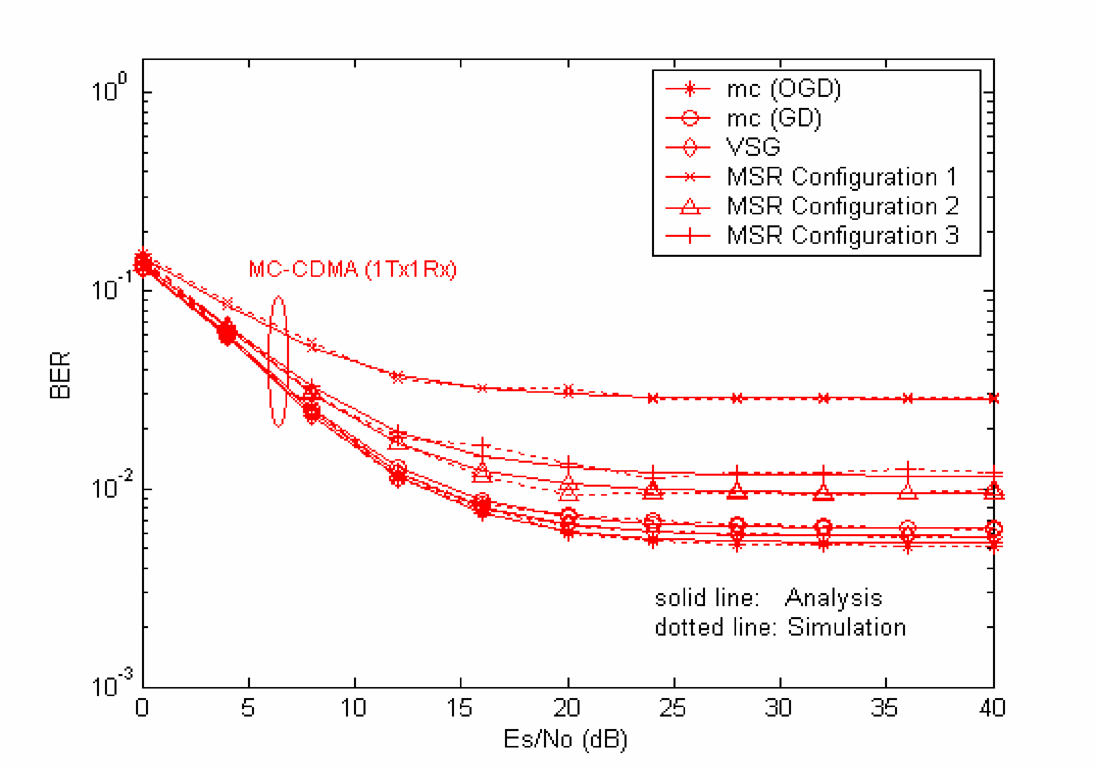

(a) MC-CDMA system

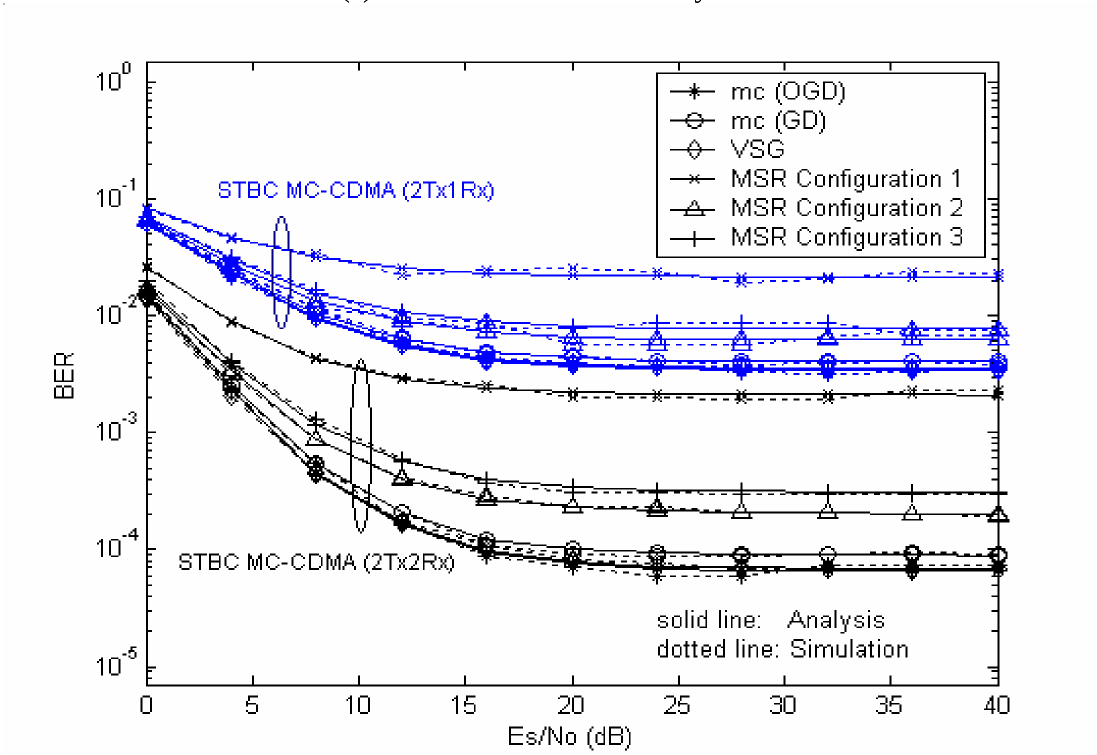

(b) STBC MC-CDMA systems

Fig. 4.7 BER performance of high rate users versus Es/No for different multirate access schemes ($K1$=32, $K2$=8 and $R2$=4$R1$)[1]

[1] OGD is abbreviation of orthogonal gold sequence, while GD is abbreviation of gold sequence.

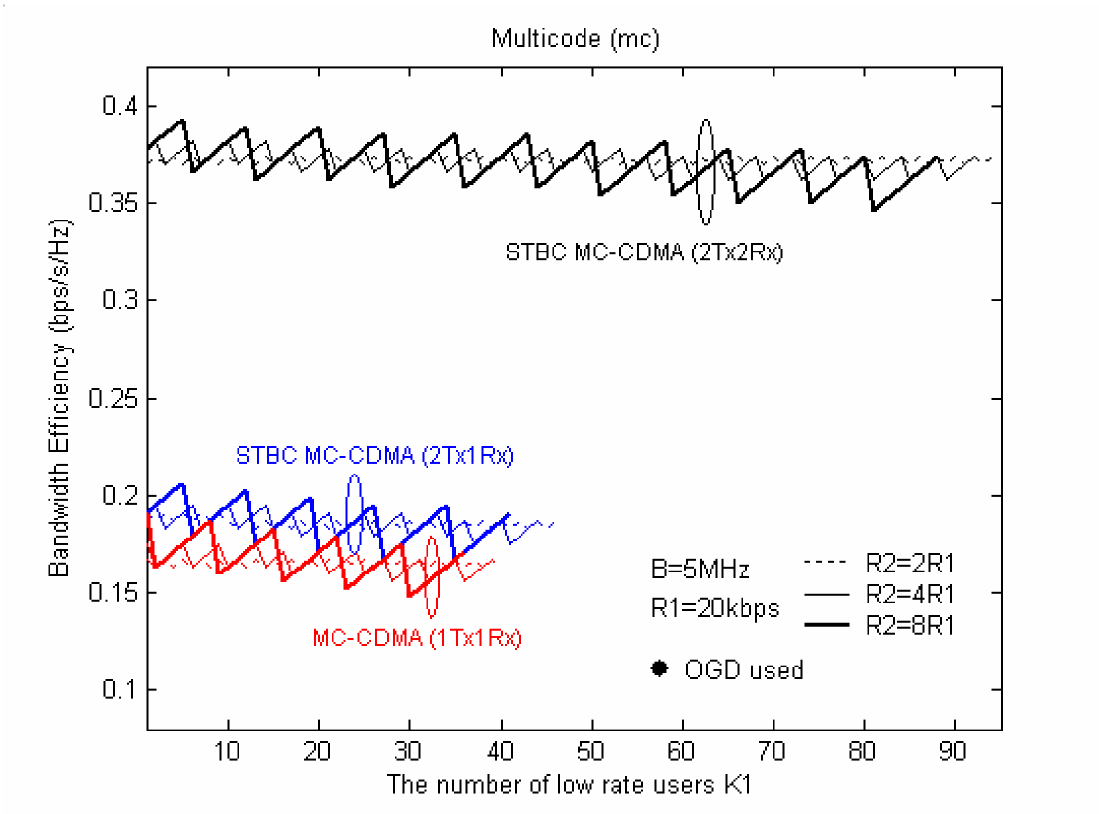

(a)

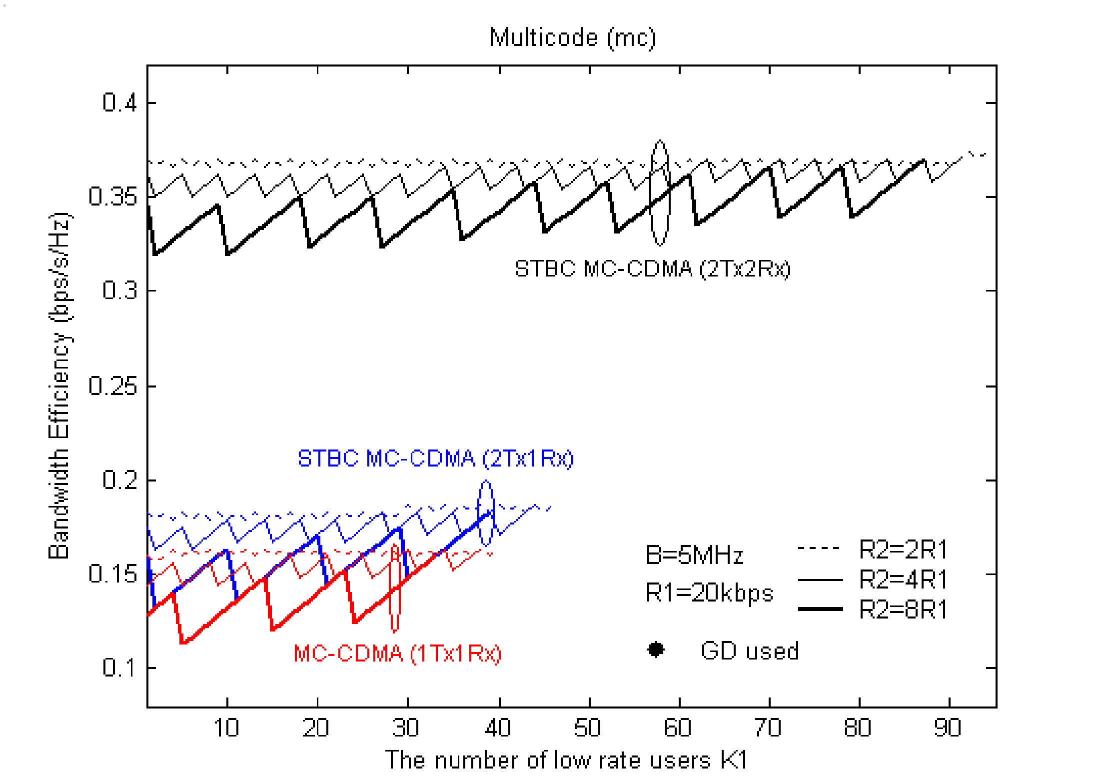

(b)

Fig. 4.8 System capacity for mc access scheme of STBC MC-CDMA system (a) orthogonal Gold sequence; (b) Gold sequence

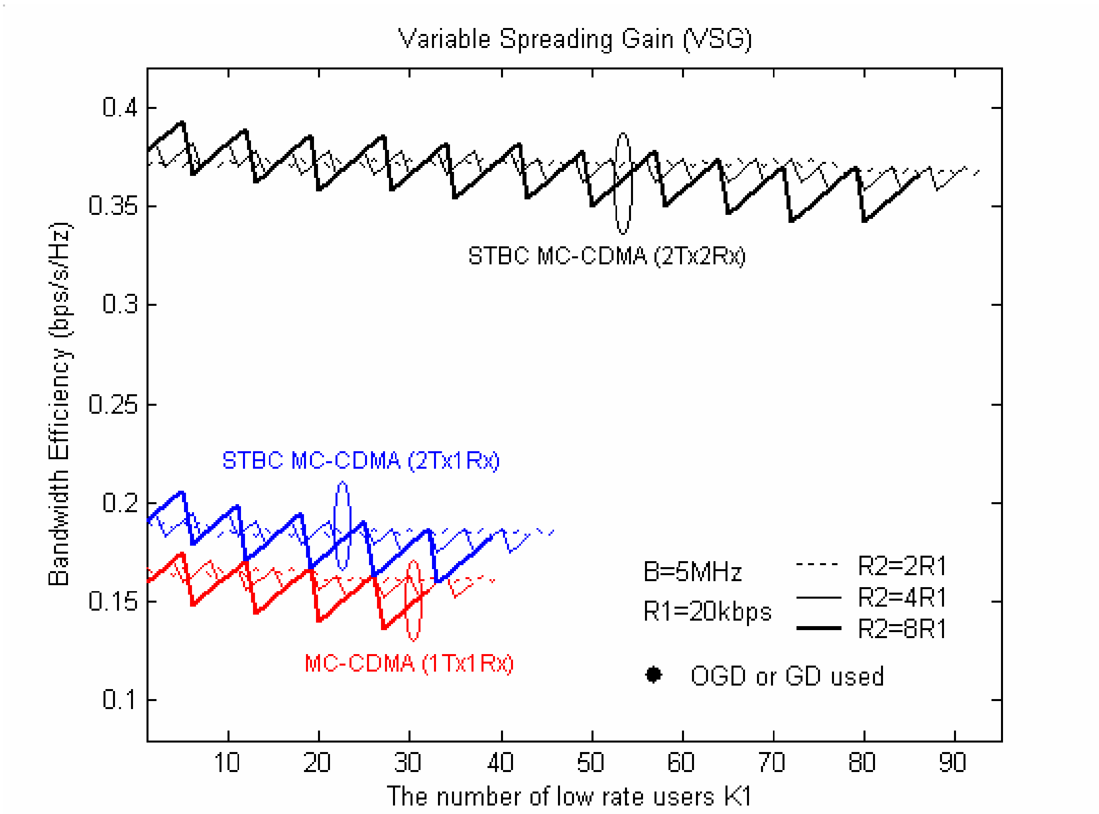

Fig. 4.9 System capacity for VSG access scheme of STBC MC-CDMA system. (Gold sequence or orthogonal Gold sequence is used)

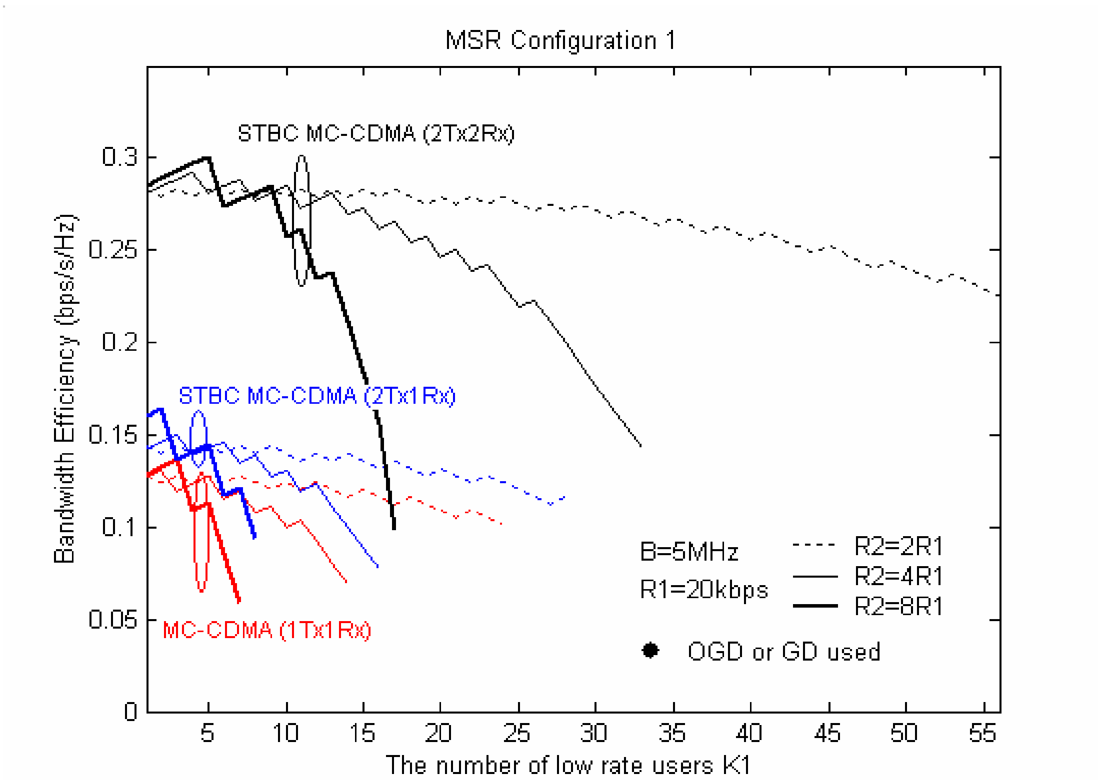

(a)

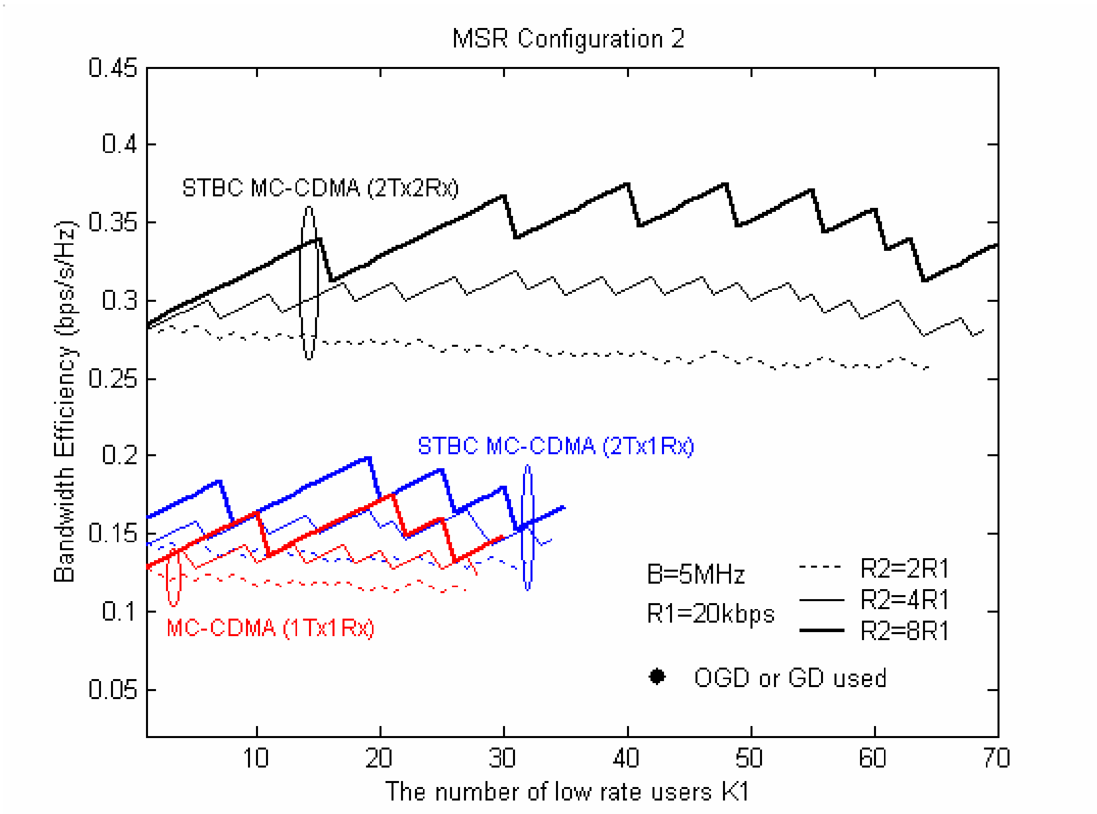

(b)

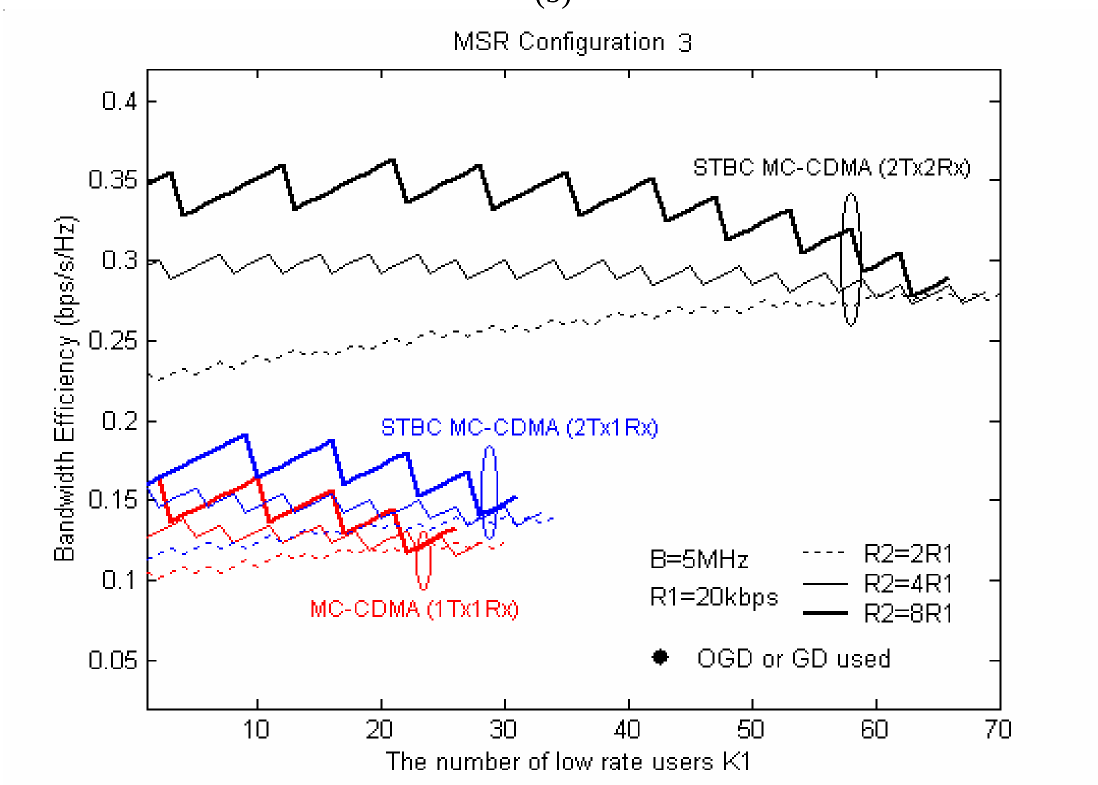

(c)

Fig. 4.10 System capacity of MSR access scheme for STBC MC-CDMA system (Gold sequence or orthogonal Gold sequence is used) (a) Spectrum Configuration 1; (b) Spectrum Configuration 2; (c)Spectrum Configuration 3

4.6 Conclusion

In this chapter, the system performances and capacities of mc, VSG and MSR multirate access schemes with transmit power control for STBC MC-CDMA systems are investigated. The system models for these three multirate access schemes are presented, then the interferences for different access schemes are given. With our proposed power control, the BER performance and system capacity analysis for the three access schemes are presented. Finally, the numerical results are given to show clear comparisons between the three multirate access schemes. And the theoretical analysis is also verified by computer simulations. It can be concluded that the systems with mc access scheme when orthogonal Gold spreading sequence is used and VSG access scheme have similar system performance and capacity, and both perform better than the system with any spectrum configurations of MSR access scheme. In case when non-orthogonal Gold sequences are used, mc access scheme shows a degrading in the system capacity as compared to VSG, due to the presence of larger self-interference (SI) among the sequences used by each user. It can be also concluded that the system performance and capacity of STBC MC-CDMA system will be better than the conventional MC-CDMA without space-time coding. The system performance and capacity will be much better when the system have more receive antennas.

Appendix 4.A

To better understand the multiuser interference for different MSR sepctrum configurations, a two-class service system ($M = 2$) is considered in this appendix. However, the analysis can be easily extended to more service classes. The two classes of users have the low and high transmission rates, R_1 and R_2, respectively, with $R_2 = N_1 R_1$. There are K_1 low rate users and K_2 high rate users in the system.

(i) *MSR Configuration 1*

In this configuration, high rate users will occupy whole bandwidth at each subcarrier, whereas, all the low rate users are allocated in only one subsystem. One of the subcarrier spectral of the two systems is shown in 0(b), where we have $\Delta f_{1,k} = \Delta f_1$ for any low rate user *k*. Thus, the variance of interference for low rate user is given by

$$\sigma_{I_1}^2 = (K_1 - 1) Var(I_{1,k}^{CSG} \mid T_m = T_u) + K_2 Var(I_{2,k}^{CSG} \mid T_m < T_u) \tag{4.A.1}$$

and the variance of interference for high rate user is given by

$$\sigma_{I_2}^2 = K_1 Var(I_{1,k}^{CSG} \mid T_m > T_u) + (K_2 - 1) Var(I_{2,k}^{CSG} \mid T_m = T_u). \tag{4.A.2}$$

(ii) *MSR Configuration 2*

In this configuration, high rate users will occupy the whole bandwidth of each subcarrier. The low rate users divide the subcarrier bandwidth into $\overline{N}_1 = 2N_1 - 1$ subsystems. The low rate users are evenly distributed among $\overline{N}_1$ subsystems. The central frequency of the *n*th subsystem at the *l*th subcarrier is given by $f_{m,l,n} = f_{M,l} - 1/T_M + n/T_m$, $n = 1, 2, \cdots, \overline{N}_1$. The spectrum allocation is shown in Fig. 4.5(c). It is expected that with such arrangement, the MUI experienced by a narrowband user is smaller so that system capacity can be improved. The allocation algorithm is presented as follows:

(1) Let $K_1 = \overline{N}_1 \overline{K}_1 + v$, where $\overline{K}_1 = \lfloor K_1 / \overline{N}_1 \rfloor$ and $v = K_1 \bmod \overline{N}_1$.

(2) Allocate $\overline{K}_1$ low rate users evenly among $\overline{N}_1$ subsystems.

(3) Finally, allocate the remaining v low rate users into the first v subsystems, one user per one subsystem.

If the user in the first subsystem is of interest, the variance of the interference for low rate user is given by

$$\sigma_{I_1}^2 = (\overline{K}_1 + g(v,1) - 1) Var(I_{1,k}^{CSG} \mid T_m = T_u) + \sum_{n=2}^{\overline{N}_1} (\overline{K}_1 + g(v,n)) Var(I_{1,k}^{CSG} \mid T_m = T_u) + K_2 Var(I_{2,k}^{CSG} \mid T_m < T_u) \quad (4.A.3)$$

where $g(v,n) = \begin{cases} 1 & v \geq n \\ 0 & v < n \end{cases}$. The variance of the interference for high rate user is given by

$$\sigma_{I_2}^2 = \sum_{n=1}^{\overline{N}_1} (\overline{K}_1 + g(v,n)) Var(I_{1,k}^{CSG} \mid T_m > T_u) + (K_2 - 1) Var(I_{2,k}^{CSG} \mid T_m = T_u) \quad . \quad (4.A.4)$$

(iii) *MSR Configuration 3*

For this configuration of MSR access scheme system, the relationship between the spreading gains (or number of subcarriers) of the low rate and high rate class is given by $L_1 = N_1 L_2 + N_1 - 1$. The variance of interference for a low rate user is given by

$$\sigma_{I_1}^2 = (K_1 - 1) Var(I_{1,k}^{VSG} \mid T_m = T_u) + K_2 Var(I_{2,k}^{VSG} \mid T_m < T_u) \quad (4.A.5)$$

and the variance of interference for a high rate user is given by

$$\sigma_{I_2}^2 = K_1 Var(I_{1,k}^{VSG} \mid T_m > T_u) + (K_2 - 1) Var(I_{2,k}^{VSG} \mid T_m = T_u) . \quad (4.A.6)$$

Chapter 5

Timing and Frequency Synchronization

In the next two chapters, we focus our studies on some receiver design and implementation issues for STBC MC-CDMA systems. Firstly, joint timing and frequency synchronization are investigated in this chapter. Then time and frequency offset information will be feed back to mobile users through the control channel, so that the mobile users adjust their clock and oscillators adapted to the base station. When the signals of all users arrived at the base station synchronously, the channel estimation and multiuser detection will be performed to recover the data of all users.

In this chapter, a subspace-based joint blind multiuser timing and frequency synchronization scheme for asynchronous STBC MC-CDMA systems over frequency selective fading channels is proposed. While formulating the joint synchronization using the maximum likelihood (ML) method [75], we find that it will inevitably result in a multi-dimensional estimation problem when multiple users are present, This means that we are not able to decouple the multiuser parameters estimation problem to a series of single user estimation problems, as a result, huge amount of computation needs to be performed. Our effort shows that subspace-based algorithm can resolve this joint timing and frequency synchronization in multiuser STBC MC-CDMA or MC-CDMA systems more efficiently. We show that through properly choosing the oversampling factor and the number of received samples, the joint timing and frequency synchronization for multiple users can be resolved using the subspace approach. The proposed subspace based algorithm is derived by taking the transmitters of all users into consideration, and the joint multiuser and multiple input multiple output (MIMO) synchronization problem will be transformed into a set of single user and single input single output (SISO) timing and frequency synchronization problems. Each single user problem is then reduced and generalized to a one-dimensional optimization, and then solved by using an numerical iterative algorithm, such as the Newton's approach. Simulation results show the robustness and effectiveness of the proposed synchronization algorithm in the presence of near far problem, multipath fading and Doppler Spread. Performance of the proposed algorithm is studied using the small perturbation analysis and is verified by computer simulations. Finally the Cramér-Rao bound (CRB) is derived and computed in this chapter.

The rest of this chapter is organized as follows. The synchronization scheme is first described in the Section 5.1. The system model is described and the problem under investigation is formulated in Section 5.2. The subspace based blind joint timing and frequency synchronization algorithm is proposed in Section 5.3. The performance analysis is presented in Section 5.4. The derivation of CRB is given in Section 5.5. The computer simulations are presented in Section 5.6. Finally, the paper is concluded in Section 5.7

5.1 Synchronization Scheme

We concentrate our work on the uplink (asynchronous) transmission of STBC MC-CDMA systems. The important difference between the uplink and downlink multiuser synchronization is how symbol and frequency synchronization is accomplished. In a downlink scenario, offsets are estimated by the mobile receiver. These offset estimates then control the adjustments of the local symbol clock and demodulation oscillator. Synchronization thus takes place at the receiver. In the uplink, on the other hand, time and frequency offset estimation is performed in the base station but the clock and oscillator adjustments are made in the mobile user's transmitter. Since all mobile users' signals must arrive at the base station aligned in time and frequency in order to maintain the orthogonality between the subcarriers, all users adapt to the base station's receiver clock and oscillator by adjusting their oscillators and scheduling their transmission according to the base station information. Therefore, in our scheme, for every connected mobile user a control channel is embedded in the downlink on which control information conveying the offset estimates is transmitted back to the mobile user. With the aid of these control parameters, the mobile user aligns its transmitted signal to the receiver reference symbol clock and to the receiver oscillator. The control channel is embedded in the downlink frequency band, which may have a similar multiuser structure as the uplink band and is set up during the initial phase of the connection. Apart from offset estimates, other control parameters for one user include, for instance, which time slots must be used for the uplink transmission and which transmission power must be applied. Successful synchronization of the user thus relies on the control channel.

5.2 System Model

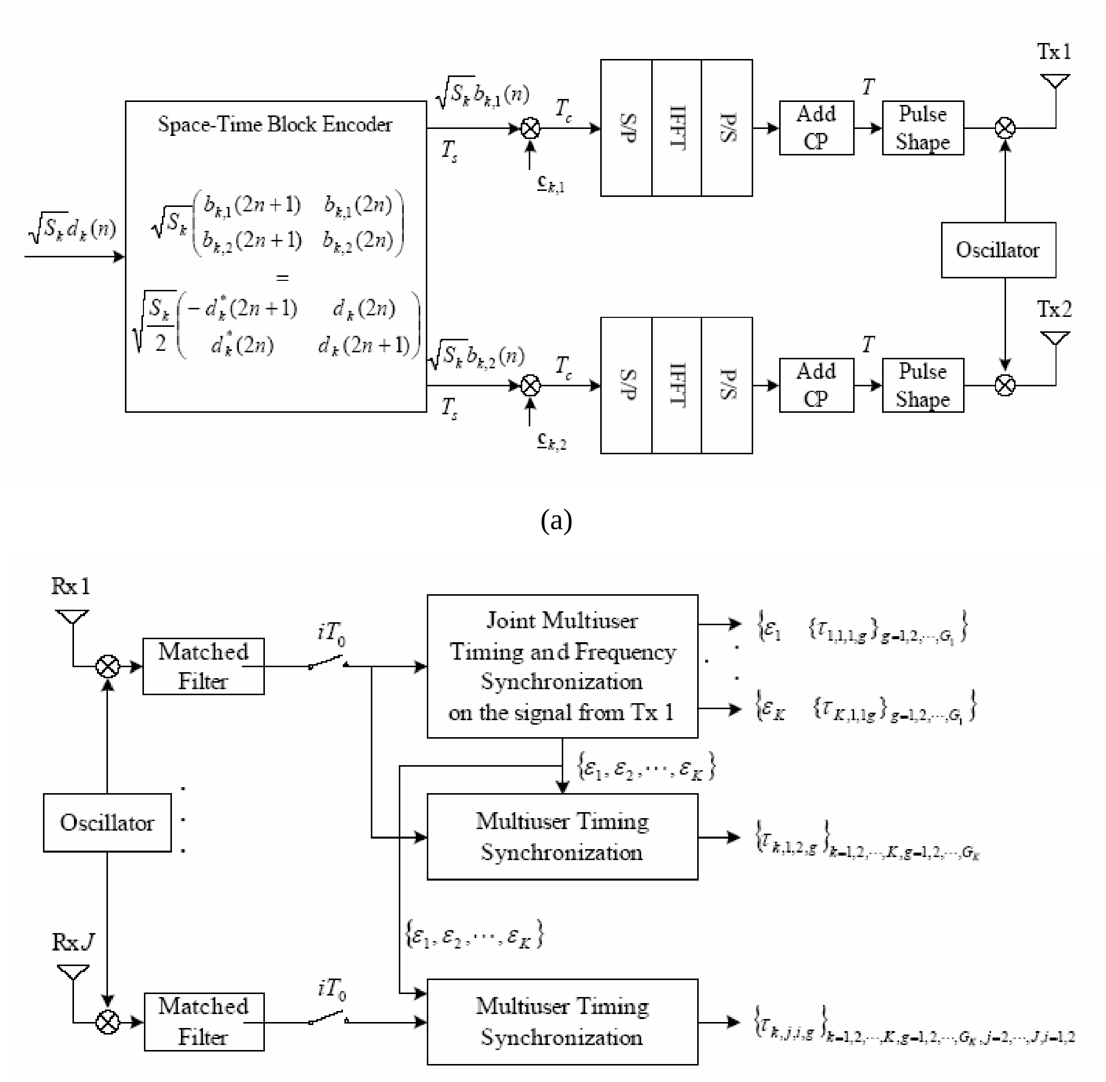

(a)

(b)

Fig. 5.1 The system model of STBC MC-CDMA (a) Transmitter; (b) Receiver

An asynchronous STBC MC-CDMA system over frequency selective fading channels is considered. We assume that there are K active asynchronous users in the system. The equivalent block diagram of the transmitter and receiver of STBC MC-CDMA system used in our analysis is shown in Fig. 5.1. The stream of symbols of the kth user first goes through the ST block encoder. Without incurring any power or bandwidth penalty, the Alamouti's orthogonal ST block coding scheme for two transmit antennas is employed [44][48], and more general ST codes for other number of transmit antennas can be found in [48]. Two successive symbols $\sqrt{S_k}\, d_k(2n)$ and $\sqrt{S_k}\, d_k(2n+1)$ for the *k*th user are mapped to the following matrix

$$\sqrt{S_k}\begin{pmatrix} b_{k,1}(2n+1) & b_{k,1}(2n) \\ b_{k,2}(2n+1) & b_{k,2}(2n) \end{pmatrix} = \sqrt{\frac{S_k}{2}}\begin{pmatrix} -d_k^*(2n+1) & d_k(2n) \\ d_k^*(2n) & d_k(2n+1) \end{pmatrix} \quad \begin{array}{l} \leftarrow \ \text{time} \\ \downarrow \ \text{space} \end{array}$$

where $d_k(n)$ denotes the *n*th symbol for *k*th user, S_k is its transmit power and $b_{k,i}(n)$ denotes the *n*th symbol at the *i*th transmit antenna for the *k*th user, and * denotes complex conjugate. The columns are transmitted in successive block time with the symbols in the upper and lower blocks simultaneously sent through the two transmit antennas, respectively. The factor $1/\sqrt{2}$ is to normalize the transmitted symbol energy.

Next the signal $b_{k,i}(n)$ at *i*th transmit antenna is spread by the spreading code $\underline{\mathbf{c}}_{k,i} = [c_{k,i,0}, \ \cdots \ c_{k,i,L-1}]^T$, where L is spreading gain and ^{T} denotes the transpose. We assume that the spreading code has unit amplitude, and normalized by $1/\sqrt{L}$. The spread signal $\sqrt{S_k / L} \cdot \underline{\mathbf{c}}_{k,i} b_{k,i}(n)$ is then serial-to-parallel converted followed by the inverse fast Fourier transform (IFFT) processing $\mathbf{F}^{\mathcal{H}}$, where $\mathbf{F}$ is the $L \times L$ matrix with its $(m,n)^{\text{th}}$ entry equal to $1/\sqrt{L} \cdot \exp[-j2\pi(m-1)(n-1)/L]$ and $^{\mathcal{H}}$ denotes the Hermitan transpose. To compensate for the channel's time-dispersive effects thus to avoid ISI, we insert redundancy in the form of cyclic prefix (CP) of the length larger than the channel order, *G*, $G = \lfloor \tau_{max}/T \rfloor$ where τ_{max} denotes the maximum delay spread among all the users, and T is the interval between two MC-CDMA samples after CP insertion, i.e., $T = LT_c / V = T_s / V$ where V is the total number of samples in one MC-CDMA symbol period T_s. The CP insertion process can be described by a $V \times L$ transmit matrix given by $\mathbf{T}_{cp} = [\mathbf{I}_{cp} \quad \mathbf{I}_L]^T$, where $\mathbf{I}_{cp}$ denotes the last

$V - L \geq G$ rows of $L \times L$ identity matrix $\mathbf{I}_L$, and the energy is normalized by $\sqrt{L/V}$. Then the transmitted signal for kth user is given by

$$\underline{\mathbf{x}}_{k,i}(n) = \sqrt{S_k/V} \cdot \mathbf{T}_{cp}\mathbf{F}^{\mathcal{H}}\underline{\mathbf{c}}_{k,i}b_{k,i}(n), \tag{5.1}$$

where $k = 1, \cdots K$, $i = 1,2$

The signal $\underline{\mathbf{x}}_{k,i}(n)$ is converted from parallel to serial (P/S), and the resulting sequence $x_{k,i}(a)$ is then shaped to obtain the continuous time signal $x_{k,i}(t) = \sum_{a=-\infty}^{\infty} x_{k,i}(a)u(t - aT)$, where $u(t)$ is the pulse shape. The transmitted signal propagates through the unknown time-dispersive channel between ith transmit antenna and jth receive antenna which has finite impulse response denoted as $\overline{\beta}_{k,j,i}(t)$. The received signal is then shaped by $\overline{u}(t)$ which is matched to $u(t)$, and then sampled at the rate $1/T_0 = H/T$, where H is an integer and denotes the oversampling factor. At the receiver of the base station, the equivalent discrete-time channel impulse response can be expressed as

$$\beta_{k,j,i}(a) = u(t) \otimes \overline{\beta}_k(t) \otimes \overline{u}(t)\Big|_{t=aT_0} = \sum_{g=1}^{G_k} \beta_{k,j,i,g}\delta(a - \tau_{k,j,i,g}) \tag{5.2}$$

where $\delta(t)$ denotes the Dirac delta function, $\beta_{k,j,i,g}$ is complex channel fading gain between ith transmit antenna and jth receive antenna for gth path of user k, respectively. G_k denotes the number of paths of user k. And $\tau_{k,j,i,g}$ is the relative time delay between the ith transmit antenna and the jth receive antenna for the gth path of user k with respect to some reference time, which can be taken as the time where samples are collected, as shown in Fig. 5.2. We assume that the relative time delay of each path from the same user is distinct and within one symbol interval, i.e., $\tau_{k,j,i,g}$ takes an integer value in $[0, VH)$ [82]-[88], and

$$0 < \tau_{k,j,i,1} < \tau_{k,j,i,2} < \cdots < \tau_{k,j,i,G_k} < VH \text{, and } \tau_{k,j,i,g} T_0 < VHT_0 = T_s \text{.} \tag{5.3}$$

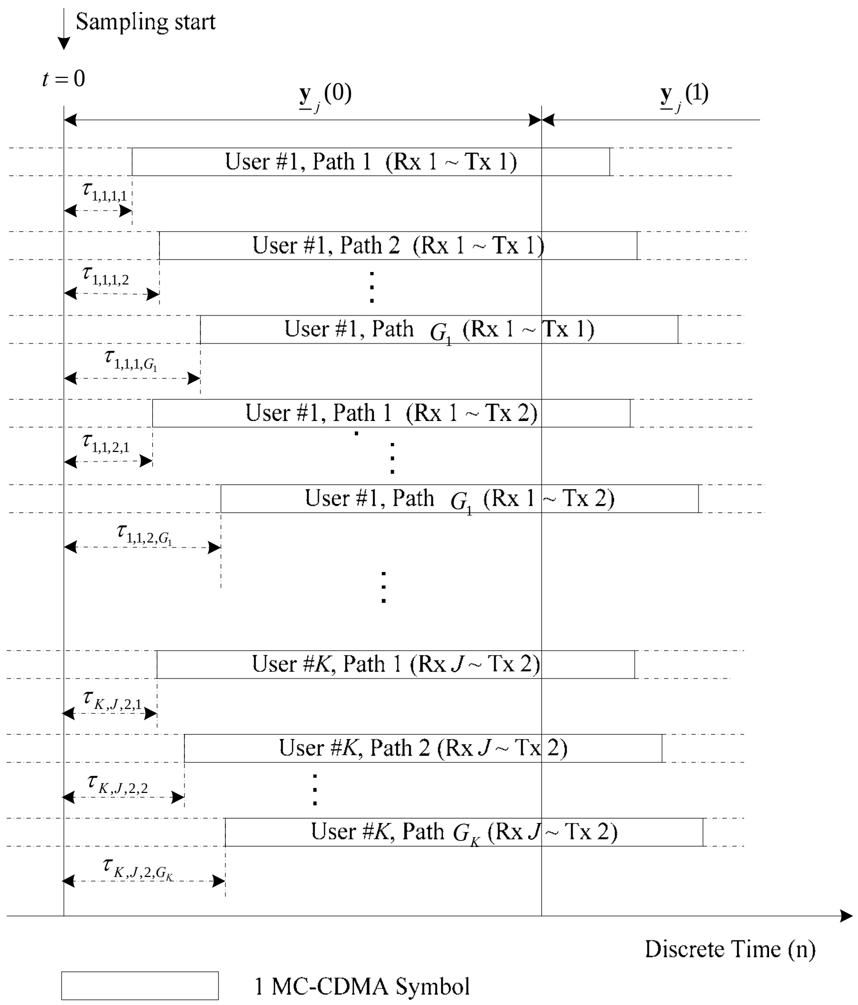

Fig. 5.2 Illustration of the timing information in the asynchronours transmission of diff erent users and multipath delay at *j*th receive antenna

Assume K asynchronous users in the system, due to the mismatch between the oscillator in the transmitters of K users and the receiver at base station, the received signal at the *j*th receive antenna ($j = 1,2,\cdots,J$), sampled at the rate $1/T_0$, can be written as

$$y_j(a) = \sum_{k=1}^{K} \exp(-j2\pi\varepsilon_k / VH) \cdot \sum_{i=1}^{2} \sum_{g=1}^{G_k} \beta_{k,j,i,g} x_{k,i}(a - \tau_{k,j,i,g}) + \eta_j(i) \text{,}$$

$$j = 1,2,\cdots,J \text{,} \tag{5.4}$$

where ε_k is the normalized carrier frequency offset (NCFO) to the subcarrier spacing $1/T_s$. $\eta_j(i)$ denotes the zero-mean additive white Gaussian noise (AWGN) with the variance σ_η^2 which is assumed to be independent of $d_k(n)$ and $x_{k,i}(\cdot)$ has been defined in (1). Denote a $VH \times 1$ vector $\underline{\mathbf{a}}_{k,i} = \left(\mathbf{T}_{cp}\mathbf{F}^{\mathcal{H}}\underline{\mathbf{c}}_{k,i} \otimes \underline{\mathbf{h}}\right)/\sqrt{V}$, where $\underline{\mathbf{a}}_{k,i} = \left[a_{k,i,0}, a_{k,i,1}, \cdots, a_{k,i,VH-1}\right]^T$. Without loss in generality, the transmission pulse shape is assumed rectangular and $\underline{\mathbf{h}}$ is $H \times 1$ vector to account for the oversampling and $\underline{\mathbf{h}} = [1,1,\cdots,1]^T / \sqrt{H}$. With some manipulation, the nth received sample block at jth receive antenna can be expressed as a $VH \times 1$ vector

$$\underline{\mathbf{y}}_j(n) = \sum_{k=1}^{K} \mathcal{D}(\underline{\mathbf{f}}(\varepsilon_k)) \sum_{i=1}^{2} \mathbf{A}_k(\underline{\boldsymbol{\tau}}_{k,j,i}) \underline{\mathbf{s}}_{k,j,i}(n) + \underline{\boldsymbol{\eta}}_j(n), \quad j = 1,2,\cdots,J, \tag{5.5}$$

where $\underline{\mathbf{y}}_j(n) = \left[y_j(nVH), \quad y_j(nVH+1), \quad \cdots \quad y_j(nVH+VH-1)\right]^T$ is the collection of the nth block of VH samples to be processed, and likewise for $\underline{\boldsymbol{\eta}}_j(n)$ takes the similar form. $\underline{\mathbf{f}}(\varepsilon_k) = [1, \exp(-j2\pi\varepsilon_k / VH), \cdots, \exp(-j2\pi\varepsilon_k (VH-1)/VH)]^T$, and

$$\underline{\mathbf{s}}_{k,j,i}(n) = \exp(-j2\pi n\varepsilon_k)\sqrt{S_k} \cdot$$
$$\left[b_{k,i}(n)\beta_{k,j,i,0} \quad b_{k,i}(n-1)\beta_{k,j,i,0} \quad \cdots \quad b_{k,i}(n)\beta_{k,j,i,G_k} \quad b_{k,i}(n-1)\beta_{k,j,i,G_k}\right].$$

Note that two consecutive MC-CDMA symbols are used because transmissions are asynchronous. To make the element of the matrix $\mathcal{D}(\underline{\mathbf{f}}(\varepsilon_k))$ independent of time index n is an important step in our algorithm. Because of this, $\mathcal{D}(\underline{\mathbf{f}}(\varepsilon_k))$ contains only the frequency offset ε_k which is of the interest, and the time dependent term $\exp(-j2\pi n\varepsilon_k)\sqrt{S_k}$ incorporated in $\underline{\mathbf{s}}_{k,j,i}(n)$ is regarded as the nuisance parameter in our algorithm. The matrix

$$\mathbf{A}_k(\underline{\boldsymbol{\tau}}_{k,j,i}) = \left[\underline{\bar{\mathbf{a}}}_k(\tau_{k,j,i,1}) \quad \underline{\tilde{\mathbf{a}}}_k(\tau_{k,j,i,1}) \quad \cdots \quad \underline{\bar{\mathbf{a}}}_k(\tau_{k,j,i,G_k}) \quad \underline{\tilde{\mathbf{a}}}_k(\tau_{k,j,i,G_k})\right], \tag{5.6}$$

where $\underline{\boldsymbol{\tau}}_{k,j,i} = \begin{bmatrix} \tau_{k,j,i,1} & \tau_{k,j,i,2} & \cdots & \tau_{k,j,i,G_k} \end{bmatrix}^T$. The definition of $\underline{\bar{\mathbf{a}}}_k(\tau_{k,j,i,g})$ and $\underline{\tilde{\mathbf{a}}}_k(\tau_{k,j,i,g})$ ($g = 1,2,\cdots,G_k$) are given by

$$\underline{\bar{\mathbf{a}}}_k(\tau_{k,j,i,g}) = \begin{bmatrix} \mathbf{0}^T_{\tau_{k,j,i,g}\times 1} & a_{k,i,0} & a_{k,i,1} & \cdots & a_{k,i,VH-\tau_{k,g}-1} \end{bmatrix}^T, \tag{5.7}$$

$$\underline{\tilde{\mathbf{a}}}_k(\tau_{k,j,i,g}) = \begin{bmatrix} a_{k,i,VH-\tau_{k,j,i,g}} & a_{k,i,VH-\tau_{k,g}+1} & \cdots & a_{k,i,VH-1} & \mathbf{0}^T_{(VH-\tau_{k,j,i,g})\times 1} \end{bmatrix}^T. \tag{5.8}$$

Note that in the derivation, two consecutive MC-CDMA symbols are involved because transmissions among all mobile users are asynchronous. Eq (5.5) can be further rewritten as

$$\begin{aligned}
\underline{\mathbf{y}}_j(n) &= \sum_{k=1}^{K} \underbrace{\mathcal{D}(\underline{\mathbf{f}}(\varepsilon_k)) \underbrace{\begin{bmatrix} \mathbf{A}_k(\underline{\boldsymbol{\tau}}_{k,j,1}) & \mathbf{A}_k(\underline{\boldsymbol{\tau}}_{k,j,2}) \end{bmatrix}}_{\mathbf{A}_{k,j}}}_{\mathbf{Q}_{k,j}} \underbrace{\begin{bmatrix} \underline{\mathbf{s}}^T_{k,j,1}(n) & \underline{\mathbf{s}}^T_{k,j,2}(n) \end{bmatrix}^T}_{\underline{\mathbf{s}}_{k,j}} + \underline{\boldsymbol{\eta}}_j(n) \\
&= \underbrace{\begin{bmatrix} \mathbf{Q}_{1,j} & \mathbf{Q}_{2,j} & \cdots & \mathbf{Q}_{K,j} \end{bmatrix}}_{\mathbf{Q}_j} \cdot \underbrace{\begin{bmatrix} \underline{\mathbf{s}}^T_{1,j}(n) & \underline{\mathbf{s}}^T_{2,j}(n) & \cdots & \underline{\mathbf{s}}^T_{K,j}(n) \end{bmatrix}^T}_{\underline{\mathbf{s}}_j(n)} + \underline{\boldsymbol{\eta}}_j(n) \\
&= \mathbf{Q}_j \underline{\mathbf{s}}_j(n) + \underline{\boldsymbol{\eta}}_j(n), \\
& \qquad\qquad j = 1,2,\cdots,J
\end{aligned} \tag{5.9}$$

Our objective here is to estimate the relative time delay $\underline{\boldsymbol{\tau}}_{k,j,i}$ ($k = 1,2,\cdots,K$, $j = 1,2,\cdots,J$, $i = 1,2$) and NCFO ε_k ($k = 1,2,\cdots,K$) from the received signal $\underline{\mathbf{y}}_j(n)$ ($j = 1,2,\cdots,J$). Before we present the subspace based estimation algorithm, the conditions and assumptions are first stated in (a1) to (a5) below.

a1) The source signal $\{d_k(n)\}$ is a sequence of independent and identical distributed (i.i.d.) random variables with zero mean and unit variance.

a2) All channels $\{\beta_{k,j,i,g}\}$ are linearly time-invariant finite impulse response (FIR) filter and assumed to be stationary over the symbol interval, and the number of paths G_k of each user is known in the receiver.

a3) The noise $\underline{\boldsymbol{\eta}}_j(n)$ is a temporally and spatially white Gaussian noise with zero mean and second-order moments $E\{\underline{\boldsymbol{\eta}}_j(n)\underline{\boldsymbol{\eta}}_j^{\mathcal{H}}(n)\} = \sigma_\eta^2 \mathbf{I}_{VH}$ and $E\{\underline{\boldsymbol{\eta}}_j(n)\underline{\boldsymbol{\eta}}_j^T(n)\} = 0$ [76]. Moreover, $\underline{\boldsymbol{\eta}}_j(n)$ is independent of the source signal $\{d_k(n)\}$ and channel fading $\{\beta_{k,j,i,g}\}$. However, if we consider the correlations in the noise samples as the result of oversampling, the estimation performance will be certainly better than when uncorrelated noise samples are assumed [77]. Therefore, the obtained performance can be considered as the upper bound to the practical systems.

5.3 Joint Timing and Frequency Synchronization Algorithm

In this section, the subspace based blind joint timing and frequency synchronization algorithm is proposed. We collect N blocks of receive samples defined in (5.9) first at jth receiver antenna and obtain

$$\mathbf{Y}_j = \mathbf{Q}_j \mathbf{S}_j + \mathbf{N}_j \qquad j = 1,2,\cdots,J, \tag{5.10}$$

where $\mathbf{Y}_j = \lfloor \underline{\mathbf{y}}_j(0) \quad \underline{\mathbf{y}}_j(1) \quad \cdots \quad \underline{\mathbf{y}}_j(N-1) \rfloor_{VH\times N}$ denotes the received signal block and $\mathbf{S}_j = \lfloor \underline{\mathbf{s}}_j(0) \quad \underline{\mathbf{s}}_j(1) \quad \cdots \quad \underline{\mathbf{s}}_j(N-1) \rfloor_{G_T\times N}$ denotes the transmitted signal block, where $G_T = 4\sum_{k=1}^{K} G_k$, and $\mathbf{N}_j = \lfloor \underline{\boldsymbol{\eta}}_j(0) \quad \underline{\boldsymbol{\eta}}_j(1) \quad \cdots \quad \underline{\boldsymbol{\eta}}_j(N-1) \rfloor_{VH\times N}$ denotes the noise block.. The follow assumptions are made in the sequel to use the subspace algorithm.

a4) Signal matrix $\mathbf{S}_j$ has full row rank, i.e. $Rank(\mathbf{S}_j) = G_T$ or $N > G_T$. Thus, the number of MC-CDMA symbols needed to perform synchronization should be greater than G_T.

a5) Matrix $\mathbf{Q}_j$ has full column rank, i.e. $Rank(\mathbf{Q}_j) = G_T$ or $VH > G_T$. Thus the oversampling factor should be properly chosen according to this constraint.

With these assumptions, $Rank(\mathbf{Y}_j) = Rank(\mathbf{Q}_j) = Rank(\mathbf{S}_j) = G_T$ i.e. $\mathbf{Y}_j$, $\mathbf{Q}_j$ and $\mathbf{S}_j$ span the same space. Properties (a4) and (a5) imply that if the channel is more severe, i.e. G_T is larger, then more MC-CDMA symbols need to be used, and concurrently the oversampling factor used should also be higher, for the subspace approach.

5.3.1 Noiseless Situation

A singular value decomposition (SVD) is then performed on noiseless received signal $\mathbf{Y}_j$ given by

$$\mathbf{Y}_j = \mathbf{Q}_j \mathbf{S}_j = \begin{pmatrix} \mathbf{U}_s & \mathbf{U}_o \end{pmatrix} \begin{pmatrix} \mathbf{\Sigma}_s & \mathbf{0} \\ \mathbf{0} & \mathbf{0} \end{pmatrix} \begin{pmatrix} \mathbf{V}_s^{\mathcal{H}} \\ \mathbf{V}_o^{\mathcal{H}} \end{pmatrix}. \qquad j = 1,2,\cdots,J \tag{5.11}$$

where $\begin{pmatrix} \mathbf{U}_s & \mathbf{U}_o \end{pmatrix}$ is an $VH \times VH$ unitary matrix. The G_T column vectors of $\mathbf{U}_s$ span the signal space, while $VH - G_T$ column vectors of $\mathbf{U}_o$ span the null space (often known as the noise space or perturbed null space in practice if SVD is applied on the noise perturbed signal matrix $\mathbf{Y}_j$) which is orthogonal to the signal space. $\mathbf{\Sigma}_s = diag(\Sigma_1, \Sigma_2, \cdots, \Sigma_{G_T})$ is diagonal matrix consisting of G_T singular values corresponding to the signal space. The orthogonality property between the signal space and noise null space asserts that

$$\mathbf{U}_o^{\mathcal{H}} \mathbf{Q}_j = \mathbf{0}. \tag{5.12}$$

Due to above orthogonality, the columns of $\mathbf{Q}_j$ are orthogonal to any vector in the null space, thus we have

$$\underline{\mathbf{u}}_m^{\mathcal{H}} \mathbf{Q}_{k,j} = \mathbf{0} \quad m = 1,2,\cdots,VH - G_T, \; k = 1,2,\cdots,K, \; j = 1,2,\cdots,J \tag{5.13}$$

where $\underline{\mathbf{u}}_m$ is mth column of null space $\mathbf{U}_o$.

It can be seen that Eq (5.13) decouples the multiuser parameter estimation to a series of K single user problems. The estimation of $\hat{\varepsilon}_k$ and $\hat{\tau}_{k,j,i,g}$ therefore only depend on the information of the kth user itself and not related to the information from the other users. Since $\mathbf{Q}_{k,j} = \mathcal{D}(\underline{\mathbf{f}}(\varepsilon_k))\mathbf{A}_{k,j} = \mathcal{D}(\underline{\mathbf{f}}(\varepsilon_k))\left[\mathbf{A}_k(\underline{\boldsymbol{\tau}}_{k,j,1}) \quad \mathbf{A}_k(\underline{\boldsymbol{\tau}}_{k,j,2})\right]$, and the relationship $\underline{\mathbf{a}}^{\mathcal{H}}\mathcal{D}(\underline{\mathbf{b}}) = \underline{\mathbf{b}}^{\mathcal{H}}\mathcal{D}(\underline{\mathbf{a}})$ holds, Eq (5.13) can be rewritten as

$$\underline{\mathbf{f}}^T(\varepsilon_k)\mathcal{D}(\underline{\mathbf{u}}_m^{\mathcal{H}})\mathbf{A}_{k,j} = \underline{\mathbf{f}}^T(\varepsilon_k)\mathcal{D}(\underline{\mathbf{u}}_m^{\mathcal{H}})\left[\mathbf{A}_k(\underline{\boldsymbol{\tau}}_{k,j,1}) \quad \mathbf{A}_k(\underline{\boldsymbol{\tau}}_{k,j,2})\right] = \mathbf{0}$$

$$k = 1,\cdots,K,\ i = 1,2,\ j = 1,\cdots,J,\ m = 1,2,\cdots,VH - G_T \quad (5.14)$$

Eq (5.14) involves the relative time delays between the multiple input antennas (two transmitters in this paper) and the jth receiver antenna, and we can further transform the parameters estimation problem in MIMO system to a series of SISO parameter estimation problem given by

$$\underline{\mathbf{f}}^T(\varepsilon_k)\mathcal{D}(\underline{\mathbf{u}}_m^{\mathcal{H}})\mathbf{A}_k(\underline{\boldsymbol{\tau}}_{k,j,i}) = \mathbf{0},$$

$$k = 1,\cdots,K,\ i = 1,2,\ j = 1,\cdots,J,\ m = 1,2,\cdots,VH - G_T. \quad (5.15)$$

The matrix $\mathbf{A}_k(\underline{\boldsymbol{\tau}}_{k,j,i})$ includes the timing delay information of total G_k paths for kth user between the *ith* transmit antenna and jth receive antenna, without the loss of generality, Eq (5.15) can be further simplified as

$$\underline{\mathbf{f}}^T(\varepsilon_k)\underbrace{\mathcal{D}(\underline{\mathbf{u}}_m^{\mathcal{H}})\left[\underline{\bar{\mathbf{a}}}_k(\tau_{k,j,i,g}) \quad \underline{\tilde{\mathbf{a}}}_k(\tau_{k,j,i,g})\right]}_{\mathbf{W}_{k,j,i,m}} = \mathbf{0}$$

$$k = 1,\cdots,K,\ i = 1,2,\ j = 1,\cdots,J,\ m = 1,2,\cdots,VH - G_T. \quad (5.16)$$

We stack all $\underline{\mathbf{u}}_m$ in (5.16), then we can obtain

$$\underline{\mathbf{f}}^T(\varepsilon_k)\underbrace{\left[\mathbf{W}_{k,j,i,1} \quad \mathbf{W}_{k,j,i,2} \quad \cdots \quad \mathbf{W}_{k,j,i,VH-\bar{G}}\right]}_{\mathbf{W}_{k,j,i}} = \underline{\mathbf{f}}^T(\varepsilon_k)\mathbf{W}_{k,j,i} = \mathbf{0}$$

$$k = 1,\cdots,K,\ i = 1,2,\ j = 1,\cdots,J,\ m = 1,2,\cdots,VH - G_T. \quad (5.17)$$

Thus the estimation of NCFO $\hat{\varepsilon}_k$ and the timing delay $\hat{\tau}_{k,j,i,g}$ can be obtained by solving (5.17).

5.3.2 Practical Situation

In practice, the received signal $\mathbf{Y}_j$ in (5.11) is corrupted by noise $\mathbf{N}_j$, only the perturbed null space $\tilde{\mathbf{U}}_o$ corresponding to the $VH - G_T$ smallest eigenvalues can be obtained. The perturbed value of $\mathbf{W}_{k,j,i}$ defined in (17), $\tilde{\mathbf{W}}_{k,j,i}$, will be used and (5.17) is no longer fulfilled. The estimation of NCFO $\hat{\varepsilon}_k$ and the timing delay $\hat{\tau}_{k,g}$ is to solve the following least square equation

$$\{\hat{\varepsilon}_k, \hat{\tau}_{k,j,i,g}\}_{k=1,\cdots K, j=1,\cdots,J, i=1,,2, g=1,\cdots,\overline{G}} = \arg\min \Lambda_k(\varepsilon_k, \tau_{k,j,j,g})$$

$$k = 1,\cdots,K,\ i = 1,2,\ j = 1,\cdots,J \qquad (5.18)$$

where the cost function is given by

$$\Lambda_k(\varepsilon_k, \tau_{k,j,i,g}) = \underline{\mathbf{f}}^T(\varepsilon_k)\tilde{\mathbf{W}}_{k,j,i}\tilde{\mathbf{W}}_{k,j,i}^{\mathcal{H}}\underline{\mathbf{f}}^*(\varepsilon_k). \qquad (5.18a)$$

Since $\tau_{k,j,i,g}$ is an integer value in $[0, VH)$, we therefore have to evaluate all the local minimums of the cost function $\Lambda_k(\varepsilon_k \mid \tau_{k,j,i,g})$ for every possible $\tau_{k,j,i,g} = 0,1,\cdots,VH-1$. This is to guarantee that the global minimum of $\Lambda_k(\varepsilon_k, \tau_{k,j,i,g})$ can be obtained. In the following, the implementation of the searching algorithm is described.

We first apply SVD to the received sample to obtain the perturbed null space $\tilde{\mathbf{U}}_o$. Given $\tau_{k,j,i,g}$, $\tilde{\mathbf{W}}_{k,j,i}$ can then be computed using its definition in (5.17) and obtain $\Lambda_k(\varepsilon_k \mid \tau_{k,j,i,g})$. The estimation of $\hat{\varepsilon}_k$ can be obtained by minimizing the cost function $\Lambda_k(\varepsilon_k \mid \tau_{k,j,i,g})$. Generally, the estimation of $\hat{\varepsilon}_k$ can be obtained by using

MUSIC [111]. In the following, we propose another easy and efficient approach to estimate NCFO $\hat{\varepsilon}_k$.

We first define angular frequency $\omega_k = 2\pi\varepsilon_k / VH \in [-\pi, \pi)$, the cost function Λ_k in (5.18a) can be expressed as

$$\Lambda_k(\omega_k \mid \tau_{k,j,i,g}) = \sum_{n=-(VH-1)}^{VH-1} \lambda_{k,n}(\tau_{k,j,i,g}) \exp(jn\omega_k), \tag{5.19}$$

where $\lambda_{k,n}(\tau_{k,j,i,g}) = \sum_{b=1}^{VH} \sum_{a=1,b-a=n}^{VH} \tilde{\mathbf{R}}_{w,j,i}(a,b)$ and $\tilde{\mathbf{R}}_{w,j,i} = \tilde{\mathbf{W}}_{k,j,i} \tilde{\mathbf{W}}_{k,j,i}^{\mathcal{H}}$. In general, the solution of ω_k is to solve the zero points of the first-order differential of $\Lambda_k(\omega_k \mid \tau_{k,j,i,g})$ with respect to ω_k, i.e.,

$$\frac{\partial \Lambda_k}{\partial \omega_k} = j \sum_{n=-(VH-1)}^{VH-1} \lambda_{k,n}(\tau_{k,j,i,g}) n \exp(jn\omega_k) = 0. \tag{5.20}$$

Let $z_k = \exp(j\omega_k)$, (5.20) is equivalent to

$$\sum_{n=-(VH-1)}^{VH-1} \lambda_{k,n}(\tau_{k,j,i,g}) n z_k^n = 0. \tag{5.21}$$

This involves solving a polynomial equation of a degree of $2(VH-1)$ for the complex random variable lying on the unit circle. Normally numerical iterative algorithm [112] can be used to search for the maximum of the cost function $\Lambda_k(\omega_k \mid \tau_{k,j,i,g})$. However, the use of direct numerical methods, such as Newton's method, is only applicable to strictly convex or concave cost function over the region investigated. Unfortunately, the cost function $\Lambda_k(\omega_k \mid \tau_{k,j,i,g})$ over $[-\pi, \pi)$ does not satisfy this requirement since it has $2(VH-1)$ extremes determined by (5.21). We proposed a two-step approach to estimate the CFO $\hat{\omega}_k$ (or $\hat{\varepsilon}_k$), which has been substantiated by the simulations.

Proposition 1: If we can first divide the whole range $[-\pi, \pi)$ into some of subranges $[-\pi+\varsigma+n\mu_{CS,\omega}, \quad -\pi+\varsigma+(n+1)\mu_{CS,\omega}]$, ($n = 0,1,\cdots,\lfloor(2\pi-2\varsigma)/\mu_{CS,\omega}\rfloor-1$), where $\mu_{CS,\omega}$ is the stepsize of ω_k and ς is a small value to avoid the ambiguity of ω_k at $-\pi$ and π, so that in each subrange the cost function $\Lambda_k(\omega_k \mid \tau_{k,j,i,g})$ will be strictly convex (or concave) function and the optimization-searching approach can be applied. In general, we choose the number of subranges $\lfloor(2\pi-2\varsigma)/\mu_{CS,\omega}\rfloor \geq 2(VH-1)$ since the cost function in (5.21) have $2(VH-1)$ extreme points. This means $\mu_{CS,\omega} \leq 2\pi \cdot 0.5/VH$. Our simulations show that it is sufficient to obtain good accuracy if $\mu_{CS,\omega} = 2\pi \cdot 0.5/VH$. Since the value of cost function $\Lambda_k(\omega_k \mid \tau_{k,j,i,g})$ over each subrange varies only slightly, we can obtain a coarse estimation of $\hat{\omega}'_k$ by examining the minimum of cost function at each value of $\omega_k = -\pi+\varsigma+n\mu_{CS,\omega}$ ($n = 0,1,\cdots,\lfloor(2\pi-2\varsigma)/\mu_{CS,\omega}\rfloor-1$). Fine estimation can be then obtained by using any numerical iterative optimization algorithm over the range of $[\hat{\omega}'_k - \mu_{CS,\omega}/2, \quad \hat{\omega}'_k + \mu_{CS,\omega}/2]$.

(i) *Coarse Estimation*

By *Proposition 1*, we find the coarse estimation of CFO $\hat{\omega}'_k$ by searching for the minimum of the cost function $\Lambda_k(\omega_k \mid \tau_{k,j,i,g})$ at the values of ω_k range from $-\pi+\varsigma$ to $\pi-\varsigma$, each with the value of ω_k increases by $\mu_{CS,\omega}$.

(ii) *Fine Estimation*

After obtaining the coarse estimation of CFO $\hat{\omega}'_k$, the actual CFO ω_k which is very close to $\hat{\omega}'_k$ can be obtained using any numerical iterative optimization algorithm. Newton approach [112] is used here to search for the actual CFO ω_k. Denote

$$\Lambda'_k(\omega_k \mid \tau_{k,j,i,g}) = \frac{\partial \Lambda_k}{\partial \omega_k} = j \sum_{n=-(VH-1)}^{VH-1} \lambda_{k,n}(\tau_{k,j,i,g}) n \exp(jn\omega_k), \tag{5.22}$$

$$\Lambda''_k(\omega_k \mid \tau_{k,j,i,g}) = \frac{\partial^2 \Lambda_k}{\partial^2 \omega_k} = -\sum_{n=-(VH-1)}^{VH-1} \lambda_{k,n}(\tau_{k,j,i,g}) n^2 \exp(jn\omega_k). \tag{5.23}$$

The iteration process is summarized as follows.

1) Set the initial point $\omega_k = \hat{\omega}'_k$;

2) Calculate $\left|\Lambda'_k(\omega_k \mid \tau_{k,j,i,g})\right|$;

3) If $\left|\Lambda'_k(\omega_k \mid \tau_{k,j,i,g})\right| < \xi$, then $\omega_k^* = \omega_k$ is the good estimation for CFO. Here, $|x|$ denotes the absolute value of x and ξ is the tolerable accuracy ($\xi \to 0^+$);

4) If $\left|\Lambda'_k(\omega_k \mid \tau_{k,j,i,g})\right| > \xi$, calculate new step size $\mu_{FN,\omega}$ using

$$\mu_{FN,\omega} = -1/\Lambda''_k(\omega_k \mid \tau_{k,j,i,g}). \tag{5.24}$$

5) The next value of ω_k is then computed from

$$\omega_k = \omega_k - \mu_{FN,\omega}\Lambda'_k(\omega_k \mid \tau_{k,j,i,g}). \tag{5.25}$$

6) Repeat from (2) until the good estimation is declared.

To summarize, the estimation CFO $\hat{\omega}_k$ (or $\hat{\varepsilon}_k$) and the relative time delay of $\tau_{k,1,1,g}$ ($g = 1,2,\cdots,G_k$) between the first transmit antenna ($i = 1$) and the first receive antenna ($j = 1$) can be jointly obtained by evaluating the global minimum of the cost function $\Lambda_k(\omega_k^* \mid \tau_{k,1,1,g})$ at each local minimum extreme pair $(\tau_{k,1.1,g}, \omega_k^*)$.

$$\hat{\omega}_k = \arg\min_{\omega_k^*} \Lambda_k(\omega_k^* \mid \tau_{k,1,1,g}), \; k = 1,2,\cdots,K,$$

$$\left\{\hat{\tau}_{k,1,1,g}\right\}_{g=1,\cdots,G_k} = \arg g^{th} \min_{\tau_{k1,1,g}} \Lambda_k(\omega_k^* \mid \tau_{k,1,1,g}), \qquad (5.26)$$

$$\hat{\varepsilon}_k = \hat{\omega}_k VH / 2\pi, \; k = 1,2,\cdots,K. \qquad (5.26a)$$

It can be seen from (5.26) that the proposed approach can estimate the NCFO ε_k within $[-VH/2, VH/2)$. The estimate of timing delay $\hat{\tau}_{k,1,1,g}$ can be obtained by evaluating the first G_k global minimums of the cost function $\Lambda_k(\omega_k^* \mid \tau_{k,1,1,g})$ at each local minimum extreme pair $(\tau_{k,1,1,g}, \omega_k^*)$.

Similar procedure can be repeated to every transmit receiver antennas pair of the same user. However, since multiple receive antennas of the same user share the same local oscillator, the frequency offset estimations are expected to be nearly the same for each transmission pair. When the estimated NCFO $\hat{\omega}_k$ (or $\hat{\varepsilon}_k$) is obtained from one of the transmission pairs, we verify that it is not necessary to repeat the evaluation of $\hat{\omega}_k$ again in simulation since the difference in values obtained are generally insignificant. Therefore, $\left\{\tau_{k,j,i,g}\right\}$ between the other transmit antennas and the receive antennas can be simplified to the following single parameter estimation problem given by

$$\left\{\hat{\tau}_{k,j,i,g}\right\}_{g=1,\cdots,G_k} = \arg g^{th} \min_{(\tau_{k,j,i,g})} \Lambda_k(\hat{\omega}_k, \tau_{k,j,i,g}), \; k = 1,2,\cdots,K, \; j = 1,2,\cdots,J, \; i = 1,2$$

and (if $j = 1$, $i \neq 1$). (5.27)

5.4 Performance Analysis

In this section, the theoretical performance analysis of frequency offset estimation in the presence of additive noise is studied. The performance is measured in terms of mean square error (MSE). The vectorization and the matrix Kronecker product have the following properties [113]

$$\begin{aligned} &vec(\mathbf{ABC}) = \left(\mathbf{C}^T \otimes \mathbf{A}\right) vec(\mathbf{B}) \\ &\left(\mathbf{A} \otimes \mathbf{B}\right)\left(\mathbf{C} \otimes \mathbf{D}\right) = \left(\mathbf{AC} \otimes \mathbf{BD}\right) \\ &\left(\mathbf{A} \otimes \mathbf{B}\right)^{\mathcal{H}} = \left(\mathbf{A}^{\mathcal{H}} \otimes \mathbf{B}^{\mathcal{H}}\right) \end{aligned} \quad . \tag{5.28}$$

We resort to the first-order perturbation approximation used in [101]. Since the CFO is performed at the first receive antenna, hereafter, the perturbation analysis will also be focused at the first receive antenna. We define $\mathbf{Y}_1$ and $\tilde{\mathbf{Y}}_1$ as the observation at the 1st receive antenna given in (10) without and with the presence of noise, respectively, i.e.,

$$\tilde{\mathbf{Y}}_1 = \mathbf{Y}_1 + \Delta \mathbf{Y}_1 = \mathbf{Y}_1 + \mathbf{N}_1 . \tag{5.29}$$

Denote $\mathbf{U}_o$ as the *true null subspace* obtained from the noise-free observation (5.11), and $\tilde{\mathbf{U}}_o$ as the *perturbed null subspace* obtained from the additive noise-corrupted observation (5.10), and

$$\tilde{\mathbf{U}}_o = \mathbf{U}_o + \Delta \mathbf{U}_o . \tag{5.30}$$

Thus, the first order of perturbation approximation of null subspace can be derived to be [101]

$$\Delta \mathbf{U}_o = -\mathbf{U}_s \mathbf{\Sigma}_s^{-1} \mathbf{V}_s^{\mathcal{H}} \mathbf{N}_1^{\mathcal{H}} \mathbf{U}_o = -\mathbf{Y}_1^{\dagger \mathcal{H}} \mathbf{N}_1^{\mathcal{H}} \mathbf{U}_o . \tag{5.31}$$

Using the relationship in (5.28), (5.31) can be expressed as

$$vec(\Delta \mathbf{U}_o) = -\left(\mathbf{U}_o^T \otimes \mathbf{Y}_1^{\dagger \mathcal{H}}\right) vec(\mathbf{N}^{\mathcal{H}}) . \tag{5.32}$$

Since the CFO is estimated by using the cost function corresponding to the signal information only between the 1st transmit antenna and the 1st receive antenna, only the information $\underline{\mathbf{f}}^T(\varepsilon_k)\mathbf{W}_{k,1,1}$ is of interest in the analysis. Performing some manipulations using (5.14)-(5.17), we can obtain

$$\underline{\mathbf{f}}^T(\varepsilon_k)\mathbf{W}_{k,1,1} = vec^{\mathcal{H}}(\mathbf{U}_o)\left(\mathbf{I}_{VH-\bar{G}} \otimes \mathbf{Q}_{k,1,1}\right). \tag{5.33}$$

Thus the cost function in (5.18) can be expressed as

$$\Lambda_k = vec^{\mathcal{H}}(\mathbf{U}_o)\left(\mathbf{I}_{VH-\bar{G}} \otimes \mathbf{Q}_{k,1,1}\mathbf{Q}_{k,1,1}^{\mathcal{H}}\right)vec(\mathbf{U}_o). \tag{5.34}$$

In the noise-free case, the cost function Λ_k will reach zeros at the true NCFO ε_k. While, in the presence of noise, Λ_k will reach its minimum at the estimated NCFO $\hat{\varepsilon}_k$. Denote $\Delta\varepsilon_k = \varepsilon_k - \hat{\varepsilon}_k$. As we describe in section III, Newton approach obtains the estimated NCFO $\hat{\varepsilon}_k$ when the first order differential of $\Lambda_k(\hat{\varepsilon}_k, \hat{\mathbf{U}}_o)$ in respect to ε_k must be zero. The first order differential of Λ_k at $(\varepsilon_k, \hat{\mathbf{U}}_o)$ can be approximated by the first order Taylor expansion at ε_k, yielding

$$0 = \frac{\partial\Lambda_k(\hat{\varepsilon}_k, \hat{\mathbf{U}}_o)}{\partial\varepsilon_k} \cong \frac{\partial\Lambda_k(\varepsilon_k, \hat{\mathbf{U}}_o)}{\partial\varepsilon_k} + \frac{\partial^2\Lambda_k(\varepsilon_k, \hat{\mathbf{U}}_o)}{\partial^2\varepsilon_k}\Delta\varepsilon_k. \tag{5.35}$$

Define $T_1 = \partial\Lambda_k / \partial\varepsilon_k$, $T_2 = \partial^2\Lambda_k / \partial^2\varepsilon_k$, then we have

$$\Delta\varepsilon_k = -T_2^{-1}(\varepsilon_k, \hat{\mathbf{U}}_o)T_1(\varepsilon_k, \hat{\mathbf{U}}_o). \tag{5.36}$$

With the first order approximation, we have

$$T_1(\varepsilon_k, \hat{\mathbf{U}}_o) = T_1(\varepsilon_k, \mathbf{U}_o) + \Delta T_1(\varepsilon_k, \mathbf{U}_o),$$

$$T_2(\varepsilon_k, \hat{\mathbf{U}}_o) = T_2(\varepsilon_k, \mathbf{U}_o) + \Delta T_2(\varepsilon_k, \mathbf{U}_o). \tag{5.37}$$

Since $T_1(\varepsilon_k, \mathbf{U}_o) = 0$, Eq (5.36) can be further approximately as

$$\Delta\varepsilon_k = -\left(T_2^{-1}(\varepsilon_k, \mathbf{U}_o) - T_2^{-1}(\varepsilon_k, \mathbf{U}_o)\Delta T_2^{1}(\varepsilon_k, \mathbf{U}_o)T_2^{-1}(\varepsilon_k, \mathbf{U}_o)\right)\cdot \Delta T_1(\varepsilon_k, \mathbf{U}_o). \tag{5.38a}$$

Ignoring the second order of perturbation, (5.38a) can be simplified as

$$\Delta\varepsilon_k \cong -T_2^{-1}(\varepsilon_k, \mathbf{U}_o)\Delta T_1(\varepsilon_k, \mathbf{U}_o). \tag{5.38b}$$

Denote $\mathbf{X}_k = \mathbf{Q}_{k,1,1}\mathbf{Q}_{k,1,1}^{\mathcal{H}}$, and $\mathbf{X}'_k = \partial\mathbf{X}_k / \partial\varepsilon_k$, $\mathbf{X}''_k = \partial^2\mathbf{X}_k / \partial^2\varepsilon_k$, then we have

$$T_2(\varepsilon_k, \mathbf{U}_o) = vec^{\mathcal{H}}(\mathbf{U}_o)\left(\mathbf{I}_{VH-\bar{G}} \otimes \mathbf{X}''_k\right)vec(\mathbf{U}_o)\,. \tag{5.39}$$

And since

$$\begin{aligned} T_1(\varepsilon_k, \hat{\mathbf{U}}_o) &= vec^{\mathcal{H}}(\hat{\mathbf{U}}_o)\left(\mathbf{I}_{VH-\bar{G}} \otimes \mathbf{X}'_k\right)vec(\hat{\mathbf{U}}_o) \\ &= vec^{\mathcal{H}}(\mathbf{U}_o + \Delta\mathbf{U}_o)\left(\mathbf{I}_{VH-\bar{G}} \otimes \mathbf{X}'_k\right)vec(\mathbf{U}_o + \Delta\mathbf{U}_o)\,. \end{aligned} \tag{5.40}$$

Using $T_1(\varepsilon_k, \mathbf{U}_o) = 0$ and (5.31), after some manipulations, we can obtain

$$\Delta T_1(\varepsilon_k, \mathbf{U}_o) = -\mathrm{Re}\left\{vec^{\mathcal{H}}(\mathbf{U}_o)\left(\mathbf{U}_o^{\mathcal{H}} \otimes \mathbf{X}'_k \mathbf{Y}_1^{\dagger\mathcal{H}}\right)vec(\mathbf{N}^{\mathcal{H}})\right\}. \tag{5.41}$$

Assuming the noise is independent complex Gaussian with zero mean and variance σ_η^2, it's easy to obtain that $E\{\Delta\varepsilon_k\} = 0$ .For arbitrary vector $\underline{\mathbf{a}}$ with compatible dimension, the following results hold:

$$\begin{aligned} &E\left\{\underline{\mathbf{a}}^{\mathcal{H}} vec(\mathbf{N}_1)\underline{\mathbf{a}}^{\mathcal{H}} vec(\mathbf{N}_1)\right\} = 0\,, \\ &E\left\{\underline{\mathbf{a}}^{\mathcal{H}} vec(\mathbf{N}_1{}^{\mathcal{H}})\underline{\mathbf{a}}^{\mathcal{H}} vec(\mathbf{N}_1{}^{\mathcal{H}})\right\} = 0\,, \\ &E\left\{\underline{\mathbf{a}}^{\mathcal{H}} vec(\mathbf{N}_1)vec^{\mathcal{H}}(\mathbf{N}_1)\underline{\mathbf{a}}\right\} = \sigma_\eta^2 E\{\underline{\mathbf{a}}^{\mathcal{H}}\,\underline{\mathbf{a}}\}\,, \\ &E\left\{\underline{\mathbf{a}}^{\mathcal{H}} vec(\mathbf{N}_1{}^{\mathcal{H}})vec^{\mathcal{H}}(\mathbf{N}_1{}^{\mathcal{H}})\underline{\mathbf{a}}\right\} = \sigma_\eta^2 E\{\underline{\mathbf{a}}^{\mathcal{H}}\,\underline{\mathbf{a}}\}\,. \end{aligned} \tag{5.42}$$

Thus, the MSE of NCFO ε_k can be obtained by

$$E\left\{\Delta\varepsilon_k^2\right\} = 2\sigma_\eta^2\left(vec^{\mathcal{H}}(\mathbf{U}_o)vec(\mathbf{X}''_k\mathbf{U}_o)\right)^{-2} \cdot vec(\mathbf{U}_o)vec(\mathbf{X}'_k\mathbf{Y}_1^{\dagger\mathcal{H}}\mathbf{Y}_1^{\dagger}\mathbf{X}'_k\mathbf{U}_o)\,. \tag{5.43}$$

It is important to point out that though seemingly complicated, the above MSE expression only contains the known parameters of the system, and thus allows us to predict the performance of the proposed algorithm directly by using the system parameters including the true CFO and the relative timing delay.

5.5 Cramér-Rao Bound

In this section, we study the Cramér-Rao bound (CRB) of the NCFO ε_k estimation, assuming that the transmitted symbols and channel coefficients are nuisance parameters. Once again, the CRB analysis is based on the received signal $\underline{\mathbf{y}}_1(n)$. With the assumptions (**a**1)-(**a**3) we have made, the probability density function (PDF) of each block of the received data $\underline{\mathbf{y}}_1(n)$ described in (5.9), conditioned on the NCFO $\underline{\boldsymbol{\varepsilon}} = [\varepsilon_1 \quad \varepsilon_2 \quad \cdots \quad \varepsilon_K]^T$ and the signal vector $\underline{\mathbf{s}}_1(n)$, is given by

$$p_{\underline{\mathbf{y}}_1|\underline{\boldsymbol{\varepsilon}},\underline{\mathbf{s}}_1(n)}(\underline{\mathbf{y}}_1 \mid \underline{\boldsymbol{\varepsilon}}, \underline{\mathbf{s}}_1(n)) = \frac{1}{(2\pi\sigma_\eta)^{VH}} \exp\left[-\left\|\underline{\mathbf{y}}_1(n) - \mathbf{Q}_1\underline{\mathbf{s}}_1(n)\right\|^2 / \sigma_\eta^2\right]. \tag{5.44}$$

Since the noise samples are uncorrelated, the joint PDF of a block received data described in (5.10) is given by

$$p_{\mathbf{Y}_1|\underline{\boldsymbol{\varepsilon}},\mathbf{S}_1}(\mathbf{Y}_1 \mid \underline{\boldsymbol{\varepsilon}}, \mathbf{S}_1) = \frac{1}{(2\pi\sigma_\eta)^{VHN}} \exp\left[-\sum_{n=0}^{N-1}\left\|\underline{\mathbf{y}}_1(n) - \mathbf{Q}_1\underline{\mathbf{s}}_1(n)\right\|^2 / \sigma_\eta^2\right]. \tag{5.45}$$

To simplify the CRB derivation, we introduce the equivalent $(2G_T N + K)\times 1$ parameter vector

$$\underline{\boldsymbol{\theta}} = \left[\underline{\boldsymbol{\varepsilon}}^T \quad \underline{\mathbf{s}}_{1,re}^T(0) \quad \cdots \quad \underline{\mathbf{s}}_{1,re}^T(N-1) \quad \underline{\mathbf{s}}_{1,im}^T(0) \quad \cdots \quad \underline{\mathbf{s}}_{1,im}^T(N-1)\right]^T \tag{5.46}$$

where $\underline{\mathbf{s}}_{1,re}(n) = \mathrm{Re}[\underline{\mathbf{s}}_1(n)]$ and $\underline{\mathbf{s}}_{1,im}(n) = \mathrm{Im}[\underline{\mathbf{s}}_1(n)]$, and we write the log-likelihood function as

$$f(\underline{\boldsymbol{\theta}}) = -VHN\ln(2\pi\sigma_\eta) - \sum_{n=0}^{N-1}\left\|\underline{\mathbf{y}}_1(n) - \mathbf{Q}_1\underline{\mathbf{s}}_1(n)\right\|^2 / \sigma_\eta^2 . \tag{5.47}$$

We assume that the SNR is high enough to neglect the estimator's bias and introduce the $(2G_T N + K)\times(2G_T N + K)$ equivalent Fisher's information matrix (FIM) given by

$$\mathcal{J}(\underline{\boldsymbol{\theta}}) = E_{\mathbf{Y}|\underline{\boldsymbol{\varepsilon}},\mathbf{S}}\left\{\frac{\partial f(\underline{\boldsymbol{\theta}})}{\partial\underline{\boldsymbol{\theta}}}\left(\frac{\partial f(\underline{\boldsymbol{\theta}})}{\partial\underline{\boldsymbol{\theta}}}\right)^T\right\}. \tag{5.48}$$

The calculation of each element of the FIM is given in Appendix 5.A. With the signal vectors $\underline{\mathbf{s}}(n)$ treated as the nuisance parameters, the CRB bound of the estimated NCFO covariance matrix is given by the $K \times K$ upper left block of $\mathcal{J}^{-1}$. Then the CRB of each NCFO for each user k can be obtained by

$$\mathrm{CRB}(\varepsilon_k) = \mathcal{J}^{-1}(k,k)\,. \tag{5.49}$$

However, directly computing the inverse of FIM matrix $\mathcal{J}(\underline{\boldsymbol{\theta}})$ involves huge amount of computation, particularly due to the large dimension of the matrices involved. By using the inherent property of $\mathcal{J}(\underline{\boldsymbol{\theta}})$, a more efficient way to compute $\mathcal{J}^{-1}$ is presented in the Appendix 5.A.

5.6 Simulation Results

In this section, we provide simulations to demonstrate the performance of the proposed blind joint timing and frequency synchronization for asynchronous STBC MC-CDMA system. For simplicity, only 1 receiver antenna is considered in the simulations, and it can be easily extended to multiple receiver antennas case. We also compare the synchronization performance between the STBC MC-CDMA and the conventional MC-CDMA system.

A STBC MC-CDMA system with K active asynchronous users using binary phase shift keying (BPSK) constellation is considered. Each user is assigned with a $L = 32$ orthogonal Gold code to spread the signal. In the following, the timing and frequency synchronization for the first user is investigated, with the transmit power $S_1 = 1$. In the sequel, we consider near-far environments without enforcing stringent power control. The power for $K-1$ interfering users follows a lognormal distribution with a mean power ddB higher than that of the desired user, and a standard deviation of 10 dB, i.e., $S_k / S_1 = 10^{\xi_k/10}$ ($k = 2,3,\cdots,K$), where $\xi_k \sim N(d,100)$. The near-far ratio (NFR) is defined as d (in decibels). The channel fading coefficients $\{\beta_{k,j,i,g}\}_{g=1}^{G_k}$ between the jth receiver antenna and ith transmit antenna were modeled as complex Gaussian random variables with zero mean and variance $\sigma^2_{k,j,i,g}$ where $\sum_{g=1}^{G_k}\sigma^2_{k,j,i,g} = 1$. And the channel fading is assumed to be quasi-stationary over a MC-CDMA symbol interval. In the simulations below, we set $G_k = 4$ ($k = 1,\cdots,K$), and $V = L + G_k$. The time delays $\{\tau_{k,j,i,g}\}_{k=1,\cdots,K,g=1,\cdots,G_k}$ are uniformly generated over $[0, VH)$, and NCFOs $\{\varepsilon_k\}_{k=1}^{K}$ are also uniformly generated over $[-VH/2, VH/2)$ for every trial. The fading processing is generated according to the Jakes model [1] with with various Doppler rate f_D. A mobile cellular system is simulated, where the carrier frequency is set to 1800 MHz, the data rate is 20 kbps, and mobiles move at a constant speed. The normalized Doppler rate is defined as $f_D T_b$ where f_D is Doppler rate. The average signal-to-noise ratio (SNR) per sample for the desired user is defined as (recall that $S_1 = 1$)

$$SNR = 10\lg\left(1/VH\sigma_\eta^2\right). \tag{5.50}$$

The performance measure for timing synchronization, the probability of acquisition, is defined as the probability that the time delay is estimated correctly, given by

$$P_a = \frac{\text{No. of correct acquisitions}}{\text{No. of time delays}}. \tag{5.51}$$

The performance measure for CFO synchronization is examined by the mean square error (MSE) given by

$$\text{MSE} = E\left\{\left|\hat{\varepsilon}_k - \varepsilon_k\right|^2\right\}. \tag{5.52}$$

The below simulation results are obtained by averaging over 500 independent Monte Carlo trials.

Fig. 5.3 and Fig. 5.4 show the probability of correct acquisition and MSE performance of frequency offset estimation versus the number of MC-CDMA symbols, N, respectively, when $L = 32$, $K = 8$, $H = 5$, $\mathrm{SNR} = 10\mathrm{dB}$, $\mathrm{NFR} = 0\mathrm{dB}$, $G_k = 4$ and $f_D T_b = 0.006$ (corresponding to the mobile speed 60km/h). It can be seen from Fig. 5.3 that (i) for STBC MC-CDMA, the performance of timing synchronization is nearly perfect since the probability of correct acquisition is very close to or equal to 100% when $N > 100$, it degrades greatly when $N \le 100$; (ii) for MC-CDMA, the probability of correct acquisition is very close to or equal to 100% when $N > 50$, it degrades greatly when $N \le 50$. It can be observed from Fig. 5.4 that the MSE performance for frequency synchronization improves as the N increases. It can be found that (i) for STBC MC-CDMA, the MSE performance degrades severely when $N \le 100$; (ii) for MC-CDMA, the MSE performance degrades significantly when $N \le 50$. This is due to the requirement of the proposed subspace-based algorithm described in section III that the number of symbols used for synchronization has to satisfy (i) $N \ge G_T = 4\sum_{k=1}^{K} G_k = 128$ for STBC MC-CDMA, (ii) $N \ge G_T = 2\sum_{k=1}^{K} G_k = 64$ for MC-CDMA. When $N \le 100$ for STBC MC-CDMA, or when $N \le 50$ for MC-CDMA, the signal space obtained by the SVD on the received signal $\mathbf{Y}_j$ will not be the same as that of $\mathbf{S}_j$, thus the subspace method fails.

It can be also seen from Fig. 5.3 and Fig. 5.4 that the synchronization performance of MC-CDMA systems is better than that of STBC MC-CDMA systems. Since the transmit signals from two transmit antennas of each user in the STBC MC-CDMA systems contribute to the signal matrix $\mathbf{S}_j$ with the dimension

$(4\sum_{k=1}^{K} G_k) \times N$, while only the transmit signals from one transmit antenna of each user in the MC-CDMA system contribute to $\mathbf{S}_j$ with the dimension $(2\sum_{k=1}^{K} G_k) \times N$, the level of the number of symbols N used for synchronization must be greater than $4\sum_{k=1}^{K} G_k$ for STBC MC-CDMA and $2\sum_{k=1}^{K} G_k$ for MC-CDMA, respectively, to apply subspace method correctly. That is to say, given N, the resolution of the signal space and null space obtained by the SVD on the received signal $\mathbf{Y}_j$ in MC-CDMA systems is better than that in STBC MC-CDMA systems.

It can be also observed from Fig. 5.4 that the simulation results present well agreement with the MSE perturbation analysis when $N > 100$ for STBC MC-CDMA or when $N > 50$ for MC-CDMA, indicating the accuracy of the perturbation analysis as long as the conditions to apply the proposed subspace-based algorithm are satisfied. And the calculated CRB also gives a good lower bound for the MSE performance of frequency offset estimation.

Fig. 5.5 and Fig. 5.6 show the probability of correct acquisition and MSE performance of frequency offset estimation versus SNR, respectively, when $L = 32$, $K = 8$, $H = 5$, $N = 200$, $\mathrm{NFR} = 0\mathrm{dB}$, $G_k = 4$, and $f_D T_b = 0.006$. It can be seen from Fig. 5.5 that (i) for MC-CDMA, the SNR has very slight effect on the performance of timing synchronization since the probability of correct acquisition will always keep at or very close to 100%, and even at $\mathrm{SNR} = -10\mathrm{dB}$; (ii) for STBC MC-CDMA, the probability of correct acquisition is very close to 100% when $\mathrm{SNR} \geq 0\mathrm{dB}$, however it can reach 77.83% when $\mathrm{SNR} = \text{-}10\mathrm{dB}$. It can be observed from Fig. 5.6 that the MSE performance improves smoothly as SNR increases. It can be also seen that simulation results show well agreement with the MSE perturbation analysis, and the good lower bound for the MSE performance of frequency offset estimation is provided by CRB.

And it can be shown again from Fig. 5.5 and Fig. 5.6 that the synchronization performance of MC-CDMA is better than that of STBC MC-CDMA since the higher resolution of signal and null space are obtained by SVD in MC-CDMA system given the number of symbols N.

Fig. 5.7 and Fig. 5.8 show the probability of correct acquisition and MSE performance of frequency offset estimation versus the near-far ratio NFR, respectively, when $L = 32$, $K = 8$, $H = 5$, $N = 200$, $\mathrm{SNR} = 10\mathrm{dB}$, $G_k = 4$, and $f_D T_b = 0.006$. From Fig. 5.7, we can observe that (i) for STBC MC-CDMA, the near-far problems result in a small variation of the probability of correct acquisition, and however, it can reach above 95% no matter how the NFR changes from 5dB to 30dB. (ii) for MC-CDMA, the near-far problems have only very slight effect on the performance of timing synchronization. It can be seen from Fig. 5.8 that (i) for STBC MC-CDMA, the MSE performance of frequency synchronization just degrades one order when $\mathrm{NFR} \geq 10\mathrm{dB}$ comparing with the performance when NFR is small; (ii) for MC-CDMA, the MSE performance of frequency synchronization has only very slight variations no matter how NFR changes.

Fig. 5.9 and Fig. 5.10 show the probability of correct acquisition and MSE performance of frequency offset estimation versus $f_D T_b$, respectively, when $L = 32$, $K = 8$, $H = 5$, $N = 200$, $\mathrm{SNR} = 10\mathrm{dB}$, $\mathrm{NFR} = 0\mathrm{dB}$ and $G_k = 4$. It can be seen from Fig. 5.9 and Fig. 5.10 that the values of $f_D T_b$ has only a slight effect on the synchronization performance both in STBC MC-CDMA systems and MC-CDMA systems. It can be concluded that the synchronization performance is only slightly affected when channel fading becomes fast.

5.7 Conclusion

In this chapter, a subspace based joint blind multiuser timing and frequency synchronization algorithm for asynchronous MC-CDMA system over frequency selective fading channels is proposed. Through properly choosing the oversampling factor and the number of received samples, the joint timing and frequency synchronization are resolved using the subspace approach. Besides, the use of the decoupled subspace approach in the algorithm makes it computational efficient in multiuser environment. Simulation results show the robustness and effectiveness of the proposed synchronization algorithm in the presence of near-far problems, multipath fading and Doppler effect. The theoretical MSE perturbation analysis gives a good prediction of the estimation, and the calculated CRB also presents a good lower bound of the estimation.

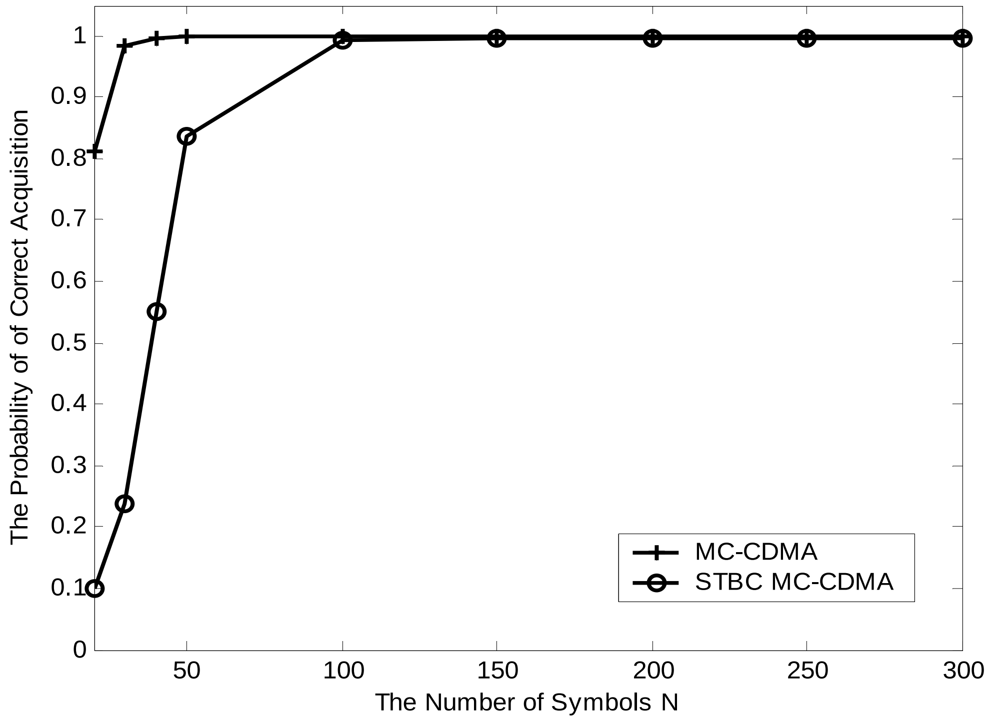

Fig. 5.3 Probability of correct acquisition versus N

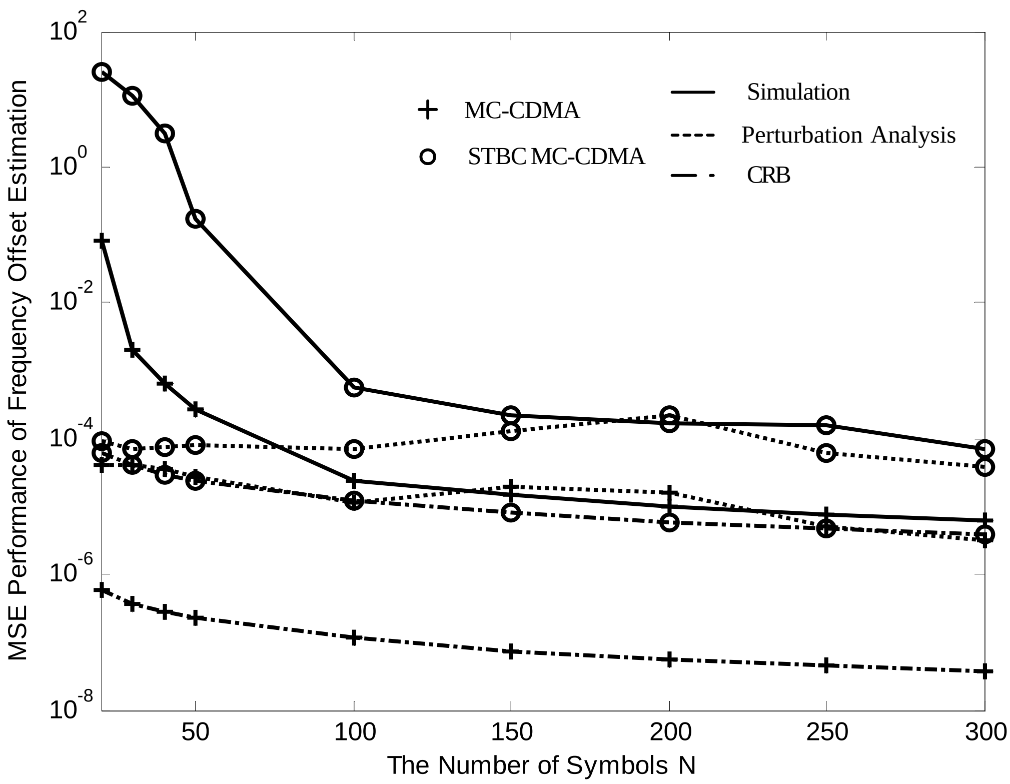

Fig. 5.4 MSE of frequency offset estimation versus N

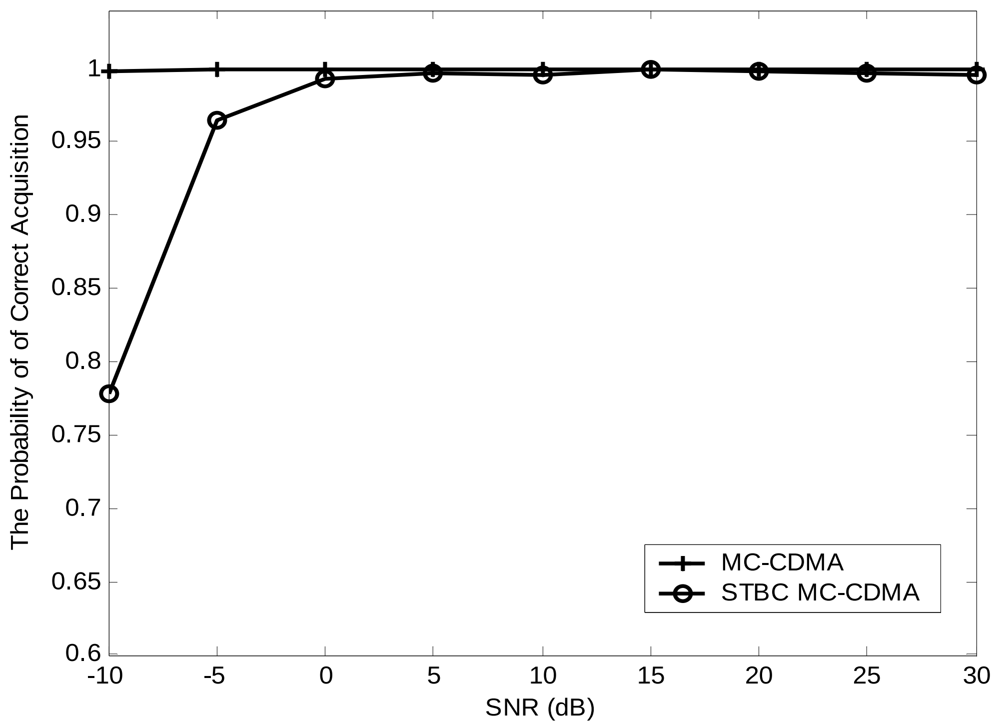

Fig. 5.5 Probability of correct acquisition versus SNR

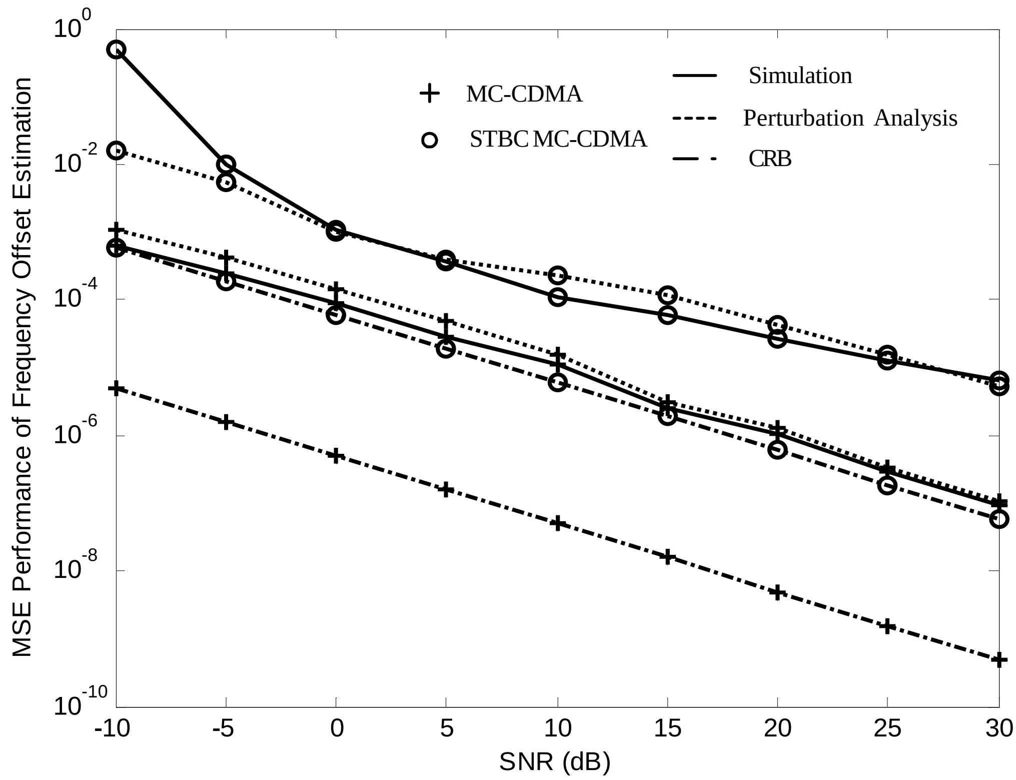

Fig. 5.6 MSE of frequency offset estimation versus SNR

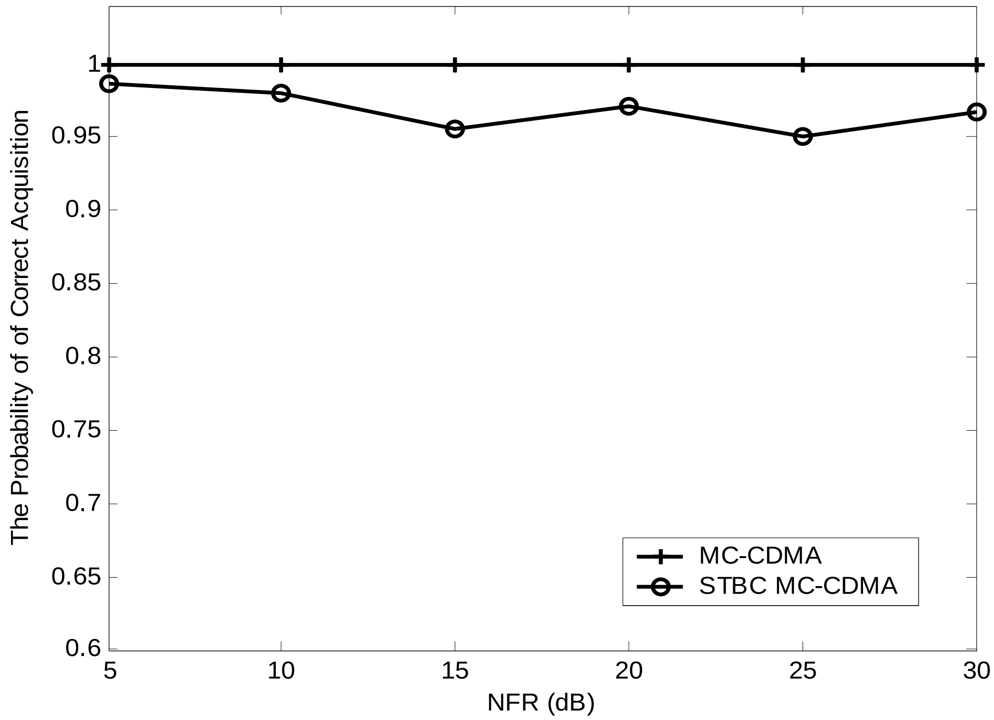

Fig. 5.7 Probability of correct acquisition versus near-far ratio NFR

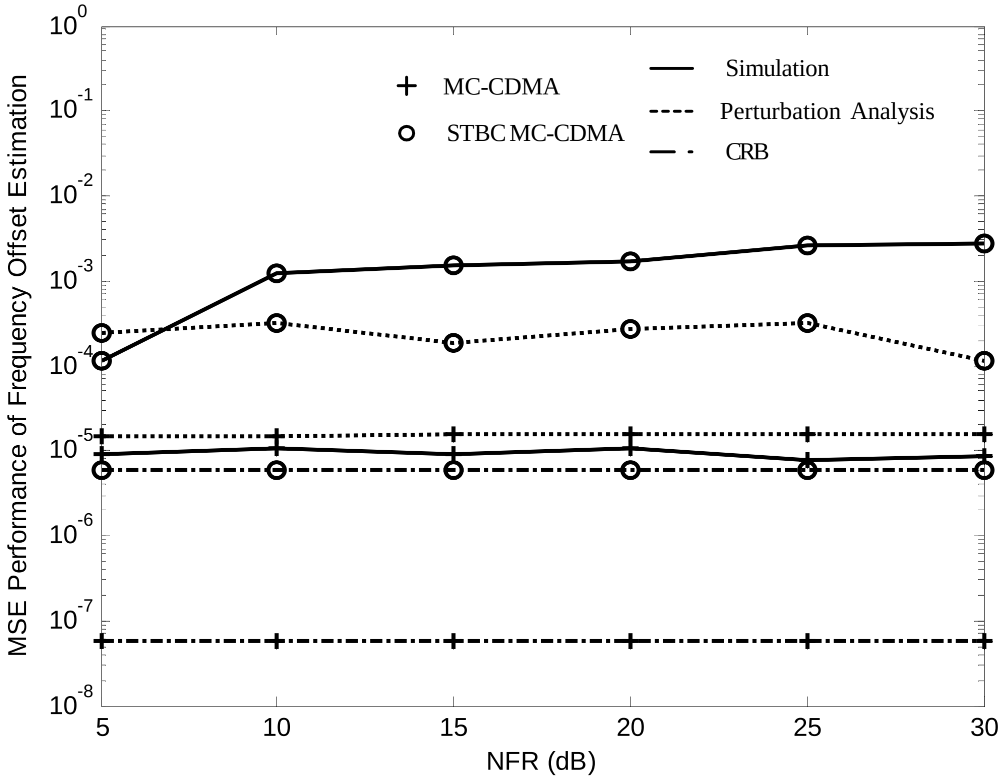

Fig. 5.8 MSE of frequency offset estimation versus near-far ratio NFR

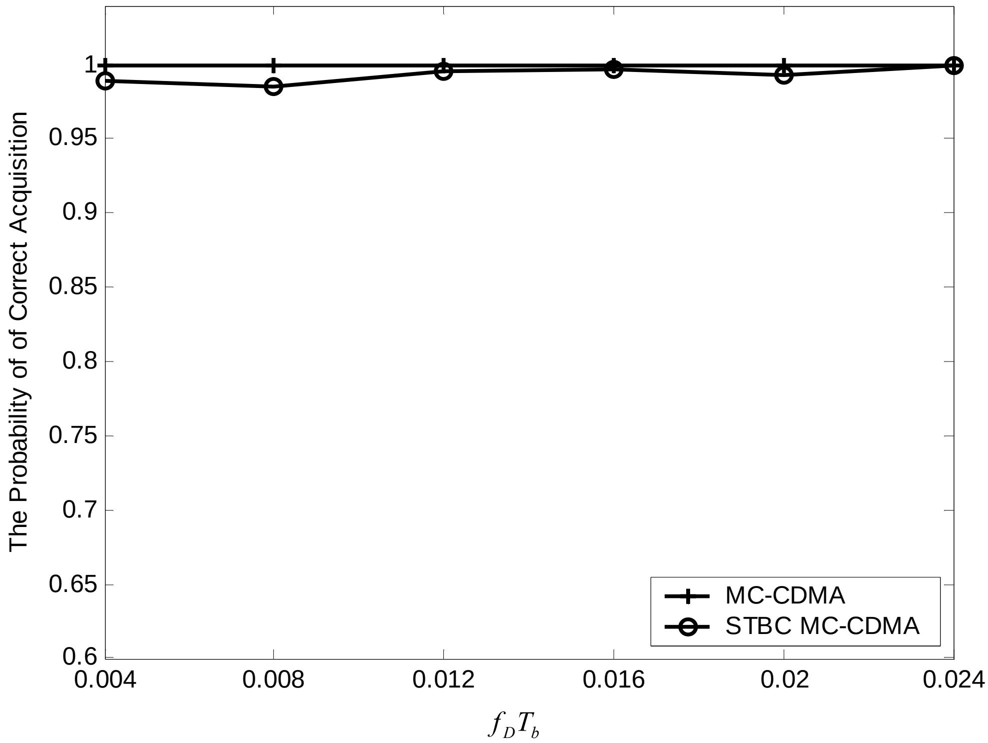

Fig. 5.9 Probability of correct acquisition versus normalized Doppler rate $f_D T_b$

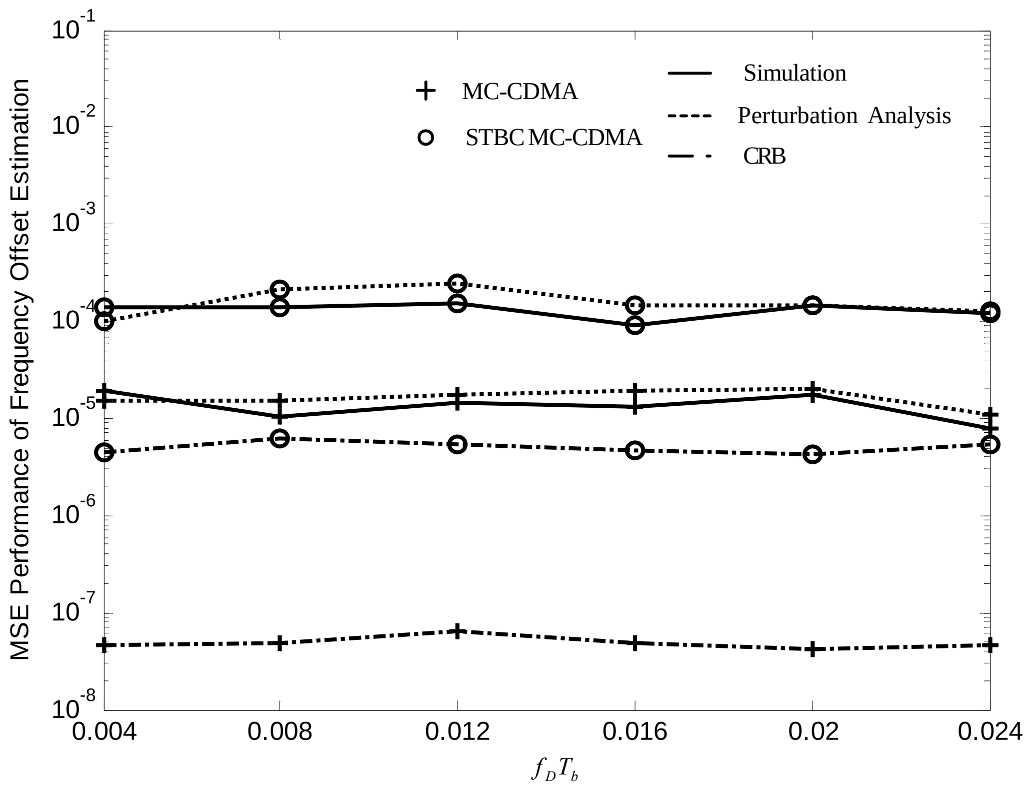

Fig. 5.10 MSE of frequency offset estimation versus normalized Doppler rate $f_D T_b$

Appendix 5.A

In this appendix, we calculate each element of the matrix $\mathcal{J}(\underline{\boldsymbol{\theta}})$ in (5.48), and the simplification of computing the inverse of the $\mathcal{J}(\underline{\boldsymbol{\theta}})$ is presented. Taking the partial differential of $f(\underline{\boldsymbol{\theta}})$ in (5.47) with respect to the unknown parameters, we obtain

$$\frac{\partial f(\underline{\boldsymbol{\theta}})}{\partial \varepsilon_k} = \frac{2}{\sigma_\eta^2}\sum_{n=0}^{N-1}\mathrm{Re}\left[\underline{\mathbf{s}}_{k,1}^{\mathcal{H}}(n)\mathbf{Q}_{k,1}^{\mathcal{H}}\boldsymbol{\chi}^{\mathcal{H}}\,\underline{\boldsymbol{\eta}}(n)\right], \tag{5.A.1}$$

$$\frac{\partial f(\underline{\boldsymbol{\theta}})}{\partial \underline{\mathbf{s}}_{1,re}(n)} = \frac{2}{\sigma_\eta^2}\mathrm{Re}\left[\mathbf{Q}_1^{\mathcal{H}}\,\underline{\boldsymbol{\eta}}(n)\right], \tag{5.A.2}$$

$$\frac{\partial f(\underline{\boldsymbol{\theta}})}{\partial \underline{\mathbf{s}}_{1,im}(n)} = \frac{2}{\sigma_\eta^2}\mathrm{Im}\left[\mathbf{Q}_1^{\mathcal{H}}\,\underline{\boldsymbol{\eta}}(n)\right], \tag{5.A.3}$$

where $\boldsymbol{\chi} = -j\mathcal{D}\left(\begin{bmatrix}0 & 2\pi/VH & \cdots & 2\pi(VH-1)/VH\end{bmatrix}\right)$ Thus, we have

$$\begin{aligned}\frac{\partial f(\underline{\boldsymbol{\theta}})}{\partial \underline{\boldsymbol{\varepsilon}}} &= \left[\left(\frac{\partial f(\underline{\boldsymbol{\theta}})}{\partial \varepsilon_1}\right)^T \quad \left(\frac{\partial f(\underline{\boldsymbol{\theta}})}{\partial \varepsilon_2}\right)^T \quad \cdots \quad \left(\frac{\partial f(\underline{\boldsymbol{\theta}})}{\partial \varepsilon_K}\right)^T\right] \\ &= \frac{2}{\sigma_\eta^2}\sum_{n=0}^{N-1}\mathrm{Re}\left[\mathbf{T}^{\mathcal{H}}(n)\underline{\boldsymbol{\eta}}(n)\right]\end{aligned} \tag{5.A.4}$$

where $\mathbf{T}(n) = \left[\boldsymbol{\chi}\mathbf{Q}_{1,1}\mathbf{s}_{1,1}(n) \quad \cdots \quad \boldsymbol{\chi}\mathbf{Q}_{K,1}\mathbf{s}_{K,1}(n)\right]$. Since the noise is white and circularly symmetric, we have

$$E\left\{\frac{\partial f(\underline{\boldsymbol{\theta}})}{\partial \underline{\boldsymbol{\varepsilon}}}\left(\frac{\partial f(\underline{\boldsymbol{\theta}})}{\partial \underline{\boldsymbol{\varepsilon}}}\right)^T\right\} = \frac{2}{\sigma_\eta^2}\sum_{n=0}^{N-1}\mathrm{Re}\left[\mathbf{T}^{\mathcal{H}}(n)\mathbf{T}(n)\right] = \mathcal{J}_1(n), \tag{5.A.5}$$

$$E\left\{\frac{\partial f(\underline{\boldsymbol{\theta}})}{\partial \underline{\boldsymbol{\varepsilon}}}\left(\frac{\partial f(\underline{\boldsymbol{\theta}})}{\partial \underline{\mathbf{s}}_{1,re}(n)}\right)^T\right\} = \frac{2}{\sigma_\eta^2}\mathrm{Re}\left[\mathbf{T}^{\mathcal{H}}(n)\mathbf{Q}_1\right] = \mathcal{J}_{2a}(n), \tag{5.A.6}$$

$$E\left\{\frac{\partial f(\underline{\boldsymbol{\theta}})}{\partial \underline{\boldsymbol{\varepsilon}}}\left(\frac{\partial f(\underline{\boldsymbol{\theta}})}{\partial \underline{\mathbf{s}}_{im}(n)}\right)^T\right\} = -\frac{2}{\sigma_\eta^2}\mathrm{Im}\left[\mathbf{T}^{\mathcal{H}}(n)\mathbf{Q}_1\right] = \mathcal{J}_{2b}(n), \tag{5.A.7}$$

$$E\left\{\frac{\partial f(\underline{\boldsymbol{\theta}})}{\partial \underline{\mathbf{s}}_{1,re}(n)}\left(\frac{\partial f(\underline{\boldsymbol{\theta}})}{\partial \underline{\mathbf{s}}_{1,re}(m)}\right)^T\right\} = \frac{2}{\sigma_\eta^2}\mathrm{Re}\left[\mathbf{Q}_1^{\mathcal{H}}\mathbf{Q}_1\right]\delta(n-m) = \mathcal{J}_{3a}(n,m)\,, \tag{5.A.8}$$

$$E\left\{\frac{\partial f(\underline{\boldsymbol{\theta}})}{\partial \underline{\mathbf{s}}_{1,re}(n)}\left(\frac{\partial f(\underline{\boldsymbol{\theta}})}{\partial \underline{\mathbf{s}}_{1,im}(m)}\right)^T\right\} = \frac{2}{\sigma_\eta^2}\mathrm{Im}\left[-\mathbf{Q}_1^{\mathcal{H}}\mathbf{Q}_1\right]\delta(n-m) = \mathcal{J}_{3b}(n,m)\,, \tag{5.A.9}$$

$$E\left\{\frac{\partial f(\underline{\boldsymbol{\theta}})}{\partial \underline{\mathbf{s}}_{1,im}(n)}\left(\frac{\partial f(\underline{\boldsymbol{\theta}})}{\partial \underline{\mathbf{s}}_{1,im}(m)}\right)^T\right\} = \frac{2}{\sigma_\eta^2}\mathrm{Re}\left[\mathbf{Q}_1^{\mathcal{H}}\mathbf{Q}_1\right]\delta(n-m) = \mathcal{J}_{3a}(n,m)\,. \tag{5.A.10}$$

The equivalent FIM defined in (5.52) can be expressed as the form

$$\mathcal{J} = \left(\begin{array}{c|c} \mathcal{J}_1 & \mathcal{J}_2 \\ \hline \mathcal{J}_2^T & \mathcal{J}_3 \end{array}\right) = \left(\begin{array}{c|cc} \mathcal{J}_1 & \mathcal{J}_{2a} & \mathcal{J}_{2b} \\ \hline \mathcal{J}_{2a}^T & \mathcal{J}_{3a} & \mathcal{J}_{3b} \\ -\mathcal{J}_{2b}^T & \mathcal{J}_{3b} & \mathcal{J}_{3a} \end{array}\right) \tag{5.A.11}$$

where the blocks have the following dimensions: $\mathcal{J}_1$ is $K \times K$, $\mathcal{J}_2$ is $K \times 2G_T N$, $\mathcal{J}_{2a}$ and $\mathcal{J}_{2b}$ are $K \times G_T N$, $\mathcal{J}_3$ is $2G_T N \times 2G_T N$, $\mathcal{J}_{3a}$ and $\mathcal{J}_{3b}$ are $G_T N \times G_T N$, with the elements defined in (5.A.5)-(5.A.10). The CRB bound of the estimated NCFO covariance matrix is given by the $K \times K$ upper left block of $\mathcal{J}^{-1}$, i.e.,

$$\mathrm{CRB}(\underline{\boldsymbol{\varepsilon}}) = \left(\mathcal{J}_1 - \mathcal{J}_2\mathcal{J}_3^{-1}\mathcal{J}_2^T\right)^{-1}. \tag{5.A.12}$$

However, directly computing the inverse of matrix in (5.A.12) is intensive complexity. In the following, a simplification of computing the inverse of $\mathcal{J}(\underline{\boldsymbol{\theta}})$ is proposed.

By the calculations in (5.A.8)-(5.A.9), the matrix $\mathcal{J}_{3a}$ and $\mathcal{J}_{3b}$ have the following form

$$\mathcal{J}_{3a} = \mathbf{I}_N \otimes \bar{\mathcal{J}}_{3a}\,, \tag{5.A.13a}$$

$$\mathcal{J}_{3b} = \mathbf{I}_N \otimes \bar{\mathcal{J}}_{3b} \tag{5.A.13b}$$

where $\bar{\mathcal{J}}_{3a}$ and $\bar{\mathcal{J}}_{3b}$ is $G_T \times G_T$ matrix. Thus, the inverse of $\mathcal{J}_3$ can be easily obtained

$$\mathcal{J}_3^{-1} = \begin{pmatrix} \mathbf{I}_N \otimes \tilde{\mathcal{J}}_{3a} & \mathbf{I}_N \otimes \tilde{\mathcal{J}}_{3b} \\ \mathbf{I}_N \otimes \tilde{\mathcal{J}}_{3b} & \mathbf{I}_N \otimes \tilde{\mathcal{J}}_{3a} \end{pmatrix} \tag{5.A.14}$$

where $\tilde{\mathcal{J}}_{3a}$ and $\tilde{\mathcal{J}}_{3b}$ has the same form shown in (A.13) with its element

$$\tilde{\mathcal{J}}_{3a} = \left(\bar{\mathcal{J}}_{3a} - \bar{\mathcal{J}}_{3b}\bar{\mathcal{J}}_{3a}^{-1}\bar{\mathcal{J}}_{3b}\right)^{-1}, \quad \tilde{\mathcal{J}}_{3b} = -\bar{\mathcal{J}}_{3a}^{-1}\bar{\mathcal{J}}_{3b}\tilde{\mathcal{J}}_{3a},$$

$$n = 0,1,\cdots,N-1. \tag{5.A.15}$$

Denote $\mathcal{J}_{2a} = \left[\mathcal{J}_{2a}(0) \quad \mathcal{J}_{2a}(1) \quad \cdots \quad \mathcal{J}_{2a}(N-1)\right]$ and $\mathcal{J}_{2b} = \left[\mathcal{J}_{2b}(0) \quad \mathcal{J}_{2b}(1) \quad \cdots \quad \mathcal{J}_{2b}(N-1)\right]$, where $\mathcal{J}_{2a}(n)$ and $\mathcal{J}_{2b}(n)$ ($n = 0,1,\cdots,N-1$) is $K \times G_T$ matrix. Substitute (5.A.14) in (5.A.12), then the CRB of NCFO covariance matrix can be simplified as

$$\begin{aligned}\mathrm{CRB}(\underline{\boldsymbol{\varepsilon}}) = \Big(\mathcal{J}_1 - \sum_{n=0}^{N-1}\mathcal{J}_{2a}(n)\tilde{\mathcal{J}}_{3a}\mathcal{J}_{2a}^T(n) + \mathcal{J}_{2b}(n)\tilde{\mathcal{J}}_{3b}\mathcal{J}_{2a}^T(n) \\ - \mathcal{J}_{2a}(n)\tilde{\mathcal{J}}_{3b}\mathcal{J}_{2b}^T(n) - \mathcal{J}_{2b}(n)\tilde{\mathcal{J}}_{3a}\mathcal{J}_{2b}^T(n)\Big)^{-1}.\end{aligned} \tag{5.A.16}$$

Chapter 6

Channel Estimation and Multiuser Detection

In this chapter, the subspace-based semi-blind channel estimation is studied in uplink STBC MC-CDMA system over frequency selective channels. We assume perfect timing and frequency synchronization of all users at the receiver of base station, and the signals from different users have been synchronized at the receiver. In the uplink context, we have to simultaneously estimate the multipath channels corresponding to the different links between the different mobile users and the base station. This is a $K \times I \times J$ -dimension estimation problem for a K active users, I transmit antennas and J receiver antennas MIMO system. Subspace-based technique is able to decouple this multiuser channel estimation to a series of single user and single-input single output (SISO) estimation problems. To resolve the inherent scalar ambiguity existing in the second-order statistic blind estimation, a training symbol is also transmitted.

To access the performance of the proposed subspace-based semi-blind channel estimation technique, we quantify its resilience to the additive noise. Using the subspace perturbation result in [101], the covariance matrix of the channel estimation error is derived and expressed in a closed form. As a benchmark to measure the relative accuracy of the proposed channel estimation algorithm, a closed-form expression for the Cramér-Rao bound (CRB) is derived by assuming the unknown transmitted symbols as the deterministic or nuisance parameters and independent AWGN samples. Next linear zero-forcing (ZF) and minimum mean squared error (MMSE) detectors are used to recover the data of the different users using the estimated channel parameters.

The remaining of the chapter is organized as follows. In Section 6.1, the system model is first presented. In Section 6.2, the subspace-based semi-blind channel estimation is studied. We first exploit the theory behind the multichannel state information estimation and illustrate how scalar ambiguity arises when subspace method is used. We next explain how to resolve such ambiguity with the use of one training symbol. In Section 6.3, the perturbation analysis is presented and the derivation of CRB is given in section 6.4. In section 6.5 ZF and MMSE detectors are used to suppress the multiuser interference. Simulation results are presented in Section 6.6. Conclusion is drawn in Section 6.7.

6.1 System Description

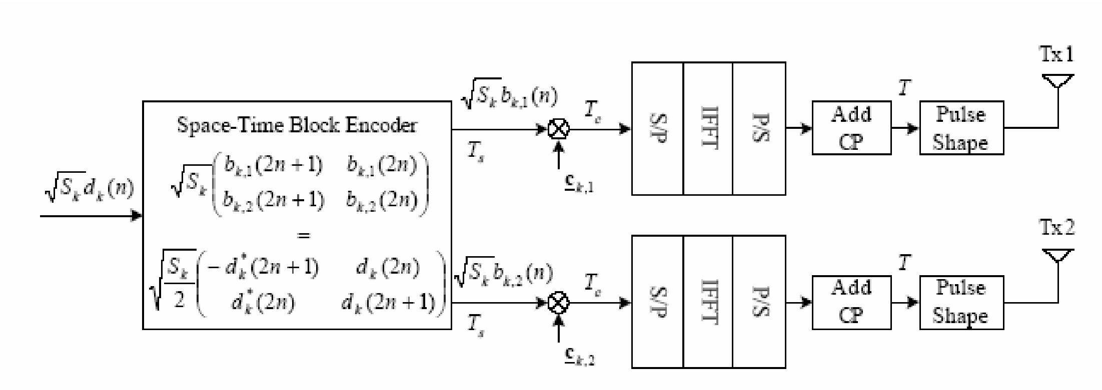

(a)

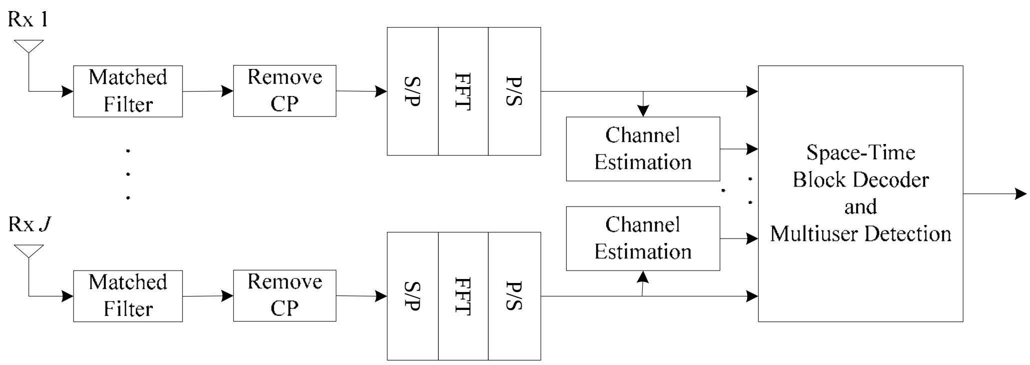

(b)

Fig. 6.1 System Model of STBC MC-CDMA (a) Transmitter; (b) Receiver

We consider a STBC MC-CDMA wireless system consists of two transmit antennas ($I = 2$) and $J \geq 1$ receive antennas. The discrete-time equivalent baseband block diagram of the transmitter and receiver of STBC MC-CDMA system used is shown in Fig. 6.1. We assume K users in the system transmit synchronously. In practice, this can be made by adjusting the user transmission time after performing the symbol timing and frequency synchronization for all users. Data bits take the value of +1 or –1 randomly. Without incurring any power or bandwidth penalty, we employ the Alamouti's orthogonal space-time block coding scheme [44][48]. Two successive symbols $\sqrt{S_k}d_k(2n)$ and $\sqrt{S_k}d_k(2n+1)$ for the k^{th} user are mapped to the following 2×2 matrix

$$\sqrt{S_k}\begin{pmatrix} b_{k,1}(2n+1) & b_{k,1}(2n) \\ b_{k,2}(2n+1) & b_{k,2}(2n) \end{pmatrix} = \sqrt{\frac{S_k}{2}}\begin{pmatrix} -d_k^*(2n+1) & d_k(2n) \\ d_k^*(2n) & d_k(2n+1) \end{pmatrix} \quad \begin{array}{l} \leftarrow \ \text{time} \\ \downarrow \ \text{space} \end{array}$$

where $d_k(n)$ denotes the nth symbol for kth user, S_k is its transmit power of kth user and $b_{k,i}(n)$ denotes the nth symbol at ith transmit antenna for kth user. The columns are transmitted in successive block time with the symbols in the upper and lower blocks simultaneously sent through the two transmit antennas, respectively. The factor $1/\sqrt{2}$ is to normalize the transmitted symbol energy.

The signal $b_{k,i}(n)$ at the ith transmit antenna is spread by $\underline{\mathbf{c}}_{k,i} = [c_{k,i,0}, \ \cdots \ c_{k,i,L-1}]^T$, where L is the spreading gain. We assume that the spreading code has unit amplitude, and normalized by a factor $1/\sqrt{L}$. The spread signal $\sqrt{S_k/L}\cdot\underline{\mathbf{c}}_{k,i}b_{k,i}(n)$ is then serial-to-parallel converted followed by the inverse fast Fourier transform (IFFT) processing $\mathbf{F}^{\mathcal{H}}$, where $\mathbf{F}$ is the $L\times L$ matrix with its $(m,n)^{\text{th}}$ entry equal to $1/\sqrt{L}\cdot\exp[-j2\pi(m-1)(n-1)/L]$. To avoid ISI, we insert redundancy in the form of cyclic prefix (CP) of the length larger than the channel order $G=\lfloor \tau_{max}/T \rfloor$. Here τ_{max} denotes the maximum delay spread among all the users and T is the time interval between two MC-CDMA samples after CP insertion, i.e., $T = LT_c/V = T_s/V$ where V is the total number of samples in one MC-CDMA symbol period T_s. The CP insertion process can be described by a $V\times L$ transmit matrix given by $\mathbf{T}_{cp} = [\mathbf{I}_{cp} \quad \mathbf{I}_L]^T$, where $\mathbf{I}_{cp}$ denotes the last $V-L\geq G$ rows of $L\times L$ identity matrix $\mathbf{I}_L$, and the energy is normalized by $\sqrt{L/V}$. The transmitted signal for kth user can be expressed as

$$\underline{\mathbf{x}}_{k,i}(n) = \sqrt{S_k/V} \cdot \mathbf{T}_{cp}\mathbf{F}^{\mathcal{H}}\underline{\mathbf{c}}_{k,i}b_{k,i}(n), \tag{6.1}$$

where $k = 1, \cdots K$, $i = 1,2$

The signal $\underline{\mathbf{x}}_{k,i}(n)$ is converted from parallel to serial (P/S), and the resulting sequence $x_{k,i}(a)$ is then shaped to obtain the continuous time signal $x_{k,i}(t) = \sum_{a=-\infty}^{\infty} x_{k,i}(a)u(t-aT)$, where $u(t)$ is the pulse shape. The transmitted signal propagates through the unknown time-dispersive channel between the *i*th transmit antenna and the *j*th receive antenna which has finite impulse response denoted as $\overline{\beta}_{k,j,i}(t)$. The received signal is then shaped by $\overline{u}(t)$ which is matched to $u(t)$, and then sampled at the rate $1/T$. At the receiver of the base station, the equivalent discrete-time channel impulse response can be expressed as

$$\beta_{k,j,i}(a) = u(t) \otimes \overline{\beta}_k(t) \otimes \overline{u}(t)\Big|_{t=aT} = \sum_{g=1}^{G} \beta_{k,j,i,g}\delta(a-gT) \tag{6.2}$$

where $\delta(t)$ denotes the Dirac delta function, $\beta_{k,j,i,g}$ is the complex channel fading gain between *i*th transmit antenna and *j*th receive antenna for *g*th path of user *k*.

For K users in the system transmit the signals through each dispersive frequency selective fading channel synchronously, the received signals at the *j*th antenna can be written as

$$\underline{\mathbf{r}}_j(n) = \sum_{k=1}^{K}\sum_{i=1}^{2}\left(\boldsymbol{\beta}_{k,j,i,0}\underline{\mathbf{x}}_{k,i}(n) + \boldsymbol{\beta}_{k,j,i,1}\underline{\mathbf{x}}_{k,i}(n-1)\right) + \underline{\dot{\boldsymbol{\eta}}}_j(n),\ j = 1,\cdots,J\ , \tag{6.3}$$

where $\boldsymbol{\beta}_{k,j,i,0}$ is the $V \times V$ lower triangular Toeplitz matrix with first column $[\beta_{k,j,i,0} \ \cdots \ \beta_{k,j,i,G} \ \ 0 \ \cdots \ 0]^T$, $\boldsymbol{\beta}_{k,j,i,1}$ is the $V \times V$ upper triangular Toeplitz matrix representing the ISI resulting from previous symbol and with its first row vector given by $[0 \ \cdots \ 0 \ \ \beta_{k,j,i,G}, \ \cdots \ \beta_{k,j,i,0}]^T$. The $V \times 1$ vector $\underline{\dot{\boldsymbol{\eta}}}_j(n)$ is the additive white Gaussian noise (AWGN) at the *j*th receive antenna with zero mean and variance

$\sigma_\eta^2\mathbf{I}$. We next remove CP of length $V-L$ from the received vector $\underline{\mathbf{r}}_j(n)$ and perform the FFT processing. The matrix $\mathbf{R}_{cp}=[\mathbf{0}_{L\times(V-L)}\quad \mathbf{I}_L]$ is to remove the CP. The recovered signal after FFT is given by

$$\underline{\mathbf{y}}_j(n)=\mathbf{F}\mathbf{R}_{cp}\underline{\mathbf{r}}_j(n)=\frac{1}{\sqrt{2V}}\sum_{k=1}^{K}\sum_{i=1}^{2}\mathbf{F}\overline{\boldsymbol{\beta}}_{k,j,i}\mathbf{F}^{\mathcal{H}}\underline{\mathbf{c}}_{k,i}s_{k,i}(n)+\underline{\ddot{\boldsymbol{\eta}}}_j(n), \tag{6.4}$$

where $\overline{\boldsymbol{\beta}}_{k,j,i}=\mathbf{R}_{cp}\boldsymbol{\beta}_{k,j,i,0}\mathbf{T}_{cp}$, $\underline{\ddot{\boldsymbol{\eta}}}_j(n)=\mathbf{F}\mathbf{R}_{cp}\underline{\boldsymbol{\eta}}_j(n)$. Since $\mathbf{R}_{cp}\boldsymbol{\beta}_{k,j,i,1}=\mathbf{0}$, ISI can be removed completely. Moreover,

$$\mathbf{F}\overline{\boldsymbol{\beta}}_{k,j,i}\mathbf{F}^{\mathcal{H}}=\mathcal{D}(\underline{\mathbf{h}}_{k,j,i}), \tag{6.5}$$

where

$$\underline{\mathbf{h}}_{k,j,i}=\begin{bmatrix}h_{k,j,i}(0) & h_{k,j,i}(1) & \cdots & h_{k,j,i}(L-1)\end{bmatrix}^T \tag{6.6}$$

is the channel frequency response vector, with its elements given by

$$h_{k,j,i}(l)=\sum_{g=0}^{G}\beta_{k,j,i,g}\exp(-j2\pi gl/L)\quad l=0,\cdots,L-1, \tag{6.6a}$$

Therefore, we can rewrite (4) as

$$\underline{\mathbf{y}}_j(n)=\frac{1}{\sqrt{2V}}\sum_{k=1}^{K}\sum_{i=1}^{2}\mathcal{D}(\underline{\mathbf{h}}_{k,j,i})\underline{\mathbf{c}}_{k,i}s_{k,i}(n)+\underline{\ddot{\boldsymbol{\eta}}}_j(n). \tag{6.7}$$

We collect the received signals in the two successive symbol intervals, and let $\underline{\mathbf{z}}_j(n)=[\underline{\mathbf{y}}_j(2n)^T\quad \underline{\mathbf{y}}_j(2n+1)^{\mathcal{H}}]^T$. We then express $\underline{\mathbf{z}}_j(n)$ as a $2L\times 1$ received signal vector with the transmitted space-time block codes.

$$\underline{\mathbf{z}}_j(n)=\frac{1}{\sqrt{2V}}\mathbf{D}_j\underline{\mathbf{s}}(n)+\underline{\boldsymbol{\eta}}_j(n)\qquad j=1,\cdots,J, \tag{6.8}$$

where

$$\mathbf{D}_j=\begin{bmatrix}\mathbf{D}_j^1, & \cdots & \mathbf{D}_j^K\end{bmatrix}_{2L\times 2K}, \tag{6.8a}$$

$$\mathbf{D}_j^k=\begin{bmatrix}\mathcal{D}(\underline{\mathbf{h}}_{k,j,1})\underline{\mathbf{c}}_{k,1} & \mathcal{D}(\underline{\mathbf{h}}_{k,j,2})\underline{\mathbf{c}}_{k,2}\\ \mathcal{D}(\underline{\mathbf{h}}_{k,j,2})^*\underline{\mathbf{c}}_{k,2} & -\mathcal{D}(\underline{\mathbf{h}}_{k,j,1})^*\underline{\mathbf{c}}_{k,1}\end{bmatrix}_{2L\times 2},\qquad k=1,2,\cdots,K, \tag{6.8b}$$

$\underline{\mathbf{s}}(n) = [\underline{\mathbf{s}}_1(n)^T \cdots \underline{\mathbf{s}}_K(n)^T]^T$ and $\underline{\mathbf{s}}_k(n) = \sqrt{S_k}[s_k(2n) \quad s_k(2n+1)]^T$ denote the samples in two successive MC-CDMA symbols for user k, $\underline{\boldsymbol{\eta}}_j(n) = [\ddot{\underline{\boldsymbol{\eta}}}_j(2n)^T \quad \ddot{\underline{\boldsymbol{\eta}}}_j(2n+1)^{\mathcal{H}}]^T$ denotes the AWGN $2L \times 1$ vector.

6.2 Subspace-Based Semi-Blind Channel Estimation

We propose a subspace algorithm to estimate the channel information of all users for the MIMO system. We stream the samples of the $2N$ successive MC-CDMA symbols $\mathbf{Z}_j = [\underline{\mathbf{z}}_j(0) \quad \cdots \quad \underline{\mathbf{z}}_j(N-1)]_{2L\times N}$ as a block at each receive antenna and denote the transmitted signal block of all users as $\mathbf{S} = [\underline{\mathbf{s}}(0) \quad \cdots \quad \underline{\mathbf{s}}(N-1)]_{2K\times N}$. We can show that

$$\mathbf{Z}_j = \frac{1}{\sqrt{2L}} \mathbf{D}_j \mathbf{S} + \mathbf{N}_j \quad , \tag{6.9}$$

where $\mathbf{N}_j = [\underline{\boldsymbol{\eta}}_j(1) \quad \cdots \quad \underline{\boldsymbol{\eta}}_j(N)]_{2L\times N}$ is the AWGN noise matrix.

Before the derivation of subspace based semi-blind channel estimation algorithm, a few assumptions are made first.

a1) The source signal $\{d_k(n)\}$ is a sequence of independent and identical distributed (i.i.d.) random variables with zero mean and unit variance.

a2) All channels $\{\beta_{k,j,i,g}\}$ are linearly time-invariant finite impulse response (FIR) filter and assumed to be stationary over the $2N$ MC-CDMA symbol intervals, and the number of paths G of each user is known in the receiver.

a3) The noise $\underline{\boldsymbol{\eta}}_j(n)$ is a temporally and spatially white Gaussian noise with zero mean and second-order moments $E\{\underline{\boldsymbol{\eta}}_j(n)\underline{\boldsymbol{\eta}}_j^{\mathcal{H}}(n)\} = \sigma_\eta^2 \mathbf{I}_L$ and $E\{\underline{\boldsymbol{\eta}}_j(n)\underline{\boldsymbol{\eta}}_j^T(n)\} = \mathbf{0}$.

Moreover, $\underline{\boldsymbol{\eta}}_j(n)$ is independent of the source signal $\{d_k(n)\}$ and channel fading $\{\beta_{k,j,i,g}\}$.

a4) Signal matrix $\mathbf{S}$ has full row rank, i.e. $Rank(\mathbf{S}) = 2K$ and $N > 2K$. The number of symbols should be large enough such as four times the number of total users.

a5) Channel information matrix $\mathbf{D}_j$ has full column rank, i.e. $Rank(\mathbf{D}_j) = 2K$ or $L > K$, the processing gain of spreading sequence should be greater than the number of total users.

With these assumptions, $Rank(\mathbf{Z}_j) = Rank(\mathbf{D}_j) = Rank(\mathbf{S}) = 2K$, i.e. $\mathbf{Z}_j$, $\mathbf{D}_j$ and $\mathbf{S}$ span the same signal space.

6.2.1 Subspace Concept

If there is no additive noise present in (6.9), a subspace decomposition can be performed on $\mathbf{Z}_j$ by the singular value decomposition (SVD)

$$\mathbf{Z}_j = \frac{1}{\sqrt{2V}} \mathbf{D}_j \mathbf{S} = \begin{pmatrix} \mathbf{U}_s & \mathbf{U}_o \end{pmatrix} \begin{pmatrix} \mathbf{\Sigma}_s & \mathbf{0} \\ \mathbf{0} & \mathbf{0} \end{pmatrix} \begin{pmatrix} \mathbf{V}_s^{\mathcal{H}} \\ \mathbf{V}_o^{\mathcal{H}} \end{pmatrix}, \tag{6.10}$$

where the vectors in $\mathbf{U}_s$ are associated with the $2K$ signal eigenvalues (λ_i) and span the *signal subspace* defined by the column of $\mathbf{D}_j$, whereas the vectors in $\mathbf{U}_o$ that are associated with zero singular values span the *null subspace*,

$$\mathbf{U}_o = \begin{bmatrix} \underline{\mathbf{u}}_1, & \cdots & \underline{\mathbf{u}}_{2L-2K} \end{bmatrix}. \tag{6.11}$$

In (6.13), $\mathbf{U}_s$, $\mathbf{U}_o$ have dimensions $2L \times 2K$ and $2L \times (2L - 2K)$ respectively, and $\mathbf{\Sigma}_s = \mathcal{D}(\lambda_1, \ \cdots \ \lambda_{2K})$. Due to the orthogonality of the null subspace and the signal subspace,

$$\mathbf{U}_o \perp \mathbf{D}_j \,. \tag{6.12}$$

6.2.2 Estimation Algorithm

Due to the orthogonality, $\mathbf{U}_o{}^{\mathcal{H}}\mathbf{D}_j = \mathbf{0}$, the columns of $\mathbf{D}_j$ are orthogonal to any vector in the null subspace. Denote $\underline{\mathbf{u}}_m$ as the mth column of null subspace, thus, we obtain

$$\underline{\mathbf{u}}_m{}^{\mathcal{H}}\mathbf{D}_j^k = \mathbf{0} \qquad m = 1, \ \cdots \ 2L - 2K \,. \tag{6.13}$$

$\underline{\mathbf{u}}_m$ is split into upper part $\underline{\mathbf{u}}_{m,1}$ and lower part $\underline{\mathbf{u}}_{m,2}$, each is a $L \times 1$ vector, i.e. $\underline{\mathbf{u}}_m = [\underline{\mathbf{u}}_{m,1}^T \quad \underline{\mathbf{u}}_{m,2}^T]^T$. Using (6.8b), (6.13) can be rewritten as

$$\begin{bmatrix}\underline{\mathbf{u}}_{m,1}^{\mathcal{H}} & \underline{\mathbf{u}}_{m,2}^{\mathcal{H}}\end{bmatrix} \cdot \begin{bmatrix} \mathcal{D}(\underline{\mathbf{h}}_{k,j,1})\underline{\mathbf{c}}_{k,1} & \mathcal{D}(\underline{\mathbf{h}}_{k,j,2})\underline{\mathbf{c}}_{k,2} \\ \mathcal{D}(\underline{\mathbf{h}}_{k,j,2})^* \underline{\mathbf{c}}_{k,2} & -\mathcal{D}(\underline{\mathbf{h}}_{k,j,1})^* \underline{\mathbf{c}}_{k,1} \end{bmatrix} = \mathbf{0}, \ m=1 \ \cdots \ 2L-2K \,. \tag{6.14}$$

We let $\overline{\mathbf{V}}_{(G_k+1)\times L}$ denote the Vandermonde matrix with $(g+1,\ l+1)^{\text{th}}$ entry equals to $\exp[-j2\pi gl/L]/\sqrt{L}$, $g = 0,\cdots G_k$ for $l = 0,\cdots L-1$. Let $\underline{\boldsymbol{\beta}}_{k,j,i} = [\beta_{k,j,i,0} \ \ \beta_{k,j,i,1} \ \cdots \ \beta_{k,j,i,G}]^T$ for $i = 1,2$, using the relationship $\underline{\mathbf{a}}^{\mathcal{H}}\mathcal{D}(\underline{\mathbf{b}}) = \underline{\mathbf{b}}^{\mathcal{H}}\mathcal{D}(\underline{\mathbf{a}})$, after taking the conjugate for the second column, we can rewrite (14) as

$$\begin{bmatrix}\underline{\boldsymbol{\beta}}_{k,j,1}^T & \underline{\boldsymbol{\beta}}_{k,j,2}^{\mathcal{H}}\end{bmatrix} \cdot \mathbf{V} \cdot \mathbf{A}_{k,j}(m) = \mathbf{0} \qquad m = 1,\cdots 2L - 2K \ , \tag{6.15}$$

where

$$\mathbf{V} = \begin{bmatrix} \overline{\mathbf{V}} & \mathbf{0} \\ \mathbf{0} & \overline{\mathbf{V}}^* \end{bmatrix}, \tag{6.15a}$$

$$\mathbf{A}_{k,j}(m) = \begin{bmatrix} \mathcal{D}(\underline{\mathbf{u}}_{m,1}^*)\underline{\mathbf{c}}_{k,1} & -\mathcal{D}(\underline{\mathbf{u}}_{m,2})\underline{\mathbf{c}}_{k,1} \\ \mathcal{D}(\underline{\mathbf{u}}_{m,2}^*)\underline{\mathbf{c}}_{k,2} & \mathcal{D}(\underline{\mathbf{u}}_{m,1})\underline{\mathbf{c}}_{k,2} \end{bmatrix} \ m=1, \ \cdots \ 2L-2K. \tag{6.15b}$$

We stack all $\underline{\mathbf{u}}_m$ in (6.15), then we can obtain

$$[\underline{\boldsymbol{\beta}}_{k,j,1}^{T} \quad \underline{\boldsymbol{\beta}}_{k,j,2}^{\mathcal{H}}]\cdot \mathbf{V}\cdot \left[\mathbf{A}_{k,j}(1) \quad \cdots \quad \mathbf{A}_{k,j}(2L-2K)\right] = \mathbf{0}. \tag{6.16}$$

We assume that all the spreading sequences $\underline{\mathbf{c}}_{k,i}$ for all K users are known at the receiver. The channel estimation can be solved by the following equation

$$\underline{\boldsymbol{\beta}}_{k,j}^{\mathcal{H}} \cdot \mathbf{G}_{k,j} = \mathbf{0} \qquad j = 1,\cdots,J \quad k = 1,\cdots K, \tag{6.17}$$

where

$$\underline{\boldsymbol{\beta}}_{k,j} = [\underline{\boldsymbol{\beta}}_{k,j,1}^{\mathcal{H}} \quad \underline{\boldsymbol{\beta}}_{k,j,2}^{T}]^{T}, \tag{6.17a}$$

$$\mathbf{A}_{k,j} = \left[\mathbf{A}_{k,j}(1) \quad \cdots \quad \mathbf{A}_{k,j}(2L-2K)\right], \tag{6.17b}$$

$$\mathbf{G}_{k,j} = \mathbf{V}\cdot \mathbf{A}_{k,j}. \tag{6.17c}$$

Eq. (6.17) provides an efficient way to identify the multi-channel state information in the multi-user and multi-antenna environment up to a scalar ambiguity. Since (6.17) is a linear overdetermined equation set, it will have unique nontrivial solution $\underline{\boldsymbol{\beta}}_{k,j}$ [②] subject to $\left\|\underline{\boldsymbol{\beta}}_{k,j}\right\|^{2} = 1$.

Next, the algorithm is modified to cope with the presence of AWGN. We apply SVD to the noise-corrupted data matrix and obtain the subspace decomposition similar to (6.10).

$$\mathbf{Z}_j = \frac{1}{\sqrt{2V}}\mathbf{D}_j\mathbf{S} + \mathbf{N}_j = \begin{pmatrix}\tilde{\mathbf{U}}_s & \tilde{\mathbf{U}}_o\end{pmatrix}\begin{pmatrix}\tilde{\boldsymbol{\Sigma}}_s & \mathbf{0}\\ \mathbf{0} & \tilde{\boldsymbol{\Sigma}}_o\end{pmatrix}\begin{pmatrix}\tilde{\mathbf{V}}_s^{\mathcal{H}}\\ \tilde{\mathbf{V}}_o^{\mathcal{H}}\end{pmatrix} \tag{6.18}$$

[②] The notation of the strikethrough channel vector $\underline{\boldsymbol{\beta}}_{k,j}$ and $\underline{\tilde{\boldsymbol{\beta}}}_{k,j}$ is to denote the solution of (6.17) and (6.20), respectively. $\underline{\boldsymbol{\beta}}_{k,j}$ and $\underline{\tilde{\boldsymbol{\beta}}}_{k,j}$ denote the actual channel vector in (6.17, without noise) and (6.20, in the presence of noise), respectively. $\underline{\hat{\boldsymbol{\beta}}}_{k,j}$ denotes the estimated channel vector.

where $\tilde{\mathbf{U}}_o$ is the perturbated null subspace (*noise subspace*) corresponding to the $2L-2K$ smallest eigenvalues. The estimated channel state information can be obtained by solving linear equations

$$\underline{\tilde{\boldsymbol{\beta}}}_{k,j}^{\mathcal{H}} \cdot \tilde{\mathbf{G}}_{k,j} \cong \mathbf{0} \qquad j=1,\cdots,J \quad k=1,\cdots K \tag{6.19}$$

subject to $\left\|\underline{\tilde{\boldsymbol{\beta}}}_{k,j}\right\|^2 = 1$, which is equivalent to solving the following least square estimation

$$\underline{\tilde{\boldsymbol{\beta}}}_{k,j} = \arg\min_{\left\|\underline{\tilde{\mathbf{h}}}_j^m\right\|^2=1} [\underline{\boldsymbol{\beta}}_{k,j}^{\mathcal{H}} \tilde{\mathbf{G}}_k \tilde{\mathbf{G}}_k^{\mathcal{H}} \underline{\mathbf{h}}_{k,j}] \quad j=1,\cdots,J \quad k=1,\cdots K\,. \tag{6.20}$$

The solution to (6.20), denoted by $\underline{\tilde{\boldsymbol{\beta}}}_{k,j}$, is the eigenvector corresponding to the smallest eigenvalue of $\tilde{\mathbf{G}}_{k,j}\tilde{\mathbf{G}}_{k,j}^{\mathcal{H}}$. However, in such blind identification employing second order statistics and subspace decompositions, there is inherent scalar ambiguity in the estimation, i.e. there is a complex scalar yet to be determined.

6.2.3 Channel Identifiablity

Firstly, the identifiablity of channel parameters depend on the properties of the matrix $\mathbf{D}_j$. This matrix has to be full column rank, and the condition is shown in *Theorem 1*.

Theorem 1: For $L > K$, the matrix $\mathbf{D}_j$, with dimension $2L \times 2K$, has full column rank, i.e., $Rank(\mathbf{D}_j) = 2K$, if and only if at least one of the subcarriers channel frequency response between any of the transmit antennas and the receive antenna of each respective user is non-zero.

Proof: The submatrix $\mathbf{D}_j^k$ defined in (6.8b) which is extracted from the ($2k-1$)th and $2k$ th ($k=1,2,\cdots,K$) columns of $\mathbf{D}_j^k$ can be rewritten as

$$\mathbf{D}_j^k = \underbrace{\begin{bmatrix} \mathcal{D}(\underline{\mathbf{h}}_{k,j,1}) & \mathbf{0} & \mathcal{D}(\underline{\mathbf{h}}_{k,j,2}) & \mathbf{0} \\ \mathbf{0} & \mathcal{D}(\underline{\mathbf{h}}_{k,j,2})^* & \mathbf{0} & -\mathcal{D}(\underline{\mathbf{h}}_{k,j,1})^* \end{bmatrix}}_{\mathbf{H}_{k,j}} \underbrace{\begin{bmatrix} \underline{\mathbf{c}}_{k,1} & \mathbf{0} \\ \underline{\mathbf{c}}_{k,2} & \mathbf{0} \\ \mathbf{0} & \underline{\mathbf{c}}_{k,2} \\ \mathbf{0} & \underline{\mathbf{c}}_{k,1} \end{bmatrix}}_{\mathbf{C}_k} = \mathbf{H}_{k,j}\mathbf{C}_k \, .$$

(6.21)

Since the spreading code $\underline{\mathbf{c}}_{k,1}$ and $\underline{\mathbf{c}}_{k,2}$ are linearly independent, and take on values from {-1, +1}, matrix $\mathbf{C}_k$ has full column rank, i.e., $Rank(\mathbf{C}_k)=2$. If each respective user has at least one nonzero subcarrier channel frequency response between the transmit antennas and *j*th receive antenna, i.e., the vector $\left[\underline{\mathbf{h}}_{k,j,1}^T \quad \underline{\mathbf{h}}_{k,j,2}^T\right]^T$ has at least one nonzero element, then the rank of $\mathbf{H}_{k,j}$ will be equal or greater than 2. From the above argument and using the relationship

$$2 \le Rank(\mathbf{H}_{k,j}) + Rank(\mathbf{C}_k) - 2 \le Rank(\mathbf{D}_j^k) \le \min\left(Rank(\mathbf{H}_{k,j}), Rank(\mathbf{C}_k)\right) = 2 \, ,$$

(6.22)

we obtain $2 \le Rank(\mathbf{D}_j^k) \le 2 \;\Rightarrow\; Rank(\mathbf{D}_j^k) = 2$. This means that $\mathbf{D}_j^k$ has full column rank. This condition in STBC MC-CDMA system is always satisfied because channel will have at least one nonzero multipaths and thus channel frequency response will have at least one none-null if $L > K$.

Since matrix $\mathbf{C}_k$ is independent for different *k* and channel frequency response $\left[\underline{\mathbf{h}}_{k,j,1}^T \quad \underline{\mathbf{h}}_{k,j,2}^T\right]^T$ is also independent for different *j* and *k* (or matrix $\mathbf{H}_{k,j}$ is also independent for different *j* and *k*), the matrix $\mathbf{D}_j$ consisting of $\mathbf{D}_j^k$ will have full column rank. Comparing the blind channel estimation in OFDM system [97], subspace-based estimation technique is much more robust in STBC MC-CDMA (and MC-CDMA) system. OFDM system requires all the subcarrier channel frequency responses to be non-zero.

Secondly, the identifiability of the channel will depend on (6.17) - the solution for channel parameter vector $\underline{\boldsymbol{\beta}}_{k,j}$ should be unique (up to a scalar ambiguity). The following theorem provides a characterization of condition under which the channel $\underline{\boldsymbol{\beta}}_{k,j}$ can be uniquely identified.

Theorem 2: The matrix $\mathbf{G}_{k,j}$ defined in (6.17) has a left null space of dimension one, and the channel parameter vector $\underline{\boldsymbol{\beta}}_{k,j}$ estimated by (6.17) is unique and up to a scalar if the spreading codes at each transmit antenna of all users are linearly independent of each other, i.e. $\underline{\mathbf{c}}_{k,1} \neq \underline{\mathbf{c}}_{k,2}$ which is used in this chapter..

Proof: Let us assume that (6.17) has two different solutions, $\underline{\boldsymbol{\beta}'}_{k,j} \neq \mathbf{0}$ and $\underline{\boldsymbol{\beta}}_{k,j} \neq \mathbf{0}$, where $\underline{\boldsymbol{\beta}}_{k,j}$ represents the actual channel vector and we shall investigate the property of $\underline{\boldsymbol{\beta}'}_{k,j}$. Since both channel $\underline{\boldsymbol{\beta}'}_{k,j}$ and $\underline{\boldsymbol{\beta}}_{k,j}$ satisfy (6.17), they both span the same space. Hence, there must exist a full rank 2×2 matrix $\mathbf{B}$ such that $\mathbf{D}_j^k\left(\underline{\boldsymbol{\beta}'}_{k,j}\right) = \mathbf{D}_j^k\left(\underline{\boldsymbol{\beta}}_{k,j}\right)\cdot\mathbf{B}$, where $\mathbf{D}_j^k(\bullet)$ is the composite channel matrix $\mathbf{D}_j^k$ defined in (6.8b) with the channel parameter $\underline{\boldsymbol{\beta}'}_{k,j}$ or $\underline{\boldsymbol{\beta}}_{k,j}$. Let us define matrix $\mathbf{B}$ as $\mathbf{B} = \begin{bmatrix} b_1 & b_2 \\ b_3 & b_4 \end{bmatrix}$, then the following equation should be satisfied

$$\begin{bmatrix} \mathcal{D}(\underline{\mathbf{h}'}_{k,j,1})\underline{\mathbf{c}}_{k,1} & \mathcal{D}(\underline{\mathbf{h}'}_{k,j,2})\underline{\mathbf{c}}_{k,2} \\ \mathcal{D}(\underline{\mathbf{h}'}_{k,j,2})^*\underline{\mathbf{c}}_{k,2} & -\mathcal{D}(\underline{\mathbf{h}'}_{k,j,1})^*\underline{\mathbf{c}}_{k,1} \end{bmatrix} = \begin{bmatrix} \mathcal{D}(\underline{\mathbf{h}}_{k,j,1})\underline{\mathbf{c}}_{k,1} & \mathcal{D}(\underline{\mathbf{h}}_{k,j,2})\underline{\mathbf{c}}_{k,2} \\ \mathcal{D}(\underline{\mathbf{h}}_{k,j,2})^*\underline{\mathbf{c}}_{k,2} & -\mathcal{D}(\underline{\mathbf{h}}_{k,j,1})^*\underline{\mathbf{c}}_{k,1} \end{bmatrix}\cdot\begin{bmatrix} b_1 & b_2 \\ b_3 & b_4 \end{bmatrix}. \tag{6.23}$$

With some manipulations, Eq (6.23) can be rewritten as

$$\begin{bmatrix} \mathcal{D}(\underline{\mathbf{c}}_{k,1})\overline{\mathbf{V}}^T \underline{\boldsymbol{\beta}}'_{k,j,1} & \mathcal{D}(\underline{\mathbf{c}}_{k,2})\overline{\mathbf{V}}^T \underline{\boldsymbol{\beta}}'_{k,j,2} \\ \mathcal{D}(\underline{\mathbf{c}}_{k,2})\overline{\mathbf{V}}^{\mathcal{H}} \underline{\boldsymbol{\beta}}'^*_{k,j,2} & -\mathcal{D}(\underline{\mathbf{c}}_{k,1})\overline{\mathbf{V}}^{\mathcal{H}} \underline{\boldsymbol{\beta}}'^*_{k,j,1} \end{bmatrix}.$$

$$= \begin{bmatrix} \mathcal{D}(\underline{\mathbf{c}}_{k,1})\overline{\mathbf{V}}^T \underline{\boldsymbol{\beta}}_{k,j,1} & \mathcal{D}(\underline{\mathbf{c}}_{k,2})\overline{\mathbf{V}}^T \underline{\mathbf{c}}_{k,2}\underline{\boldsymbol{\beta}}_{k,j,2} \\ \mathcal{D}(\underline{\mathbf{c}}_{k,2})^*\overline{\mathbf{V}}^{\mathcal{H}} \underline{\boldsymbol{\beta}}^*_{k,j,2} & -\mathcal{D}(\underline{\mathbf{c}}_{k,1})^*\overline{\mathbf{V}}^{\mathcal{H}} \underline{\boldsymbol{\beta}}^*_{k,j,1} \end{bmatrix} \cdot \begin{bmatrix} b_1 & b_2 \\ b_3 & b_4 \end{bmatrix}. \tag{6.24}$$

Since $\overline{\mathbf{V}}\overline{\mathbf{V}}^{\mathcal{H}} = \mathbf{I}$, and $\mathcal{D}(\underline{\mathbf{c}}_{k,i})^{-1} = \mathcal{D}(\underline{\mathbf{c}}_{k,i})$ ($i = 1,2$), we can obtained the following equations by (6.24)

$$\underline{\boldsymbol{\beta}}'_{k,j,1} = b_1 \cdot \underline{\boldsymbol{\beta}}_{k,j,1} + b_3 \cdot \mathbf{Q}_k \cdot \underline{\boldsymbol{\beta}}_{k,j,2}, \tag{6.25a}$$

$$\underline{\boldsymbol{\beta}}'_{k,j,2} = b_2 \cdot \mathbf{Q}_k \cdot \underline{\boldsymbol{\beta}}_{k,j,1} + b_4 \cdot \underline{\boldsymbol{\beta}}_{k,j,2}, \tag{6.25b}$$

$$\underline{\boldsymbol{\beta}}'_{k,j,2} = b_1^* \cdot \underline{\boldsymbol{\beta}}_{k,j,2} + b_3^* \cdot \mathbf{Q}_k \cdot \underline{\boldsymbol{\beta}}_{k,j,1}, \tag{6.25c}$$

$$\underline{\boldsymbol{\beta}}'_{k,j,1} = b_2^* \cdot \mathbf{Q}_k \cdot \underline{\boldsymbol{\beta}}_{k,j,2} + b_4^* \cdot \underline{\boldsymbol{\beta}}_{k,j,1}, \tag{6.25d}$$

where $\mathbf{Q}_k = \overline{\mathbf{V}}^*\mathcal{D}(\underline{\mathbf{c}}_{k,1})\mathcal{D}(\underline{\mathbf{c}}_{k,2})\overline{\mathbf{V}}^T$. In the sequel, we will discuss the two cases of spreading codes.

i) $\underline{\mathbf{c}}_{k,1} \neq \underline{\mathbf{c}}_{k,2}$,

From (6.25a), (6.25d) and (6.25b), (6.25c), we can obtain

$$\underline{\boldsymbol{\beta}}_{k,j,2} = \frac{b_4^* - b_1}{b_2^* + b_3}\mathbf{Q}_k^{-1} \cdot \underline{\boldsymbol{\beta}}_{k,j,1}, \tag{6.26a}$$

$$\underline{\boldsymbol{\beta}}_{k,j,1} = \frac{b_1^* - b_4}{b_2^* + b_3}\mathbf{Q}_k^{-1} \cdot \underline{\boldsymbol{\beta}}_{k,j,2}, \tag{6.26b}$$

respectively. Substitute (6.26a) in (6.25a) and (6.26b) in (6.25b), the following equations can be obtained

$$\underline{\boldsymbol{\beta}}'_{k,j,1} = \frac{b_1 b_2^* + b_3 b_4^*}{b_2^* + b_3} \cdot \underline{\boldsymbol{\beta}}_{k,j,1}, \tag{6.27a}$$

$$\underline{\boldsymbol{\beta}}'_{k,j,2} = \frac{b_1^* b_2 + b_3^* b_4}{b_2 + b_3^*} \cdot \underline{\boldsymbol{\beta}}_{k,j,2}. \tag{6.27b}$$

Substitute (6.27a) and (6.27b) into (6.17), we can show that $\underline{\boldsymbol{\beta}}'_{k,j} = \alpha \cdot \underline{\boldsymbol{\beta}}_{k,j}$, where α is a complex scalar defined by $\alpha = \dfrac{b_1^* b_2 + b_3^* b_4}{b_2 + b_3^*}$. Thus, the two solutions are different by a complex scalar. This proves that the matrix $\mathbf{G}_{k,j}$ has a left null space of dimension one, which implies that it loses its rank by one. Hence the channel vector can be identified up to a complex scalar factor when spreading codes at each transmit antenna of the users are linearly independent each other.

ii) when $\underline{\mathbf{c}}_{k,1} = \underline{\mathbf{c}}_{k,2}$,

In this case, the matrix $\mathbf{Q}_k$ is simplified as an identity matrix $\mathbf{Q}_k = \mathbf{I}$, from (6.25a), (6.25d) and (6.25b), (6.25c), we can obtain different relations between $\underline{\boldsymbol{\beta}}_{k,j,1}$ and $\underline{\boldsymbol{\beta}}_{k,j,1}$ given as

$$\underline{\boldsymbol{\beta}}_{k,j,1} = \frac{b_2^* + b_3}{b_4^* - b_1} \cdot \underline{\boldsymbol{\beta}}_{k,j,2}, \tag{6.28a}$$

$$\underline{\boldsymbol{\beta}}_{k,j,2} = \frac{b_2^* + b_3}{b_1^* - b_4} \cdot \underline{\boldsymbol{\beta}}_{k,j,1}, \tag{6.28b}$$

respectively. Substitute (6.28a) in (6.25a) and (6.28b) in (6.25b), the following equations can be obtained

$$\underline{\boldsymbol{\beta}}'_{k,j,1} = \frac{b_1 b_2^* + b_3 b_4^*}{b_4^* - b_1} \cdot \underline{\boldsymbol{\beta}}_{k,j,2}, \tag{6.29a}$$

$$\underline{\boldsymbol{\beta}}'_{k,j,2} = \frac{b_1^* b_2 + b_3^* b_4}{b_1^* - b_4} \cdot \underline{\boldsymbol{\beta}}_{k,j,1}. \tag{6.29b}$$

Unlike the previous case, (6.29a) and (6.29b) implies that $\underline{\boldsymbol{\beta}}'_{k,j} = \left[\underline{\boldsymbol{\beta}}'^{\mathcal{H}}_{k,j,1} \quad \underline{\boldsymbol{\beta}}'^{T}_{k,j,2}\right]^T = \alpha \cdot \left[-\underline{\boldsymbol{\beta}}^{\mathcal{H}}_{k,j,2} \quad \underline{\boldsymbol{\beta}}^{T}_{k,j,1}\right]^T$ is another solution of (6.17), where α is a complex scalar defined by $\alpha = \dfrac{b_1^* b_2 + b_3^* b_4}{b_1^* - b_4}$. Therefore, both channel vector $\underline{\boldsymbol{\beta}}'_{k,j}$ and

$\underline{\boldsymbol{\beta}}_{k,j}$, as well as their any linear combinations, satisfied (6.17). This indicates that the matrix $\mathbf{G}_{k,j}$ has a left null space of dimension two, which implies that it loses rank by two, and that the channel vector does not necessarily yield a unique solution by (6.17).

In the presence of the noise, the proof to (6.19) can be performed similarly. The matrix $\tilde{\mathbf{G}}_{k,j}$ defined in (6.19) has a left null space of dimension one, and the channel parameter vector $\tilde{\underline{\boldsymbol{\beta}}}_{k,j}$ estimated by (6.19) is unique and up to a complex scalar if the spreading codes at each transmit antenna of the users are linearly independent to each other.

6.2.4 Resolving the Scalar Ambiguity

In this chapter, different spreading codes are used at each transmit antenna for every user, i.e., $\underline{\mathbf{c}}_{k,1} \neq \underline{\mathbf{c}}_{k,2}$. As we discussed in the subsection *6.2.3*, the channel vector estimated by (6.20) is unique and up to a complex scalar. I We then specify a training symbol to resolve this scalar ambiguity. Assuming

$$\hat{\underline{\boldsymbol{\beta}}}_{k,j} = \alpha_{k,j} \cdot \tilde{\underline{\boldsymbol{\beta}}}_{k,j}, \tag{6.30}$$

where $\alpha_{k,j}$ means the complex scalar, $\tilde{\underline{\boldsymbol{\beta}}}_{k,j}$ is the $2(G+1)\times 1$ channel coefficients vector obtained by the subspace solution in (6.20). We require one training symbol in every data block of each user, which means

$$s_k(2n-1) = a \qquad n = 1 \qquad\qquad k = 1,\cdots,K \tag{6.31}$$

where a is known symbol. Eq.(6.30) can be written as

$$\hat{\underline{\boldsymbol{\beta}}}_{k,j,1} = \alpha^*_{k,j} \cdot \tilde{\underline{\boldsymbol{\beta}}}_{k,j,1}, \tag{6.32a}$$

$$\hat{\underline{\boldsymbol{\beta}}}_{k,j,2} = \alpha_{k,j} \cdot \tilde{\underline{\boldsymbol{\beta}}}_{k,j,2}. \tag{6.32b}$$

Therefore, we can obtain

$$\mathcal{D}(\hat{\underline{\mathbf{h}}}_{k,j,1})\underline{\mathbf{c}}_{m,1} = \alpha_{k,j}^{*} \cdot \mathcal{D}(\tilde{\underline{\mathbf{h}}}_{k,j,1})\underline{\mathbf{c}}_{k,1} \ , \tag{6.33a}$$

$$\mathcal{D}(\hat{\underline{\mathbf{h}}}_{k,j,2})\underline{\mathbf{c}}_{k,2} = \alpha_{k,j} \cdot \mathcal{D}(\tilde{\underline{\mathbf{h}}}_{k,j,2})\underline{\mathbf{c}}_{k,2} \, . \tag{6.33b}$$

Let us collect the received data in first two successive symbol intervals for every block, apply (6.33a) (6.33b) to (6.8), we can have

$$\underline{\mathbf{z}}_j(1) = \frac{1}{\sqrt{2L}} \tilde{\mathbf{Đ}}_j \cdot \mathcal{D}[\alpha_{1,j}^{*} \quad \alpha_{1,j} \quad \cdots \quad \alpha_{K,j}^{*} \quad \alpha_{K,j}] \cdot \left[a \quad s_1(2) \quad \cdots \quad a \quad s_K(2)\right]^T + \underline{\boldsymbol{\eta}}_j(1) \, . \tag{6.34}$$

Since $\tilde{\mathbf{Đ}}_j$ is full column rank, there exists Moore-Penrose pseudo inverse $\tilde{\mathbf{Đ}}_j^{\dagger}$ which satisfies $\tilde{\mathbf{Đ}}_j^{\dagger}\tilde{\mathbf{Đ}}_j = \mathbf{I}_{2K}$. We let

$$\underline{\mathbf{b}}_j = \sqrt{2L}\tilde{\mathbf{Đ}}_j^{\dagger}\underline{\mathbf{z}}_j(1) \tag{6.35}$$

which is $2K \times 1$ vector, therefore, the scalar ambiguity can be solved by

$$\hat{\alpha}_{k,j} \cong b_j^{*}(2k-1)\big/a^{*}; \quad k = 1, \cdots, K \ . \tag{6.36}$$

6.3 Performance Analysis of Estimation

In the section, the theoretical performance when using the above semi-blind subspace-based channel estimation method in the presence of AWGN is studied. The vectorization and the matrix Kronecker product between matrices have the following properties [113]

$$\begin{aligned} vec(\mathbf{ABC}) &= \left(\mathbf{C}^T \otimes \mathbf{A}\right)vec(\mathbf{B}) \\ \left(\mathbf{A} \otimes \mathbf{B}\right)\left(\mathbf{C} \otimes \mathbf{D}\right) &= \left(\mathbf{AC} \otimes \mathbf{BD}\right) \\ \left(\mathbf{A} \otimes \mathbf{B}\right)^{\mathcal{H}} &= \left(\mathbf{A}^{\mathcal{H}} \otimes \mathbf{B}^{\mathcal{H}}\right) \end{aligned} \ . \tag{6.37}$$

We resort to the first-order perturbation approximation used in [101]. We define $\mathbf{Z}_j$ as the observation to (6.9) without noise and $\tilde{\mathbf{Z}}_j$ is the observation in the presence of noise, which means

$$\tilde{\mathbf{Z}}_j = \mathbf{Z}_j + \Delta\mathbf{Z}_j = \mathbf{Z}_j + \mathrm{N}_j \,. \tag{6.38}$$

Denote $\mathbf{U}_o$ as the *true null subspace* obtained from the noise-free observation (6.10), and $\tilde{\mathbf{U}}_o$ as the *perturbated null subspace* obtained from the additive noise-corrupted observation (6.18), then we can write

$$\tilde{\mathbf{U}}_o = \mathbf{U}_o + \Delta\mathbf{U}_o \,. \tag{6.39}$$

Thus, the first order of perturbation approximation of null subspace can be derived to be [101]

$$\Delta\mathbf{U}_o = -\mathbf{U}_s \mathbf{\Sigma}_s^{-1} \mathbf{V}_s^{\mathcal{H}} \mathbf{N}_j^{\mathcal{H}} \mathbf{U}_o = -\mathbf{Z}_j^{\dagger\mathcal{H}} \mathbf{N}_j^{\mathcal{H}} \mathbf{U}_o \,. \tag{6.40}$$

Applying the relationship given in (6.37),

$$vec(\Delta\mathbf{U}_o) = -\left(\mathbf{U}_o^T \otimes \mathbf{Z}_j^{\dagger\mathcal{H}}\right) vec(\mathbf{N}_j^{\mathcal{H}}) \,. \tag{6.41}$$

Let $\tilde{\underline{\boldsymbol{\beta}}}_{k,j} = \underline{\boldsymbol{\beta}}_{k,j} + \Delta\underline{\boldsymbol{\beta}}_{k,j}$, $\tilde{\mathbf{G}}_{k,j} = \mathbf{G}_{k,j} + \Delta\mathbf{G}_{k,j}$, then from (6.19),

$$(\underline{\boldsymbol{\beta}}_{k,j}^{\mathcal{H}} + \Delta\underline{\boldsymbol{\beta}}_{k,j}^{\mathcal{H}}) \cdot (\mathbf{G}_{k,j} + \Delta\mathbf{G}_{k,j}) \cong \mathbf{0} \,. \tag{6.42}$$

Ignore the second order perturbation in (6.42), we have

$$\Delta\underline{\boldsymbol{\beta}}_{k,j}^{\mathcal{H}} \mathbf{G}_{k,j} = -\underline{\boldsymbol{\beta}}_{k,j}^{\mathcal{H}} \Delta\mathbf{G}_{k,j} \,. \tag{6.43}$$

Define a $(4G+4)\times(4L-4K)$ matrix $\vec{\mathbf{G}}_{k,j}$ given by

$$\vec{\mathbf{G}}_{k,j}(:,2m-1) = \begin{bmatrix} \mathbf{G}_{k,j}(:,2m-1) \\ \mathbf{0} \end{bmatrix}, \tag{6.44a}$$

$$\vec{\mathbf{G}}_{k,j}(:,2m) = \begin{bmatrix} \mathbf{0} \\ \mathbf{G}_{k,j}(:,2m)^* \end{bmatrix}. \tag{6.44b}$$

e.g., if $\mathbf{G}_{k,j} = \begin{bmatrix} a_1 & a_2 & a_3 & a_4 \\ b_1 & b_2 & b_3 & b_4 \end{bmatrix}$, then $\vec{\mathbf{G}}_{k,j} = \begin{bmatrix} a_1 & 0 & a_3 & 0 \\ b_1 & 0 & b_3 & 0 \\ 0 & a_2^* & 0 & a_4^* \\ 0 & b_2^* & 0 & b_4^* \end{bmatrix}$. Then from Eq (6.43) the following equation holds

$$\Delta\vec{\underline{\boldsymbol{\beta}}}_{k,j}^{\mathcal{H}}\vec{\mathbf{G}}_{k,j} = -\vec{\underline{\boldsymbol{\beta}}}_{k,j}^{\mathcal{H}}\Delta\vec{\mathbf{G}}_{k,j} . \tag{6.45}$$

where $\vec{\underline{\boldsymbol{\beta}}}_{k,j} = \left[\underline{\boldsymbol{\beta}}_{k,j}^T \quad \underline{\boldsymbol{\beta}}_{k,j}^{\mathcal{H}}\right]^T$. From *Theorem 2*, since $\mathbf{G}_{k,j}$ loses its rank by one, $\vec{\mathbf{G}}_{k,j}$ will lose its rank by two. Thus we are unable to find a matrix $\vec{\mathbf{G}}_{k,j}^{\dagger}$ to satisfy $\vec{\mathbf{G}}_{k,j}\vec{\mathbf{G}}_{k,j}^{\dagger} = \mathbf{I}$ since $\vec{\mathbf{G}}_{k,j}$ has no full row rank. We then reconstruct the matrix $\mathbf{G}_{k,j}$ by removing the *d*th row where *d* is the index whose element in vector $\underline{\boldsymbol{\beta}}_{k,j}$ is having the largest amplitude [114]. Therefore from (45), we can express the channel error vector as

$$\Delta\vec{\vec{\underline{\boldsymbol{\beta}}}}_{k,j}^{\mathcal{H}} \cong -\vec{\underline{\boldsymbol{\beta}}}_{k,j}^{\mathcal{H}}\Delta\vec{\mathbf{G}}_{k,j}\vec{\vec{\mathbf{G}}}_{k,j}^{\dagger} . \tag{46}$$

where $\Delta\vec{\vec{\underline{\boldsymbol{\beta}}}}_{k,j}$ and $\vec{\vec{\mathbf{G}}}_{k,j}$ are obtained from $\vec{\underline{\boldsymbol{\beta}}}_{k,j}$ and $\vec{\mathbf{G}}_{k,j}$ by removing its *d*th and (2*G* + 2 + *d*)th rows.

Performing some manipulations using (6.14)-(6.17) we can obtain

$$\vec{\underline{\boldsymbol{\beta}}}_{k,j}^{\mathcal{H}}\vec{\mathbf{G}}_{k,j} = vec^{\mathcal{H}}(\mathbf{U}_o)\left(\mathbf{I}_{2L-2K} \otimes \mathbf{D}_j^k\right) . \tag{6.47}$$

Therefore,

$$\vec{\underline{\boldsymbol{\beta}}}_{k,j}^{\mathcal{H}}\Delta\vec{\mathbf{G}}_{k,j} = vec^{\mathcal{H}}(\Delta\mathbf{U}_o)\left(\mathbf{I}_{2L-2K} \otimes \mathbf{D}_j^k\right). \tag{6.48}$$

By substituting (6.40) in (6.48), we obtain

$$\begin{aligned}\vec{\underline{\boldsymbol{\beta}}}_{k,j}^{\mathcal{H}}\Delta\vec{\mathbf{G}}_{k,j} &= -vec^{\mathcal{H}}(\mathbf{N}_j^{\mathcal{H}})\left(\mathbf{U}_o \otimes \mathbf{Z}_j^{\dagger}\right)\left(\mathbf{I}_{2L-2K} \otimes \mathbf{D}_j^k\right) \\ &= -vec^{\mathcal{H}}(\mathbf{N}_j^{\mathcal{H}})\left(\mathbf{U}_o \otimes \mathbf{Z}_j^{\dagger}\mathbf{D}_j^k\right).\end{aligned} \tag{6.49}$$

Using (6.9),

$$\mathbf{Z}_j^{\dagger}\mathbf{D}_j^k = (\mathbf{D}_j\mathbf{S}\big/\sqrt{2V})^{\dagger}\mathbf{D}_j^k = \sqrt{2V}\mathbf{S}^{\dagger}(\mathbf{D}_j^{\dagger}\mathbf{D}_j^k) = \sqrt{2V}\mathbf{S}^{\dagger}\boldsymbol{\gamma}_k\,, \tag{6.49a}$$

where $\boldsymbol{\gamma}_k$ is $2K\times 2$ matrix whose (2k-1, 1)th and (2k, 2)th entries are unity with other elements equal zero, e.g. $\boldsymbol{\gamma}_1 = [\mathbf{I}_{2\times 2} \quad \mathbf{0}_{2\times 2(K-1)}]^T$. Substitute (6.49) in (6.46), the channel error vector is equal to

$$\Delta\underline{\overleftrightarrow{\boldsymbol{\beta}}}_{k,j}^{\mathcal{H}} = -\sqrt{2V}vec^{\mathcal{H}}(\mathbf{N}_j^{\mathcal{H}})\left(\mathbf{U}_o\otimes\mathbf{S}^{\dagger}\boldsymbol{\gamma}_k\right)\overleftrightarrow{\mathbf{G}}_{k,j}^{\dagger}\,. \tag{6.50}$$

Since the channel is estimated with the scalar to resolve the ambiguity, the perturbation of the estimated channel is given by

$$\Delta\underline{\overleftrightarrow{\boldsymbol{\beta}}}_{k,j} = \hat{\alpha}_{k,j}\cdot\underline{\Delta\overleftrightarrow{\boldsymbol{\beta}}}_{k,j}\,. \tag{6.51}$$

However, the amplitude of the scalar is nearly equal or equal to unity, i.e., $\left\|\hat{\alpha}_{k,j}\right\|\cong 1$, then we have

$$\Delta\underline{\overleftrightarrow{\boldsymbol{\beta}}}_{k,j}\Delta\underline{\overleftrightarrow{\boldsymbol{\beta}}}_{k,j}^{\mathcal{H}} \cong \Delta\underline{\overleftrightarrow{\boldsymbol{\beta}}}_{k,j}\Delta\underline{\overleftrightarrow{\boldsymbol{\beta}}}_{k,j}^{\mathcal{H}}\,. \tag{6.52}$$

Thus, the covariance of channel estimation error is given by

$$\begin{aligned}
\mathbf{R}_{\underline{\boldsymbol{\beta}}_k} &= E\left\{\Delta\underline{\overleftrightarrow{\boldsymbol{\beta}}}_{k,j}\Delta\underline{\overleftrightarrow{\boldsymbol{\beta}}}_{k,j}^{\mathcal{H}}\right\} \cong E\left\{\Delta\underline{\overleftrightarrow{\boldsymbol{\beta}}}_{k,j}\Delta\underline{\overleftrightarrow{\boldsymbol{\beta}}}_{k,j}^{\mathcal{H}}\right\} \\
&= 2V\sigma_\eta^2\overleftrightarrow{\mathbf{G}}_{k,j}^{\dagger\,\mathcal{H}}\left(\mathbf{U}_o^{\mathcal{H}}\otimes\boldsymbol{\gamma}_k^T\mathbf{S}^{\dagger\mathcal{H}}\right)\left(\mathbf{U}_o\otimes\mathbf{S}^{\dagger}\boldsymbol{\gamma}_k\right)\overleftrightarrow{\mathbf{G}}_{k,j}^{\dagger} \\
&= 2V\sigma_\eta^2\overleftrightarrow{\mathbf{G}}_{k,j}^{\dagger\,\mathcal{H}}\left(\mathbf{U}_o^{\mathcal{H}}\mathbf{U}_o\otimes\boldsymbol{\gamma}_k^T\mathbf{S}^{\dagger\mathcal{H}}\mathbf{S}^{\dagger}\boldsymbol{\gamma}_k\right)\overleftrightarrow{\mathbf{G}}_{k,j}^{\dagger} \\
&= 2V\sigma_\eta^2\cdot E\left\{\overleftrightarrow{\mathbf{G}}_k^{\dagger\mathcal{H}}\left(\mathbf{I}_{2L-2K}\otimes\boldsymbol{\gamma}_k^{\dagger}\left(\mathbf{S}\mathbf{S}^{\mathcal{H}}\right)^{-1}\boldsymbol{\gamma}_k\right)\overleftrightarrow{\mathbf{G}}_k^{\dagger}\right\}.
\end{aligned} \tag{6.53}$$

To derive (6.53), we have made used of (6.50) and the fact that $\mathbf{U}_o$ is an unitary matrix. When the number of data symbols (2N) is large enough, (6.53) can be simplified to

$$\mathbf{R}_{\Delta\underline{\boldsymbol{\beta}}_k} = \frac{2V\sigma_\eta^2}{S_k}\cdot E\left\{\overleftrightarrow{\mathbf{G}}_{k,j}^{\dagger\ \mathcal{H}}\mathbf{W}_k\overleftrightarrow{\mathbf{G}}_{k,j}^{\dagger}\right\}$$

$$= 2 \cdot 10^{-SNR/10} \cdot E\left\{ \overleftrightarrow{\mathbf{G}}_{k,j}^{\dagger\ \mathcal{H}} \mathbf{W}_k \overleftrightarrow{\mathbf{G}}_{k,j}^{\dagger} \right\} \tag{6.54}$$

where $\mathbf{W}_k = \left(\mathbf{I}_{2L-2K} \otimes \boldsymbol{\gamma}_k^{\dagger} \left(\mathcal{D}\left(\left[S_1 / S_k \quad \cdots \quad 1 \quad \cdots \quad S_K / S_k \right] \right) \otimes \mathbf{I}_2 \right)^{-1} \boldsymbol{\gamma}_k \right)$, and SNR is defined as the received sample signal energy to noise ratio per receive antenna.

6.4 Cramér-Rao Bound

In this section, the Cramér-Rao Bound (CRB) of the channel impulse response estimation is studied to compare the channel estimation accuracy by assuming that the transmitted symbols are nuisance parameters.

Given the observation vector in (6.8), with the assumption **a**1) – **a**5) we made neforer, the probability density function (PDF) of each block of the received data vector $\underline{\mathbf{z}}_j(n)$, conditioned on the channel parameter vector $\underline{\boldsymbol{\beta}}_j$ and the source symbol vector $\underline{\mathbf{s}}(n)$, is given by

$$p_{\underline{\mathbf{z}}_j|\underline{\boldsymbol{\beta}}_j,\underline{\mathbf{s}}(n)}(\underline{\mathbf{z}}_j \mid \underline{\boldsymbol{\beta}}_j, \underline{\mathbf{s}}(n)) = \frac{1}{(2\pi\sigma_\eta)^V} \exp\left[-\left\| \underline{\mathbf{z}}_j(n) - \frac{1}{\sqrt{2V}} \mathbf{D}_j \underline{\mathbf{s}}(n) \right\|^2 / \sigma_\eta^2 \right] \tag{6.55}$$

where $\|\cdot\|^2$ denotes vector norm, and $\underline{\boldsymbol{\beta}}_j = \left[\underline{\boldsymbol{\beta}}_{1,j}^T \quad \underline{\boldsymbol{\beta}}_{2,j}^T \quad \cdots \quad \underline{\boldsymbol{\beta}}_{K,j}^T \right]^T$. Since the noise samples are uncorrelated, the joint PDF of a block received data $\mathbf{Z}_j = [\underline{\mathbf{z}}_j(0) \quad \cdots \quad \underline{\mathbf{z}}_j(N-1)]$ described in (6.9) is given by

$$p_{\mathbf{Z}_j|\underline{\boldsymbol{\beta}}_j,\mathbf{S}}(\mathbf{Z}_j \mid \underline{\boldsymbol{\beta}}_j, \mathbf{S}) = \frac{1}{(2\pi\sigma_\eta)^{VN}} \exp\left[-\sum_{n=0}^{N-1} \left\| \underline{\mathbf{z}}_j(n) - \frac{1}{\sqrt{2V}} \mathbf{D}_j \underline{\mathbf{s}}(n) \right\|^2 / \sigma_\eta^2 \right]. \tag{6.56}$$

To simplify the CRB derivation, we introduce the equivalent $4K(N+G+1) \times 1$ parameter vector

$$\underline{\boldsymbol{\theta}} = \left[\underline{\boldsymbol{\beta}}_{j,re}^T \quad \underline{\boldsymbol{\beta}}_{j,im}^T \quad \underline{\mathbf{s}}_{re}^T(0) \quad \cdots \quad \underline{\mathbf{s}}_{re}^T(N-1) \quad \underline{\mathbf{s}}_{im}^T(0) \quad \cdots \quad \underline{\mathbf{s}}_{im}^T(N-1) \right]^T \tag{6.57}$$

where $\underline{\boldsymbol{\beta}}_{j,re}(n) = \mathrm{Re}[\underline{\boldsymbol{\beta}}_j(n)]$, $\underline{\boldsymbol{\beta}}_{j,im}(n) = \mathrm{Im}[\underline{\boldsymbol{\beta}}_j(n)]$, $\underline{\mathbf{s}}_{re}(n) = \mathrm{Re}[\underline{\mathbf{s}}(n)]$ and $\underline{\mathbf{s}}_{im}(n) = \mathrm{Im}[\underline{\mathbf{s}}(n)]$, and we write the log-likelihood function as

$$f(\underline{\boldsymbol{\theta}}) = -VN\ln(2\pi\sigma_\eta) - \sum_{n=0}^{N-1}\left\| \underline{\mathbf{z}}_j(n) - \frac{1}{\sqrt{2V}}\mathbf{D}_j\underline{\mathbf{s}}(n)\right\|^2 / \sigma_\eta^2 . \tag{6.58}$$

We assume that the SNR is high enough to neglect the estimator's bias and introduce the $4K(N+G+1)\times 4K(N+G+1)$ equivalent Fisher's information matrix (FIM) given by

$$\mathcal{J}(\underline{\boldsymbol{\theta}}) = E_{\mathbf{z}_j|\underline{\boldsymbol{\beta}}_j,\mathbf{s}}\left\{ \frac{\partial f(\underline{\boldsymbol{\theta}})}{\partial\underline{\boldsymbol{\theta}}}\left(\frac{\partial f(\underline{\boldsymbol{\theta}})}{\partial\underline{\boldsymbol{\theta}}}\right)^T \right\}. \tag{6.59}$$

The calculation of each element of the FIM is given in Appendix A. With the signal vectors $\underline{\mathbf{s}}(n)$ treated as the nuisance parameters, the CRB bound of the covariance matrix of channel estimation error is given by the $4K(G+1)\times 4K(G+1)$ upper left block of $\mathcal{J}^{-1}$, i.e.

$$\mathrm{CRB}(\underline{\boldsymbol{\beta}}_j) = \mathcal{J}^{-1}\left(1{:}4K(G+1), 1{:}4K(G+1)\right). \tag{6.60}$$

However, directly computing the inverse of FIM matrix $\mathcal{J}(\underline{\boldsymbol{\theta}})$ is computationally intensive. With the inherent property of $\mathcal{J}(\underline{\boldsymbol{\theta}})$, a more efficient way to compute $\mathcal{J}^{-1}$ is presented in the Appendix 6.A.

6.5 Multiuser Detection

With the estimated channel state information $\hat{\underline{\boldsymbol{\beta}}}_{k,j}$ available at the receiver for all users, the symbols of desired user can be detected by using standard linear methods such as Zero-Forcing (ZF) detection or Minimum Mean Square Error (MMSE) detection [104]. We stack all received data symbols at every j^{th} receiver in the successive two symbol intervals to a data vector, and let $\underline{\mathbf{z}}(n) = \left[\underline{\mathbf{z}}_1(n)^T \quad \cdots \quad \underline{\mathbf{z}}_J(n)^T\right]^T_{2LJ\times 1}$, $\mathbf{D} = \left[\mathbf{D}_1^T \quad \cdots \quad \mathbf{D}_J^T\right]^T_{2LJ\times 2K}$, then we have

$$\underline{\mathbf{z}}(n) = \frac{1}{\sqrt{2V}}\mathbf{D}\underline{\mathbf{s}}(n) + \underline{\boldsymbol{\eta}}(n) \quad . \tag{6.61}$$

and the channel information matrix can be rewritten as $\mathbf{D} = \left[\mathbf{D}^1 \quad \cdots \quad \mathbf{D}^K\right]$, where $\mathbf{D}^k$ ($k = 1,2,\cdots,K$) is a ($2LJ \times 2$) matrix consisting of the channel information of kth user.

After the estimated channel information matix $\hat{\mathbf{D}}$ is obtained, in the following, we use this to recover the desired symbols at the receiver. We assume that the first user is of interest.

6.5.1 Zero Forcing Detection

A simple linear design that can completely eliminate the MUI is the ZF detection. In this approach, the detector $\hat{\boldsymbol{\omega}}_{ZF,1}$ for the desired 1st user is chosen such that in the absence of the noise. Since the estimated $\hat{\mathbf{D}}$ in (6.61) has full column rank $2K$, there always exists a Moore-Penrose pseudo inverse $\hat{\mathbf{D}}^\dagger$ so that $\hat{\mathbf{D}}^\dagger\hat{\mathbf{D}} = \mathbf{I}_{2K}$. Therefore, the ZF detector for the desired kth user is given by

$$\hat{\boldsymbol{\omega}}^{\mathcal{H}}_{ZF,1} = \sqrt{2V}\boldsymbol{\gamma}_1\hat{\mathbf{D}}^\dagger. \tag{6.62}$$

It follows that

$$\hat{\underline{\mathbf{s}}}_1(n) = \hat{\boldsymbol{\omega}}^{\mathcal{H}}_{ZF,1}\underline{\mathbf{z}}(n) = \underbrace{\boldsymbol{\gamma}_1^T\hat{\mathbf{D}}^\dagger\mathbf{D}^1\underline{\mathbf{s}}_1(n)}_{\text{desired signal}} + \underbrace{\sum_{k=2}^{K}\boldsymbol{\gamma}_1^T\hat{\mathbf{D}}^\dagger\mathbf{D}^m\underline{\mathbf{s}}_k(n)}_{\text{MUI}} + \underbrace{\sqrt{2V}\boldsymbol{\gamma}_1^T\hat{\mathbf{D}}^\dagger\underline{\boldsymbol{\eta}}(n)}_{\text{noise}}. \tag{6.63}$$

The conditional signal to interference and noise ratio SINR is given by

$$\text{SINR} = \frac{E\left\{\left\|\boldsymbol{\gamma}_1^T \hat{\mathbf{D}}^\dagger \mathbf{D}^1\right\|^2\right\}}{\sum_{k=2}^{K} E\left\{\left\|\boldsymbol{\gamma}_1^T \hat{\mathbf{D}}^\dagger \mathbf{D}^k S_k / S_1\right\|^2\right\} + 2\cdot 10^{-SNR/10} E\left\{\left\|\boldsymbol{\gamma}_1^T \hat{\mathbf{D}}^\dagger\right\|^2\right\}} \ . \qquad (6.64)$$

6.5.2 MMSE Detection

The ZF detector might enhance the effect of noise, especially when the noise is large. It is well known that the MMSE detector reduces to the ZF detector when $\text{SNR} = \infty$ and yields a better performance than the latter for finite SNR. The MMSE detector also maximizes the receiver output SINR among all linear detectors, and, thus, is the optimum linear detectors in that sense. The MMSE detection $\boldsymbol{\omega}_{MMSE}$ can be obtained by minimizing the mean square error criterion

$$\boldsymbol{\omega}_{MMSE} = \arg\min \quad \mathcal{L}(\boldsymbol{\omega}_{MMSE}) \qquad (6.65)$$

where $\mathcal{L}(\boldsymbol{\omega}_{MMSE}) = E\left\{\left\|\underline{\mathbf{s}}_1(n) - \boldsymbol{\omega}_{MMSE}^{\mathcal{H}} \underline{\mathbf{z}}(n)\right\|^2\right\}$

$$= E\left\{\left\|\underline{\mathbf{s}}_1(n) - \boldsymbol{\omega}_{MMSE}^{\mathcal{H}}\left(\frac{1}{\sqrt{2V}}\mathbf{D}^1 \underline{\mathbf{s}}_1(n) + \sum_{k=2}^{K}\frac{1}{\sqrt{2V}}\mathbf{D}^k \underline{\mathbf{s}}_k(n) + \underline{\boldsymbol{\eta}}(n)\right)\right\|^2\right\}.$$

(6.65a)

Through minimizing (6.65a) we have

$$\frac{\partial \mathcal{L}}{\partial \boldsymbol{\omega}_{MMSE}} = \frac{S_1}{2V}\sum_{k=1}^{K}\mathbf{D}^k \aleph \mathbf{D}^{k\mathcal{H}} \boldsymbol{\omega}_{MMSE} + \sigma_\eta^2 \mathbf{I}\cdot\boldsymbol{\omega}_{MMSE} - \frac{S_1}{\sqrt{2V}}\mathbf{D}^1 = \mathbf{0} \qquad (6.66)$$

where $\aleph = \mathbf{I}_2 \otimes \mathcal{D}([1 \quad S_2/S_1 \quad \cdots \quad S_K/S_1])$. Therefore

$$\boldsymbol{\omega}_{MMSE} = \sqrt{2V}\left(\mathbf{D}\aleph\mathbf{D}^{\mathcal{H}} + 2\cdot 10^{-SNR/10}\cdot\mathbf{I}\right)^{-1}\mathbf{D}^1 \ . \qquad (6.67)$$

Since in practice, only estimated $\hat{\mathbf{D}}$ and $\hat{\mathbf{D}}^1$ are available, the MMSE detector will follow that

$$\hat{\underline{\mathbf{s}}}_1(n) = \hat{\boldsymbol{\omega}}_{MMSE}^{\mathcal{H}} z(n) \quad = \underbrace{\frac{1}{\sqrt{2V}} \hat{\boldsymbol{\omega}}_{MMSE}^{\mathcal{H}} \mathbf{D}^1 \underline{\mathbf{s}}_1(n)}_{\text{desired signal}} + \underbrace{\sum_{k=2}^{K} \frac{1}{\sqrt{2V}} \hat{\boldsymbol{\omega}}_{MMSE}^{\mathcal{H}} \mathbf{D}^k \underline{\mathbf{s}}_k(n)}_{\text{MUI}} + \underbrace{\hat{\boldsymbol{\omega}}_{MMSE}^{\mathcal{H}} \underline{\boldsymbol{\eta}}(n)}_{\text{noise}}. \tag{6.68}$$

Similarly, the conditional signal to interference and noise ratio is given by

$$\text{SINR} = \frac{E\left\{\left\|\hat{\boldsymbol{\omega}}_{MMSE}^{\mathcal{H}} \mathbf{D}^1\right\|^2\right\}}{\sum_{k=2}^{K} E\left\{\left\|\hat{\boldsymbol{\omega}}_{MMSE}^{\mathcal{H}} \mathbf{D}^k S_k / S_1\right\|^2\right\} + 2 \cdot 10^{-SNR/10} E\left\{\left\|\hat{\boldsymbol{\omega}}_{MMSE}^{\mathcal{H}}\right\|^2\right\}}. \tag{6.69}$$

6.6 Simulations

In this section, the performance of the proposed semi-blind channel estimation technique and the system BER performance when using our ZF and MMSE detectors are investigated through simulations. The theoretical perturbation analysis and the CRB for the channel estimation are also verified by simulations.

A STBC MC-CDMA system with K active synchronous users using 16 phase shift keying (16-PSK) constellation is considered. Each user is assigned with a $L = 32$ orthogonal Gold code to spread the signal. In the following, the channel estimation and BER performance for the first user is investigated, with the transmit power $S_1 = 1$. In the sequel, we consider near-far environments without enforcing stringent power control. The power for $K-1$ interfering users follows a lognormal distribution with a mean power ddB higher than that of the desired user, and a standard deviation of 10 dB, i.e., $S_k / S_1 = 10^{\xi_k/10}$ ($k = 2,3,\cdots,K$), where $\xi_k \sim N(d,100)$. The near-far ratio (NFR) is defined as d (in decibels). The channel fading coefficients $\{\beta_{k,j,i,g}\}_{g=0}^{G}$ between the jth receiver antenna and ith transmit antenna were modeled as complex Gaussian random variables with zero mean and variance $\sigma_{k,j,i,g}^2$ where

$\sum_{g=0}^{G}\sigma_{k,j,i,g}^{2}=1$. In the simulations below, we set $G=5$, and $V=L+G$. The average signal-to-noise ratio (SNR) per sample for the desired user is defined as (recall that $S_1=1$)

$$\mathrm{SNR}=10\lg\left(1/V\sigma_{\eta}^{2}\right). \tag{6.70}$$

The performance measure for channel estimation is examined by the mean square error (MSE) given by

$$\mathrm{MSE}=E\left\{\left|\hat{\beta}_{k,j,i,g}-\beta_{k,j,i,g}\right|^{2}\right\}. \tag{6.71}$$

In the following numerical results, the performance of the proposed channel estimation and system BER performance of (i) conventional MC-CDMA systems with 1 transmitter and 1 receiver, (ii) STBC MC-CDMA systems with 2 transmitters and 1 receiver, and (iii) STBC MC-CDMA systems with 2 transmitters and 2 receivers are investigated.

Fig. 6.2 shows the MSE of channel estimation versus the SNR when $L=32$, $K=10$, $N=100$, $\mathrm{NFR}=0$ and $G=5$. t can be seen that the MSE improves gradually as SNR increases. It can be also found that the MSE of channel estimation for STBC MC-CDMA system is a bit worse than that for MC-CDMA system. This is due to the fact that for a given *N*, the SVD in (10) for MC-CDMA system can obtain a higher accurate null space than that for STBC MC-CDMA system since the requirement to guarantee the signal matrix **S** has full row rank is $N>K$ for MC-CDMA system, while it is $N>2K$ for STBC MC-CDMA system. As we expected, the MSE of channel estimation for STBC MC-CDMA system will degrades gradually when the number of transmit antennas increases. It can be also observed that the MSE of channel estimation for STBC MC-CDMA system with different receive antennas has nearly the same performance. This indicates that the MSE performance of channel estimation is independent of the number of receiver antennas for STBC MC-CDMA system.

It can be seen from Fig. 6.2 that the simulation results show well agreement with the theoretical MSE perturbation analysis, and the good lower bound for the MSE performance of channel estimation is provided by CRB.

Fig. 6.3 shows the MSE of channel estimation versus NFR when $L=32$, $K=10$, $N=100$, $\mathrm{SNR}=10$ and $G=5$. It can be seen that the near far problem has very slight effect on the MSE performance of channel estimation since the MSE remains nearly the same values as NFR increases. It shows the proposed the channel estimation algorithm is robust with the resistance to the near far problems.

Fig. 6.4 presents the MSR of channel estimation versus the number of users K when $L=32$, $N=100$, $\mathrm{SNR}=10$, $\mathrm{NFR}=0$ and $G=5$. It can be observed that MSE performance of channel estimation degrades slightly as the number of users K increases. This indicates that the number of users has only a slight effect on the MSE performance of channel estimation.

In Fig. 6.5, we present the BER performance versus SNR when $L=32$, $K=10$, $N=100$, $\mathrm{NFR}=0$ and $G=5$, using either ZF or MMSE detection, both for the case when channel estimation is performed and when perfect channel information is available. We demonstrate how the practical channel estimation technique affects the performance of the system. Since channel estimation error exists, it will obviously result in performance loss and this loss is estimated to 4dB for a 2 transmitters 2 receiver STBC-MC-CDMA system, 3-4dB for a 2 transmitters 1 receiver MC-CDMA system. On the other hand, the loss is only 2-3dB for MC-CDMA system. It can be also seen that the BER performance of STBC MC-CDMA system with two receivers will achieve much better performance regardless of whether channel state information is through estimated or perfectly known, and the BER performance of STBC MC-CDMA system shows a bit better than that of MC-CDMA system. In our system, there is only a slight loss in the BER performance by Zero-Forcing detection compared to that by MMSE detection and the curves overlapped and are not presented.

Fig. 6.6 shows the BER performance versus NFR when $L=32$, $K=10$, $N=100$, $\mathrm{SNR}=10$ and $G=5$. It can be seen that the near far problems has only a slight effect on the BER performance both for estimated channel or true channel when either MMSE (or ZF) detection is used.

Fig. 6.7 presents the BER performance versus the number of users K when $L=32$, $N=100$, $\mathrm{SNR}=10$, $\mathrm{NFR}=0$ and $G=5$. It can be observed that the BER performance degrades gradually as the number of users K increases. And the BER performance of STBC MC-CDMA system degrades quicker than that of MC-CDMA system when the number of users increases.

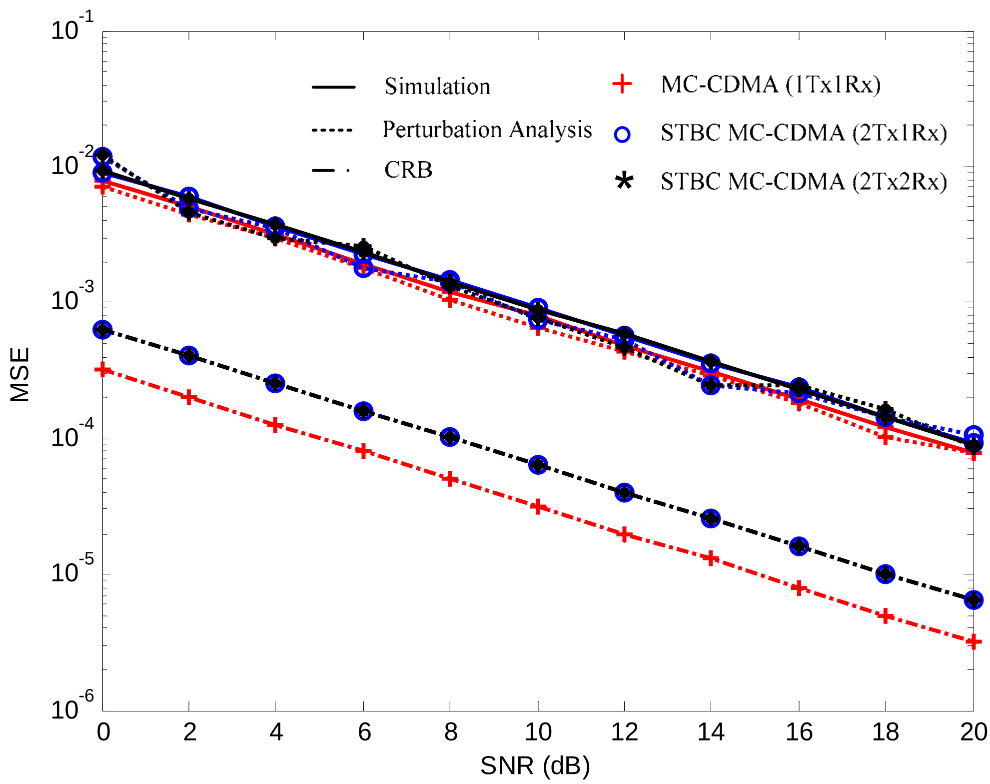

Fig. 6.2 MSE of Channel Estimation versus SNR

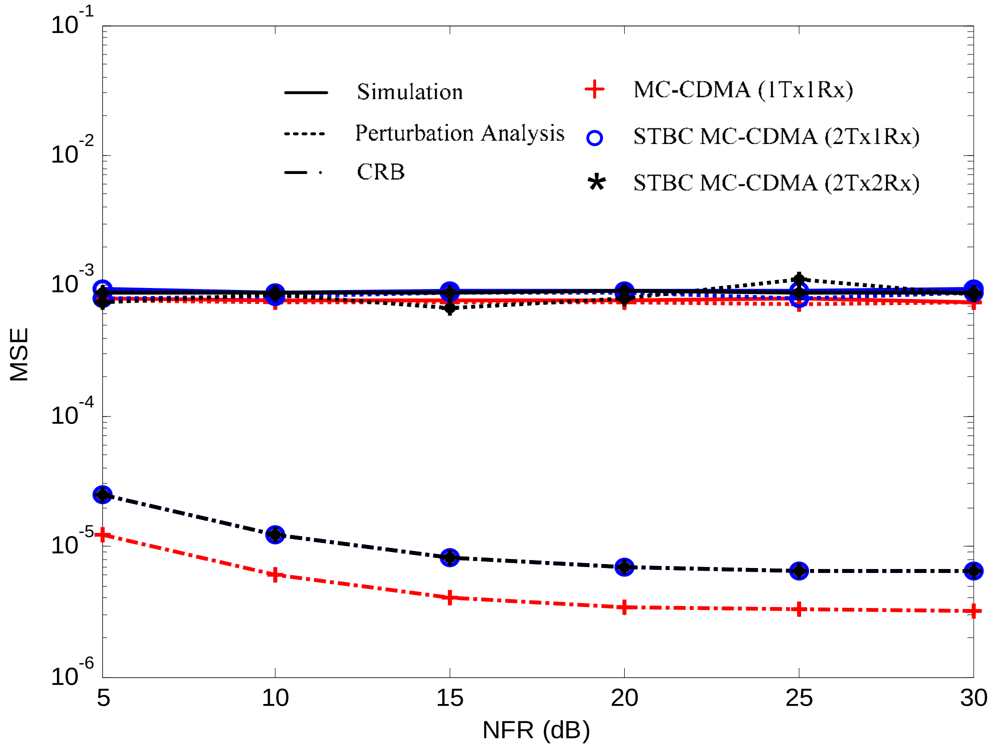

Fig. 6.3 MSE of Channel Estimation versus NFR

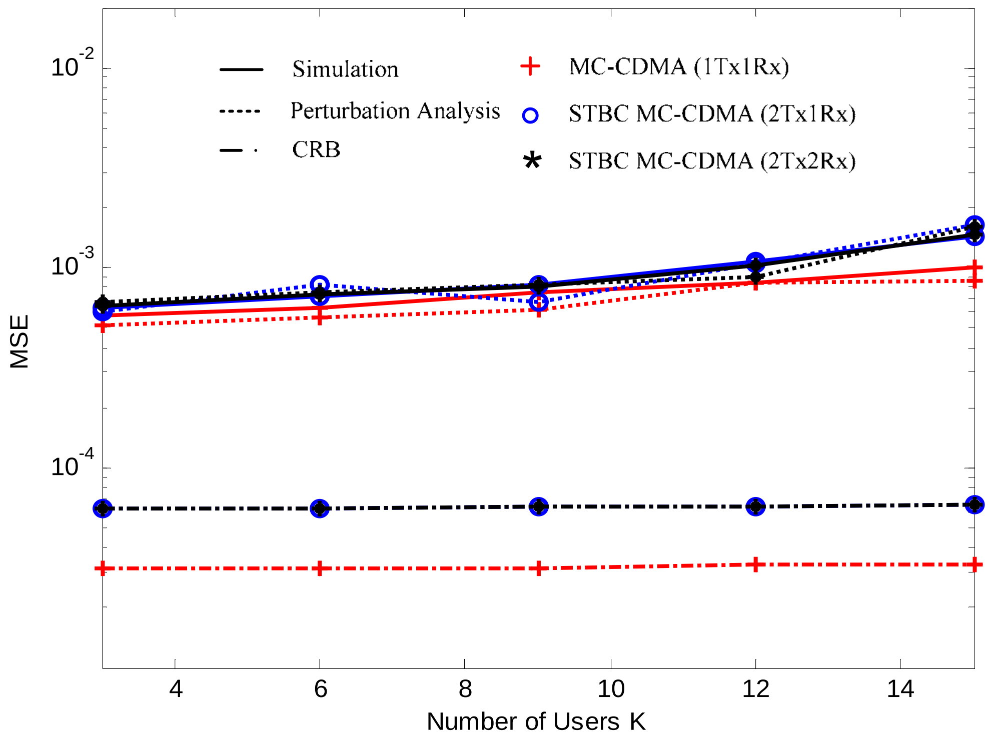

Fig. 6.4 MSE of Channel Estimation versus the Number of Users *K*

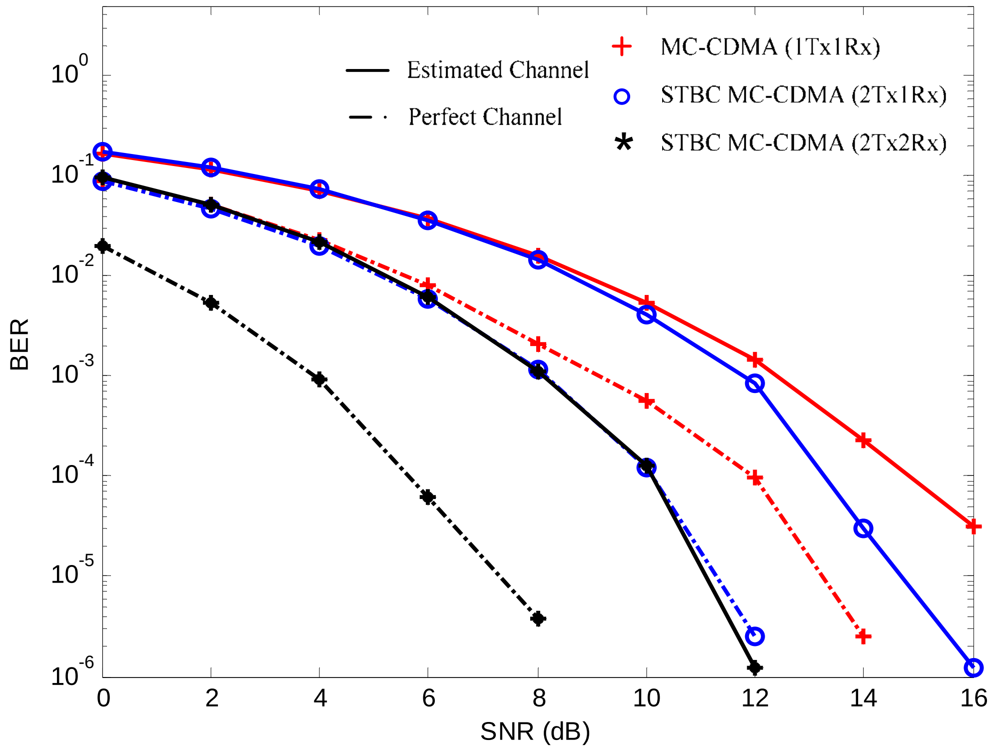

Fig. 6.5 BER Performance versus SNR

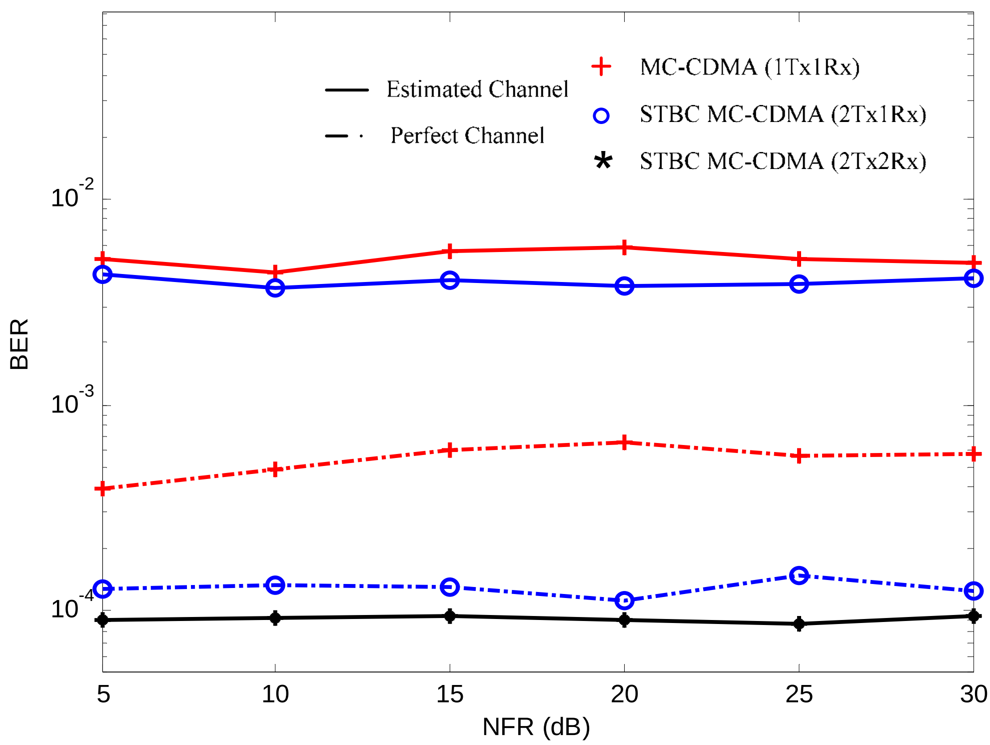

Fig. 6.6 BER versus NFR

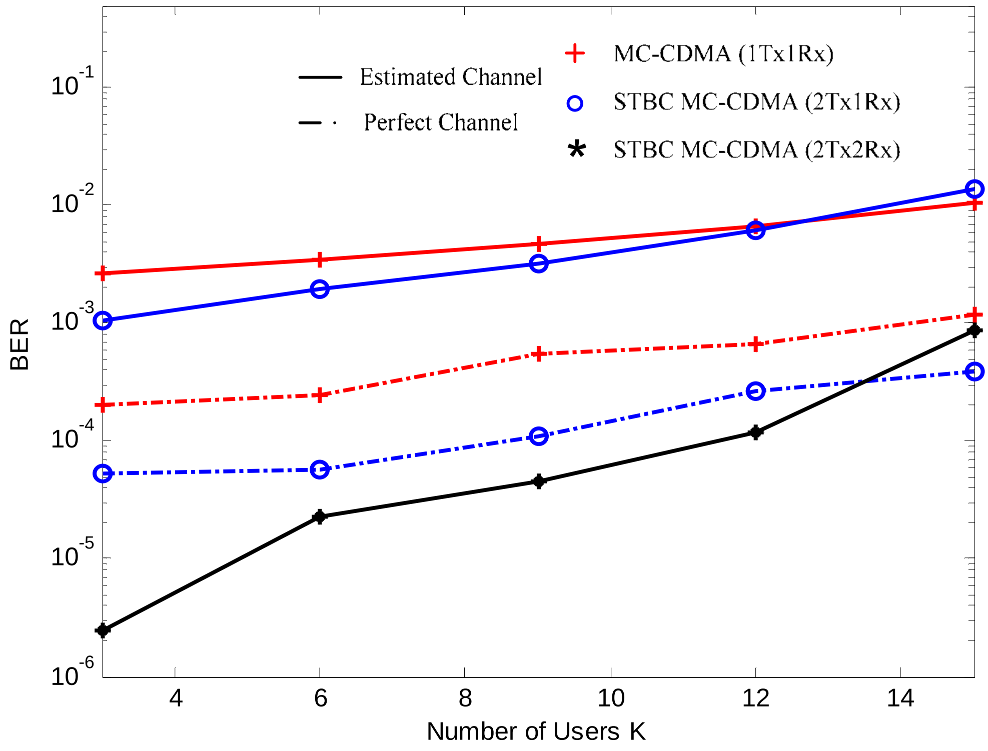

Fig. 6.7 BER versus Number of users *K*

6.7 Conclusion

In this chapter, a semi-blind channel estimation and multiuser detection for uplink space-time block coded (STBC) multicarrier (MC-) CDMA system are studied. Subspace-based technique decouples the multiuser and MIMO channel estimation to a series of single user and SISO estimation problems. To resolve the inherent scalar ambiguity existing in all the second-order statistic blind estimation, a training symbol is introduced to obtain this scalar. Using small perturbation analysis, the approximate expression of the covariance matrix of the channel estimation error is derived. The Cramér-Rao bound (CRB) is also calculated to compare the channel estimation accuracy, and is proved that the estimation algorithm is statistically efficient at practical SNR values. Simulation results show that the proposed channel estimation algorithm is effective and robust, and with the resistance to the near far problems, multipath fading and number of users. The estimated channel state information is used to examine the BER performance of ZF and MMSE detectors. The implementation loss in system BER performance as a result of imperfect channel estimation is generally 4dB and 3-4 dB for two receivers and one receiver STBC MC-CDMA system, respectively. It can be concluded that the STBC MC-CDMA system with multiple receivers will obtain much better system performance.

Appendix 6.A

In this appendix, we calculate each element of the matrix $\mathcal{J}(\underline{\boldsymbol{\theta}})$ in (6.59), and the simplification of computing the inverse of the $\mathcal{J}(\underline{\boldsymbol{\theta}})$ is also presented.

Firstly, we rewritten the channel information matrix from the *k*th user at the *j*th receive antenna as

$$\mathbf{D}_{k,j} = \begin{bmatrix} \mathcal{D}(\underline{\mathbf{c}}_{k,1})\overline{\mathbf{V}}^T \underline{\boldsymbol{\beta}}_{k,j,1} & \mathcal{D}(\underline{\mathbf{c}}_{k,2})\overline{\mathbf{V}}^T \underline{\mathbf{c}}_{k,2}\underline{\boldsymbol{\beta}}_{k,j,2} \\ \mathcal{D}(\underline{\mathbf{c}}_{k,2})^* \overline{\mathbf{V}}^{\mathcal{H}} \underline{\boldsymbol{\beta}}^*_{k,j,2} & -\mathcal{D}(\underline{\mathbf{c}}_{k,1})^* \overline{\mathbf{V}}^{\mathcal{H}} \underline{\boldsymbol{\beta}}^*_{k,j,1} \end{bmatrix}. \tag{6.A.1}$$

Let

$$\underline{\boldsymbol{\beta}}_{k,j,re} = \begin{bmatrix} \underline{\boldsymbol{\beta}}^T_{k,j,1,re} & \underline{\boldsymbol{\beta}}^T_{k,j,2,re} \end{bmatrix}^T, \tag{6.A.2a}$$

$$\underline{\boldsymbol{\beta}}_{k,j,im} = \begin{bmatrix} \underline{\boldsymbol{\beta}}^T_{k,j,1,im} & \underline{\boldsymbol{\beta}}^T_{k,j,2,im} \end{bmatrix}^T. \tag{6.A.2b}$$

where $\underline{\boldsymbol{\beta}}_{k,j,i,re} = \mathrm{Re}[\underline{\boldsymbol{\beta}}_{k,j,i}]$ and $\underline{\boldsymbol{\beta}}_{k,j,i,im} = \mathrm{Im}[\underline{\boldsymbol{\beta}}_{k,j,i}]$ (i = 1,2). Taking the partial differential of $f(\underline{\boldsymbol{\theta}})$ in (6.58) with respect to the unknown channel impulse response, we obtain

$$\frac{\partial f(\underline{\boldsymbol{\theta}})}{\partial \underline{\boldsymbol{\beta}}_{k,j,1,re}} = \frac{\sqrt{2}}{V\sigma_\eta^2} \sum_{n=0}^{N-1} \mathrm{Re}\left[\mathbf{T}_{k,1}(n)\underline{\boldsymbol{\eta}}(n)\right], \tag{6.A.3}$$

where $\mathbf{T}_{k,1}(n) = \left[s_k^*(2n)\overline{\mathbf{V}}^*\mathcal{D}(\underline{\mathbf{c}}_{k,1}) \quad -s_k^*(2n+1)\overline{\mathbf{V}}\mathcal{D}(\underline{\mathbf{c}}_{k,1})\right]$;

$$\frac{\partial f(\underline{\boldsymbol{\theta}})}{\partial \underline{\boldsymbol{\beta}}_{k,j,1,im}} = \frac{\sqrt{2}}{V\sigma_\eta^2} \sum_{n=0}^{N-1} \mathrm{Im}\left[\mathbf{T}_{k,2}(n)\underline{\boldsymbol{\eta}}(n)\right], \tag{6.A.4}$$

where $\mathbf{T}_{k,2}(n) = \left[s_k^*(2n)\overline{\mathbf{V}}^*\mathcal{D}(\underline{\mathbf{c}}_{k,1}) \quad s_k^*(2n+1)\overline{\mathbf{V}}\mathcal{D}(\underline{\mathbf{c}}_{k,1})\right]$;

$$\frac{\partial f(\underline{\boldsymbol{\theta}})}{\partial \underline{\boldsymbol{\beta}}_{k,j,2,re}} = \frac{\sqrt{2}}{V\sigma_\eta^2} \sum_{n=0}^{N-1} \mathrm{Re}\left[\mathbf{T}_{k,3}(n)\underline{\boldsymbol{\eta}}(n)\right], \tag{6.A.5}$$

where $\mathbf{T}_{k,3}(n) = \left[s_k^*(2n+1)\overline{\mathbf{V}}^* \mathcal{D}(\underline{\mathbf{c}}_{k,2}) \quad s_k^*(2n)\overline{\mathbf{V}}\mathcal{D}(\underline{\mathbf{c}}_{k,2}) \right]$;

$$\frac{\partial f(\underline{\boldsymbol{\theta}})}{\partial \underline{\boldsymbol{\beta}}_{k,j,2,im}} = \frac{\sqrt{2}}{V\sigma_\eta^2} \sum_{n=0}^{N-1} \mathrm{Im}\left[\mathbf{T}_{k,4}(n)\underline{\boldsymbol{\eta}}(n) \right], \tag{6.A.6}$$

where $\mathbf{T}_{k,4}(n) = \left[s_k^*(2n+1)\overline{\mathbf{V}}^* \mathcal{D}(\underline{\mathbf{c}}_{k,2}) \quad -s_k^*(2n)\overline{\mathbf{V}}\mathcal{D}(\underline{\mathbf{c}}_{k,2}) \right]$.

Thus

$$\frac{\partial f(\underline{\boldsymbol{\theta}})}{\partial \underline{\boldsymbol{\beta}}_{k,j,re}} = \begin{bmatrix} \dfrac{\partial f(\underline{\boldsymbol{\theta}})}{\partial \underline{\boldsymbol{\beta}}_{k,j,1,re}} \\ \dfrac{\partial f(\underline{\boldsymbol{\theta}})}{\partial \underline{\boldsymbol{\beta}}_{k,j,2,re}} \end{bmatrix} = \frac{\sqrt{2}}{V\sigma_\eta^2} \sum_{n=0}^{N-1} \mathrm{Re}\Big[\underbrace{\begin{pmatrix} \mathbf{T}_{k,1}(n) \\ \mathbf{T}_{k,3}(n) \end{pmatrix}}_{\overline{\mathbf{T}}_k(n)} \underline{\boldsymbol{\eta}}(n) \Big] = \frac{\sqrt{2}}{V\sigma_\eta^2} \sum_{n=0}^{N-1} \mathrm{Re}\left[\overline{\mathbf{T}}_k(n)\underline{\boldsymbol{\eta}}(n) \right], \tag{6.A.7}$$

$$\frac{\partial f(\underline{\boldsymbol{\theta}})}{\partial \underline{\boldsymbol{\beta}}_{k,j,im}} = \begin{bmatrix} \dfrac{\partial f(\underline{\boldsymbol{\theta}})}{\partial \underline{\boldsymbol{\beta}}_{k,j,1,im}} \\ \dfrac{\partial f(\underline{\boldsymbol{\theta}})}{\partial \underline{\boldsymbol{\beta}}_{k,j,2,im}} \end{bmatrix} = \frac{\sqrt{2}}{V\sigma_\eta^2} \sum_{n=0}^{N-1} \mathrm{Im}\Big[\underbrace{\begin{pmatrix} \mathbf{T}_{k,2}(n) \\ \mathbf{T}_{k,4}(n) \end{pmatrix}}_{\tilde{\mathbf{T}}_k(n)} \underline{\boldsymbol{\eta}}(n) \Big] = \frac{\sqrt{2}}{V\sigma_\eta^2} \sum_{n=0}^{N-1} \mathrm{Im}\left[\tilde{\mathbf{T}}_k(n)\underline{\boldsymbol{\eta}}(n) \right]. \tag{6.A.8}$$

Then, the partial differentials of $f(\underline{\boldsymbol{\theta}})$ with respect to $\underline{\boldsymbol{\beta}}_{j,re}$ and $\underline{\boldsymbol{\beta}}_{j,im}$ are given by

$$\frac{\partial f(\underline{\boldsymbol{\theta}})}{\partial \underline{\boldsymbol{\beta}}_{j,re}} = \frac{\sqrt{2}}{V\sigma_\eta^2} \sum_{n=0}^{N-1} \mathrm{Re}\left[\overline{\mathbf{T}}(n)\underline{\boldsymbol{\eta}}(n) \right], \tag{6.A.9}$$

where $\overline{\mathbf{T}}(n) = \left[\overline{\mathbf{T}}_1^T(n) \quad \overline{\mathbf{T}}_2^T(n) \quad \cdots \quad \overline{\mathbf{T}}_K^T(n) \right]^T$;

$$\frac{\partial f(\underline{\boldsymbol{\theta}})}{\partial \underline{\boldsymbol{\beta}}_{j,im}} = \frac{\sqrt{2}}{V\sigma_\eta^2} \sum_{n=0}^{N-1} \mathrm{Im}\left[\tilde{\mathbf{T}}(n)\underline{\boldsymbol{\eta}}(n) \right], \tag{6.A.10}$$

where $\tilde{\mathbf{T}}(n) = \left[\tilde{\mathbf{T}}_1^T(n) \quad \tilde{\mathbf{T}}_2^T(n) \quad \cdots \quad \tilde{\mathbf{T}}_K^T(n) \right]^T$.

Taking the partial differential of $f(\underline{\boldsymbol{\theta}})$ in (58) with respect to the other unknown parameters, we obtain

$$\frac{\partial f(\underline{\boldsymbol{\theta}})}{\partial \underline{\mathbf{s}}_{re}(n)} = \frac{\sqrt{2}}{V\sigma_\eta^2} \mathrm{Re}\left[\mathbf{D}_j^{\mathcal{H}} \underline{\boldsymbol{\eta}}(n) \right], \tag{6.A.11}$$

$$\frac{\partial f(\underline{\boldsymbol{\theta}})}{\partial \underline{\mathbf{s}}_{im}(n)} = \frac{\sqrt{2}}{V\sigma_\eta^2}\mathrm{Im}\left[\mathbf{D}_j^{\mathcal{H}}\,\underline{\boldsymbol{\eta}}(n)\right]. \tag{6.A.12}$$

Since the noise $\underline{\boldsymbol{\eta}}(n)$ is i.i.d zero mean, complex Gaussian random variables uncorrelated with the symbol sequence $\underline{\mathbf{s}}(n)$ and channel vector $\underline{\boldsymbol{\beta}}_j$, we have

$$E\left\{\frac{\partial f(\underline{\boldsymbol{\theta}})}{\partial \underline{\boldsymbol{\beta}}_{j,re}}\left(\frac{\partial f(\underline{\boldsymbol{\theta}})}{\partial \underline{\boldsymbol{\beta}}_{j,re}}\right)^T\right\} = \frac{1}{V\sigma_\eta^2}\sum_{n=0}^{N-1}\mathrm{Re}\left[\overline{\mathbf{T}}(n)\overline{\mathbf{T}}^{\mathcal{H}}(n)\right], \tag{6.A.13}$$

$$E\left\{\frac{\partial f(\underline{\boldsymbol{\theta}})}{\partial \underline{\boldsymbol{\beta}}_{j,re}}\left(\frac{\partial f(\underline{\boldsymbol{\theta}})}{\partial \underline{\boldsymbol{\beta}}_{j,im}}\right)^T\right\} = -\frac{1}{V\sigma_\eta^2}\sum_{n=0}^{N-1}\mathrm{Im}\left[\overline{\mathbf{T}}(n)\tilde{\mathbf{T}}^{\mathcal{H}}(n)\right], \tag{6.A.14}$$

$$E\left\{\frac{\partial f(\underline{\boldsymbol{\theta}})}{\partial \underline{\boldsymbol{\beta}}_{j,re}}\left(\frac{\partial f(\underline{\boldsymbol{\theta}})}{\partial \underline{\mathbf{s}}_{re}(n)}\right)^T\right\} = \frac{1}{V\sigma_\eta^2}\mathrm{Re}\left[\overline{\mathbf{T}}(n)\mathbf{D}_j\right], \tag{6.A.15}$$

$$E\left\{\frac{\partial f(\underline{\boldsymbol{\theta}})}{\partial \underline{\boldsymbol{\beta}}_{j,re}}\left(\frac{\partial f(\underline{\boldsymbol{\theta}})}{\partial \underline{\mathbf{s}}_{im}(n)}\right)^T\right\} = -\frac{1}{V\sigma_\eta^2}\mathrm{Im}\left[\overline{\mathbf{T}}(n)\mathbf{D}_j\right], \tag{6.A.16}$$

$$E\left\{\frac{\partial f(\underline{\boldsymbol{\theta}})}{\partial \underline{\boldsymbol{\beta}}_{j,im}}\left(\frac{\partial f(\underline{\boldsymbol{\theta}})}{\partial \underline{\boldsymbol{\beta}}_{j,im}}\right)^T\right\} = \frac{1}{V\sigma_\eta^2}\sum_{n=0}^{N-1}\mathrm{Im}\left[\tilde{\mathbf{T}}(n)\tilde{\mathbf{T}}^{\mathcal{H}}(n)\right], \tag{6.A.17}$$

$$E\left\{\frac{\partial f(\underline{\boldsymbol{\theta}})}{\partial \underline{\boldsymbol{\beta}}_{j,im}}\left(\frac{\partial f(\underline{\boldsymbol{\theta}})}{\partial \underline{\mathbf{s}}_{re}}\right)^T\right\} = \frac{1}{V\sigma_\eta^2}\mathrm{Im}\left[\tilde{\mathbf{T}}(n)\mathbf{D}_j\right], \tag{6.A.18}$$

$$E\left\{\frac{\partial f(\underline{\boldsymbol{\theta}})}{\partial \underline{\boldsymbol{\beta}}_{j,im}}\left(\frac{\partial f(\underline{\boldsymbol{\theta}})}{\partial \underline{\mathbf{s}}_{im}}\right)^T\right\} = \frac{1}{V\sigma_\eta^2}\mathrm{Re}\left[\tilde{\mathbf{T}}(n)\mathbf{D}_j\right], \tag{6.A.19}$$

$$E\left\{\frac{\partial f(\underline{\boldsymbol{\theta}})}{\partial \underline{\mathbf{s}}_{re}(n)}\left(\frac{\partial f(\underline{\boldsymbol{\theta}})}{\partial \underline{\mathbf{s}}_{re}(m)}\right)^T\right\} = \frac{1}{V\sigma_\eta^2}\mathrm{Re}\left[\mathbf{D}_j^{\mathcal{H}}\mathbf{D}_j\right]\delta(n-m), \tag{6.A.20}$$

$$E\left\{\frac{\partial f(\underline{\boldsymbol{\theta}})}{\partial \underline{\mathbf{s}}_{re}(n)}\left(\frac{\partial f(\underline{\boldsymbol{\theta}})}{\partial \underline{\mathbf{s}}_{im}(m)}\right)^T\right\} = -\frac{1}{V\sigma_\eta^2}\mathrm{Im}\left[\mathbf{D}_j^{\mathcal{H}}\mathbf{D}_j\right]\delta(n-m), \tag{6.A.21}$$

$$E\left\{\frac{\partial f(\underline{\boldsymbol{\theta}})}{\partial \underline{\mathbf{s}}_{im}(n)}\left(\frac{\partial f(\underline{\boldsymbol{\theta}})}{\partial \underline{\mathbf{s}}_{im}(m)}\right)^T\right\} = \frac{1}{V\sigma_\eta^2}\mathrm{Re}\left[\mathbf{D}_j^{\mathcal{H}}\mathbf{D}_j\right]\delta(n-m) \ . \tag{6.A.22}$$

The equivalent FIM defined in (6.59) can be expressed as the form

$$\mathcal{J} = \left(\begin{array}{c|c} \mathcal{J}_1 & \mathcal{J}_2 \\ \hline \mathcal{J}_4 & \mathcal{J}_3 \end{array}\right) = \left(\begin{array}{c|cc} \mathcal{J}_1 & \mathcal{J}_{2A} & \mathcal{J}_{2B} \\ \hline \mathcal{J}_{4A} & \mathcal{J}_{3a} & \mathcal{J}_{3b} \\ \mathcal{J}_{4B} & \mathcal{J}_{3b} & \mathcal{J}_{3a} \end{array}\right) = \left(\begin{array}{cc|cc} \mathcal{J}_{1a} & \mathcal{J}_{1b} & \mathcal{J}_{2a} & \mathcal{J}_{2b} \\ -\mathcal{J}_{1b}^T & \mathcal{J}_{1c} & \mathcal{J}_{2c} & \mathcal{J}_{2d} \\ \hline \mathcal{J}_{2a}^T & -\mathcal{J}_{2c}^T & \mathcal{J}_{3a} & \mathcal{J}_{3b} \\ -\mathcal{J}_{2b}^T & \mathcal{J}_{2d}^T & \mathcal{J}_{3b} & \mathcal{J}_{3a} \end{array}\right) \tag{6.A.23}$$

where the blocks have the following dimensions: $\mathcal{J}_{1a}$, $\mathcal{J}_{1b}$ and $\mathcal{J}_{1c}$ are $2K(G+1)\times 2K(G+1)$, $\mathcal{J}_{2a}$, $\mathcal{J}_{2b}$, $\mathcal{J}_{2c}$ and $\mathcal{J}_{2d}$ are $2K(G+1)\times 2KN$, $\mathcal{J}_{3a}$ and $\mathcal{J}_{3b}$ are $2KN\times 2KN$, with the elements defined in (6.A.13)-(6.A.22). The CRB bound of the covariance matrix of channel estimation error is given by the $4K(G+1)\times 4K(G+1)$ upper left block of $\mathcal{J}^{-1}$, i.e.,

$$\mathrm{CRB}(\underline{\boldsymbol{\beta}}_j) = \left(\mathcal{J}_1 - \mathcal{J}_2\mathcal{J}_3^{-1}\mathcal{J}_4\right)^{-1}. \tag{6.A.24}$$

However, directly computing the inverse of matrix in (6.A.12) is intensive complexity. In the following, a simplification of computing the inverse of $\mathcal{J}(\underline{\boldsymbol{\theta}})$ is proposed.

By the calculations in (6.A.20)-(6.A.22), the matrix $\mathcal{J}_{3a}$ and $\mathcal{J}_{3b}$ have the following form

$$\mathcal{J}_{3a} = \mathbf{I}_N \otimes \bar{\mathcal{J}}_{3a} \,, \tag{6.A.25a}$$

$$\mathcal{J}_{3b} = \mathbf{I}_N \otimes \bar{\mathcal{J}}_{3b} \tag{6.A.25b}$$

where $\bar{\mathcal{J}}_{3a}$ and $\bar{\mathcal{J}}_{3b}$ is $2K\times 2K$ matrix. Thus, the inverse of $\mathcal{J}_3$ can be easily obtained

$$\mathcal{J}_3^{-1} = \begin{pmatrix} \mathbf{I}_N \otimes \tilde{\mathcal{J}}_{3a} & \mathbf{I}_N \otimes \tilde{\mathcal{J}}_{3b} \\ \mathbf{I}_N \otimes \tilde{\mathcal{J}}_{3b} & \mathbf{I}_N \otimes \tilde{\mathcal{J}}_{3a} \end{pmatrix} \tag{6.A.26}$$

where $\tilde{\mathcal{J}}_{3a}$ and $\tilde{\mathcal{J}}_{3b}$ with its element

$$\tilde{\mathcal{J}}_{3a} = \left(\bar{\mathcal{J}}_{3a} - \bar{\mathcal{J}}_{3b}\bar{\mathcal{J}}_{3a}^{-1}\bar{\mathcal{J}}_{3b}\right)^{-1}, \tag{6.A.27a}$$

$$\tilde{\mathcal{J}}_{3b} = -\bar{\mathcal{J}}_{3a}^{-1}\bar{\mathcal{J}}_{3b}\tilde{\mathcal{J}}_{3a}, \tag{6.A.27b}$$

Denote $\mathcal{J}_{2A} = \left[\mathcal{J}_{2A}(0) \quad \mathcal{J}_{2A}(1) \quad \cdots \quad \mathcal{J}_{2A}(N-1)\right]$, $\mathcal{J}_{2B} = \left[\mathcal{J}_{2B}(0) \quad \mathcal{J}_{2B}(1) \quad \cdots \quad \mathcal{J}_{2B}(N-1)\right]$, $\mathcal{J}_{4A} = \left[\mathcal{J}_{4A}^T(0) \quad \mathcal{J}_{4A}^T(1) \quad \cdots \quad \mathcal{J}_{4A}^T(N-1)\right]^T$, and $\mathcal{J}_{4B} = \left[\mathcal{J}_{4B}^T(0) \quad \mathcal{J}_{4B}^T(1) \quad \cdots \quad \mathcal{J}_{4B}^T(N-1)\right]^T$, where $\mathcal{J}_{2A}(n)$ and $\mathcal{J}_{2B}(n)$ ($n = 0,1,\cdots,N-1$) are $4K(G+1)\times 2K$, $\mathcal{J}_{4A}(n)$ and $\mathcal{J}_{4B}(n)$ ($n = 0,1,\cdots,N-1$) are $2K\times 4K(G+1)$ matrix. Substitute (6.A.26) in (6.A.24), then the CRB of the estimated channel covariance matrix of can be simplified as

$$\begin{aligned}\mathrm{CRB}(\underline{\boldsymbol{\beta}}_j) = \Big(\mathcal{J}_1 - \sum_{n=0}^{N-1}\mathcal{J}_{2A}(n)\tilde{\mathcal{J}}_{3a}\mathcal{J}_{4A}(n) + \mathcal{J}_{2B}(n)\tilde{\mathcal{J}}_{3b}\mathcal{J}_{4A}(n)\\ + \mathcal{J}_{2A}(n)\tilde{\mathcal{J}}_{3b}\mathcal{J}_{4B}(n) + \mathcal{J}_{2B}(n)\tilde{\mathcal{J}}_{3a}\mathcal{J}_{4A}(n)\Big)^{-1}.\end{aligned} \tag{6.A.28}$$

Chapter 7

Conclusion

Next generation wireless mobile communication systems need to support high data rate and multimedia services with different QoS requirement. This thesis looks into the performance and capacity of STBC MC-CDMA systems, and investigates some receiver design and implementation issues of STBC MC-CDMA systems.

The thesis begins with the theoretical performance and capacity analysis of the STBC MC-CDMA system. Firstly, the BER performance and system capacity (bandwidth efficiency) for STBC MC-CDMA system in the presence of carrier frequency offset between the transmitter and receiver oscillators were studied. The exact BER expression when using EGC and the approximate BER expression when using MRC are derived. These BER expressions are verified through simulations. Using these derived expressions, the achievable system capacity satisfying a minimum BER requirement can be studied for the two cases when EGC and MRC are used, and hence possible to compare the achievable capacity of STBC MC-CDMA systems with that of MC-CDMA systems. It is concluded that small CFO has insignificant effect on the BER and capacity of STBC MC-CDMA systems, and this range of CFO is important in transceiver design. Besides, STBC MC-CDMA systems with multiple receive antennas can achieve higher capacity than that of the MC-CDMA systems, and this amount can be obtained analytically using the theoretical BER expressions derived.

Then, the BER performance and system capacity of three multirate access schemes (multicode, VSG, MSR access schemes) for STBC MC-CDMA system are studied. Transmit power control is adjusted according to the service rates and the number of active users in each service class to maintain the link quality and to improve the system capacity. The multiple access interferences and hence the BER performance and system capacities of the three multirate access schemes for STBC MC-CDMA systems are studied. From the numerical results obtained, it can be concluded that the systems with mc access scheme when orthogonal Gold spreading sequence is applied and the VSG access scheme have similar system performance and capacity, and both perform better than the system with MSR access scheme for any spectrum configurations. In case when non-orthogonal Gold sequences are used, mc access scheme shows a degrading in the system capacity as compared to VSG, due to the presence of larger self-interference (SI) among the sequences used by each user.

The thesis next focuses on some studies on receiver designs and implementations for STBC MC-CDMA. First, the development of a timing and frequency synchronization algorithm is made. The subspace-based joint timing and frequency synchronization algorithm is proposed. Through properly choosing the oversampling factor and the number of received samples, the joint timing and frequency synchronization are resolved using the subspace approach. Besides, the use of subspace approach allows that multiuser estimations can be decoupled and hence makes it computational efficient in multiuser environment. Using small perturbation analysis, the approximate MSE of the proposed algorithm is derived, which can be used to quantify the resilience of the proposed algorithm to additive white Gaussian noise. The CRB is also evaluated to illustrate. Simulation results show the robustness and effectiveness of the proposed synchronization algorithm in the presence of near-far problems, multipath fading and Doppler Effect. The theoretical perturbation analysis also shows good agreement with the simulation results. Finally, the computed CRB is shown to be a good lower bound.

When the timing and frequency synchronization is completed at the base station, synchronous transmission in the uplink can be achieved. At the base station, channel estimation and multiuser detection are then performed to recover the data from all users. The subspace-based semi-blind channel estimation and multiuser detection are proposed. The method assumes that the channel is finite impulse response (FIR) and time-invariant, and the channel order is assumed to be known at the receiver. Using small perturbation analysis, the approximate expression of the covariance matrix of the channel estimation error is derived, which can be used to quantify the resilience of the estimation algorithm to AWGN. The CRB is also calculated to compare the channel estimation accuracy, and is proved that the estimation algorithm is statistically efficient at practical SNR values. Simulation results show the robustness and effectiveness of the estimation algorithm in the presence of near-far problems, multipath fading and large number of users. The theoretical perturbation analysis shows the good agreement with the simulation results and computed CRB is shown to be a good lower bound. Finally BER performances of STBC MC-CDMA system when using ZF and MMSE multiuser detection techniques using the estimated channel gain are obtained through simulations.

References

[1] T. S. Rappaport, *Wireless communications: Principles and Practice*, Prentice Hall, 1996.

[2] W.C.Y. Lee, *Mobile Communications Engineering, Theory and Applications.* New York, McGraw-Hill, 2nd edn, 1997.

[3] D.J. Goodman, "Cellular packet communications". *IEEE Transactions on Communications,* vol. 38, pp. 1272-1280, Aug 1990.

[4] J. Rapeli, "UMTS: Targets, system concept, and standardization in a global framework", *IEEE Personal Communications*, vol. 2, pp. 20-28, Feb. 1995.

[5] M. Callendar, "Future public land mobile telecommunication systems", *IEEE Personal Communications*, vol. 12, no. 4, pp. 18-22, 1994.

[6] A. Viterbi, *CDMA: Principles of Spread Spectrum Communication.* Addison-Wesley, June 1995.

[7] S. Glisic and B. Vuvetic, *Spread Spectrum CDMA Systems for Wireless Communications*. Artech House, April 1997.

[8] J. E. Padgett, C. G. Gunther, T. Hattori, "Overview of wireless personal communications," *IEEE Communications Magazine,* pp. 28-41, Jan. 1995.

[9] *The 3GPP Website*: http://www.3gpp.org

[10] *The 3GPP2 Website*: http://www.3gpp2.org

[11] R.W. Chang, "Synthesis of band-limited orthogonals for multi-channel data transmission", *Bell Labs Technical Journals*, no. 45, pp. 1775-1796, Dec, 1966.

[12] R.W. Chang and R.A. Gibby, “A theoretical study of performance of an orthogonal multiplexing data transmisson scheme”, *IEEE Transactions on Communications*, vol. 16, pp. 529-540, Aug. 1968.

[13] B.R. Saltzberg, “Performance of anefficient parallel data transmission system”, *IEEE Transactions on Communications*, vol 15, pp. 805-811, Dec. 1967.

[14] S.B. Weinstein and P.M. Ebert, “Data transmission by frequency-division multiplexing using the discrete Fourier transform”, *IEEE Transactions on. Communications,* vol. 19, pp. 628-634, Oct. 1971

[15] M. Alard. and R. Lassalle, “Principles of modulation and channel coding for digital broadcasting for mobile receivers”, *European Broadcast Union Review,* no. 224, pp. 47-69, Aug. 1987.

[16] J.A.C. Bingham, “Multicarrier modulation for data transmission: an idea start of the 21st century”, *IEEE Communications Magazine,* vol. 39, pp. 110-116, Jan. 2001.

[17] A. Chouly, A. Brajal and S. Jourdan, “Orthogonal multicarrier techiques applied to direct sequence spread spectrum CDMA systems”, *IEEE Global Telecommunications Conference (GLOBECOM’93)*, Houston, USA, pp. 1723-1728, Dec, 1993

[18] V. Dasilva and E.S. Sousa, “Performance of orthogonal CDMA codes for quasi-synchronous communication systems”, *IEEE International Conference on Universal Personal Communications (ICUPC’93)*, Ottawa, Canada, pp. 995-999, Oct. 1993.

[19] K. Fazel, “Performance of CDMA/OFDM for mobile communications system”, *IEEE International Conference on Universal Personal Communications (ICUPC’93)*, Ottawa, Canada, pp. 975-979, Oct. 1993

[20] K. Fazel and L. Papke, "On the performance of convolutionally coded CDMA/OFDM for mobile communications system", *IEEE International Symposium on Personal, Indoor and Mobile Radio Communications (PIMRC'93)*, Yokohama, Japan, pp. 468-472, Sept. 1993

[21] S. Kondo and L.B. Milstein, "On the use of multicarrier direct sequence spread spectrum systems", *IEEE Military Communications Conference (MILCOM'93)*, Boston, USA, pp. 52-56, Oct. 1993

[22] N. Yee, J.P. Linnartz and G. Fettweis, "Multicarrier CDMA for indoor wireless radio networks", *IEEE International Symposium on Personal, Indoor and Mobile Radio Communications (PIMRC'93)*, Yokohama, Japan, pp. 109-113, Sept. 1993.

[23] J. Uddenfeldt, "Digital cellular – Its roots and its future," *Proceedings of the IEEE*, Vol. 86, pp. 1319-1324, Jul 1998.

[24] S. Hara, R. Prasad, "Overview of multi-carrier CDMA", *IEEE Communications Mag*azine, vol . 35, pp. 126-133, Dec. 1997.

[25] N. Yee, J.P.Linnartz, *Multi-Carrier CDMA in an Indoor Wireless Radio Channel*, Univ. of California at Berkeley, Berkeley, California 94720.

[26] M. Schilpp, W. Sauer-Greff, W. Rupprecht, E.Bogenfeld, "Influence of oscillator phase noise and clipping on OFDM for terrestrial broadcasting of digital HDTV", *IEEE International Conference on Communications (ICC'95)*, Seattle, USAm pp. 1678-1682, Jun. 1995.

[27] K. Fazel, S. Kaiser, *Multi-Carrier and Spread Spectrum Systems*, John wiley, New York, USA, 2003.

[28] L. Hanzo, M. Münster, B,J, Choi and T. Keller, *OFDM and MC-CDMA for Broadband Multi-user Communications, WLANs and Broadcasting*, John Wiley, New York, USA, 2003

[29] R.Prasad, *CDMA for Wireless Personal Communications*, Artech House Publishers, 1996

[30] R.A. Scholtlz, "The origins of spread spectrum communications", *IEEE Transactions on Communications*, vol. 30, no.5, pp. 822-854, 1982.

[31] S. Roy, j.R. Foerster, V.S. Somayazulu, and D.G. Leeper, "Ultrawideband radio design: The promising of high-speed, short-range wireless connectivity", *Proceesdings of the IEEE*, vol. 92, No. 2, Feb. 2004.

[32] R.S. Ahmad, Bahai and Bourton R.Saltzberg, *Multi-Carrier Digital Communications Theory and Applications of OFDM*, Kluwer Academic/Plenum Publishers, New York

[33] J. S. Lee and L. E. Miller, *CDMA Systems Engineering Handbook*, Artech House Publishers, 1998.

[34] S. B. Weinstein and P. M. Ebert, "Data transmission by frequency-division multiplexing using the discrete Fourier transform," *IEEE Transactions on Communications*, vol. COM-19, pp. 628-634, Oct. 1971.

[35] L. J. Cimini Jr., "Analysis and simulation of a digital mobile channel using orthogonal frequency division multiplexing," *IEEE Transactions on Communications*, Vol. 33, pp. 665-675, July 1985.

[36] J. A. C. Bingham, "Multicarrier modulation for data transmission: An idea whose time has come," *IEEE Communications Magazine,* vol. 28, pp. 5-14, May 1990.

[37] L. Vandendorpe, "Multitone Direct Sequence CDMA System in an Indoor Wireless Environment," *IEEE First Symposium of Communications and Vehicular Technology in the Benelux, Delft, The Netherlands,* pp 4.1.1-4.1.8, Oct. 1993.

[38] N. Seshadri and J.H. Winters, "Two schemes for improving the performance of frequency-division duplex (FDD) transmission systems using transmitter antenna diversity", *International Journal of Wireless Information Networks*, vol. 1, pp. 49-60, Jan. 1994.

[39] A. Wittneben, "A new bandwidth efficient transmit antenna modulation diversity scheme for linear digital modulation", in *IEEE International Conference on Communications (ICC'93)*, vol. 3, pp. 1630-1634, Geneva, Switzerland, 1993.

[40] A.J. Paulraj, C.B. Papadias, "Space-time processing for wireless communications", *IEEE Signal Processing Magazine* , vol 14, pp. 49 –83, Nov. 1997.

[41] G.J. Foschini and M.J. Gans, "On Limits of Wireless Communications in a Fading Enviroment when Using Multiple Antennas", *Wireless Personal Communications*, vol. 6, pp. 311-335, Mar. 1998.

[42] A.F. Naguib, N. Seshadri, A.R. Calderbank, "Increasing data rate over wireless channels", *IEEE Signal Processing Magazine*, vol 17, pp. 76 –92, May 2000.

[43] V. Tarokh, N. Seshadri, A.R. Calderbank, "Space-time codes for high data rate wireless communication: performance criterion and code construction", *IEEE Transactions on Information Theory* , vol 44, pp.744 –765. March 1998.

[44] S.M. Alamouti, "A simple transmit diversity technique for wireless communications", *IEEE Journal on Selected Areas in Communications*, vol 16, pp. 1451 –1458, Oct. 1998.

[45] A. Wittneben, “Base station modulation diversity for digital SIMULCAST,” in *IEEE Vehicular Technology Conference (VTC’93),* May 1993, pp. 505–511.

[46] N. Seshadri and J. H. Winters, “Two signaling schemes for improving the error performance of frequency-division-duplex (FDD) transmission systems using transmitter antenna diversity,” *International Journal of Wireless Information Networks,* vol. 1, no. 1, 1994.

[47] V. Tarokh, H. Jafarkhani, A.R. Calderbank, “Space-time block coding for wireless communications: Performance results”, *IEEE Journal on Select Area in Communications*, vol. 17, No. 3, pp. 451-460, Mar. 1999

[48] V. Tarokh, H. Jafarkhani, A.R. Calderbank, “Space-Time block codes from orthogonal designs”, *IEEE Transactions on Information Theory*, vol 45, pp. 1456-1467, July 1999.

[49] G. J. Foschini, Jr., “Layered space–time architecture for wireless communication in a fading environment when using multi-element antennas,” *Bell Labs Technical Journals,* pp. 41–59, Autumn 1996.

[50] P.W. Wolniansky, G.J. Foschini, G.D. Golden, and R.A. Valenzuela, “V-BLAST: An architecture for realizing very high data rates over the rich-scattering wireless channel.”, *International Symposium on Advanced Radio Technologies,* Boulder, USA, Sept. 1998.

[51] E. Telatar, “Capacity of multi-antenna Gaussian channels,” AT&T-Bell Laboratories, Internal Tech. Memo., June 1995

[52] C.E.W. Sundberg and N. Seshadri, “Digital cellular systems for North America”, *IEEE Global Telcommunications Conference (GLOBECOM’90)*, pp. 533-537, Dec. 1990.

[53] N. Balaban and J. Salz, "Dual diversity combining and equalization in digital cellular mobile radio", *IEEE Transactions on Vehicular Technology*, vol. 40, pp. 342-354, May. 1991.

[54] M. Engels, *Wireless OFDM Systems: How to make them work*, Boston, Kluwer Academic Publishers, 2002.

[55] R.V. Nee, R. Prasad, *OFDM for Wireless Multimedia Communications*, Boston, Artech House Publishers, 2000.

[56] J.R. Schott, *Matrix Analysis for Statistics*, John-Willey, New York, 1996

[57] X. Hu, Y.H. Chew, "Performance of space-time block coded MC-CDMA system over frequency selective fading channel using semi-blind channel estimation technique", *IEEE Wireless Communications and Networking Conference (WCNC'03),* vol. 1, pp. 414-419, Mar, 2003, USA.

[58] X. Cai. A.N. Akansu, "Multicarrier CDMA systems with transmit diversity", *IEEE Vehicular Technology Conference 2000 Fall (VTC'00 Fall)*, vol 6, pp. 2817 –2821, 2000.

[59] Z. Yang; B. Lu; X. Wang, "Bayesian Monte Carlo multiuser receiver for space-time coded multicarrier CDMA systems", *IEEE Journal on Selected Areas in Communications*, vol 19, Aug. 2001, pp.1625 –1637.

[60] P.L. Kafle, A.B. Sesay, "Iterative semi-blind space-time multiuser detection for MC-CDMA uplink system", *IEEE Vehicular Technology Conference 2002 Fall (VTC'02 Fall)*l, 2002.

[61] X. Gui, T.S. Ng, "Performance of asychrounous orthogonal multicarrier CDMA system in frequency selective fading channel", *IEEE Transactions on Communications*, vol. 47,pp.1084-1091, Jul. 1999

[62] L. Tomba and W.A. Krzymien, “Effect of carrier phase noise and frequency offset on the performance of multicarrer CDMA systems”, *IEEE Internatioanl Conference on Communications (ICC’96)*, pp.1513-1517, Dallas, TX, June, 1996

[63] J. Jang, K.B. Lee, “Effects of frequency offset on MC-CDMA system performance”, *IEEE Communications Letters*, vol. 3, pp.196-198, Jul. 1999.

[64] D. Kivanc and H. Liu, “Uplink performance of MC-CDMA in the presence of frequency offset”, *IEEE Vehicular Technology Conference (VTC’99)*, vol. 5, pp.2855-2859.

[65] T. Kim and K. Bang, etc, “Performance of an MC-CDMA system with frequency offsets in correlated fading”, *IEEE International Conference on Communications (ICC’00)*, vol. 2, pp.1095-1099.

[66] Q. Shi, M. Latva-aho, “Effect of frequency offset on the performance of asynchronous MC-CDMA systems in a correlated rayleigh fading channel”, *Info-Tech and Info-Net International Conference (ICII’*01), vol. 2, pp. 448-452, Nov. 2001.

[67] Z. Yang; B. Lu; X. Wang, “Bayesian Monte Carlo multiuser receiver for space-time coded multicarrier CDMA systems”, *IEEE Journal on Selected Areas in Communications*, vol 19, Aug. 2001, pp.1625 –1637.

[68] U.Mitra, “Comparison of maximum-likelihood-based detection for two multirate access schemes for CDMA signals”, *IEEE Transactions on Communications*, vol 47, Jan. 1999.

[69] R.Srinivasan, U.Mitra, R.L.Moses, “Design and analysis of receiver filters for multiple chip-rate DS-CDMA systems”, *IEEE Journal on Selected Areas in Communications*, vol 17, pp. 2096-2109, Dec, 1999.

[70] R.Mo, X.Hu, Y.H.Chew, “On the Design of Spectrally Overlaid CDMA Systems under a Practical Interference Environment”, *IEEE International Symposium on Personal, Indoor, and Mobile Radio Communications (PIMRC’03),* pp.661-665, Beijing, Sep. 2003.

[71] K.S.Lim, J.H.Lee, “Performance of multirate transmisstion schemes for a multicarrier DS/CDMA system”, *IEEE Vehicular Technology Conference (VTC’01*), vol 2, pp.767-771, Oct. 2001.

[72] Z.Wang, G.B.Giannakis, “Block precoding for MUI/ISI-resilient generalize multicarrier CDMA with multirate capabilities”, *IEEE Transactions on Communications*, vol 49, pp.2016-2027, Nov. 2001.

[73] Steendam, H.; Moeneclaey, M., “The effect of synchronisation errors on MC-CDMA performance”, *IEEE International Conference on Communications (ICC’99)*, vol. 3, pp. 1510-1514, June, 1999.

[74] X. Hu, Y.H. Chew, “On the Performance and Capacity of Asynchronous Space-Time Block Coded MC-CDMA System in the presence of Carrier Frequency Offset”, *IEEE Trans on Vehicular Technology*, vol. 53, pp. 1327-1340, Sept. 2004.

[75] X. Hu, Y.H. Chew, “Maximum likelihood multiuser timing synchronization scheme for asynchronous multirate multicarrier CDMA System”, to appear in Military Communications Conference *(MILCOM’04)*, USA, Nov, 2004.

[76] E. G. Ström, S. Parkvall, S. L. Miller, B. E. Ottersten, “Propagation Delay Estimation in asynchronous direct-seqeunce code-division multiple access systems”, *IEEE Transactions on Communications*, vol. 44, pp. 84-93, Jan. 1996.

[77] B.Chen, H.Wang, “Blind estimation of OFDM carrier frequency offset via oversampling”, *IEEE Transactions on Signal Processing*, vol. 52, pp. 2047-2057, July 2004.

[78] J.C. Lin, “Maximum-likelihood frame timing instant and frequency offset estimation for OFDM communication over a fast Rayleigh-fading channel”, *IEEE Transactions on Communications*, vol. 52, pp. 1049-1062, Jul. 2003.

[79] H. Minn, V.K. Bhargava, K.B. Letaief, “A robust timing and frequency synchronization for OFDM systems”, *IEEE Transactions on Wireless Communications*, vol. 2, pp. 822-839, Jul. 2003.

[80] Y. Zhang, S.L. Miller, “ Code acquisition in transmit diversity DS-CDMA systems”, *IEEE Transactions on Communications*, vol. 51, pp. 1378-1388, Aug. 2003.

[81] H. Li, J. Li, S.L. Miller, “Decoupled multiuser code-timing estimation for code-division multiple-access communication systems”, *IEEE Transactions on Communications*, vol. 49, pp. 1425-1436, Aug. 2001.

[82] Y. Luan, J. Li, J. Yang, “Timing estimator for MC-CDMA system”, *Electronics Letters*, vol. 38, pp. 1061-1063, Aug. 2002.

[83] K. Ha, Y.C. Seo, C.W. Lee, “On a frame synchronization scheme for MC-CDMA systems in up-link asynchronous channels”, *IEEE Vehicular Technology Conference (VTC’99)*, vol. 1, pp. 193-197, Sep. 1999.

[84] B. Seo, H.M. Kim, “Frequency offset estimation and multiuser detection for MC-CDMA systems”, *IEEE Military Communications Conferencec (MILCOM’*02)., vol. 2, pp. 804-807, Oct. 2002.

[85] A. Feng, Q. Yin, Z.Zhao, H. Zhang, “Blind space-time equalization/ decoding with carrier frequency synchronization in multicarrier CDMA systems”, *IEEE*

International Symposium on Circuits and Systems (ISCAS'02), vol. 2, pp. 500-503, May. 2002.

[86] Y. Luan, J. Li, "New timing acquisition method for MC-CDMA system with frequency offset", *IEEE Vehicular Technology Conference (VTC'02)*, vol. 3, pp. 1477-1481, May. 2002.

[87] Y. Jiao, C.H. Hong, X. Sun, Z.Zhou, "An low-complex and faster synchronization method for MC-CDMA systems", *IEEE Vehicular Technology Conference (VTC'02)*, vol. 3, pp. 1482-1486, May. 2002

[88] S. Hahm, W. Sung, "A synchronization scheme for multi-carrier CDMA systems", *IEEE International Conference on Communications (ICC'98)*, vol. 3, pp. 1330-1334, Jun. 1998.

[89] X. Cai; A.N. Akansu, Multicarrier CDMA systems with transmit diversity, VTC, 2000. *IEEE Vehicular Technology Conference (VTC'00 Fall)*, vol 6, pp. 2817 –2821, 2000.

[90] C. Fragouli, N. Al-Dhahir, W. Turin, "Training-based channel estimation for multiple-antenna broadband transmissions", *IEEE Transactions on Wireless Communications*, vol 2, pp. 384-391, Mar, 2003.

[91] E. Moulines, P. Duhamel, J.F. Cardoso, S. Mayrargue, "Subspace methods for the blind identification of multichannel FIR filters", *IEEE Transactions on Signal Processing*, vol 43, pp. 516 –525, Feb. 1995.

[92] S.E. Bensley, B. Aazhang, "Subspace-based channel estimation for code division multiple access communication systems", *IEEE Transactions on Communications*, vol 44, pp. 1009 –1020, Aug. 1996.

[93] W. Sun, H. Li, "A subspace-based channel identification algorithm for forward link in space-time coded MC-CDMA systems", *IEEE Wireless Communications and Networking Conference (WCNC'02)*, vol.1, pp. 445-448, Mar, 2002.

[94] C.J. Escudero, D.I.Iglesia, L.Castedo, " A novel channel identification method for downlink multicarrier CDMA systems", *IEEE International Symposium on Personal, Indoor, and Mobile Radio Communications (PIMRC'00*), vol.1, pp. 103-107, Sept. 2000

[95] X. Hu, Y.H. Chew, "Performance of space-time block coded MC-CDMA system over frequency selective fading channel using semi-blind channel estimation technique", *IEEE Wireless Communications and Networking Conference (WCNC'03)*, vol. 1, pp. 414-419, Mar, 2003.

[96] Z. Li, M. Latva-aho, "Semil-blind space-time-frequency multiuser receiver for STBC MC-CDMA", *IEEE International Symposium on Spread Spectrum Techniques and Applications (ISSSTA'04)*, pp. 140-144, Sept. 2004.

[97] S. Zhou; Muquet, B.; G.B. Giannakis, Subspace-based (semi-) blind channel estimation for block precoded space-time OFDM, *IEEE Transactions on Signal Processing*, vol 50, pp.1215 -1228, May 2002.

[98] H. Li, X. Lu, G.B. Giannakis, "Capon multiuser Receiver for CDMA systems with space-time coding", *IEEE Transactions on Signal Processing. On*, vol. 50, pp. 11930-1204, May, 2002.

[99] J. Altuna, B. Mulgrew, J.M. Zabalegui, "Semi-blind equalisation for multiple-input multiple-output MC-CDMA", *3G Mobile Comm. Tech., 2001. 2nd Inter. Conf. On*, pp. 387 –391, 2001, *IEEE Transactions on Signal Processing*, vol 50, pp. 1699 –1712, Jul 2002.

[100] F. Lin, L.B.Milstein, "Successive interference cancellation in multicarrier DS/CDMA", *IEEE Transactions on Communications.*, vol. 48, pp1530-1540, Sep. 2000.

[101] F. Li, H. Liu, R.J. Vaccaro, "Performance analysis for DOA estimation algorithms: unification, simplification, and observations" *IEEE Transactions on Aerospace and Electronics Systems*, vol 29, pp. 1170 –1184, Oct. 1993.

[102] X. Hu, Y.H. Chew, "A New Approach to Study the Effect of Carrier Frequency Offset on the BER Performance of Asynchronous MC-CDMA Systems", to appear in *IEEE Wireless Communications and Networking Conference 2005 (WCNC'05)*, New Orleans, USA, 2005.

[103] J.P. Imhof, "Computing the distribution of quadratic forms in normal variables", *Biometrika*, Vol 48, 3/4, pp.419-426, Dec. 1961.

[104] J.G. Proakis, *Digital Communications*, McGraw-Hill, New York, 2001.

[105] A. Papoulis, S.U. Pillai, *Probability, Random Variables and Stochastic Processes,* McGraw-Hill, New York, 2002.

[106] M.K. Simon, M. Alouini, *Digital Communication over Fading Channels – A Unified Approach to Performance Analysis,* John Wiley & Sons, New York, 2000.

[107] M. Abramowitz, I.A. Stegun, *Handbook of Mathematical Functions.* New York, Dover, 1972.

[108] I.S. Gradshteyn, I.M. Ryzhik, *Table of Integrals, Series, and Products*. New York, 1980.

[109] Frank H.P. Fitzek, "Quality of service support in multi-code CDMA systems", Ph.D. thesis, University of Technology, RWTH, Aachen, Germany, 1997.

[110] Q.Shi, M.Latva-aho, “Spreading sequences for asynchrounous MC-CDMA revisited: accurate bit error rate analysis”, *IEEE Transactions on Communications*, vol 51, pp 8-11, Jan. 2003

[111] A.J.Barabell, “Improving the resolution performance of eigenstructure-based direction-finding algorithms”, *IEEE International Conference on Acoustics, Speech, and Signal Processing (ICASP*’83), vol. 49, pp. 336-339, 1983

[112] K. Erwin, *Advanced engineering mathematics*, John Wiley, 1999.

[113] Peter Lancaster, Miron Tismenetsky, *The theory of matrices : with applications*, Orlando, Academic Press , 1985

[114] S. Barbarossa, A. Scaglione, G.B. Giannakis, “Performance analysis of a deterministic channel estimator for block transmission systems with null guard intervals”, *IEEE Transactions on Singal Processing*, vol. 50, pp. 684-695, Mar. 2002.

Publications and Submissions

Journal

[1]. X. Hu, Y.H. Chew, "On the performance and capacity of asynchronous space-time block coded MC-CDMA system in the presence of carrier frequency offset", *IEEE Transactions on Vehicular Technology*, Vol. 53, pp. 1327-1340, Sept, 2004

[2]. X. Hu, Y.H. Chew, "On the performance and system capacity comparisons of multicode, variable spreading gain and multiple-symbol-rate multirate access schemes for asynchronous space-time block coded multicarrier CDMA systems over frequency selective Rayleigh fading channel", submitted to *IEEE Transactions on Vehicular Technology*

[3]. X. Hu, Y.H. Chew, "A subspace-based joint blind multiuser timing and frequency synchronization for asynchronous space-time block coded multicarrier CDMA system", submitted to *IEEE Transactions on Wireless Communications*

[4]. X. Hu, Y.H. Chew, "Subspace-based semi-blind channel estimation and multiuser detection for uplink space-time block coded multicarrier CDMA System over frequency selective fading channel", submitted to *IEEE Transactions on Vehicular Technology*

Conference

[1]. X. Hu, Y.H. Chew, “A New Approach to Study the Effect of Carrier Frequency Offset on the BER Performance of Asynchronous MC-CDMA Systems”, *IEEE Wireless Communications and Networking Conference 2005 (WCNC’05)*, New Orleans, LA, USA, Mar 2005.

[2]. X. Hu, Y.H. Chew, “Maximum likelihood multiuser timing synchronization scheme for asynchronous multirate multicarrier CDMA System”, *IEEE Military Communications Conference 2004 (MILCOM’04)*, Monterey, CA, USA, Nov 2004

[3]. X. Hu, Y.H. Chew, “On the capacity of multicode and variable spreading gain access scheme for multicarrier CDMA systems supporting multirate services with transmit power control”, *IEEE International Conference on Communication Systems 2004 (ICCS’04)*, pp. 666-671, Singapore, Sept 2004.

[4]. X. Hu, Y.H. Chew, “On the capacity of multicode and variable spreading gain multirate space-time blocked coded multicarrier CDMA systems over frequency selective Rayleigh fading channel”, *IEEE Vehicular Technology Conference 2004-Fall (VTC’04-Fall)*, vol. 1, pp. 353-357, LA, CA, USA, Sept 2004.

[5]. X. Hu, Y.H. Chew, "On the capacity of spectrally overlaid multiple-symbol-rate space-time block coded multicarrier CDMA systems over frequency selective Rayleigh fading channel ”, *IEEE International Symposium on Personal, Indoor, and Mobile Radio Communications 2004 (PIMRC’04)*, pp. 1652-1657, Barcelona, Spain, Sept 2004.

[6]. X. Hu, Y.H. Chew, “On the design of spectrally overlaid multiple symbol-rate multicarrier CDMA systems”, *IEEE International Symposium on Spread*

Spectrum Techniques and Applications 2004 (ISSSTA'04), pp. 72-76, Sydney, Australia, Aug 2004.

[7]. R. Mo, X. Hu, Y.H. Chew, "On the design of spectrally overlaid CDMA system under a practical interference environment", *IEEE International Symposium on Personal, Indoor, and Mobile Radio Communications 2003 (PIMRC'03),* vol. 1, pp.661-665, Beijing, China, Sept 2003.

[8]. X. Hu, Y.H. Chew, "Performance of space-time block coded MC-CDMA system over frequency selective fading channel using semi-blind channel estimation technique", *IEEE Wireless Communications and Networking Conference 2003 (WCNC'03),* vol. 1, pp. 414-419, USA, Mar 2003.

[9]. X. Hu, Y.H. Chew, "A joint blind timing and frequency synchronization algorithm using decoupled subspace approach for asynchronous multicarrier CDMA systems", submitted to *IEEE Global Telecommunications Conference 2005 (GlobeCom'05)*, St. Louis, USA.